Title
Complete Electrochemical Characterization of Ion Transport in Polymer Electrolytes

Author
Pesko, Danielle

Publication Date
2018

Peer reviewed|Thesis/dissertation

Complete Electrochemical Characterization of Ion Transport in Polymer Electrolytes

By

Danielle Pesko

A dissertation submitted in partial satisfaction of the

requirements for the degree of

Doctor of Philosophy

in

Chemical Engineering

in the

Graduate Division

of the

University of California, Berkeley

Committee in charge:

Professor Nitash P. Balsara, Chair
Professor Bryan D. McCloskey
Professor Susan J. Muller
Professor Andrew M. Minor

Summer 2018

Complete Electrochemical Characterization of Ion Transport in Polymer Electrolytes

Abstract

Complete Electrochemical Characterization of Ion Transport in Polymer Electrolytes

By

Danielle Pesko

Doctor of Philosophy in Chemical Engineering

University of California, Berkeley

Professor Nitash P. Balsara, Chair

Next-generation lithium batteries with high energy densities are desired for powering the future fleet of electric vehicles. The implementation of these batteries hinges upon the development of novel electrolyte materials that exhibit stability against the lithium metal anode in addition to favorable transport properties. Conventional liquid electrolytes, such as the carbonate-based solvents that are standard in lithium-ion batteries, have high ionic conductivities but lack compatibility with lithium metal. In these systems, brittle, unstable interface layers form on the lithium surface leading to uneven plating and rapid cell failure. Polymer electrolytes offer a promising alternative to conventional liquid electrolytes, as they form stable interfaces with lithium metal and exhibit solid-like material properties. However, despite four decades of persistent research, the transport properties of the most promising solvent-free polymer electrolytes remain insufficient for use in commercial batteries. Our ability to design new polymers with improved electrolyte properties is compromised by a lack of understanding of ion transport in these materials. In this work, we employ a wide variety of electrochemical characterization techniques, supplemented with theory and simulations, to identify the factors that govern ion transport in polymer electrolytes.

The performance of battery electrolytes depends on three independent transport properties: ionic conductivity, diffusion coefficient, and transference number. We perform a complete characterization of all three transport properties in mixtures of 5 kg/mol polyethylene oxide (PEO) and lithium bis(trifluoromethanesulfonyl) imide (LiTFSI) salt over a wide range of salt concentrations. Three different approaches were used to measure the transference number: the steady-state current measurement, pulsed-field gradient NMR, and a new approach proposed by Balsara and Newman. The latter approach is rigorous and based on concentrated solution theory, while the other two approaches only yield the true transference number in ideal solutions. The values obtained from the steady-state current method and pulsed-field gradient NMR are positive at all concentrations. In contrast, the transference number obtained by the approach of Balsara and Newman exhibits a complex dependence on the addition of salt, with negative values obtained at intermediate salt concentrations. Negative transference numbers suggest that ion transport

is dominated by highly-mobile ionic clusters. These ion-ion interactions are neglected in the approaches that are derived using dilute solution theory.

There are a variety of techniques that can, in theory, be used to measure the transference number of concentrated electrolytes. We perform a comparison of two different electrochemical approaches: the method proposed by Balsara and Newman and a more well-established technique by Ma and coworkers. Both approaches are experimentally intensive and rely on concentrated solution theory. In high molecular weight PEO electrolytes, the data from the two techniques are in perfect agreement. In contrast, in low molecular weight PEO there is a disagreement between the two approaches, which is attributed to the presence of a complex interface layer on the surface of the lithium electrodes. The parameters measured in technique of Ma and coworkers are thought to be inherently sensitive to the nature of the electrode-electrolyte interface, which may not be representative of the bulk electrolyte. For this reason, the Balsara and Newman approach is taken as the more robust measure of transference number.

Complete characterization of ion transport in an electrolyte enables full cell modeling. In this work, the theory is presented for predicting the cycling characteristics of a lithium-polymer-lithium cell containing an electrolyte with known transport properties. Using the ionic conductivity, diffusion coefficient, and transference number of PEO/LiTFSI electrolytes as inputs to our model, we calculate salt concentration and potential profiles in the electrolyte under a constant dc polarization. At steady-state, these profiles are nonlinear due to the strong concentration dependence of the transport properties of the electrolyte. Predictions of the limiting current in PEO/LiTFSI electrolytes were obtained using the model. Experimentally-measured cycling data from a series of symmetric cells with different salt concentrations were used to test the validity of the model. The time-dependence and steady-state value of the potential measured during cycling experiments were in excellent agreement with model predictions, requiring no adjustable parameters or simplifying assumptions.

Our modeling work supports the notion that the transport properties of PEO/LiTFSI electrolytes are insufficient for immediate commercialization. Thus, there is a great deal of interest in developing next-generation polymer electrolytes with improved transport properties. Designing new polymers is hindered by the complex relationship between the transport of ions in the polymer and the structure of the monomer. For example, the ionic conductivity of a polymer electrolyte depends on a variety of interconnected factors: interactions between the polymer chains and the salt, extent of dissociation of the salt, and polymer dynamics in the vicinity of the ions. All of these are affected by the monomer structure. In this work, we attempt to unravel these factors through systematic analysis of electrolytes comprised of newly-designed polymers and LiTFSI salt. In all cases, PEO/LiTFSI electrolytes are used as a baseline for comparison.

A set of aliphatic polyesters with systematic variations to the monomer structure were characterized using ionic conductivity and glass transition temperature measurements over a wide range of salt concentrations. A novel analysis approach was introduced to factor out the effect of segmental motion on conductivity; the parameter calculated in this analysis is referred to as the reduced conductivity. The dependence of the reduced conductivity on salt concentration helps to clarify the relationship between monomer structure and ionic

conductivity, and highlights differences between PEO and the polyesters. This study also demonstrates that polymers, such as polyesters, which are comprised of multiple polar groups are not an ideal choice for fundamental studies due to the complexity of solvation and ion transport in these systems.

Linear polyethers (C_xEO_y) were synthesized as a systematic set wherein aliphatic linkers were added to a PEO backbone. The carbon linkers change the glass transition temperature and dilute the polar groups relative to PEO; both factors influence ionic conductivity. The analysis introduced in the previous study was used to factor out the effect of glass transition temperature on conductivity; the results show a clear dependence of the reduced conductivity on the mole fraction of oxygen of the polymer. MD simulations were used to study the solvation site around Li^+, which were found to be similar in all polymers. A comparison of experimental measurements and simulation results highlights the importance of solvation-site connectivity, a parameter which is thought to affect the hopping rate of Li^+. A polymer with a higher solvation-site connectivity than PEO is predicted to exhibit superior transport properties.

A newly-synthesized polymer, P(2EO-MO), was characterized using a variety of electrochemical and NMR experiments in addition to MD simulations. The maximum conductivity of P(2EO-MO) is comparable to that of PEO, but the glass transition temperature exhibits a more precipitous increase with the addition of salt. The transference number measured using the steady-state current method and NMR are about a factor of two higher in P(2EO-MO) compared to PEO. In lieu of complete electrolyte characterization, the product $\sigma t_{+,SS}$ is identified as the most important transport characteristic for comparison of electrolytes. This product is higher in P(2EO-MO), thus it is predicted to be a more efficacious electrolyte than PEO for battery applications. MD simulations reveal that the promising transport properties of P(2EO-MO) are likely attributed to the high solvation-site density which facilitates the transport of Li^+ in this material.

Table of Contents

List of Figures

List of Tables

Acknowledgements

This work would not have been possible without the gentle guidance and unwavering support of my advisor, Nitash Balsara. He helped me to navigate this project while allowing me ample space to learn and grow as an independent researcher. I admire his enthusiasm for science, his love for electrochemistry derivations, and his ability to craft a story out of seemingly meaningless data. As a mentor, Nitash is patient, thoughtful, and genuinely cares about the progress and well-being of each individual in his lab. He continues to cultivate an environment where students feel encouraged to collaborate and help each other. It is through his guidance that the Balsara Lab has evolved into a tightknit community. I cannot imagine having worked with anyone else over these past five years.

My colleagues and friends in the Balsara Lab have contributed to my work and shaped my overall experience in graduate school. I am indebted to the older graduate students for the time they spent showing me the ropes of scientific research. Kevin Wujcik had a huge influence on my decision to come to Berkeley and ultimately join the Balsara Lab. He trained me on x-ray absorption spectroscopy and assisted over the years as I struggled with the technique. I look up to him as a role model both personally and professionally. Katherine Harry also served as a mentor. I admire her ability to present research in a manner that is accessible to everyone, a skill I have tried to emulate with my own work. The singing component of our musical group hasn't been the same since she graduated. In many ways Jacob Thelen embodies what it means to be a member of the Balsara Lab: no matter how busy he is, he always finds the time to collaborate with others in lab and life. Mahati Chintapalli is a fun and cheerful colleague whose love of science, music, and fungi is contagious. I cherish our impromptu brainstorming sessions about future research directions and the nuances of electrochemistry. Her free-spirited nature, physics expertise, and violin/banjo playing skills are sorely missed in the lab. Chaeyoung Shin is a brilliant researcher who taught the battery lovers in the group about the importance of biofuels. She contributed significantly to the lab culture and frequently performed underappreciated tasks such as designing the group website. Chaeyoung seems to excel at anything she sets her mind to. I'm sure she is crushing it at her startup. Adriana Rojas bravely explored the realm of single-ion conductors and synthesized more materials than most grad students would dream of accomplishing. She also ensured our lab upheld the highest of safety standards, a thankless job. Hanging out next to her in the glovebox was always a good time. Alex Wang is easily one of the kindest, most sincere people I know. His witty humor and ambitious nature make him super enjoyable to be around. I cannot quite find the words to describe Doug as he is quite possibly one of the most unique individuals I know. He is the master of board games, snowball fight instigator, musical prodigy, water sport extraordinaire, and a man willing to hike 20 miles without shoes. He is also an ambitious researcher who courageously switched projects midway through graduate school and has educated me a great deal about polymer self-assembly.

It's difficult to emphasize how grateful I am to have spent five years working alongside Ksenia Timachova and Rita Wang. In terms of research progress, I truly believe that together Ksenia and I were greater than the sum of our parts. Through constant communication and collaboration, we have collectively contributed to the field of ion

transport in polymers. She is a brilliant researcher, a compelling presenter, and a dedicated friend who has taught me to enjoy the finer details in life. I cannot imagine having survived graduate school without her as my counterion. Rita made day-to-day life in the building 62 lab so fun and memorable. Every morning I would look forward to chatting with Rita about the excitement of life and the difficulties of science. Despite the challenging nature of the lithium-sulfur battery project, she valiantly explored a wide variety of electrochemical, spectroscopy, and computational techniques and never lost her optimistic outlook on research. We worked as a team in lab and as opponents on the ultimate frisbee field. I am lucky to call Rita a close friend.

I have also had the opportunity to learn a great deal from the younger students in the lab. There is no doubt that Whitney, Jackie, and Deep will continue to uphold the reputation and culture of the Balsara Lab as senior members of the group. Whitney's love of block copolymers might rival that of Nitash. Her fast-and-furious approach to research has allowed her to synthesize an impressive number of polymers and make rapid progress developing the theory of asymmetric block copolymers. She also is a force to be reckoned with on the softball field and in the yoga studio. Her enemy, Jackie, has also made impressive strides in lab; the two make an incredible duo. Studying failure modes in electrochemical cells is never easy, but this is especially true for Jackie because she can only synthesize polymers that are so mechanically robust they prevent dendrites altogether. She is a softball hero, fellow lover of magic erasers, knower of random facts, and genuine friend. We were usually on the same wavelength… unless we were playing Codenames. I am so impressed with how far Deep has come since he joined the lab. He has heroically explored an array of approaches and apparatuses for the electrochemical characterization of liquid electrolytes. Deep is never low on energy or sass, except after he loses in a footrace with Piper. It's hard to believe that Mike and Gumi are only second years, as they have already both taken on leadership roles in lab and continue to present research results that boggle my mind. Mike is a diligent researcher who has already dabbled in an astonishing assortment of techniques, which are likely to be useful as his recent discovery leads him in a new direction. He is incredibly level headed and down-to-earth, likely a result of his New Hampshire roots. Gumi is a ball of energy who has a hard time containing her enthusiasm for all things science. Her work ethic is unprecedented as are her makeup skills. I am also very proud of the progress she has made learning the names and functions of the tools in the toolbox; tinkering around lab with her and the rest of the 62-crew are some of my fondest memories. It is already clear that Kevin and Lorena have great intellect and are extremely dedicated researchers. I am excited to see what direction their projects take over the next few years.

The postdocs in our lab were also greatly influential in my development as a scientist. When I joined the lab, Didier Devaux took me under his wing and taught me the ins and outs of cell preparation and electrochemical characterization, skills that ended up being the foundation of my project. I learned how to properly maintain the gloveboxes and take care of the lab from Mahesh Bhatt. He was an excellent officemate with whom I spent a great deal of time discussing science and life. I overlapped with Irune Villaluenga the most out of any postdoc, which was lucky for me. She is a jack-of-all-trades who has mastered everything from polymer/inorganic synthesis to battery cycling. Over the past five years, I have learned from her how to approach difficult research questions and feel fortunate that

we were able to collaborate on the transference number measurements discussed in Chapter 2. Sebnem Inceoglu is one of the most pleasant, thoughtful, and supportive people I have ever worked with. She was always wearing a smile and truly looked out for the graduate students in the lab. Nikos Petzetakis, Pepa Cotanda, and Chelsea Chen asked difficult questions in group meeting, which helped to improve my understanding of the results I was presenting. Irune, Sebnem, Nikos, Pepa and Chelsea collectively formed a synthesis powerhouse that brought a variety of new and exciting materials into the lab. Working in conjunction with Kim Mongcopa on the ion transport characterization of homopolymers has been wonderful. I am thankful for all the help she has provided with spectroscopy and excited to learn about her future discoveries. Hee-Jeung Oh is the definition of a hard-working postdoc; she has completely revolutionized our lab's understanding of drug capture and has the best work ethic of anyone I know. She is also a pleasure to be around. I am fortunate to have had the opportunity to work with Louise Frenck on two separate occasions, during her stay as a visiting scholar and more recently as a postdoc. I look up to her a great deal and hope someday I will reach her level of understanding of electrochemistry. The lab is a brighter place with her bubbly personality.

The undergrads that I have had the opportunity to work with over the past five years have blown me away. Lexi Hasan is incredible in so many ways. She has excellent intuition, is eager to learn, and can communicate effectively, all of which made her a pleasure to work with for three years. Her independent project was so successful that she was granted the opportunity to give an oral presentation at the APS conference, making me a very proud mentor. Mackensie Smith was also a powerhouse in lab. She was quick to pick up new concepts and produced more data than most undergrads would dream of. She also bravely conquered the mysterious pychnometer and used it to make density measurements that are a cornerstone of many calculations in our lab. It's difficult to express my appreciation that I had the opportunity to work with Simar over the last year. We are so different and yet we worked seamlessly together in lab. He has the intellect and the work ethic to achieve any future direction he may wish to pursue. The Balsara Lab is lucky to have him for two more years.

I have greatly benefited from various collaborations throughout graduate school. I would like to acknowledge Tom Miller III, ZhenGang Wang, and Goeff Coates for leading the DMREF group through four successful years of collaboration. Working with the students on this team was an incredibly rewarding experience. Michael Webb, Brett Savoie, and Umi Yamamoto employed theory and simulations which helped provide insight into our experimental results. Qi Zheng and Yukyung Jung developed novel approaches to synthesize the novel polymers discussed in Chapters 5-7. I also have had the pleasure of collaborating with John Newman, whom some might call the modern-day father of electrochemistry. I sincerely value the contributions he made to the work in Chapters 2, 3 and 4.

Last but certainly not least, I want to acknowledge my family and non-work friends who have helped keep me sane through the ups and downs of a PhD program. My mom and dad have been so incredibly supportive throughout my educational journey, and I certainly would not have made it this far if it weren't for their encouragement. Every time I visited home in New Hampshire, my entire family including my sister, brother-in-law,

niece, and nephew would shower me with love and pepper me with questions about batteries. I am so thankful to have remained so close with them despite the 3000-mile separation between us. Also instrumental to my success in grad school was my future mother-in-law, Jeanne. She patiently listened and provided valuable advice as I disclosed my frustrations with academia. I am also grateful for the fun and relaxing vacations she treated me to, which undoubtedly helped alleviate stress. I know for a fact that I would not have made it through graduate school without my fiancé, Derrick. He has given me infinite pep talks and shoulder rubs through the late nights of writing, and also gladly provided comic relief when it was necessary. Moving across the country to allow me to pursue my dreams at Berkeley is the greatest gift he could ever give me. I truly hope someday I can repay the favor. I feel incredibly blessed for the community that has supported me through this journey.

1 Introduction

The widespread implementation of renewable energy technologies will alleviate the dependence of our economy on fossil fuels and help to decelerate the caustic effects of global warming on the environment. The transition to sustainable energy resources such as wind and solar hinges on the development of energy storage solutions that are both versatile and reliable.[1,2] Rechargeable batteries have the potential to transform the energy landscape by enabling integrated electrical energy storage through the grid as well as providing mobile power for transportation applications.[3–5] Batteries for these applications must satisfy an extensive set of criteria including high capacity, extensive cycle lifetime, low cost, and assured safety. One route towards improving upon existing technology is by increasing the energy density of batteries through the use of novel chemistries and next-generation materials.

1.1 High Energy Density Lithium Batteries

Lithium is the third-lightest element and offers the highest oxidation potential (3 V above the standard hydrogen electrode), making it an excellent prospect for high-power electrochemical applications. Lithium-ion batteries are the industry standard for powering electric vehicles and storing energy in the grid. A conventional lithium-ion cell is comprised of a graphite anode, a metal oxide cathode, and an organic solvent electrolyte contained within an inert separator. The theoretical energy density of the lithium-ion battery is 385 Wh/kg, and current industry technology is rapidly approaching this upper threshold.[6] While this technology is most promising in the short-term, it is clear that the lithium-ion battery will remain insufficient to meet long-term requirements for powering electric vehicles.[4,5] Thus, a transition to higher energy density batteries is desired.

Achieving a battery with increased energy density requires implementation of new active materials and/or a reduction in the mass of the components within the cell. A wide variety of novel battery chemistries offer improvements in energy density over the conventional lithium-ion chemistry;[5] a majority rely on replacing the graphite anode with pure lithium-metal. This simple substitution leads to a 40% increase in the theoretical energy density of the system. In addition, the lithium metal anode is a requirement for next-generation technology such as lithium-sulfur and lithium-air batteries, both of which have theoretical energy densities on par with gasoline.[7,8] While significant challenges preclude the immediate adoption of these chemistries, it is likely that future batteries will rely on lithium metal anodes. We thus focus our efforts on developing materials that are compatible with lithium metal.

1.1 Limitations of Nonaqueous Liquid Electrolytes

The electrolyte solvent chosen for a given battery application must satisfy a long list of basic requirements: it must (1) be able to dissolve lithium salts, (2) be able to conduct ions, (3) remain inert to the electrode materials and separator during cell operation, (4) be a liquid over a wide temperature window, (5) be economical, and (6) be safe.[9] Aqueous electrolytes are not compatible with lithium-ion technology, as the reduction and oxidation potentials at the electrodes are outside the stability window of water. Nonaqueous solvents containing polar groups such as carbonyls

(C=O), ethers (-O-), sulfonyls (S=O) and nitriles (N≡O) are promising candidates due to their ability to dissolve lithium salts in high concentrations.[9] A wide variety of nonaqueous solvents have been explored as electrolyte materials including those based on carbonates, esters, and ethers. The electrolyte that best satisfies the aforementioned criteria for the lithium-ion battery consists of blends of carbonates (e.g. ethylene carbonate, EC, and dimethyl carbonate, DMC) mixed with lithium salt.[9–11] These electrolytes offer high ionic conductivities of 10^{-2} S/cm at ambient temperatures. Today, carbonate solvents account for the vast majority of electrolytes in commercial lithium-ion batteries.

History has proven that traditional organic solvent-based electrolytes are not compatible with lithium metal.[12,13] This incompatibility is ascribed to irreversible reactions that take place on the surface of the lithium metal leading to capacity fade and dendrite formation, both of which result in cell failure.[14–16] Replacing these organic solvents with materials are stable against lithium metal is a crucial step toward the development of next-generation batteries.

1.2 Polymer Electrolytes for Next-Generation Batteries

Polymers are desirable electrolyte materials as they offer fluid-like properties on the microscale with solid-like properties on the macroscale and provide a promising path towards an entirely solid-state battery. They have proven stable against the lithium metal anode.[17] In addition, their structural properties can be easily tuned through the incorporation of crosslinks or microphase-segregated blocks;[18,19] using these strategies to increase the modulus may thwart the propagation of lithium dendrites during cell cycling.[20,21] However, the solvation and transport mechanisms of ions in polymers is fundamentally different from that of conventional liquids.[22–25] At this point, the factors that underlie ion transport in polymer electrolytes is not well understood. This compromises our ability for rational design of novel polymer electrolytes with improved transport properties.

The field of polymer electrolytes was set forth in 1973 when Fenton, Parker, and Wright discovered that polyethylene oxide (PEO) could solvate and conduct alkali metal salts based on sodium and potassium.[26] Later that decade, Armand demonstrated the ability of PEO to conduct lithium salts, and identified it as a promising material for electrochemical applications.[27] Since then, a vast amount of literature has been dedicated to characterizing the ion transport properties in PEO-based electrolytes with an array of lithium salts.[28–36] At this point, the most promising candidate is PEO mixed with lithium bis(trifluoromethanesulfonyl) imide (LiTFSI) salt, which has a conductivity on the order of 10^{-3} S/cm at 90°C.[28] Due to its high ionic conductivity and stability against lithium metal, the PEO/LiTFSI electrolyte is now used as a benchmark against all other polymer electrolytes.

The desire to improve upon the transport characteristics of PEO has motivated studies of conductivity in a wide variety of polymers. Dating back to the 1980's, reports of conductivity in polyethers,[37–43] polyesters,[44–48] polycarbonates,[49,50] polysiloxanes,[51–54] polyphosphazenes,[55] and perflouropolyethers[56] have been prevalent in the literature. The majority of reports rely on a guess-and-check approach, wherein a new polymer is synthesized and the conductivity of the electrolyte is measured to determine if the electrolyte is of practical interest. Designing new polymers for improved ion transport is challenging due to a lack of understanding of the relationship between monomer chemistry and electrolyte properties. A simple measure of conductivity gives little

insight into the factors that affect ion transport in a given system. Differences in conductivity could be attributed to differences in the glass transition temperature, dielectric constant, ion solvation mechanism, salt dissociation, or ion hopping rates, all of which are inherently dependent on monomer chemistry. Few studies take a systematic approach to characterizing and understanding ion transport in these materials.

1.3 Electrochemical Characterization of Electrolytes

Ionic conductivity is the most important transport property of a battery electrolyte, as it describes the amount of current that is achieved for a given voltage based on Ohm's law. In addition, conductivity is the most facile characterization measurement, relying on ac impedance spectroscopy which is a fast and well-defined technique. It is, therefore, not surprising that most studies of newly-designed electrolytes report on the conductivity over a range of conditions such as temperature and salt concentration.

Complete characterization of ion transport in a battery electrolyte depends on three independent properties: ionic conductivity, salt diffusion coefficient, and cation transference number.[57] Measurement of all three transport properties over a wide range of salt concentrations is required for full-scale modeling of electrolyte performance in a battery. It also can provide insight into the mechanisms through which ions transport on the microscale in a given solvent. Few reports in the literature make an attempt to characterize all three transport properties. While the correct experimental techniques for measuring conductivity and the salt diffusion coefficient are widely accepted, the appropriate technique for measuring the transference number remains to be determined. The majority of transference numbers reported in the literature are obtained using experimental techniques that rely on dilute solution assumptions; these techniques are not valid in concentrated electrolytes but nonetheless continue to be applied to a variety of systems at high concentrations.

1.4 Outline of this Dissertation

The overarching goal of this work is to use electrochemical characterization as a means to gain a better fundamental understanding of the factors that govern ion transport in polymer electrolytes. The remainder of this dissertation is organized into two parts: Chapters 2-4 describe an investigation of electrochemical characterization and modeling techniques using PEO/LiTFSI electrolytes, and Chapters 5-7 focuses on developing next-generation polymer electrolytes using a systematic approach.

Chapter 2 shows the complete electrochemical characterization of PEO/LiTFSI electrolytes over a wide range of salt concentrations employing three different techniques for measuring the transference number. We demonstrate the importance of characterization techniques that do not rely on ideal solution assumptions. Chapter 3 is a direct comparison between two rigorous approaches for measuring transference number, both of which rely on concentrated solution theory. Chapter 4 uses the transport properties reported in Chapter 2 to model the cycling characteristics of lithium-polymer-lithium symmetric cells with PEO/LiTFSI electrolytes. A direct comparison between experiment and theory highlights the accuracy of our electrochemical measurements and demonstrates the validity of our model. Chapter 5 provides a new approach for analyzing conductivity measurements that offers insight into the relationship between ion transport

and monomer structure in a systematic set of polyester-based electrolytes. Chapter 6 details a joint experimental and computational investigation of a set of polyether electrolytes that introduces the importance of the solvation-site connectivity. Chapter 7 describes the characterization of a new ether-based polymer electrolyte with transport properties that exceed that of PEO/LiTFSI. In this chapter, we define the parameter that is most relevant for comparing battery electrolytes in lieu of complete characterization.

2 Negative Transference Numbers in Poly(ethylene oxide)-based Electrolytes[†]

ABSTRACT

The performance of battery electrolytes depends on three independent transport properties: ionic conductivity, diffusion coefficient, and transference number. While rigorous experimental techniques for measuring conductivity and diffusion coefficients are well-established, popular techniques for measuring the transference number rely on the assumption of ideal solutions. We employ three independent techniques for measuring transference number, t_+, in mixtures of polyethylene oxide (PEO) and lithium bis(trifluoromethanesulfonyl) imide (LiTFSI) salt. Transference numbers obtained using the steady-state current method pioneered by Bruce and Vincent, $t_{+,SS}$, and those obtained by pulsed-field gradient NMR, $t_{+,NMR}$, are compared against a new approach detailed by Newman and coworkers, $t_{+,Ne}$, for a range of salt concentrations. The latter approach is rigorous and based on concentrated solution theory, while the other two approaches only yield the true transference number in ideal solutions. Not surprisingly, we find that $t_{+,SS}$ and $t_{+,NMR}$ are positive throughout the entire salt concentration range, and decrease monotonically with increasing salt concentration. In contrast, $t_{+,Ne}$ has a non-monotonic dependence on salt concentration and is negative in the highly-concentrated regime. Our work implies that ion transport in PEO/LiTFSI electrolytes at high salt concentrations is dominated by the transport of ionic clusters.

2.1 Introduction

Energy density and safety of conventional lithium-ion batteries is limited by the use of liquid electrolytes comprising mixtures of flammable organic solvents and lithium salts. Polymer electrolytes have the potential to address both limitations. However, the power and lifetime of batteries containing solvent-free polymer electrolytes remain inadequate for most applications. The performance of electrolytes in batteries depends on three independent transport properties: ionic conductivity, σ, salt diffusion coefficient, D, and cation transference number, t_+.[57] The poor performance of batteries with polymer electrolytes is generally attributed to low conductivity, which is on the order of 10^{-3} S/cm at 90°C for mixtures of polyethylene oxide (PEO) and lithium bis(trifluoromethanesulfonyl) imide (LiTFSI) salt,[28,58] compared to that of liquid electrolytes which is 10^{-2} S/cm at ambient temperatures.[9] Much of the literature in this field has been devoted to increasing the ionic conductivity of these materials.[41,44–48,50–53,55,59–75] The purpose of our work is to shed light on another transport property of polymer electrolytes, the transference number.

In a pioneering study, Ma and coworkers showed that the transference number of a mixture of PEO and a sodium salt is negative.[76] Following this approach, others have obtained $t_+ < 0$ in

[†] This chapter was reported in *J. Electrochem. Soc.* **2017**, *164* (11), E3569–E3575

polymers containing lithium or sodium salts.[77–79] Nevertheless, the majority of reports for t_+ in polymer electrolytes fall between zero and one.[30,36,49,56,80–90] In contrast, all reports of t_+ in non-aqueous liquid electrolytes containing lithium salts fall between zero and one, including those that followed the techniques outlined by Ma and coworkers.[91–95] Zugmann and coworkers presented a comparative study using four different methods for measuring t_+ in nonaqueous liquid electrolytes. In all cases, t_+ fell in the range of 0.25 to 0.35. Similar comprehensive studies of t_+ in polymer electrolytes have not yet been conducted. It is clear that more work is needed to clarify the value of t_+ in polymer electrolytes.

The most popular approach for estimating t_+ in polymer electrolytes is that developed by Bruce and Vincent.[88,96] In this approach, the electrolyte of interest is sandwiched between two lithium electrodes, and the current, i, obtained under a fixed applied potential, ΔV, is monitored as a function of time, t. Bruce and Vincent showed that for electrolytes that exhibit ideal solution behavior

$$t_{+,SS} = \frac{i_{SS}}{i_0}, \tag{2.1}$$

where i_0 is the initial current, i_{ss} is the steady-state current, and the subscript SS in $t_{+,SS}$ indicates the approach used to obtain the transference number. It is now fairly routine to report both σ and $t_{+,SS}$ of newly-developed polymer electrolytes.[80–82,87,90,97–99] The question of limits on i_{ss}/i_0, or equivalently, $t_{+,SS}$ is an interesting open question. While most papers have reported i_{ss}/i_0 values between 0 and 1, there is at least one report wherein i_{ss}/i_0 obtained from an electrolyte was greater than 1.[100] Since there are no bounds on the value of t_+, eq. 2.1 suggests that there may be no bounds on i_{ss}/i_0.

In more recent work by Newman and coworkers,[101,102] it was shown that for concentrated electrolytes,

$$\frac{i_{SS}}{i_0} = \frac{1}{1+Ne}, \tag{2.2}$$

where

$$Ne = a\frac{\sigma RT\left(1-t_{+,Ne}\right)^2}{F^2Dc}\left(1+\frac{d\ln\gamma_{\pm}}{d\ln m}\right). \tag{2.3}$$

Here R is the gas constant, T is the temperature, F is Faraday's constant and c is the bulk concentration of the electrolyte. The parameter a is related to the stoichiometry of the salt, which is equal to 2 for monovalent salts such as LiTFSI. The thermodynamic factor, $1+d\ln\gamma_{\pm}/d\ln m$, quantifies the change in the mean molal activity coefficient of the salt, $\gamma_{\pm}$, with the molality, m, of the solution. Measurements of i_{ss}/i_0, σ, D, and $1+d\ln\gamma_{\pm}/d\ln m$ are combined to obtain $t_{+,Ne}$. Note that all of the terms on the right side of eq. 2.3 are positive. This indicates that i_{ss}/i_0 must lie between zero and one, regardless of the magnitude or sign of t_+ (see eq. 2.2); measurements outside this range must be affected by side reactions or some other artifact. It was shown in reference 102 that eq. 2.3 reduces to eq. 2.1 in the limit of infinitely-dilute ideal solutions.

Complimentary information can be obtained by ^{7}Li and ^{19}F pulsed-field gradient NMR experiments. These experiments enable determination of the self-diffusion coefficients of species containing Li and F, D_{Li} and D_F. For fully dissociated electrolytes, D_{Li} represents the diffusion coefficient of the cation while D_F represents the diffusion coefficient of the anion. It is customary to define a transference number based on NMR as

$$t_{+,NMR} = \frac{D_{Li}}{D_{Li} + D_F}. \tag{2.4}$$

The purpose of this paper is to report on the dependence of $t_{+,SS}$, $t_{+,Ne}$, and $t_{+,NMR}$ on salt concentration in mixtures of PEO and LiTFSI, a standard polymer electrolyte. It is important to recognize that the transference number required for modeling battery performance[57] is $t_{+,Ne}$, not $t_{+,SS}$ nor $t_{+,NMR}$.

2.2 Experimental

2.2.1 Electrolyte Preparation and Density Measurements

Electrolytes were prepared according to the procedures outlined in reference 103. All electrolytes are homogeneous mixtures of 5 kg/mol PEO with –OH endgroups (Polymer Source) and lithium bis(trifluoromethanesulfonyl)imide (LiTFSI) salt (Novalyte). Electrolytes are prepared at varying salt concentrations, ranging from $r = 0.01$ to $r = 0.3$, where $r = [Li^+]/[O]$ is the molar ratio of lithium ions to ether oxygens.

The density, ρ, at each salt concentration was obtained by measuring the mass of electrolyte within a known volume at 90°C. Results are shown in Table 2.1, where the reported density is based on a single measurement due to limited sample. We measured neat PEO density three times and found the standard deviation to be about 2%. We take this to be the error for all of our measurements.

Salt concentration, c, was calculated from r and ρ according to

$$c = \frac{\rho r}{M_{EO} + r M_{salt}}, \tag{2.5}$$

where M_{EO} is the molar mass of the ethylene oxide repeat unit (44.05 g/mol) and M_{LiTFSI} is the molar mass of LiTFSI (287.09 g/mol). The molality of the electrolyte, m, is calculated according to

$$m = \frac{r}{M_{EO}}. \tag{2.6}$$

Table 2.1 provides values of ρ, c, and m for all electrolytes in this study.

Table 2.1. Measured values of density and calculated values of salt concentration (eq. 2.5) and molality (eq. 2.6) for each electrolyte based on *r*.

r	*ρ* (g/L)	*c* (mol/L)	*m* (mol/kg)
0.00	1128	0.00	0.00
0.01	1160	0.25	0.23
0.02	1180	0.47	0.45
0.04	1210	0.87	0.91
0.06	1230	1.20	1.36
0.08	1330	1.59	1.81
0.10	1365	1.87	2.27
0.12	1380	2.11	2.72
0.14	1430	2.38	3.17
0.16	1450	2.58	3.63
0.18	1470	2.76	4.08
0.21	1516	3.05	4.76
0.24	1580	3.36	5.44
0.27	1572	3.49	6.12
0.30	1640	3.78	6.80

2.2.2 Electrochemical Characterization

All sample preparation was performed inside of an argon glovebox (MBraun) in order to maintain water and oxygen levels below 1 and 5 ppm respectively. Conductivity samples were prepared according to the procedures outlined in reference 103. Lithium symmetric cells were prepared for steady-state current and restricted diffusion measurements of the electrolytes. Samples were made by pressing the polymer electrolyte into a 508 µm thick silicone spacer and sandwiching between two 150 µm thick lithium foils (MTI Corporation) backed with nickel foil. A stainless-steel shim was placed on either side of the sample to prevent the sample from deforming, which could lead to a change in electrolyte thickness or a cell short. Nickel tabs were secured to the stainless-steel shims to serve as electrical contacts. The assembly was vacuum sealed in a laminated aluminum pouch material (Showa-Denko) before removal from the glovebox. All samples were annealed at 90°C for 4 hours prior to electrochemical characterization.

Steady-state current and restricted diffusion measurements were performed using a Biologic VMP3 potentiostat. All measurements were performed at 90°C. At the beginning of the experiment, cells were conditioned for 4 charge/discharge cycles at a low current density of 0.02 mA/cm^2 to ensure a stable interfacial layer was introduced. Each conditioning cycle consisted of a 4 h charge followed by a 45 min rest and a 4 h discharge. Ac impedance spectroscopy was performed prior to potentiostat polarization. Complex impedance measurements were acquired for a frequency range of 1 MHz to 1 Hz at an amplitude of 80 mV. The data were analyzed in the form of a Nyquist plot and fit to an equivalent electrical circuit suitable for a symmetric cell with nonblocking electrodes. This circuit is shown in Figure 2.1, where Q_b and Q_i are the bulk and interfacial pseudo-capacitance, and R_b and R_i are the bulk and interfacial resistance of the cell. During the steady-state current experiment, current was measured at time intervals of 5 s while the cell was polarized for 4 h, long enough to reach a steady-state current. Potentials of ΔV = 10 mV, -10 mV, 20 mV, and -20 mV were used to ensure that the ion transport characteristics were independent of the sign and magnitude of the applied potential. Each data point in this study represents an average of all applied potentials. The cell resistances were measured as a function of time by performing ac impedance spectroscopy every 20 minutes during polarization. Here, the

center of the ac input signal was offset by ΔV, and the amplitude was set to 10 mV to minimize disturbance of the polarization signal.

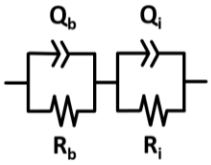

Figure 2.1. Equivalent electrical circuit for a symmetric cell with nonblocking electrodes. This circuit was fit to ac impedance spectroscopy data to obtain bulk resistance, R_b, and interfacial resistance, R_i, of the cell.

In the absence of a concentration gradient, current is defined by Ohm's law,

$$i_\Omega = \frac{\Delta V}{R_{i,0} + R_{b,0}}, \tag{2.7}$$

where ΔV is the applied potential and $R_{i,0}$ and $R_{b,0}$ are cell resistances measured by ac impedance spectroscopy prior to polarization.[87]

The steady-state current experiment is used to determine the transference number defined by the work of Bruce and Vincent,[88,96]

$$t_{+,SS} = \frac{i_{SS}(\Delta V - i_\Omega R_{i,0})}{i_\Omega(\Delta V - i_{SS} R_{i,SS})}, \tag{2.8}$$

where ΔV is the applied potential, i_Ω is the initial current calculated according to eq. 2.7, i_{SS} is the current measured at steady-state, and $R_{i,0}$ and $R_{i,SS}$ are the initial and steady-state resistances of the interface, respectively.

Restricted diffusion measurements are performed using the polarization induced by the steady-state current experiment. The applied potential was removed, and the cells were allowed to relax for 2 h while the open-circuit voltage, U, was measured at time intervals of 5 s. The salt diffusion coefficient, D, is calculated using

$$-\frac{d \ln U}{dt} = \frac{\pi^2 D}{L^2}, \tag{2.9}$$

where the left side of the equation is the slope from the least-squares fit of –ln U vs. time from t = 5 min to t = 2 h. We exclude t = 0 to 5 min to allow the electric double layer to discharge fully prior to the diffusion measurement. L is the thickness of the electrolyte, here assumed to be 508 μm, which is the thickness of the spacer.

Concentration cells were prepared using a similar cell configuration as that described in reference 76 with a diffusion length of several centimeters to prevent the concentration gradient from relaxing too quickly. Unlike the solid electrolyte films described in previous reports,[76–79,85] the electrolytes in this study were contained within a spacer to prevent leakage at high temperatures. A channel approximately 3 cm long and 2 mm wide was cut in a 508 μm thick silicone spacer. Half of the channel was filled with reference electrolyte (r_{ref} = 0.06), and the other half was filled with electrolytes at various r. Lithium electrodes backed with nickel foil were placed on either end of the channel. Nickel tabs were secured to the nickel foil, and the assembly was

vacuum sealed in a laminated aluminum pouch material. Each cell was annealed at 90°C for 20 hours before the open-circuit voltage, U, was measured using a Biologic VMP3 potentiostat. Two or three concentration cells were prepared for each salt concentration.

Measurements of σ, D, and $t_{+,SS}$, were combined with the concentration cell data to calculate $t_{+,Ne}$. For both stainless-steel and lithium symmetric cells (σ, D, and $t_{+,SS}$), three samples were prepared, the measurements were averaged, and the standard deviation is reported as the error ($\delta\sigma$, δD, and $\delta t_{+,SS}$). The error for $t_{+,Ne}$, $\delta t_{+,Ne}$, is propagated according to

$$\delta t_{+,Ne} = \left|t_{+,Ne}\right| \sqrt{\left(\frac{\delta D}{D}\right)^2 + \left(\frac{\delta \sigma}{\sigma}\right)^2 + \left(\frac{\delta t_{+,SS}}{t_{+,SS}}\right)^2}. \tag{2.10}$$

Typical values for $\delta D/D$ fell in the range of 0.05 to 0.37, $\delta\sigma/\sigma$ fell in the range of 0.03 to 0.36, and $\delta t_{+,SS}/t_{+,SS}$ fell in the range of 0.02 to 0.20.

Determination of $t_{+,Ne}$ requires three independent measurements conducted using lithium/polymer cells: $t_{+,SS}$ and D from lithium symmetric cells and the thermodynamic factor from concentration cells. All of these could theoretically be influenced by the presence of the solid electrolyte interface (SEI) that forms spontaneously at the lithium-polymer interface. To address this issue, lithium symmetric cells are always conditioned prior to electrochemical measurements. These low-current polarizations are used to set up a stable lithium-polymer interface that does not change throughout the course of the measurements. The Bruce and Vincent measurement of $t_{+,SS}$ accounts for SEI formation, as the time-dependence of the interfacial resistance is accounted for in the calculation (see equation 2.8). In the experiments reported here there is no change in either bulk or interfacial impedance during the $t_{+,SS}$ and D measurements. We deliberately chose to work with 500 μm thick samples to ensure that the potential relaxation in our restricted diffusion experiments is dominated by salt diffusion in the bulk (i.e. to minimize interfacial relaxation contributions). Concentration cells cannot be conditioned prior to the measurement as this may change the concertation gradient within the cells. We thus allowed for stable SEI formation by annealing the cells for 20 hours prior to measurement of the OCV. Between hours 0 to 20, the OCV of the cell varies with time, an observation that we attribute to interfacial reactions related to SEI formation. It is unclear at this point what role these SEI layers play in data obtained from the concentration cells. The same limitation applies to all of the concentration cell data in the literature.

2.2.3 Pulsed-Field Gradient NMR (PFG-NMR) Characterization

Electrolytes were placed into NMR tubes and sealed with high pressure polyethylene caps before measurement. NMR measurements were performed on a Bruker Avance 600 MHz instrument fitted with a Z-gradient direct detection broad-band probe and a variable temperature unit maintained at 90°C throughout the experiments. Measurements were performed on the isotopes of ^{7}Li and ^{19}F to probe the diffusion of lithiated and fluorinated salt species, respectively. All samples produced peaks around 233 MHz for lithium and 565 MHz for fluorine corresponding to all lithium- and TFSI-containing ions. The 90° pulse lengths were optimized for each sample to achieve maximum signal amplitude. T1 relaxation times were independently measured for each sample nuclei using inversion-recovery (180-τ-90-acq.) to insure the choice of an appropriate

diffusion time interval, Δ. A bipolar gradient pulse sequence was used to measure the self-diffusion coefficients, D_i. The attenuation of the echo E was fit to,

$$E = e^{-\gamma^2 g^2 \delta^2 D_i \left(\Delta - \frac{\delta}{3}\right)}, \tag{2.11}$$

where γ is the gyromagnetic ratio, g is the gradient strength, δ is the duration of the gradient pulse, Δ is the interval between gradient pulses, τ is the separation between pulses, and D_i is the self-diffusion coefficient. Parameters used for acquisition were diffusion intervals Δ = 0.55 to 0.85 s (^{7}Li) and 0.96 to 1.2 s (^{19}F), and pulse lengths δ = 5 to 10 ms (^{7}Li) and 1 to 2.5 ms (^{19}F). For each diffusion measurement, 32 experiments of varying gradient strength were performed, and the change in amplitude of the attenuated signal was fit to obtain the parameter D_i. All measured signal attenuations were single exponential decays, and R^2 values for all fits were greater than 0.99 for both ^{19}F and ^{7}Li. Only one data point was collected for each r value, because of the complexity and length of the PFG-NMR measurements at slow diffusion times.

2.3 Results and Discussion

We determine ionic conductivity, diffusion coefficient, and transference number in PEO/LiTFSI mixtures as a function of salt concentration using three separate experiments: ac impedance spectroscopy, restricted diffusion, and measurement of the steady-state current.

Ionic conductivity, σ, measured using ac impedance, is plotted as a function of salt concentration in Figure 2.2a. Here, salt concentration is expressed in terms of r, the molar ratio of lithium ions to ether oxygens. Figure 2.2a indicates that σ has a complex dependence on r, reaching a maximum of 2.2×10^{-3} S/cm at $r = 0.08$ and then a second maximum of 1.6×10^{-3} S/cm at $r = 0.18$. The values we obtain for $r \leq 0.14$ are in agreement with literature and the nonmonotonic dependence of conductivity on salt concentration is well-established.[28,58,103–105] At low salt concentrations, conductivity increases with increasing salt concentration due to an increase in in the concentration of charged species. However, ion transport in polymer electrolytes is coupled to segmental motion, which slows down in the presence of salt due to interactions between ether oxygen atoms and lithium ions. This effect dominates conductivity at $r > 0.08$. We are not aware of any reports that show two maxima for ionic conductivity. The foundations of this observation have yet to be determined.

Figure 2.2b shows the salt diffusion coefficient, D, over the same range of salt concentrations, determined by restricted diffusion. The dependence of D on r appears to be complicated, exhibiting a low concentration maximum of 1.8×10^{-7} cm^2/s at $r = 0.06$ and a high concentration maximum of 9.4×10^{-8} cm^2/s at $r = 0.16$. It appears that the concentration-dependence of D mirrors the concentration dependence of σ observed in Figure 2.2a. Qualitatively similar behavior was reported for PEO/NaTFSI mixtures in the same concentration range (PEO molecular weight = 5000 kg/mol).[77] In contrast, D of PEO/NaTf (soldium triflate) mixtures decreased monotonically with increasing r (PEO molecular weight = 5000 kg/mol).[76] To our knowledge, there are no published reports on the dependence of D on salt concentration in mixtures of PEO and LiTFSI. There are, however, three separate studies of D in PEO/LiTFSI mixtures at fixed salt concentrations. Mullin et al. reported $D = 1.1 \times 10^{-7}$ cm^2/s for 27 kg/mol PEO at r=0.085 and 90°C,[106] Edman et al. reported $D = 4.6 \times 10^{-8}$ cm^2/s for 5,000 kg/mol PEO at r=0.083 and 85°C,[85] and Geiculescu et al. reported $D = 4.2 \times 10^{-8}$ cm^2/s for 4,000 kg/mol PEO at r=0.033 and 90°C.[98]

Our results are in agreement with that of Mullin et al. In contrast, D determined by Edman et al. and Geiculescu et al. are significantly lower than those reported here. More work is needed to establish the dependence of D on polymer molecular weight and salt concentration.

Transference numbers measured by the steady-state current method, $t_{+,SS}$, are given in Figure 2.2c. We find that $t_{+,SS}$ decreases monotonically with increasing salt concentration from a value of 0.18 at r=0.01 to a value of 0.06 at r = 0.16, and exhibits a sharp increase at r > 0.16. Our values are in excellent agreement with a recent report of transference number in PEO/LiTFSI electrolytes measured using the steady-state current method.[99] Note that our value of $t_{+,SS}$ is based on the ratio i_{ss}/i_{Ω} rather than i_{ss}/i_0, where i_0 is the experimentally determined initial current and i_{Ω} is the calculated initial current (see Experimental Section).

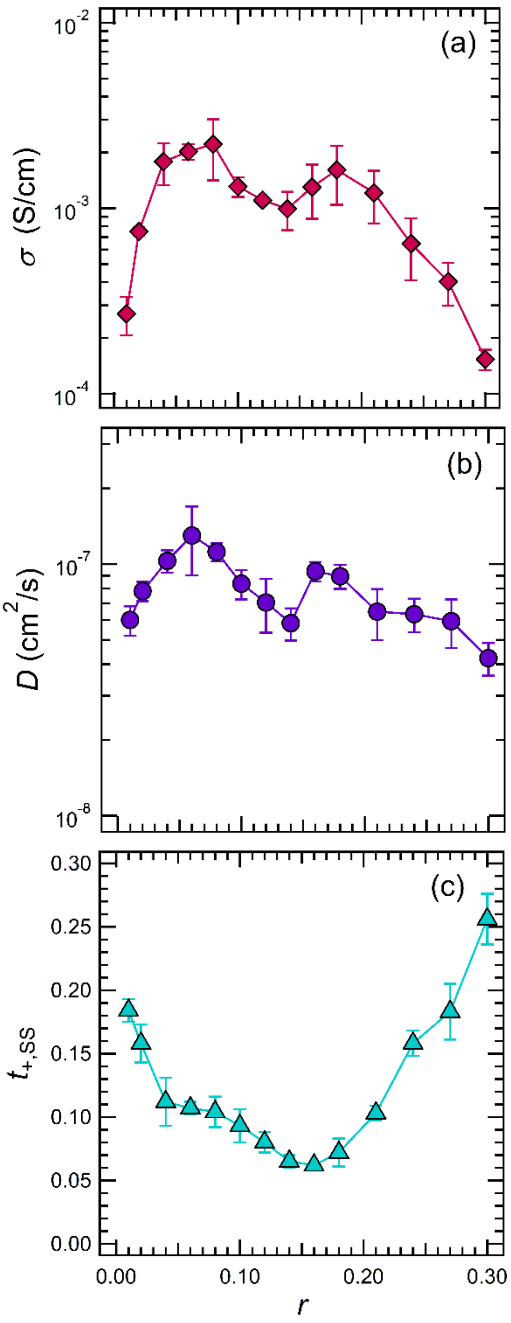

Figure 2.2. (a) Conductivity from ac impedance spectroscopy of symmetric cells with blocking electrodes. (b) Salt diffusion coefficient obtained by restricted diffusion in a lithium symmetric cell. (c) Transference number obtained using the steady-state current technique in a lithium symmetric cell. All data are for 5 kg/mol PEO with LiTFSI at 90°C.

Combining equations 2.1, 2.2, and 2.3 we obtain

$$t_{+,\mathrm{Ne}} = 1 - \sqrt{\frac{\frac{F^2 Dc}{a\sigma RT}\left(\frac{1}{t_{+,SS}} - 1\right)}{\left(1 + \frac{d\ln\gamma_{\pm}}{d\ln m}\right)}}, \tag{2.12}$$

Equation 2.12 indicates that four independent measurements must be performed in order to obtain the true transference number of an electrolyte: σ, D, $t_{+,\mathrm{SS}}$, $1+d\ln\gamma_{\pm}/d\ln m$. We have shown data for σ, D, and $t_{+,\mathrm{SS}}$ as a function of r in Figure 2.2. Next, we focus on the measurement of $1+d\ln\gamma_{\pm}/d\ln m$, often referred to as the thermodynamic factor in the literature, using concentration cells.

Concentration cells are of the form Li | PEO/LiTFSI (r_{ref}) | PEO/LiTFSI (r) | Li. The open circuit potential, U, of these cells was measured as a function of r with r_{ref} held fixed at 0.06. For consistency, we averaged values of U recorded between t = 20 h and t = 25 h in all of the experiments. The results of these experiments are shown in Figure 2.3; independent cells with the same nominal salt concentration exhibited slightly different values of U. We take U to be positive when $r < r_{\mathrm{ref}}$ and negative when $r > r_{\mathrm{ref}}$. The data in Figure 2.3 are consistent with those published by Edman et al. for mixtures of 5000 kg/mol PEO and LiTFSI.[85] The dependence of U on m is assumed to follow a power series of $\ln m$. The dashed line in Figure 2.3 shows the best fit polynomial equation of the form

$$U = 47.478 - 70.320\,(\ln m) - 33.145\,(\ln m)^2 - 8.052\,(\ln m)^3, \tag{2.13}$$

where m has units of mol/kg and U is in mV. The important quantity is the derivative of eq. 2.13, $dU/d\ln m$, because

$$\left(1 + \frac{d\ln\gamma_{\pm}}{d\ln m}\right) = -\frac{F}{2RTt_{-}}\left(\frac{dU}{d\ln m}\right). \tag{2.14}$$

Our approach for measuring the thermodynamic factor is well established, and has been applied to a variety of systems including polymer electrolytes[76–79,85] and liquid electrolytes.[92,94,107]

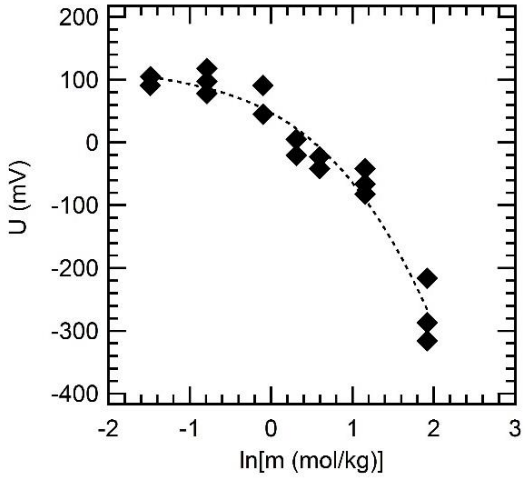

Figure 2.3. Measured open circuit potential, U, from concentration cells of the form Li | PEO/LiTFSI (r_{ref}) | PEO/LiTFSI (r) | Li at 90°C. Here, r_{ref} is the reference held at r=0.06, and r is varied. Each point represents data from one concentration cell. The dashed line shows the polynomial fit given by eq. 2.13.

Self-diffusion coefficients measured by ^{7}Li and ^{19}F pulsed-field gradient NMR (PFG-NMR) in our PEO/LiTFSI mixtures are shown in Figure 2.4. At all concentrations, the self-diffusion coefficient of the fluorine-containing species (D_F) is greater than that of the lithium-containing species (D_{Li}), consistent with previous reports in the literature for PFG-NMR in polymer electrolytes.[30,36,83,108,109] Both self-diffusion coefficients decrease with increasing salt concentration. These measurements enable determination of $t_{+,NMR}$ as a function of r using eq. 2.4.

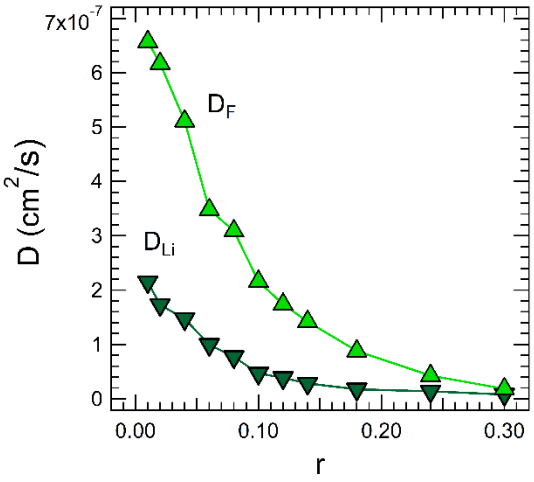

Figure 2.4. Self-diffusion coefficients for lithium-containing species, D_{Li}, and fluorine-containing species, D_F, measured using PFG-NMR at 90°C.

Results for $t_{+,SS}$, $t_{+,NMR}$ and $t_{+,Ne}$ as a function of r are shown in Figure 2.5. We find that $t_{+,NMR}$ and $t_{+,SS}$, values obtained using approaches that rely on ideal solution assumptions, are positive over the entire range of salt concentrations, and exhibit a simple dependence on salt concentration, decreasing with concentration at $r \leq 0.16$ and increasing with concentration at $r > 0.16$. In contrast, $t_{+,Ne}$ has a complex dependence on r. At intermediate salt concentrations $t_{+,Ne}$ is negative, reaching a value as low as -0.38 at $r = 0.16$. There is also a significant difference between $t_{+,Ne}$ and $t_{+,SS}$ in the dilute limit at $r = 0.01$; while $t_{+,SS}$ is about 0.18 (and $t_{+,NMR}$ is about 0.22), $t_{+,Ne}$ is 0.07 (see Figure 2.5b). It is evident that the true transference number in PEO/LiTFSI mixtures is very different from those obtained using approximate methods such as the Bruce-Vincent method and PFG-NMR.

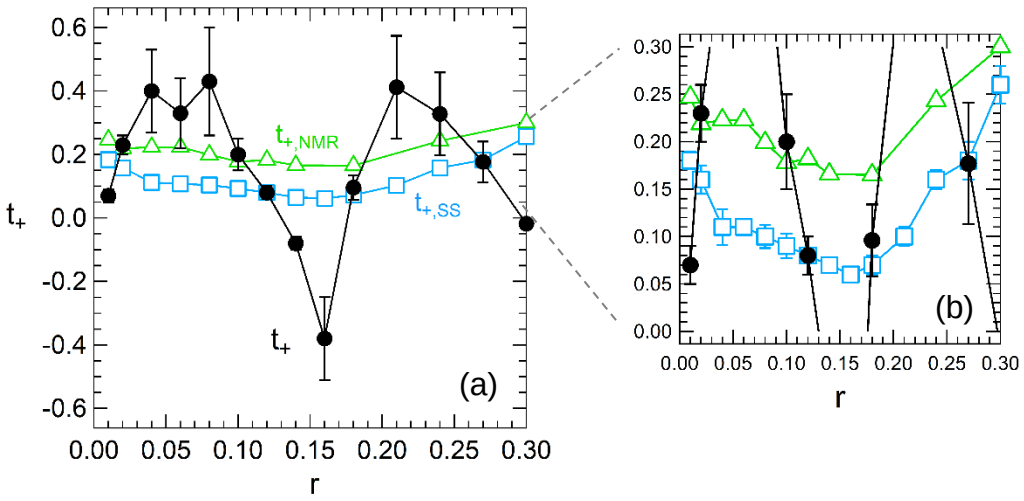

Figure 2.5. (a)Transference number, t_+, for mixtures of PEO and LiTFSI at varying salt concentration, r, using three different methods: $t_{+,NMR}$ is obtained by PFG-NMR measurements of D_{Li} and D_F, and is calculated using eq. 2.4; $t_{+,SS}$ is measured using the steady-state current method calculated using eq. 2.8; $t_{+,Ne}$ combines measurements of conductivity, restricted diffusion, $t_{+,SS}$, and the thermodynamic factor and is calculated using eq. 2.12. (b) Same data on an expanded scale.

For completeness, we use $t_{+,Ne}$ to calculate the thermodynamic factor, $(1+d\ln\gamma_{\pm}/d\ln m)$, according to eq. 2.14. The dependence of $(1+d\ln\gamma_{\pm}/d\ln m)$ on salt concentration is shown in Figure 2.6. We find that $(1+d\ln\gamma_{\pm}/d\ln m)$ is not a simple function of r, reaching a local maximum of 3.3 at $r = 0.08$ and then a global maximum of 6.0 at $r = 0.21$. For ideal solutions, $\gamma_{\pm} = 1$, independent of salt concentration; thus, $(1+d\ln\gamma_{\pm}/d\ln m) = 0$ for ideal solutions. Our results suggest that PEO/LiTFSI mixtures are closest to ideal solutions in the vicinity of $r = 0.03$. It is interesting to note that there is agreement between the three different measurements of transference numbers near this concentration ($r = 0.02$, see Figure 2.5). In contrast, the most dilute PEO/LiTFSI mixture that we have studied, $r = 0.01$, is non-ideal. The underpinnings of this observation remain to be established. The value of $(1+d\ln\gamma_{\pm}/d\ln m)$ at $r = 0.06$ reported by Georen and Lindbergh for PEO/LiTFSI (PEO molecular weight 5,000 kg/mol) at 85°C was approximately 12.[110] This differs substantially from the value that we report (3.3 at $r = 0.08$). We also note that the transference number of this system was found to be positive at all salt concentrations.[85] It is not clear if differences in molecular weight are responsible for these differences.

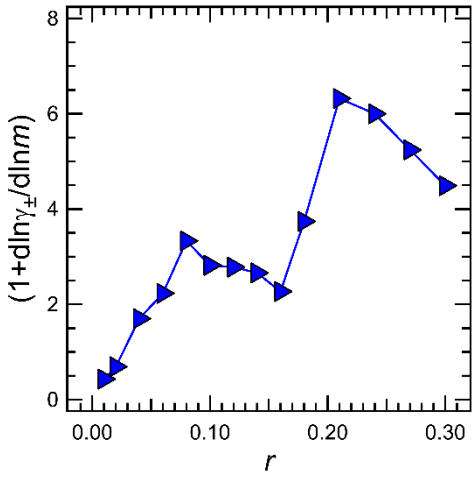

Figure 2.6. Thermodynamic factor for 5 kg/mol PEO with LiTFSI at 90°C as a function of salt concentration.

Negative transference numbers indicate the presence of ion clusters such as negatively-charged triplets in addition to free cations and anions. All of the charged species in the electrolyte contribute to the measured transference number. If we assume that the electrolyte contains both cations (Li^+) and negatively-charged triplets ($Li(TFSI)_2^-$), then negative transference numbers are obtained when ion transport is dominated by the negatively-charged triplets.[76] The presence of ion clusters in PEO/LiTFSI mixtures has been established by Raman spectroscopy.[111,112] Both studies concluded that free ions are the dominant species at lower concentrations, but at $r > 0.125$ ion pairs or aggregates are present. Interestingly, this concentration is where $t_{+,Ne}$ changes sign from positive to negative (Figure 2.5). Further studies are needed to establish the underpinnings of negative transference numbers in polymer electrolytes, as well as the underlying factors that lead to the reemergence of positive transference numbers at high salt concentrations.

2.4 Conclusions

We employ a new approach for determining the transference number of polymer electrolytes. It is based on the measurement of conductivity by ac impedance, salt diffusion coefficient by restricted diffusion, steady-state current under dc polarization, and the thermodynamic factor using concentration cells. Our approach, based on concentrated solution theory, is very similar to that proposed by Ma et al.[76] A majority of t_+ values reported in the literature[56,80–82,87–90,97,98,100] are based on the steady-state current method pioneered by Bruce and Vincent.[88,96] In a few cases[77–79,85] where the approach of Ma et al. is used to determine t_+, there is no attempt to relate t_+ values thus obtained with those that might be obtained using the steady-state current method. This paper provides a bridge between these two distinct approaches.

We report measurements of t_+ in mixtures of PEO and LiTFSI using the steady-state current method, $t_{+,SS}$, pulsed-field gradient NMR, $t_{+,NMR}$, and the present approach, $t_{+,Ne}$, for a range of salt concentrations. We find that methods that rely on ideal solution assumptions ($t_{+,SS}$ and $t_{+,NMR}$) yield positive values for t_+ falling within the narrow range of $0.06 < t_{+,SS} < 0.26$ and $0.17 < t_{+,NMR} < 0.30$. Both transference numbers show a nonmonotonic dependence on salt concentration, reaching a minima near $r = 0.16$. In contrast, $t_{+,Ne}$ has a complex dependence on salt concentration with two peaks at low and high salt concentrations ($r = 0.08$ and $r = 0.21$). In addition, $t_{+,Ne}$ is negative at

intermediate salt concentrations reaching a value as low as -0.38 at $r = 0.16$. Our work implies that charged triplets are likely to be the dominant species in PEO/LiTFSI electrolytes in the intermediate concentration regime. The nature of the species present at high concentrations is unknown. Further studies are needed to characterize the concentration dependence of the species present in in this system.

2.5 Acknowledgements

The work reported here was supported by the National Science Foundation grant NSF-CHE-383 1333736 in the Designing Materials to Revolutionize and Engineer our Future Program.

2.6 Nomenclature

PEO	polyethylene oxide
LiTFSI	lithium bis(trifluoromethanesulfonyl) imide
σ	ionic conductivity (S/cm)
D	salt diffusion coefficient (cm^2/s)
t_+	cation transference number
i	current density (mA)
ΔV	applied potential (mV)
t	time (h)
i_0	initial current (mA/cm^2)
i_{ss}	steady-state current (mA/cm^2)
$t_{+,SS}$	transference number obtained using stead-state current method
Ne	dimensionless number defined by Equation 1.3
$t_{+,Ne}$	transference number obtained using Balsara and Newman method[102]
R	gas constant (J/mol K)
T	temperature (K)
F	Faraday's constant (96485 C/mol)
c	salt concentration (mol/L)
a	stoichiometric parameter
$1+d\ln\gamma_{\pm}/d\ln m$	thermodynamic factor
$\gamma_{\pm}$	mean molal activity coefficient of the salt
m	molality (mol/kg)
D_{Li}	self-diffusion coefficients of the species containing Li (cm^2/s)
D_F	self-diffusion coefficients of the species containing F (cm^2/s)
$t_{+,NMR}$	transference number obtained using pulsed-field gradient NMR
r	moles of Li^+ per mole of ethylene oxide
ρ	density of the electrolyte (g/L)
c	salt concentration (mol/L)
M_{LiTFSI}	molar mass of LiTFSI (287.09 g/mol)
M_{EO}	molar mass of the ethylene oxide repeat unit (44.05 g/mol)
Q_b	bulk capacitance (F)
Q_i	interfacial capacitance (F)
R_b	bulk resistance ($\Omega\ cm^2$)
R_i	interfacial resistance ($\Omega\ cm^2$)
$R_{b,0}$	initial bulk resistance ($\Omega\ cm^2$)

$R_{i,0}$	initial interfacial resistance (Ω cm^2)
$R_{i,SS}$	steady-state interfacial resistance (Ω cm^2)
U	open-circuit voltage (mV)
L	thickness of the electrolyte (508 μm)
r_{ref}	concentration of reference electrolyte used in concentration cells
D_i	self-diffusion coefficient (cm^2/s)
E	attenuation of the echo
g	gyromagnetic ratio
Δ	duration of the gradient pulse (s)
δ	interval between gradient pulses (s)
τ	separation between pulses (s)

2.7 Supporting Information

2.7.1 Transference Numbers in Polymer and Liquid Electrolytes

In this work we measured t_+ in PEO/LiTFSI electrolytes using three different approaches: $t_{+,SS}$ from the steady-state current measurement, $t_{+,NMR}$ from pfg-NMR, and t_+ from the approach proposed by Balsara and Newman. Our results, shown in Figure 2.S1a as a function of concentration, demonstrate the need to use rigorous approaches based on concentrated solution theory when measuring t_+ in polymer electrolytes. The disagreement between the different approaches indicates that the dilute solution assumptions in the derivations of $t_{+,SS}$ and $t_{+,NMR}$ are not valid in polymer electrolytes, even in the dilute regime. Thus, electrostatic interactions are likely to be significant in these electrolytes. A negative transference number suggests that complex speciation is likely to be present at concentrations above 2 mol/L. In the inset of Figure 2.S1a we represent this speciation as a mixture of cations, anions, and negatively-charged triplets, although the true composition of the speciation in these electrolytes has yet to be determined.

An exact study of this nature has yet to be performed in liquid electrolytes, with different techniques to obtain t_+ in the same system over a wide range of salt concentrations. Nonetheless, it is instructive to compare reports on these systems from the literature. The Balsara and Newman approach is fairly new and has yet to be applied to a liquid system. There are, however, other approaches for measuring transference number that rely on concentrated solution theory. One example is the classical Hittorf method, which relies on the measurement of the concentration in electrolytes during polarization. Valoen and Reimers have performed this technique on electrolytes comprised of $LiPF_6$ in PC:EC:DMC over a range of concentrations.[92] An alternative is the approach proposed by Ma et al.,[76] where a variety of electrochemical measurements are combined to obtain t_+. Zugmann performed these measurements in mixtures of $LiPF_6$ in EC/PC/DMC and $LiPF_6$ in EC/DEC, and compared them against $t_{+,SS}$ obtained using the steady-state current technique.[94] Other data has been reported by Zhao et al. for $t_{+,SS}$ and $t_{+,NMR}$ in $LiPF_6$ mixed with PC,[93] Capiglia et al. for $t_{+,NMR}$ in $LiPF_6$ and LiTFSI in EC/EMC,[91] and Aihara et al. in a variety of salts in GBL.[95] Figure 2.S1b shows a summary of these results, which highlight the agreement between t_+ from concentrated solution theory, and $t_{+,SS}$ and $t_{+,NMR}$ from dilute solution theory, all of which are more-or-less independent of concentration. The agreement observed in Figure 2.S1b is surprising given the variety of salts and solvents used in these studies. The fact that approaches based on dilute solution theory agree with approaches based on concentrated solution theory is

indicative of the existence of simple dissociation in these systems. We thus represent the speciation in liquid electrolytes as cations and anions.

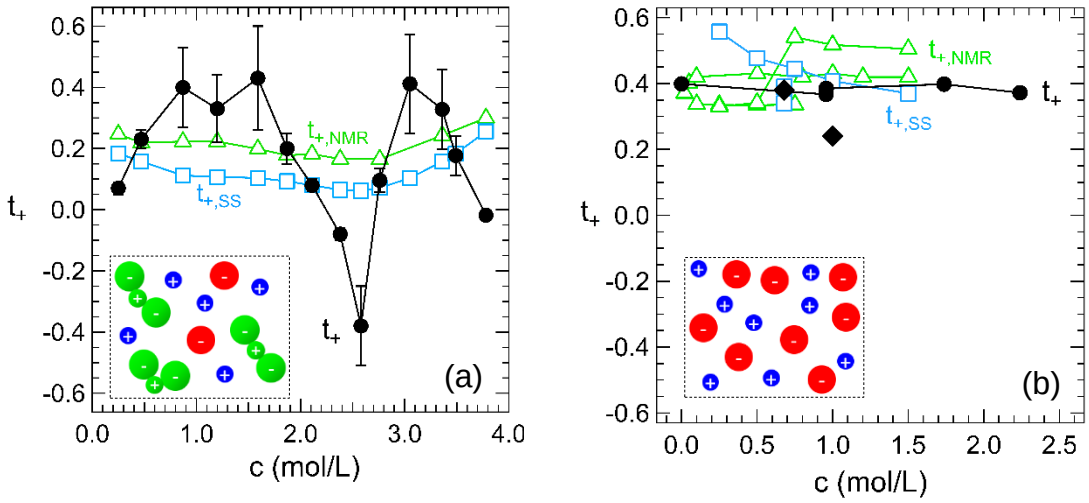

Figure 2.S1. Comparison of the concentration dependence of transference number from different measurement techniques in (a) PEO/LiTFSI in this work and (b) liquid electrolytes from literature. The data in (a) is taken at 90°C whereas the data in (b) were at room temperature. Our results suggest the existence of complex ionic speciation in polymers, whereas liquids are likely to have simple dissociation.

The difference between the speciation in polymer and liquid systems may stem from the difference in the dielectric constant of these materials, which is 5 for PEO and anywhere from 30 to 90 in liquid electrolytes.[9] Additional studies are needed to establish the concentration dependence of transference number in electrolytes with high dielectric constants.

2.7.2 Speciation Model Equations

The ion transport properties of an electrolyte are determined by underlying transport mechanisms of ionic species existing on the microscale. Writing the conductivity, NMR diffusion, and transference number in terms of these mobilities provides insight into the sign and magnitude of the transport properties.

In an ideal electrolyte, all dissolved salt molecules exist in the form of cations (1+) and anions (1-). In Figure 2.S2 we show an explicit example of a non-ideal solution wherein charged triplets (3+ and 3-) and neutral ion pairs (2) are present in addition to dissociated salt ions. Concentrated electrolytes may also contain higher-order aggregates which are not accounted for in this model.

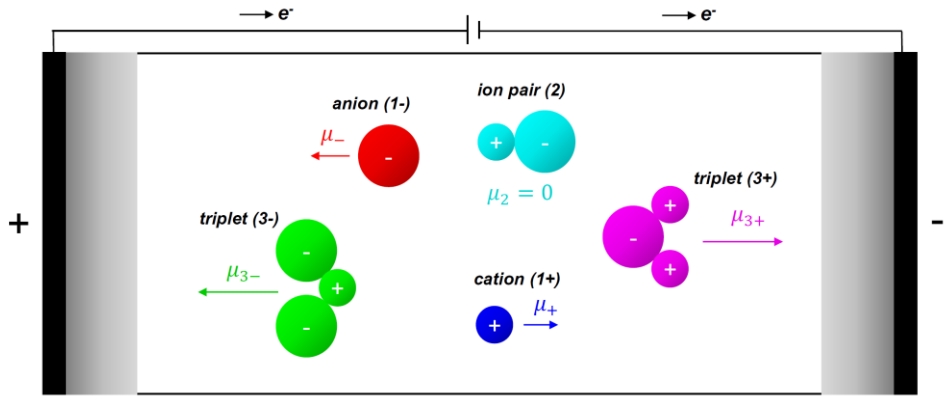

Figure 2.S2. A concentrated solution with cations, anions, ion pairs, and charged triplets. If the mobilities of the triplets dominate over that of the other charged species, then the net mobility for either ion can be negative. A negative average cation mobility results in $t_+ < 0$ and a negative average anion mobility results in $t_+ > 1$.

The transference number in a binary electrolyte with a univalent salt is defined as

$$t_+ = \frac{\mu_{+,av}}{\mu_{+,av} + \mu_{-,av}}, \tag{2.S1}$$

where $\mu_{+,av}$ and $\mu_{-,av}$ are the average electric mobilities of species containing cations and anions respectively. In an ideal solution where the salt is completely dissociated and electrostatic interactions between ions are negligible, eq. 2.S1 can be simplified to

$$t_+ = \frac{\mu_+}{\mu_+ + \mu_-}, \tag{2.S2}$$

where μ_+ and μ_- are the electric mobilities of the cation and anion, respectively. Given that the mobilities of dissociated species are defined as positive in the direction of the electrode with opposite charge, all terms in eq. 2.S2 are positive. Thus, in an ideal solution $0 < t_+ < 1$.

If, on the other hand, the solution is non-ideal then $\mu_{+,av}$ and $\mu_{-,av}$ represent the concentration-weighted averaged mobilities of all charged species. (The mobility of clusters with a neutral net charge is zero.) In this case, $\mu_{+,av}$ is given by

$$\mu_{+,av} = \frac{r_{1+}\mu_{1+} + 2r_{3+}\mu_{3+} - r_{3-}\mu_{3-}}{(r - r_2)}, \tag{2.S3}$$

where r is the total moles of lithium per ethylene oxide moiety, r_i represents the moles of species i per mole of ethylene oxide moieties, and μ_i is the mobility of that species. Here the contribution of the $r_{3-}\mu_{3-}$ term is negative because the negatively-charged triplet is drawn toward the positive electrode. It is obvious that

$$r = r_{1+} + r_2 + 2r_{3+} + r_{3-}. \tag{2.S4}$$

Combining eq. 2.S1 and 2.S3 we obtain

$$t_+ = \frac{r_{1+}\mu_{1+} + 2r_{3+}\mu_{3+} - r_{3-}\mu_{3-}}{r_{1+}\mu_{1+} + r_{3+}\mu_{3+} + r_{1-}\mu_{1-} + r_{3-}\mu_{3-}}. \quad (2.S5)$$

Thus, in non-ideal solutions, it is possible to obtain $t_+ < 0$ if the numerator in eq. 2.S5 is dominated by the $r_{3-}\mu_{3-}$ term. It is important to note that $t_+ + t_- = 1$, which implies that t_- must be greater than one if t_+ is negative. Eq. 2.S5 also shows that it is possible to obtain $t_+ > 1$ if the migration of the positively-charged triplet dominates; in this case $t_- < 0$. There are no bounds on t_+ or t_- in non-ideal solutions.

Pulsed-field gradient NMR can also be used to study the diffusion of ionic species in electrolytes. Probing a specific element of interest, NMR gives the average self-diffusion coefficient of all species containing these elements. It is customary to define a transference number based on NMR as

$$t_{+,NMR} = \frac{D_{+,av}}{D_{+,av} + D_{-,av}}, \quad (2.S6)$$

where $D_{+,av}$ and $D_{-,av}$ are average self-diffusion coefficients of the cation and anion, analogous to the average mobilities in eq. 2.S1. If we assume that the Nernst Einstein relationship holds for particular species ($\mu_i = D_i / RT$) then one may write an equation analogous to eq. 2.S3 for $D_{+,av}$ measured by NMR:

$$D_{+,av} = \frac{r_{1+}\mu_{1+} + r_2\mu_2 + 2r_{3+}\mu_{3+} + r_{3-}\mu_{3-}}{r}, \quad (2.S7)$$

The transference number measured by NMR is then

$$t_{+,NMR} = \frac{r_{1+}\mu_{1+} + r_2\mu_2 + 2r_{3+}\mu_{3+} + r_{3-}\mu_{3-}}{r_{1+}\mu_{1+} + r_{1-}\mu_{1-} + 2r_2\mu_2 + 3r_{3+}\mu_{3+} + 3r_{3-}\mu_{3-}}, \quad (2.S8)$$

Two important distinctions exist between $\mu_{i,av}$ obtained by electrochemical methods and $D_{i,av}$ determined by NMR: (1) neutral ion pairs contribute to $D_{i,av}$ and not $\mu_{i,av}$, and (2) all species will have positive contributions in $D_{i,av}$, whereas species may negatively contribute to $\mu_{i,av}$ (eq. 2.S3).

3 Comparing Two Electrochemical Approaches for Measuring Transference Numbers in Concentrated Electrolytes‡

ABSTRACT

We compare two experimental approaches for measuring the cation transference number in mixtures of polyethylene oxide (PEO) and lithium bis(trifluoromethanesulfonyl)imide (LiTFSI) salt: the well-established current-interrupt method proposed by Ma et al.,[76] and a more recent method based on measuring the steady-state current proposed by Balsara and Newman.[102] In electrolytes comprised of high molecular weight PEO, the data from the two techniques agree, highlighting the equivalence of these two approaches. However, in lower molecular weight PEO electrolytes the values of the two approaches diverge at low salt concentrations. We posit this is because the approach of Ma et al. requires measurements that are sensitive to the nature of the interface between the electrolyte and the electrode. The transference numbers measured by the approach of Balsara and Newman for both low and high molecular weight samples vary from 0.7 to -0.8 are within experimental error throughout the entire salt concentration window.

3.1 Introduction

The development of high energy density rechargeable batteries may enable the widespread adoption of mass market electric vehicles, thereby offering a promising route toward reducing the overall carbon footprint of our economy. The industry standard for rechargeable batteries is the lithium-ion battery, comprised of a graphite anode, a composite cathode, and an organic liquid electrolyte through which lithium ions are shuttled to and from the electrodes during charge and discharge. Next generation battery technology centers around increasing the energy density by employing novel active materials that are generally incompatible with traditional liquid electrolytes. Promising alternatives for liquid electrolytes include those based on polymers such as mixtures of polyethylene oxide (PEO) and lithium bis(trifluoromethanesulfonyl)imide (LiTFSI) salt.[17,27,113,114] Complete characterization of a battery electrolyte material requires knowledge of three independent transport properties: ionic conductivity, σ, salt diffusion coefficient, D, and cation transference number, t_+.[57] The experimental techniques for accurate measurement of σ and D are well established; data of σ from ac impedance spectroscopy and D from restricted diffusion are prevalent in the literature. In contrast, the best technique for measuring t_+ remains a topic of discussion.

The history of the transference number dates back to the 19th century, when Hittorf devised an experimental approach based on passing a known amount of charge through a cell with non-blocking electrodes and measuring the concentration of salt within compartmentalized sections of the electrolyte.[115] This technique is straightforward for liquid electrolytes and has been applied to

‡ This chapter was submitted for publication in June 2018.

a wide variety of systems.[116] An extension of this approach was later developed for solid electrolytes by Tubandt,[117] where the mass of the electrolyte compartments are measured instead of the salt concentration. Since then, a wide variety of approaches for determining the transference number have emerged. Techniques such as the moving boundary method,[118] electromotive force measurement,[119] and electrophoretic NMR[120] are experimentally rigorous, requiring complex experimental setups, special salts, or unique cell architecture. Other techniques commonly used to measure t_+ such as impedance spectroscopy[121,122] and pulsed-field gradient NMR[91,123] rely on assumptions that are invalid for concentrated electrolytes. Due to experimental simplicity, the steady-state current approach outlined by Bruce and Vincent[88,96] is perhaps the most prevalent technique reported in the literature. In this experiment, a polarization is applied across a symmetric cell with non-blocking electrodes, and the transference number is calculated by the ratio of the steady-state current to the initial current. We refer to this parameter as $t_{+,SS}$, where the subscript is used to denote the experimental approach. Despite its popularity, $t_{+,SS}$ is derived using ideal solution assumptions and thus does not reflect the true transference number of an electrolyte.[101,102] Values for $t_{+,SS}$ are bounded by zero and one, whereas the transference number has no bounds.

A more rigorous electrochemical approach has been recently identified by Balsara and Newman.[102] They use concentrated solution theory to derive the relationship between $t_{+,SS}$ and the true transference number of the electrolyte, referred to as $t_{+,Ne}$. Experimental determination of $t_{+,Ne}$ requires four different electrochemical measurements: σ from ac impedance spectroscopy, D from restricted diffusion, $t_{+,SS}$ from the steady-state current measurement, and U, the potential of concentration cells. This technique has been used by Pesko et al. to obtain the transport properties of electrolytes comprised of PEO and LiTFSI salt.[124] The observed dependence of $t_{+,Ne}$ on salt concentration was complex, exhibiting negative values at intermediate concentrations.

A similar electrochemical approach has been defined by Ma and coworkers and is also based on concentrated solution theory.[76] In this approach, data obtained from current interrupt experiments are combined with measurements of D and U in order to determine $t_{+,CI}$. Numerous studies have used this approach to measure $t_{+,CI}$ in polymer electrolytes[76–79] and liquid electrolytes,[92,94] including that of Edman et al. who characterized mixtures of PEO and LiTFSI.[85] The results of Edman suggest that $t_{+,CI}$ has a simple, monotonic dependence on salt concentration and is positive at all concentrations. Thus, the results of Pesko et al. and those of Edman et al. for the transference number of PEO/LiTFSI electrolytes are not in agreement. One possible reason for this discrepancy could be the difference of molecular weight of the PEO polymer used in these studies.

We set out to resolve this issue by performing a direct comparison of $t_{+,Ne}$ and $t_{+,CI}$ over a wide range of salt concentrations in two electrolytes: 5 kg/mol and 275 kg/mol PEO mixed with LiTFSI salt. Our results demonstrate the reproducibility of the $t_{+,Ne}$ measurements, and also highlight the experimental factors that may lead to discrepancies between the two techniques.

3.2 Experimental

The polymers used in this study are 5 kg/mol and 275 kg/mol poly(ethylene oxide) (PEO) with –OH end groups purchase from Polymer Source, and the salt is lithium bis(trifluoromethanesulfonyl)imide (LiTFSI) purchased from Novalyte. We refer to the 5 kg/mol polymer as PEO-5K and the 275 kg/mol polymer as PEO-275K. All sample preparation was performed inside of an argon glovebox where water and oxygen levels remained below 1 and 5

ppm respectively. Both the polymer and salt were dried thoroughly under vacuum (12 hours at 90°C for PEO, 3 days at 120°C for LiTFSI) in the glovebox antechamber before being transferred into the glovebox. Electrolytes were prepared by fully dissolving PEO and LiTFSI in anhydrous tetrahydrofuran (THF) at 60°C, then subsequently evaporating off the THF to produce a homogeneous polymer/salt mixture. The PEO/LiTFSI electrolytes were dried under vacuum for 12 hours at 90°C to remove any excess solvent.

The salt concentrations of the electrolytes ranged from $0.01 \leq r \leq 0.3$ for PEO-5K and $0.005 \leq r \leq 0.3$ for PEO-275K, where r is the molar ratio of lithium ions to ether oxygens, $r = [Li^+]/[O]$. We have previously reported measurements of density, ρ, and calculations of molarity, c, over a wide range of r in mixtures of 5 kg/mol PEO and LiTFSI at 90°C.[124] We use these values for ρ and c in both PEO-5K and PEO-275K. The molality, m, of the electrolytes are calculated according to $m = r/ M_{EO}$, where M_{EO} is the molar mass of the ethylene oxide repeat unit (44.05 g/mol). Table 3.1 provides values of ρ, c, and m for all electrolytes in this study.

Table 3.1. Values for density, molarity, and molality of PEO-5K and PEO-275K electrolytes based on r. We assume that these values are the same in both electrolytes.

r	ρ (g/L)	c (mol/L)	m (mol/kg)
0.00	1128	0.00	0.00
0.005*	1144	0.13	0.11
0.01	1160	0.25	0.23
0.02	1180	0.47	0.45
0.04	1210	0.87	0.91
0.06	1230	1.20	1.36
0.08	1330	1.59	1.81
0.10	1365	1.87	2.27
0.12	1380	2.11	2.72
0.14	1430	2.38	3.17
0.16	1450	2.58	3.63
0.18	1470	2.76	4.08
0.21†	1516	3.05	4.76
0.24	1580	3.36	5.44
0.27†	1572	3.49	6.12
0.30	1640	3.78	6.80

†only PEO-5K, *only PEO-275K

Ionic conductivity was obtained by performing ac impedance spectroscopy on symmetric cells with blocking electrodes. We assembled stainless steel-polymer-stainless steel symmetric cells by pressing the PEO/LiTFSI electrolyte into a 508 μm thick silicone spacer and sandwiching between two 200 μm stainless steel shims. The entire assembly was vacuum sealed in an airtight pouch material (Showa-Denko) with aluminum tabs serving as electrical contacts. Once the sealing was complete, the sample was removed from the glovebox for electrochemical characterization. Cells were annealed at 110°C prior to the conductivity measurement which obtained at 90°C. Ac impedance spectroscopy was performed with a Biologic VMP3 potentiostat, where complex impedance measurements were acquired for a frequency range of 100 mHz to 1 MHz at an amplitude of 80 mV. The low-frequency minimum on the Nyquist impedance plot is taken to be the bulk electrolyte resistance, R_b, which is used along with electrolyte thickness, l, and electrolyte area, a, to calculate the electrolyte conductivity, σ, according to eq. 3.1,

$$\sigma = \frac{l}{a\, R_b} \tag{3.1}$$

The inner diameter of the spacer, 3.175 mm, is used to calculate *a*. Thickness, *l*, is taken to be the final thickness of the electrolyte, measured after conductivity measurements were completed.

The steady-state current, restricted diffusion, and current interrupt measurements were performed on lithium-polymer-lithium cells. These samples were prepared by pressing the electrolyte into a 508 μm thick silicone spacer and sandwiching between two 150 μm thick lithium foils purchased from the MTI Corporation. Each lithium electrode was backed with a layer of nickel foil to keep the surface of the lithium pristine and a stainless-steel shim to prevent cell deformation. Nickel tabs were secured to the stainless-steel shims to serve as electrical contacts. The cells were vacuum sealed in pouch material to maintain an air free environment upon removal from the glovebox.

All electrochemical characterization data were obtained using a Biologic VMP3 potentiostat and the temperature was 90°C. At the beginning of the experiment, cells were annealed for 4 hours to ensure good contact at the lithium-electrolyte interface. Conditioning cycles were performed for 5 charge/discharge cycles at a low current density of 0.02 mA/cm^2. Each conditioning cycle consisted of a 4 hour charge, 45 min rest, 4 hour discharge, and 45 min rest. Ac impedance spectroscopy was performed before and after the conditioning cycles, and then again at the end of the electrochemical measurements to track the interfacial resistance, R_i, over the course of the experiment. Steady-state current and restricted diffusion measurements were performed at potentials of ΔV = 10 mV, -10 mV, 20 mV, and -20 mV to ensure the results were independent of the sign and magnitude of the applied potential. Here, we provide a brief description of these experiments; additional details are included in reference 124.

The steady-state current experiment was performed by polarizing the cell at constant potential, ΔV, for 4 hours and measuring the current density reached steady-state, i_{SS}. The resistances of the cell initially ($R_{i,0}$ and $R_{b,0}$) and at steady-state ($R_{i,SS}$ and $R_{b,SS}$) were measured using impedance spectroscopy. The steady-state current transference number, $\underline{t}_{+,SS}$, derived by Bruce and Vincent[88,96] is calculated according to the relationship

$$t_{+,SS} = \frac{i_{SS}(\Delta V - i_\Omega R_{i,0})}{i_\Omega(\Delta V - i_{SS}R_{i,SS})}, \tag{3.2}$$

where i_Ω is the initial current density calculated according to Ohm's law,[87]

$$i_\Omega = \frac{\Delta V}{R_{i,0} + R_{b,0}}. \tag{3.3}$$

It is important to note that the properties of the electrode-electrolyte interface are subtracted from the measured data to obtain $\underline{t}_{+,SS}$.

Restricted diffusion measurements were obtained using the concentration polarization introduced by the steady-state current experiment. Upon removal of the applied potential, the open-circuit voltage, OCV, of the cell relaxed with time, *t*. The salt diffusion coefficient, *D*, is calculated using

$$-\frac{d\ln(\mathrm{OCV})}{dt}=\frac{\pi^2 D}{L^2}, \tag{3.4}$$

where the left side of the equation is the slope from the least-squares linear fit of –ln(OCV) vs. t from 5 min $\leq t \leq$ 2 hours. L is the thickness of the electrolyte, measured by disassembling each cell after the completion of all electrochemical experiments.

The current interrupt technique was performed following the details outlined in reference 76. A polarization was applied to the lithium-polymer-lithium cell at a constant current density, i, for a short period of time: 5 seconds $\leq$ t $\leq$ 2 min. The values of i used in this experiment were i = 0.1, 0.2, 0.3, and 0.4 mA/cm^2. Upon the interruption of the current, the OCV of the cell was recorded immediately following the discharge of the double layer. The slope of the data plotted in the form of OCV versus $it^{0.5}$ gives the value for m_{CI}.

The thermodynamic factor is obtained by measuring the voltage, U, of a concentration cell of the form Li | PEO/LiTFSI (r_{ref}) | PEO/LiTFSI (r) | Li. These samples were prepared by creating a channel (approximately 3 cm by 2 mm) in a 508 µm thick silicone spacer, and filling half of the channel with reference electrolyte (r_{ref} = 0.06), and the other half with electrolytes at various r. Lithium backed with nickel foil was placed on either end of the channel to serve as electrodes. Nickel tabs were secured as electrical contacts, and the assembly was vacuum sealed in pouch material. Each cell was annealed at 90°C for 20 hours before the value of U was recorded; this length of time enables the formation of stable interface layers prior to the electrochemical measurement. The diffusion length of 3 cm resulted in a concentration gradient relaxation process that occurred over the course of several days. Two or three concentration cells were prepared for each salt concentration.

For experiments using stainless-steel and lithium symmetric cells (σ, D, $t_{+,\mathrm{SS}}$, and m_{CI}), three samples were prepared, the measurements were averaged, and the standard deviation is reported as the error. The error of $t_{+,\mathrm{Ne}}$ and $t_{+,\mathrm{CI}}$ is determined through propagation of these errors, not including that of the concentration cell measurements.

3.3 Results and Discussion

We measured the ionic conductivity, σ, salt diffusion coefficient, D, steady-state current transference number, $t_{+,\mathrm{SS}}$, and concentration cell potential, U, over a wide range of salt concentrations in 5 kg/mol (PEO-5K) and 275 kg/mol (PEO-275K) PEO electrolytes with LiTFSI salt at 90ºC. Here, we use r to denote salt concentration, defined as the molar ratio of lithium ions per ether oxygen on the polymer, $r = [\mathrm{Li}^+]/[\mathrm{O}]$.

Figure 3.1a shows σ as a function of r, obtained by performing ac impedance spectroscopy on symmetric cells with blocking electrodes. The maximum σ in both polymers is approximately 2 × 10^{-3} S/cm, occurring at r = 0.08 in PEO-5K and r = 0.06 in PEO-275K. The dependence of conductivity on the molecular weight of PEO at r = 0.08 has been previously established by Teran and coworkers.[58] At this concentration, conductivity is independent of molecular weight above 5 kg/mol, consistent with our results (Figure 3.1a). Both PEO-5K and PEO-275K show a non-monotonic dependence of σ on r. The most prominent difference between the concentration dependence of σ in our electrolytes is that PEO-5K has two local maxima at r = 0.08 and r = 0.18, whereas PEO-275K exhibits one broad peak, ranging from r = 0.04 to r = 0.18. At this point, it is

not clear from where this difference arises. The data in Figure 3.1a are largely consistent with previous reports on PEO/LiTFSI electrolytes.[28,99,103–105,125]

In Figure 3.1b, we show D as a function of r, obtained from restricted diffusion measurements using lithium-polymer-lithium cells. The concentration dependence of D in our electrolytes shows two peaks in PEO-5K and one broad peak in PEO-275K, analogous to the concentration dependence of σ observed in Figure 3.1a. The values of D in PEO-5K are greater than those obtained in PEO-275K throughout most of the concentration range. The maximum D in PEO-5K is 1.3×10^{-7} cm^2/s ($r = 0.06$), which is approximately double that observed in PEO-275K, 6.9×10^{-8} cm^2/s ($r = 0.08$). The molecular weight dependence of the salt diffusion coefficient in polymer electrolytes is not well understood. Two previous studies have reported on D in PEO/LiTFSI mixtures with salt concentrations near $r = 0.08$: Mullin et al. reported $D = 1.1 \times 10^{-7}$ cm^2/s for 27 kg/mol ($r = 0.085$, 90°C)[106] and Edman et al. reported $D = 4.6 \times 10^{-8}$ cm^2/s for 5,000 kg/mol ($r = 0.083$, 85°C).[85] Our measurements of D in PEO-5K fall close to the value reported by Mullin et al., while our measurements of D in PEO-275K are between the values reported by Mullin and Edman. It is clear that D exhibits a significant dependence on molecular weight above 5 kg/mol, in contrast to σ which is independent of molecular weight above 5 kg/mol.

Figure 3.1c shows $t_{+,SS}$, the transference number obtained by measuring the steady-state current in lithium-polymer-lithium cells, as function of r in our PEO electrolytes. It has been established that this is not the true transference number.[101,102,124] Nonetheless, $t_{+,SS}$ is an important parameter as it describes the fraction of the initial current that is sustained at steady-state for a given electrolyte. In Figure 3.1c, the values of $t_{+,SS}$ of PEO-5K and PEO-275K fall within error of one another, with the exception of $r = 0.3$. In both cases, $t_{+,SS}$ decreases as a function of r until $r = 0.16$, and then increases monotonically. Our data is in excellent agreement with a previous report of $t_{+,SS}$ in PEO/LiTFSI electrolytes by Pożyczka et al.[99]

Figure 3.1d shows U as a function of $\ln(m)$, where U is the potential measured in a concentration cell of the form Li | PEO/LiTFSI (r_{ref}) | PEO/LiTFSI (r) | Li, and m is the molality of the electrolyte. The reference salt concentration, r_{ref}, was 0.06 in both PEO-5K and PEO-275K. The relevant parameter for our study is $dU/d\ln(m)$; thus the choice of r_{ref} is arbitrary. We take U to be positive when $r < r_{ref}$ and negative when $r > r_{ref}$. While there is good agreement between U at high salt concentrations ($\ln(m) > 0$), the values of U in PEO-5K and PEO-275K deviate slightly at lower salt concentrations ($\ln(m) \leq 0$). Following the approach introduced by Ma et al.,[76] each data set is fit to an expression as a function of $\ln(m)$. The polynomial expression thus obtained for PEO-5K is

$$U = 47.50 - 69.88\,(\ln m) - 32.98\,(\ln m)^2 - 8.19\,(\ln m)^3, \tag{3.5}$$

and for PEO-275K is

$$U = 15.92 - 68.51\,(\ln m) - 29.61\,(\ln m)^2 - 6.65\,(\ln m)^3. \tag{3.6}$$

These equations are shown as solid curves in Figure 3.1d. Taking the derivative of eq. 3.5 and eq. 3.6 gives us the concentration dependence of $dU/d\ln(m)$ for both PEO polymers, which are consistent with those published by Edman et al. using a 5000 kg/mol PEO/LiTFSI electrolyte.[85]

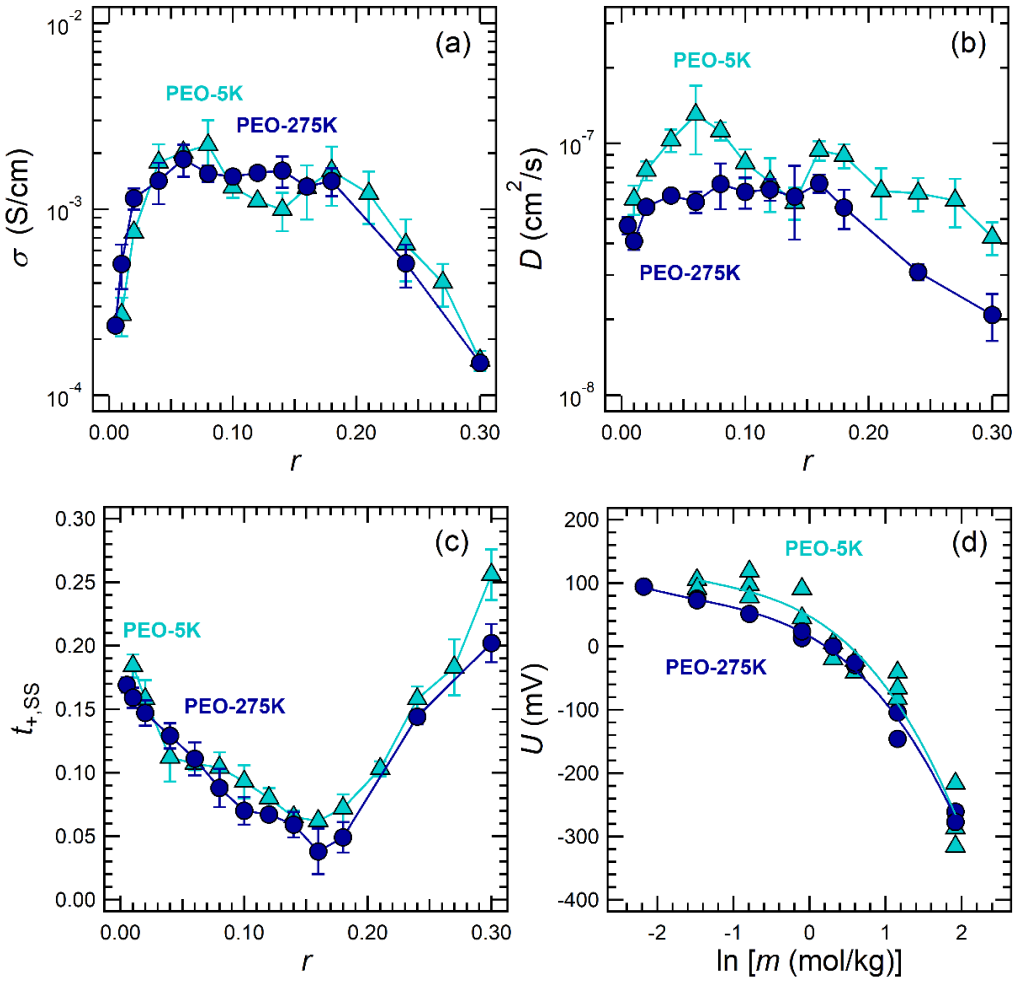

Figure 3.1. (a) Ionic conductivity, (b) restricted diffusion, (c) steady-state current transference number, and (d) open-circuit potential of concentration cells of 5 kg/mol and 275 kg/mol PEO electrolytes as a function of LiTFSI salt concentration at 90ºC.

The relationship between the electrolyte characteristics shown in Figure 3.1 and the cation transference number, $t_{+,Ne}$, has been defined by Newman and coworkers.[102,124,126]

$$t_{+,Ne} = 1 - \frac{(v_+ z_+)^2}{v}\frac{2FDc}{\sigma}\left(1 - \frac{1}{t_{+,SS}}\right)\left(\frac{d\ln m}{dU}\right) \tag{3.7}$$

Figure 3.2a shows $t_{+,Ne}$ as a function of r in PEO-5K and PEO-275K. The concentration dependence of $t_{+,Ne}$ observed in both electrolytes is complex, exhibiting two local maxima at high and low salt concentrations (r = 0.08 and r = 0.21 for PEO-5K, r = 0.06 and r = 0.24 for PEO-275K) and one local minima at intermediate salt concentrations (r = 0.16). Comparing the values of $t_{+,Ne}$ in both electrolytes, we find that PEO-275K lies above that of PEO-5K at low salt concentrations ($r \leq 0.06$), but there is excellent agreement at intermediate and high salt concentrations ($r \geq 0.08$). Further work is required to determine the underpinnings of the molecular weight dependence of $t_{+,Ne}$ at low salt concentrations.

The sign of $t_{+,Ne}$ at r = 0.16 is negative in both PEO electrolytes. The existence of negative transference numbers in polymer electrolytes has been acknowledged in previous literature,[76,77,79]

and is the topic of recent work from our group.[103,126] The sign of the transference number provides some insight into the ionic speciation in the electrolyte. If all ions in the system exist as free cations and anions, the transference number must be positive. A negative transference number suggests that a majority of ions exist as complex species such as charged triplets or higher order aggregates.[76] At r = 0.16, the concentration at which $t_{+,Ne}$ exhibits a sharp minimum, the ratio of ether oxygens to Li^+ is approximately 6:1. Molecular simulations of PEO/LiTFSI electrolytes indicate that the solvation shell of Li^+ comprises six ether oxygens.[23,127] Thus, in the vicinity of r = 0.16, all solvation sites on the polymer are likely to be saturated, and one might expect that additional salt molecules dissolved into the electrolyte will form aggregates due to the absence of available solvation sites. Our conclusion is in reasonable agreement with previously published spectroscopic studies of PEO/LiTFSI electrolytes, which have concluded that ionic aggregation is present in $r > 0.12$.[111,112]

The thermodynamic factor, $(1-d\ln\gamma_{\pm}/d\ln m)$, provides information about how the mean molal activity coefficient, $\gamma_{\pm}$, of the electrolyte changes with m of the solution. This quantity is calculated using the following relationship[124]

$$\left(1+\frac{dln\gamma_{\pm}}{dlnm}\right)=-\frac{F}{2RT(1-t_{+})}\left(\frac{dU}{dlnm}\right), \tag{3.8}$$

where t_+ is the cation transference number that, in principle, can be determined using a variety of approaches. We use $t_{+,Ne}$ (Figure 3.2a) and $dU/d\ln(m)$ (Figure 3.1d) to calculate $(1-d\ln\gamma_{\pm}/d\ln m)$ as a function of r. In Figure 3.2b, we report on the thermodynamic factor of PEO-5K and PEO-275K electrolytes. The value for thermodynamic factor in an ideal solution is unity. Given that our data for $(1-d\ln\gamma_{\pm}/d\ln m)$ are greater than one throughout much of the concentration range (Figure 3.2b), we conclude that our electrolytes are nonideal at most concentrations ($r \geq 0.04$). It is clear that the thermodynamic factor in both PEO electrolytes is similar, suggesting that the activity coefficient of PEO/LiTFSI mixtures is independent of polymer molecular weight above 5 kg/mol.

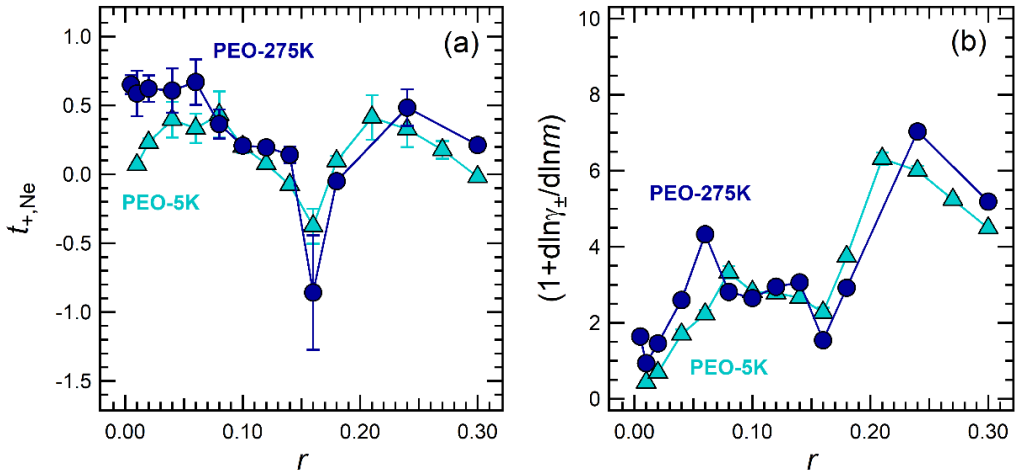

Figure 3.2. (a) Transference number obtained using the Balsara-Newman technique (eq. 3.7) and (b) Thermodynamic factor (eq. 3.8) for 5 kg/mol and 275 kg/mol PEO electrolytes as a function of LiTFSI salt concentration at 90 ºC.

An alternative approach for measuring t_+ using concentrated solution theory relies on the current interrupt technique. This technique consists of polarizing a lithium-polymer-lithium cell at

current density, i, for time, t, and measuring the open-circuit potential (OCV) of the cell immediately after the current is interrupted. Figure 3.3a shows typical data obtained from this experiment, plotted in the form of OCV versus $it^{0.5}$ as suggested by Ma et al.[76] These plots are expected to be linear in the limit of small $it^{0.5}$. The important experimental quantity is the slope, m_{CI}, of the OCV versus $it^{0.5}$ plot. Comparing the slopes of the data in Figure 3.3a, at r = 0.08 the slope of the PEO-5K data is larger than that of PEO-275K, while at r = 0.14 the slope of the data from both electrolytes is approximately the same. It is clear that the concentration dependence of m_{CI} is different in PEO-5K and PEO-275K. Figure 3.3b shows m_{CI} as a function of r for both electrolytes. There is a significant difference between m_{CI} in our electrolytes at low concentrations ($r \leq 0.12$), where the values of m_{CI} in PEO-5K are more than double those in PEO-275K at many concentrations. At high concentrations we observe good agreement.

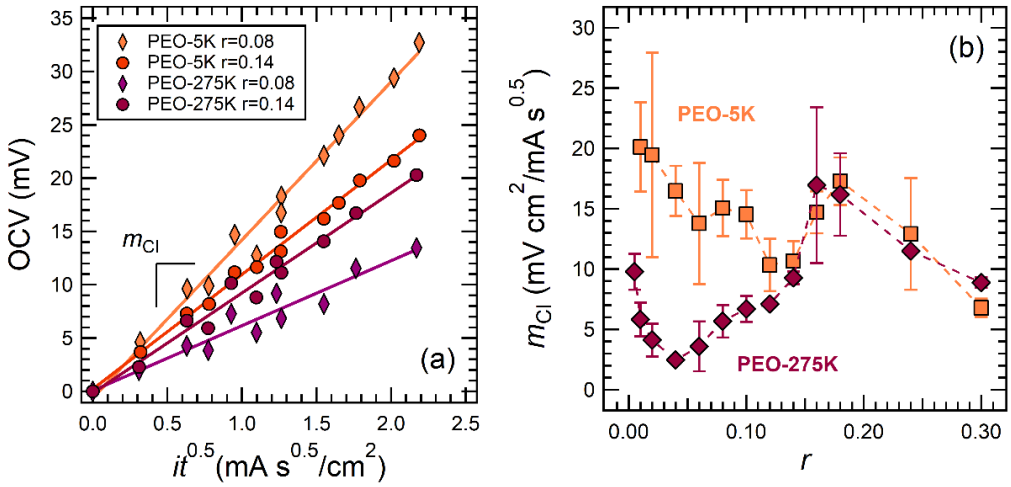

Figure 3.3. (a) Current interrupt data from 5 kg/mol and 275 kg/mol PEO at r = 0.08 and r = 0.14. Data represents an average of multiple samples; error bars are excluded for clarity. (b) The slope, m_{CI}, of the OCV versus $it^{0.5}$ plots at all salt concentrations in this study. Error bars represent the standard deviation of the data taken from multiple samples.

We calculate the transference number based on the current interrupt technique, $t_{+,CI}$, using an equation derived by Ma et al.,[76]

$$t_{+,\mathrm{CI}} = 1 - \frac{m_{CI} c F (\pi D)^{\frac{1}{2}}}{4} \left(\frac{d \ln c}{dU} \right), \tag{3.9}$$

where m_{CI} is given in Figure 3.3b, D is given in Figure 3.1b, and $d\ln(c)/dU$ is obtained by fitting the concentration cell data in Figure 3.1d in terms of $\ln(c)$, instead of $\ln(m)$. The dependence of m on c in PEO/LiTFSI is given in Table 3.1.

In Figure 3.4a, we compare our results for $t_{+,Ne}$ and $t_{+,CI}$ in PEO-275K. The results from both approaches are in excellent agreement and fall within error at most concentrations in this study. The maximum value of $t_{+,CI}$ is 0.65 ± 0.06 (r = 0.04), while that of $t_{+,Ne}$ is 0.67 ± 0.17 (r = 0.06). The minimum value of $t_{+,CI}$ is -0.78 ± 0.30 (r = 0.16), while that of $t_{+,Ne}$ is -0.86 ± 0.42 (r = 0.16). The agreement observed in Figure 3.4a is noteworthy given the complexity of the dependence of t_+ on r. The comparison of $t_{+,Ne}$ and $t_{+,CI}$ in PEO-5K electrolytes is given in Figure 3.4b. Here we observe significant disagreement between these two parameters, particularly at low salt concentrations. The sign of $t_{+,CI}$ negative at all values of r with the exception of r = 0.3, whereas

the sign of $t_{+,Ne}$ is negative only at r = 0.14, 0.16, and 0.3. The minimum value of $t_{+,CI}$ is -3.0 ± 1.3 (r = 0.02), while that of $t_{+,Ne}$ is -0.38 ± 0.13 (r = 0.16). The reason for this disagreement is an interesting, open question. In theory, both approaches should yield the same results. However, our results shown in some instances experimental factors may lead to a discrepancy between $t_{+,Ne}$ and $t_{+,CI}$.

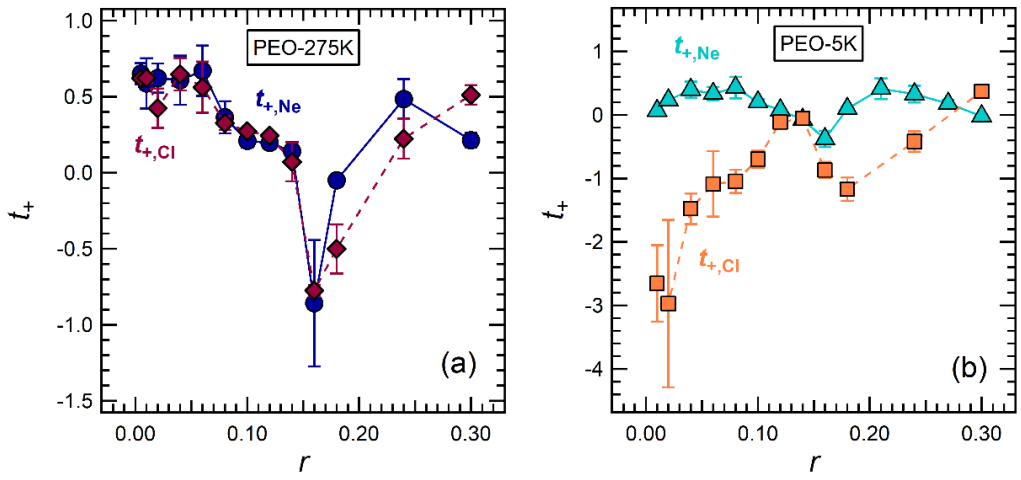

Figure 3.4. Comparison between different transference number measurements ($t_{+,Ne}$ and $t_{+,CI}$) for (a) 275 kg/mol and (b) 5 kg/mol PEO electrolytes as a function of LiTFSI salt concentration at 90ºC.

We posit that the discrepancy in Figure 3.4b arises due to differences in the electrode-electrolyte interfaces formed in our lithium-polymer-lithium cells. At the beginning of our experiments, cells were cycled 5 times using a constant current density of 0.02 mA/cm^2; we refer to these as conditioning cycles. Our objective was to complete the formation of stable solid electrolyte interface (SEI) layers prior to making electrochemical measurements (D, $t_{+,SS}$, and m_{CI}). To evaluate the nature of the SEI layers, we perform ac impedance spectroscopy on our lithium-polymer-lithium cells over the course of our experiments. The impedance data exhibited the standard signatures seen in symmetric cells with non-blocking electrodes: a bulk resistance, R_b, reflecting the resistance of ion transport in the polymer electrolyte, and an interfacial resistance, R_i, reflecting the resistance of charge transfer at the polymer-lithium interface. The values of R_b were independent of time and consistent with that expected based on our ac impedance measurements using blocking electrodes (Figure 3.1a). In contrast, R_i showed a significant dependence on time and salt concentration in some cases. Further analysis of R_i provides insight into the disagreement observed between $t_{+,Ne}$ and $t_{+,CI}$ in Figure 3.4b.

Measurements of interfacial resistance obtained initially, $R_{i,0}$, post conditioning cycles, $R_{i,c}$, and at the end of the experiments, $R_{i,f}$, are reported for PEO-275K (Figure 3.5a) and PEO-5K (Figure 3.5b). Note that $R_{i,0}$ is measured after annealing the cells for 4 hours at 90°C, thus the system is expected to be thermally equilibrated. The dependence of interfacial resistance on salt concentration is clearly affected by polymer molecular weight. In PEO-275K, $R_{i,0}$ is a strong non-monotonic function of r, reaching a maximum value of 554 Ωcm^2 (r = 0.16). In contrast, in PEO-5K, $R_{i,0}$ is nearly independent of r, reaching a maximum value of 51 Ωcm^2 (r = 0.16). The underpinnings of this observation are not well understood. In the case of PEO-275K, $R_{i,0}$, $R_{i,c}$, and $R_{i,f}$ are within experimental error across the entire salt concentration window (Figure 3.5a). In the case of PEO-5K, only $R_{i,c}$ and $R_{i,f}$ are in agreement at all r, both significantly greater than $R_{i,0}$ at

low salt concentrations (Figure 3.5b). It is important to note that the agreement between $R_{i,c}$ and $R_{i,f}$ in Figure 3.5a and b demonstrates that the SEI layer has reached steady-state prior to the point where electrochemical measurements are being conducted for both PEO-5K and PEO-275K. To our knowledge, the data in Figure 3.5 represent the first report of the effect of salt concentration and polymer molecular weight on interfacial impedance.

Comparing $R_{i,0}$ and $R_{i,c}$ provides information about the evolution of the charge transfer resistance at the lithium-polymer interface over the course of the conditioning cycles. In PEO-275K, the charge transfer resistance is stable during the conditioning cycles, demonstrated by the fact that there is reasonable agreement between $R_{i,0}$ and $R_{i,c}$ in Figure 3.5a. In PEO-5K however, at many concentrations $R_{i,c}$ is significantly larger than $R_{i,0}$ indicating that the conditioning cycles lead to the formation of resistive electrode-electrolyte interfaces that impede charge transfer. The concentration of chain ends in PEO-5K is significantly higher than that in PEO-275K. The formation of resistive layers in PEO-5K may be attributed to reactions between the end groups and Li metal; the reaction between –OH groups and Li metal is well-established.[34] The increase in R_i during conditioning cycles in PEO-5K is most pronounced at low salt concentrations ($r < 0.12$). Perhaps, the presence of LiTFSI at high concentrations slows down the reaction between –OH groups and Li metal. We note that $r < 0.12$ is also the concentration range where the differences between $t_{+,Ne}$ and $t_{+,CI}$ in PEO-5K are most significant (Figure 3.4b). Further study is required to determine the influence of interface layers on the measurements of on $t_{+,CI}$.

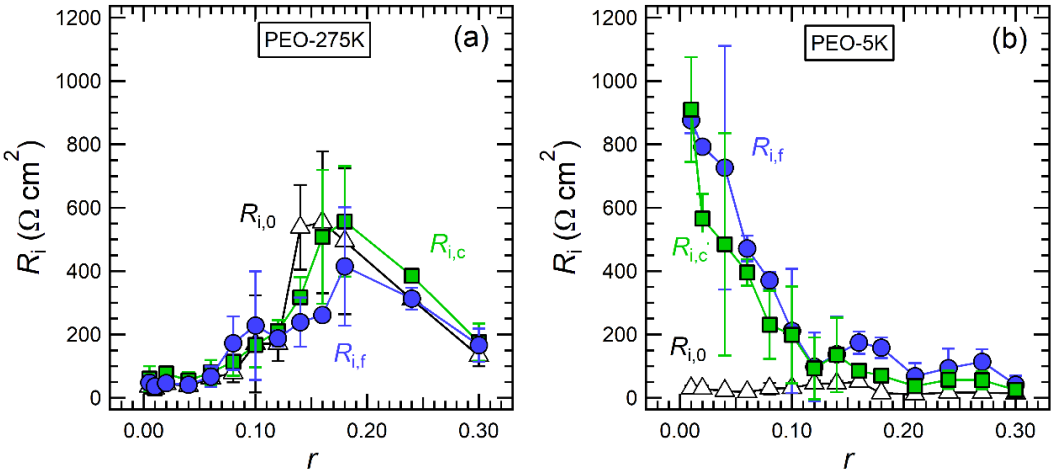

Figure 3.5. Interfacial resistance taken initially, $R_{i,0}$, after the conditioning cycles, $R_{i,c}$, and at the end of the experiment, $R_{i,f}$, from lithium-polymer-lithium cells with (a) 275 kg/mol and (b) 5 kg/mol PEO with LiTFSI at 90ºC.

It is important to recognize that $t_{+,Ne}$ is derived from measurements of σ, $t_{+,SS}$, D and U (see eq. 3.7), whereas $t_{+,CI}$ is derived from measurements of m_{CI}, D, and U (see eq. 3.9). Thus, discrepancies between these two approaches must originate from the effect of interface layers on σ, $t_{+,SS}$ and m_{CI}; D and U are used in both approaches and the effect of interface layers on these parameters cannot be the cause of the observed discrepancies. One notable difference is the length scales over which the measurements take place. Ac impedance spectroscopy and the steady-state current measurement are both techniques that probe the bulk of the electrolyte: σ is obtained by measuring the bulk resistance in a stainless steel symmetric cell and $t_{+,SS}$ is obtained by polarizing a lithium-polymer-lithium cell for long periods of time generating concentration gradients that span the

electrolyte. In contrast, the current interrupt technique is a more surface-sensitive technique, as m_{CI} is obtained by polarizing a lithium-polymer-lithium cell for short periods of time generating concentration gradients that are localized near the electrode surface. In a perfect system where the electrolyte near the electrode surface is representative of the bulk electrolyte, $t_{+,Ne}$ and $t_{+,CI}$ should be in agreement. This appears to be true for PEO-275K (Figure 3.4a). However, if the electrolyte near the electrode surface is more resistive than the bulk, as is suspected to be the case for PEO-5K, then there might be a discrepancy between $t_{+,Ne}$ and $t_{+,CI}$ (Figure 3.4b). We believe $t_{+,Ne}$ to be the more robust approach for measuring the transference number of an electrolyte because the measurements required to determine this parameter are not sensitive functions of interfacial impedance.

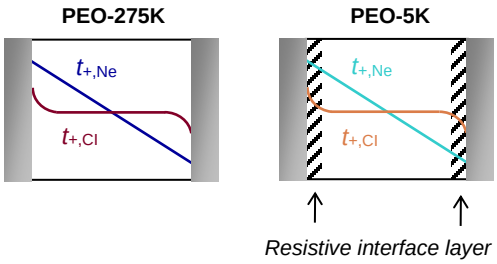

Figure 3.6. Representation of the length scales over which salt concentration gradients form in the electrolyte during our transference number measurements in lithium-polymer-lithium cells: $t_{+,CI}$ probes the electrolyte near the electrode surface whereas $t_{+,Ne}$ probes the bulk electrolyte. This may explain the discrepancy between $t_{+,Ne}$ and $t_{+,CI}$ in PEO-5K (Figure 3.4b) where a resistive interfacial layer is thought to be present at the lithium surface.

3.4 Conclusions

We have compared two different electrochemical approaches for measuring the transference number of an electrolyte. A new approach proposed by Balsara and Newman[102] ($t_{+,Ne}$) is compared against the well-established approach by Ma et al.[76] ($t_{+,CI}$) using two different electrolytes: 5 kg/mol PEO (PEO-5K) and 275 kg/mol PEO (PEO-275K) mixed with LiTFSI. Both approaches are derived using concentrated solution theory and require a combination of electrochemical measurements. Many of the measurements involve symmetric cells with lithium electrodes.

The complex dependence of $t_{+,Ne}$ on salt concentration in PEO-5K and PEO-275K is similar, both exhibiting two maxima at low and high salt concentrations, and a sharp minima at intermediate salt concentrations where the value of $t_{+,Ne}$ is negative. For PEO-275K, $t_{+,CI}$ and $t_{+,Ne}$ are within error across most of the salt concentration window. In contrast, in PEO-5K there is a substantial difference between the $t_{+,CI}$ and $t_{+,Ne}$, especially at low salt concentrations. We attribute this to the fact that the parameters measured to obtain $t_{+,CI}$ are sensitive to the nature of the lithium electrode-electrolyte interfaces. In contrast, the parameters measured to obtain $t_{+,Ne}$ are insensitive to the nature of the lithium electrode-electrolyte interfaces. Our work thus suggests that $t_{+,Ne}$ is a more robust measure of the transference number.

3.5 Acknowledgements

This work was intellectually led by the Joint Center for Energy Storage Research (JCESR), an Energy Innovation Hub funded by the U.S. Department of Energy (DOE), Office of Science, Basic Energy Sciences (BES), under Contract No. DEAC02-06CH11357.

3.6 Nomenclature

PEO	polyethylene oxide
LiTFSI	lithium bis(trifluoromethanesulfonyl) imide
THF	tetrahydrofuran
OCV	open circuit voltage (mV)
σ	ionic conductivity (S/cm)
D	salt diffusion coefficient (cm^2/s)
t_+	cation transference number
U	potential of a concentration cell (mV)
$t_{+,SS}$	transference number obtained using stead-state current method
$t_{+,Ne}$	transference number obtained by the approach of Balsara and Newman[102]
$t_{+,CI}$	transference number obtained by the approach of Ma et al.[102]
r	molar ratio of lithium ions to ether oxygens, $r = [Li^+]/[O]$
ρ	density (g/L)
c	salt molarity (mol/L)
m	salt molality (mol/kg)
M_{EO}	molar mass of the ethylene oxide repeat unit (44.05 g/mol)
R_b	bulk resistance ($\Omega\ cm^2$)
$R_{b,0}$	initial bulk resistance ($\Omega\ cm^2$)
$R_{b,SS}$	bulk resistance at steady-state ($\Omega\ cm^2$)
R_i	interfacial resistance ($\Omega\ cm^2$)
$R_{i,0}$	initial interfacial resistance ($\Omega\ cm^2$)
$R_{i,SS}$	interfacial resistance at steady-state ($\Omega\ cm^2$)
L	thickness of the electrolyte (μm)
a	area of electrolyte (cm^2)
ΔV	applied potential (mV)
i_Ω	initial current density calculated according to Ohm's law (mA/cm^2)
i_{ss}	steady-state current (mA/cm^2)
t	time (h)
i	current density
m_{CI}	slope of the OCV versus $it^{0.5}$ data ($mV\ cm^2/mA\ s^{0.5)}$
r_{ref}	reference concentration used in concentration cells
$1+d\ln\gamma_\pm/d\ln m$	thermodynamic factor
$\gamma_\pm$	mean molal activity coefficient of the salt
z_+, z_-	charge number of cation and anion
ν_+, ν_-	the number of cations and anions into which the salt dissociates
ν	total number of ions into which the salt dissociates
F	Faraday's constant (96485 C/mol)
R	gas constant (J/mol K)
T	temperature (K)
$R_{i,c}$	interfacial resistance post conditioning cycles ($\Omega\ cm^2$)
$R_{i,f}$	interfacial resistance at the end of the experiments ($\Omega\ cm^2$)

4 Comparing Cycling Characteristics of Symmetric Lithium-Polymer-Lithium Cells with Theoretical Predictions*

ABSTRACT

We develop a model based on concentrated solution theory for predicting the cycling characteristics of a lithium-polymer-lithium symmetric cell containing an electrolyte with known transport properties. The electrolytes used in this study are mixtures of polyethylene oxide (PEO) and lithium bis(trifluoromethanesulfonyl) imide (LiTFSI) salt, prepared over a wide range of salt concentrations. The transport properties of PEO/LiTFSI previously reported in the literature are used as inputs for our model. We calculate salt concentration and potential profiles, which develop in these electrolytes under a constant dc polarization, as a function of current density, electrolyte thickness, and salt concentration. These profiles are nonlinear at steady-state due to the strong concentration dependence of the transport properties of this electrolyte. The effect of this nonlinearity on limiting current is demonstrated. Cycling characteristics of a series of lithium symmetric cells were measured to test the validity of our model, without resorting to any adjustable parameters. The time-dependence and steady-state value of the potential measured during cycling experiments were in excellent agreement with model predictions.

4.1 Introduction

Next-generation lithium batteries with high energy densities are desired for applications such as electric vehicles and personal electronics. The implementation of these batteries hinges upon the development of novel electrolyte materials with both stability against the lithium metal anode and excellent transport properties. The efficacy of newly-developed electrolytes is usually established in symmetric lithium-electrolyte-lithium cells. In a typical experiment, the cell is polarized in one direction using a constant dc current for a predetermined amount of time, and then the polarization direction is switched. Numerous researchers have reported cycling data from such experiments using potential versus time plots, with an emphasis on the total number of cycles that could be sustained before failure.[100,128–132] Little attention has been paid to the time-dependence of the cycling profile and the steady-state potential attained at a given current density. While the necessary equations for predicting the cycling behavior of symmetric cells are well established in the concentrated solution theory of Newman,[57,133] we are not aware of any comparisons of these predictions with experimental data. Most of the comparisons between the Newman approach and experimental data focus on cells with porous electrodes and require adjustable parameters or simplifying assumptions.[134–138]

Polymer electrolytes have been identified as promising candidates for lithium metal batteries.[17,27,113,114] They are also convenient model systems for measurement of transport

* This chapter was submitted for publication in June 2018.

coefficients. Ion transport in electrolytes is governed by three transport coefficients: conductivity, σ, the salt diffusion coefficient, D, and the transference number, t_+.[57] In addition, modeling these systems requires knowledge of the thermodynamic factor, $(1+d\ln\gamma_\pm/d\ln m)$, which quantifies the change in the mean molal activity coefficient of the salt, $\gamma_\pm$, with the molality, m, of the solution. We note in passing that measuring these four parameters in conventional liquid electrolytes is complicated due to convection;[139–141] convection is suppressed in polymers due to high viscosity.

Figure 4.1 shows the cycling profiles of lithium symmetric cells containing polymer electrolytes that differ in salt concentration. Our electrolytes are comprised of mixtures of polyethylene oxide (PEO) and lithium bis(trifluoromethanesulfonyl) imide (LiTFSI) salt. We use r_{av} to denote the average salt concentration of the electrolyte, where r_{av} is defined as the molar ratio of lithium ions to ether oxygens in the system: $r_{av} = [Li^+]/[O]$. Although both cells in Figure 4.1 were cycled at the same current density of $i_{ss} = \pm 0.02$ mA/cm^2, the cell containing an electrolyte with a lower salt concentration ($r_{av} = 0.02$) reaches a much lower potential at steady-state compared to the cell with the higher concentration electrolyte ($r_{av} = 0.14$). The concentration-dependence of σ, D, t_+, and $(1+d\ln\gamma_\pm/d\ln m)$ of this PEO/LiTFSI electrolyte have been previously reported,[124,126] At $r_{av} = 0.02$, the ionic conductivity is $\sigma = 7.5 \times 10^{-4}$ S/cm, while at $r_{av} = 0.14$ it is $\sigma = 9.9 \times 10^{-4}$ S/cm. If conductivity were the only relevant transport parameter, then the steady-state potential would be lower for the $r_{av} = 0.02$ cell. Figure 4.1 shows that this is clearly not the case. The theoretical work presented in this paper resolves this issue.

Our objective is to compare cycling data of the type presented in Figure 4.1 with theoretical predictions based on concentrated solution theory. Our theory enables calculation of both potential gradients and salt concentration profiles in an electrolyte at steady-state with no adjustable parameters. It also addresses the time-dependence of potential as a function of applied current.

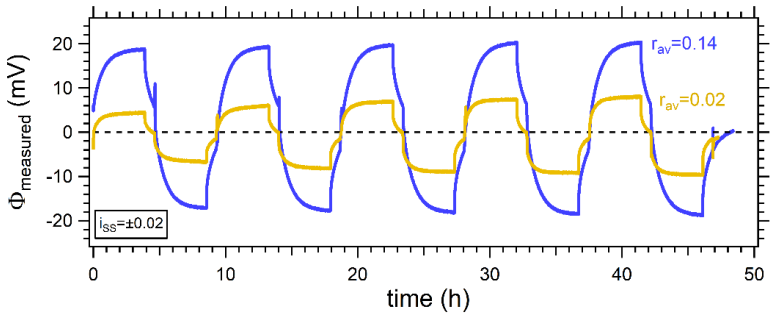

Figure 4.1. Cycling profiles showing measured potential, $\Phi_{measured}$, as a function of time for lithium symmetric cells with PEO/LiTFSI electrolytes at two different salt concentrations. The cells were cycled at a constant current density of i_{ss}=±0.02 mA/cm^2, and the thickness of the electrolytes were approximately 500 µm.

4.2 Theory

We use concentrated solution theory[57] to model a cell containing a binary electrolyte wherein the cation is produced at the anode and consumed at the cathode in response to an applied potential, and both the anion and solvent do not participate in the redox reactions. The current is applied in the x-direction across a symmetric cell containing a salt $(M^{z+})_{\nu_+}(X^{z-})_{\nu_-}$ with electrodes of pure metal M. The applied current creates gradients in the salt concentration and the potential across the electrolyte. The reference electrode used to measure the potential at any position in the electrolyte follows the reaction

$$-\mathrm{M}^{z+} + \mathrm{M}_{(s)} \rightleftharpoons n\,e^{-}. \tag{4.1}$$

The anode is located at $x = 0$ and the cathode at $x = L$, where L is the thickness of the electrolyte. We take the potential at the cathode to be zero, and surface overpotentials are taken to be zero at both electrodes.

4.2.1 Steady-State Model

The relationship between the anion flux, N_-, and the current density, i, is given by

$$N_- = -\frac{\mathfrak{D}c_T c v_-}{RTc_0 v}\frac{d\mu_e}{dx} + \frac{it_-}{z_- F}, \tag{4.2}$$

where $\mathfrak{D}$ is the diffusion coefficient of the salt based on a thermodynamic driving force, μ_e is the chemical potential of the electrolyte, t_- is the anion transference number ($t_- = 1 - t_+$), and F is Faraday's constant. The concentration terms are c_0, c, and c_T, where c_0 is the solvent concentration, c is the salt concentration, and c_T is the total solution concentration ($c_T = c_0 + \nu c$).

At steady-state, the net flux of the anion is zero at all values of x. In this case, eq. 4.1 reduces to the following expression in terms of i_{ss}, the steady-state current.

$$\frac{d\mu_e}{dx} = i_{ss}\frac{t_-}{z_- F}\frac{RTc_0 v}{\mathfrak{D}c_T c v_-} \tag{4.3}$$

The chemical potential of the electrolyte is defined in terms of the molality of the solution,

$$\mu_e = \mu_e^0 + \nu RT\ln(m\,\gamma_\pm) + RT\ln({v_+}^{v_+}{v_-}^{v_-}), \tag{4.4}$$

where μ_e^0 is the chemical potential of the reference state and $\gamma_\pm$ is the mean molal activity coefficient of the electrolyte. Combining eq. 4.3 and 4.4, we get

$$\frac{d\mu_e}{dx} = \frac{\nu RT}{m}\left(1 + \frac{d\ln\gamma_\pm}{d\ln m}\right)\frac{dm}{dx} = i_{ss}\frac{t_-}{z_- F}\frac{RTc_0 v}{\mathfrak{D}c_T c v_-}. \tag{4.5}$$

The salt diffusion coefficient D measured in a restricted diffusion experiment is based on the relaxation of a concentration gradient and is related to $\mathfrak{D}$ by

$$D = \mathfrak{D}\frac{c_T}{c_0}\left(1 + \frac{d\ln\gamma_\pm}{d\ln m}\right). \tag{4.6}$$

In this work, we prefer to describe salt concentration in terms of r, the molar ratio of lithium ions to ether oxygens in the system. Given that $r = mM_0$, where M_0 is the molar mass of the solvent, it is straightforward to convert from m to r in these equations. Combining eq. 4.5 and 4.6 and performing this conversion, we get

$$\frac{dr}{dx} = \frac{i_{ss}}{Fz_- v_-}\frac{r\,t_-(r)}{D(r)\,c(r)}. \tag{4.7}$$

Collecting the r-dependent terms and integrating over them gives an implicit expression for the concentration profile, $r(x)$, for a given $r(x{=}0)$ and $i_{ss}L$.

$$\int_{r(x=0)}^{r(x)} \frac{D(r)\, c(r)}{r\, t_-(r)}\, dr = \frac{i_{ss} L}{F z_- \nu_-} \left(\frac{x}{L}\right). \tag{4.8}$$

In an experiment one controls the average concentration of the electrolyte, r_{av}, which is obtained by integrating $r(x)$ from $x = 0$ to $x = L$. The spatial dependence of the molar salt concentration, $c(x)$, can then be readily obtained from $r(x)$ as long as the concentration-dependence of the density of the electrolytes is known.

The potential gradient $\mathrm{d}\Phi/\mathrm{d}x$ in the cell can be determined for a given current density using the relationship

$$i = -\sigma \frac{d\Phi}{dx} - \frac{\sigma}{F} \left(-\frac{1}{n\nu_+} + \frac{t_+}{z_+ \nu_+}\right) \frac{d\mu_e}{dx}, \tag{4.9}$$

where σ is the conductivity of the electrolyte and t_+ is the cation transference number. Since the electrolyte is electrically neutral, μ_e depends only on local concentration, and is independent of Φ. Charge balance implies that $z_+ = n$. Eq. 4.9 applies to both steady-state wherein both terms on the right contribute and the initial state wherein the second term on the right is zero because the solution is initially uniform in concentration. At the initial state, $\mathrm{d}\Phi/\mathrm{d}x$ will be constant. Thus, the initial current, i_0, at $t = 0$ is related to the initial potential, Φ_0, by

$$i_0 = \sigma \frac{\Phi_0}{L}. \tag{4.10}$$

The relationship between the current and potential at steady-state is given by combining eq. 4.3, 4.6, and 4.9,

$$i_{SS} = -\sigma \frac{d\Phi_{SS}}{dx} - i_{ss}\mathrm{Ne}, \tag{4.11}$$

where Ne is given by[102]

$$\mathrm{Ne} = \frac{\nu}{(\nu_+ z_+)^2} \frac{\sigma RT (t_-)^2}{F^2 D c} \left(1 + \frac{d \ln \gamma_\pm}{d \ln m}\right). \tag{4.12}$$

The parameter Ne can be measured by a steady-state current experiment and is related to the quantity i_{ss}/i_0, often referred to as the steady-state current transference number, $t_{+,SS}$.

$$t_{+,SS} = \frac{i_{ss}}{i_0} = \frac{1}{1 + Ne}. \tag{4.13}$$

Eq. 4.11 can be integrated to obtain the spatial dependence of potential,

$$\Phi_{SS}(x) = -F z_- \nu_- \int_{r(x=L)}^{r(x)} \frac{D(r)\, c(r)}{r\, t_{+,SS}(r)\, \sigma(r)\, t_-(r)}\, dr. \tag{4.14}$$

where $\mathrm{d}r/\mathrm{d}x$ determined above is used. Thus, prediction of Φ_{SS} across an electrolyte using eq. 4.14 requires knowledge of the concentration-dependence of three independent transport properties, σ, D, and t_-, in addition to $t_{+,SS}$ and c.

4.2.2 Transient Model

For unsteady-state problems, it is customary to start with eq. 12.14 from reference 57 which describes the mass transport of the salt in the electrolyte based on concentrated solution theory. This relationship, simplified to one-dimensional transport along the *x*-direction in the absence of convection, is given by

$$\frac{dc}{dt} = \frac{d}{dx}\left[D\left(1 - \frac{d\ln c_0}{d\ln c}\right)\frac{dc}{dx}\right] - \frac{i_{ss}}{z_+ v_+ F}\left(\frac{dt_+}{dx}\right) \tag{4.15}$$

with boundary conditions

$$-D\frac{dc}{dx}\Big|_{x=0} = \frac{1-t_+}{F} i_{ss} \tag{4.16}$$

$$-D\frac{dc}{dx}\Big|_{x=L} = -\frac{1-t_+}{F} i_{ss}\,. \tag{4.17}$$

Equation 4.15 can be solved numerically to obtain transient concentration profiles, $c(x,t)$, across an electrolyte.

In order to obtain transient potential profiles, $\Phi(x,t)$, across an electrolyte, we use the relationship between i_{SS} and Φ given by a modified Ohm's law that includes the overpotential due to concentration gradients in the electrolyte.

$$i_{ss} = -\sigma\frac{d\Phi}{dx} - \frac{2\sigma RT}{F}\left(1 + \frac{d\ln f_{\pm}}{d\ln c}\right)(1-t_+)\frac{d\ln c}{dx} \tag{4.18}$$

Equation 4.18 is solved numerically with Butler-Volmer kinetics used to account for the charge-transfer reaction at the electrode boundaries.

$$i_{ss}\,|_{x=0} = i_0\left[\exp\left(\frac{\alpha_a F}{RT}(\Phi_1 - \Phi(x=0))\right) - \exp\left(-\frac{\alpha_c F}{RT}(\Phi_1 - \Phi(x=0))\right)\right] \tag{4.19}$$

$$i_{ss}\,|_{x=L} = i_0\left[\exp\left(-\frac{\alpha_a F}{RT}\Phi(x=L)\right) - \exp\left(\frac{\alpha_c F}{RT}\Phi(x=L)\right)\right] \tag{4.20}$$

Here, i_0 is the exchange current density, and α_a and α_c are the anodic and cathodic transfer coefficients, respectively. The electrode potential at $x = 0$ is Φ_1. The parameters used in our unsteady-state model are: $\alpha_a = \alpha_c = 0.5$, and $i_0 = 0.5$ mA/cm^2, based on previous work on a closely related system.[142] Under these conditions, the difference between the electrode potential and that in the electrolyte at $x = 0$ and $x = L$ are negligible.

At steady-state dc/dt = 0, and eq. 4.15 simplifies to

$$D\left(1 - \frac{d\ln c_0}{d\ln c}\right)\frac{dc}{dx} = \frac{i_{ss}\,t_+}{z_+ v_+ F} + K\,. \tag{4.21}$$

The constant K is determined using the condition dc/dx = 0 when $t_+ = 1$. This gives

$$D\left(1-\frac{d\ln c_0}{d\ln c}\right)\frac{dc}{dx}=-\frac{i_{ss}}{z_+\nu_+F}(1-\ t_+)\,. \tag{4.22}$$

Collecting the concentration-dependent terms and integrating gives

$$\int_{c(x=0)}^{c(x)}\frac{D(c)}{t_-(c)}\left(1-\frac{d\ln c_0}{d\ln c}\right)dc=-\frac{i_{ss}L}{z_+\nu_+F}\left(\frac{x}{L}\right). \tag{4.23}$$

Eq. 4.23 is formally equivalent to eq. 4.8 due to the interrelations between c, r, and c_0.

4.3 Methods

4.3.1 Experiment – Cell Preparation and Cycling

All sample preparation was performed inside an argon glovebox (MBraun) in order to maintain water and oxygen levels below 1 and 5 ppm, respectively. Electrolytes were prepared by mixing PEO purchased from PolymerSource (5 kg/mol with a polydispersity of 1.08) with LiTFSI salt purchased from Novolyte. The polymers were dried at 90°C under vacuum in the glovebox antechamber for 24 h. The salt was dried at 120°C under vacuum in the glovebox antechamber for 3 days. Electrolytes were prepared by dissolving dry polymer and LiTFSI salt into tetrahydrofuran (THF) at 55°C until completely dissolved. The THF was evaporated, leaving behind a polymer/salt mixture. After 12 hours of drying on the hot plate at 55°C, the electrolytes were transferred to the glovebox antechamber to dry under vacuum at 90°C for 24 h to remove any excess THF. The average salt concentration in the electrolyte is described as r_{av}, the molar ratio of lithium ions to ether oxygens on the polymer: $r_{av} = [Li^+]/[O]$. Electrolytes were prepared in a wide range of salt concentrations of $0.01 \leq r_{av} \leq 0.30$.

Lithium symmetric cells were assembled by pressing the polymer electrolyte into a silicone spacer with a diameter of 3.175 mm and a thickness of 508 µm. The electrolyte was then sandwiched between two 150 µm thick lithium foils (MTI Corporation) backed with nickel foil. A stainless-steel shim was placed on either side of the sample to prevent the sample from deforming, which could lead to a change in electrolyte thickness or a cell short. Nickel tabs were secured to the stainless-steel shims to serve as electrical contacts. The assembly was vacuum sealed in a laminated aluminum pouch material (Showa-Denko) before removal from the glovebox. All samples were annealed at 90°C for 4 hours prior to electrochemical characterization.

Cycling was performed using a Biologic VMP3 potentiostat, and the cells were maintained at 90°C using a home-built heating stage. Cells were polarized at a low current density of i_{ss} = 0.02 mA/cm^2, and the potential, $\Phi_{measured}$, was recorded as a function of time for five charge/discharge cycles. Each cycle consisted of a 4 h charge, a 45 min rest, a 4 h discharge, and a 45 min rest. Examples of cycling data ($\Phi_{measured}$ vs. t) obtained from lithium symmetric cells with electrolytes of different salt concentrations is shown in Figure 4.1. Between each cycle, ac impedance spectroscopy was performed to track the cell impedance as a function of time. For each of these measurements, complex impedance was acquired for a frequency range of 1 MHz to 100 mHz at an amplitude of 80 mV. The data were analyzed in the form of a Nyquist plot and fit to an equivalent electrical circuit suitable for a symmetric cell with nonblocking electrodes to obtain R_i, the interfacial resistance of the cell, as described in previous publications.[124,125] The value of R_i

taken immediately subsequent to a given charge/discharge measurement is used to correct $\Phi_{measured}$ for the potential drop across the interface according to eq. 4.26.

Cells prepared with an electrolyte concentration of $r_{av} = 0.18$ were cycled at higher current densities following the initial five cycles at i_{ss} = 0.02 mA/cm^2. In this case, one full charge/discharge cycle was performed at each of the following current densities: i_{ss} = 0.05, 0.09, 0.12, 0.15, 0.20, and 0.25 mA/cm^2.

After the cycling experiments were completed, the cells were disassembled in the glovebox, and the final electrolyte thickness, L, was measured using a micrometer. These values are used in our analysis to normalize the potential of each cell according to thickness.

4.3.2 Transient Model – Comsol Parameters

The transient model, based on a macro-homogeneous model by Newman and coworkers,[135,143,144] is used to calculate the time-dependence of the potential across a lithium-PEO/LiTFSI-lithium symmetric cell during dc polarization. The governing equations for this model (eq. 4.15-4.20), are solved numerically using Comsol 5.3. The exchange current density, i_0, is taken to be 0.5 mA/cm^2, and the anodic and cathodic transfer coefficients, α_a and α_c, are both taken to be 0.5, based on a previous report using similar materials.[142]

To solve these equations, it is necessary to fit each transport property and the thermodynamic factor as continuous functions of salt concentration. The thermodynamic factor used in these equations is $(1+d\ln f_{\pm}/d\ln c)$, which quantifies the change in the mean molar activity of the salt, $f_{\pm}$, with the molarity, c, of the solution; this parameter is different from $(1+d\ln \gamma_{\pm}/d\ln m)$, which is based on the molality of the solution. The polynomial expression used for fitting and the results thus obtained are given in Table 4.1.

Table 4.1. Fitting parameters used for each transport and thermodynamic property used in the Comsol modeling. All parameters, P, are given as functions of concentration, c, in mol/L. Units for conductivity are S/cm and diffusion are cm^2/s. Most parameters were broken up into two concentration ranges to obtain the most accurate fits.

$$P(c) = K_0 + K_1 c + K_2 c^2 + K_3 c^3 + K_4 c^4 + K_5 c^5$$

P(c)	range	K_0	K_1	K_2	K_3	K_4	K_5
σ	$c \le 2.58$	2.53×10^{-4}	-1.48×10^{-3}	7.73×10^{-3}	-5.69×10^{-3}	1.16×10^{-3}	-
	$c > 2.58$	-7.26×10^{-2}	7.13×10^{-2}	-2.24×10^{-2}	2.29×10^{-3}	-	-
D	$c \le 2.38$	6.92×10^{-8}	-1.04×10^{-7}	3.51×10^{-7}	-2.50×10^{-7}	4.93×10^{-8}	-
	$c > 2.38$	-7.87×10^{-5}	1.21×10^{-4}	-7.31×10^{-5}	2.19×10^{-5}	-3.24×10^{-6}	1.90×10^{-7}
t_+	$c \le 2.58$	-8.95×10^{-2}	0.768	-0.258	-3.08×10^{-2}	-	-
	$c > 2.58$	-68.2	59.9	-17.2	1.63	-	-
$\left(1+\frac{d\ln f_{\pm}}{d\ln c}\right)$	$c \le 2.58$	3.34×10^{-3}	0.857	2.23	-0.785	-	-
	$c > 2.58$	-352	295	-78.8	6.85	-	-
$\left(1-\frac{d\ln c_0}{d\ln c}\right)$	*all c*	0.964	-0.108	-2.94×10^{-2}	-	-	-

4.4 Results and Discussion

In order to model concentration or potential profiles in an electrolyte, measurements of transport properties (conductivity, σ, salt diffusion coefficient, D, cation transference number, t_+) and the thermodynamic factor, $(1+d\ln\gamma_\pm/d\ln m)$, must be obtained over a wide range of salt concentrations.[57] Table 4.2 shows the transport properties of an electrolyte composed of 5 kg/mol PEO mixed with LiTFSI salt obtained from previous studies.[124,126] Here, salt concentration is defined in two ways: r is the molar ratio of lithium ions to ether oxygens in the system, $r = [Li^+]/[O]$, and c is the molarity of the solution. We have added the steady-state transference number, $t_{+,SS}$, defined by eq. 4.13 in Table 4.2 as it convenient for the calculations given below.

Table 4.2. Transport properties of a 5 kg/mol PEO/LiTFSI electrolyte at 90 ºC.

r	c (mol/cm^3)	D (cm^2/s)	σ (S/cm)	t_+	$(1+d\ln\gamma_\pm/d\ln m)$	$t_{+,SS}$
0.01	2.47×10^{-4}	$[6.0\pm0.8]\times10^{-8}$	$[2.7\pm0.6]\times10^{-4}$	0.07 ± 0.02	0.43	0.18 ± 0.009
0.02	4.73×10^{-4}	$[7.8\pm0.7]\times10^{-8}$	$[7.5\pm0.4]\times10^{-4}$	0.23 ± 0.03	0.69	0.16 ± 0.015
0.04	8.71×10^{-4}	$[1.0\pm0.1]\times10^{-7}$	$[1.8\pm0.5]\times10^{-3}$	0.40 ± 0.13	1.70	0.11 ± 0.019
0.06	1.20×10^{-3}	$[1.3\pm0.4]\times10^{-7}$	$[2.0\pm0.2]\times10^{-3}$	0.33 ± 0.11	2.23	0.11 ± 0.005
0.08	1.59×10^{-3}	$[1.1\pm0.1]\times10^{-7}$	$[2.2\pm0.8]\times10^{-3}$	0.43 ± 0.17	3.33	0.10 ± 0.012
0.10	1.87×10^{-3}	$[8.4\pm1.1]\times10^{-8}$	$[1.3\pm0.2]\times10^{-3}$	0.20 ± 0.05	2.82	0.09 ± 0.013
0.12	2.11×10^{-3}	$[7.0\pm1.7]\times10^{-8}$	$[1.1\pm0.0]\times10^{-3}$	0.08 ± 0.02	2.78	0.08 ± 0.008
0.14	2.38×10^{-3}	$[5.8\pm0.9]\times10^{-8}$	$[9.9\pm2.3]\times10^{-4}$	-0.08 ± 0.02	2.66	0.07 ± 0.005
0.16	2.58×10^{-3}	$[9.4\pm0.8]\times10^{-8}$	$[1.3\pm0.4]\times10^{-3}$	-0.38 ± 0.13	2.27	0.06 ± 0.001
0.18	2.76×10^{-3}	$[9.0\pm1.0]\times10^{-8}$	$[1.6\pm0.6]\times10^{-3}$	0.10 ± 0.04	3.74	0.07 ± 0.011
0.21	3.05×10^{-3}	$[6.5\pm1.5]\times10^{-8}$	$[1.2\pm0.4]\times10^{-3}$	0.41 ± 0.16	6.32	0.10 ± 0.006
0.24	3.36×10^{-3}	$[6.3\pm1.0]\times10^{-8}$	$[6.4\pm2.4]\times10^{-4}$	0.33 ± 0.13	6.00	0.16 ± 0.010
0.27	3.49×10^{-3}	$[5.9\pm1.3]\times10^{-8}$	$[4.0\pm1.0]\times10^{-4}$	0.18 ± 0.06	5.24	0.18 ± 0.022
0.30	3.78×10^{-3}	$[4.2\pm0.6]\times10^{-8}$	$[1.5\pm0.2]\times10^{-4}$	-0.02 ± 0.00	4.49	0.26 ± 0.020

To calculate concentration gradients in any system using eq. 4.8, the transport properties of the electrolyte must be fit as a continuous function of salt concentration. Based on the data in Table 4.2, we calculate the parameter $(D\,c)/(r\,t_-)$ for our PEO/LiTFSI electrolytes, shown in Figure 4.2. The anion transference number, t_-, is equal to $1 - t_+$. The solid curve shows a least-squares fit to the equation

$$\frac{D\,c}{r\,t_-} = a\,r^5 + b\,r^4 + cr^3 + dr^2 + er + f, \tag{4.24}$$

with fitting parameters

$$a = 1.088\times10^{-4} \qquad b = -9.889\times10^{-5} \qquad c = 3.280\times10^{-5}$$
$$d = -4.750\times10^{-6} \qquad e = 2.670\times10^{-7} \qquad f = -9.425\times10^{-10}$$

where D is in cm^2/s and c is in mol/cm^3. Alternatively, one could fit each parameter (D, t_-, c) individually as a function of r. It is important to note that our data are limited to the range $0.01 <$

$r < 0.3$. Thus, our model can only be used to study symmetric cell data wherein the entire salt concentration profile in the cell falls within these bounds.

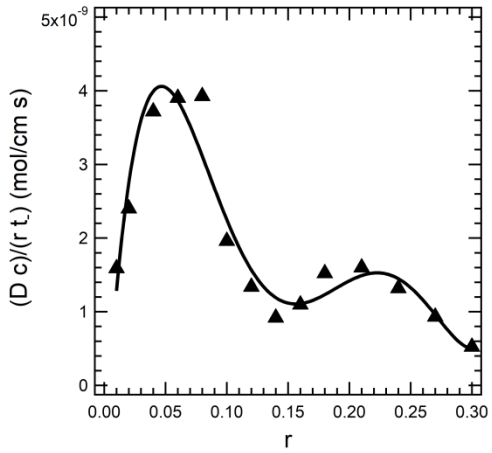

Figure 4.2. Fit of the transport coefficient term, (D c)/(r t-), with LiTFSI salt concentration. The solid curve shows the least-squares polynomial fit given by eq. 4.24.

The concentration profile in a symmetric cell under steady-state operation is governed by the initial salt concentration of the electrolyte which we call r_{av}, the steady-state current, i_{ss}, and the thickness of the electrolyte, L. Before the cell is polarized, the salt concentration at all locations is r_{av}. At steady-state, the salt concentration profile is governed by eq. 4.8; solution to this equation gives the position-dependent salt concentration, $r(x)$. It is convenient to determine the concentration profile as a function of x/L. Calculating the concentration profile for a given value of the product $i_{ss}L$ requires a three-step iterative process: (1) Choose a value for r at the point $x/L = 0$. (2) Calculate r as a function of x/L from $0 \leq x/L \leq 1$ using eq. 4.8. (3) Integrate $r(x/L)$ from 0 to 1 to determine the average salt concentration, r_{av}, of the electrolyte. The process is repeated, adjusting the value of r at $x/L = 0$, until the desired r_{av} is reached.

Figure 4.3 shows salt concentration profiles for PEO/LiTFSI electrolytes with different salt concentrations: $r_{av} = 0.08$, 0.10, 0.12, and 0.14. Each panel corresponds to a different value of $i_{ss}L$. Figure 4.3 could represent three cells with the same thickness at different current densities (L = 500 μm and (a) $i_{ss} = 0.8$ mA/cm^2, (b) $i_{ss} = 0.2$ mA/cm^2, and (c) $i_{ss} = 0.02$ mA/cm^2) or with different thicknesses at the same current density ($i_{ss} = 1$ mA/cm^2 and (a) L = 400 μm (b) L = 100 μm and (c) L = 10 μm). At the lowest value of $i_{ss}L = 0.001$ mA/cm (Figure 4.3a), the concentration profiles are linear. Nonlinear concentration profiles are evident when $i_{ss}L$ is increased 0.01 mA/cm (Figure 4.3b). Further increase in $i_{ss}L$ to 0.04 mA/cm results in highly nonlinear concentration profiles (Figure 4.3c). For the $r_{av} = 0.08$ electrolyte, $r(x)$ approaches zero at $x/L = 1$. The minimum value of $r(x/L=1)$ is zero; this condition is defined as the limiting current of an electrolyte. It is evident that an electrolyte with $r_{av} < 0.08$ would not be able to sustain $i_{ss}L = 0.04$ mA/cm. The nonlinear concentration profiles in Figure 4.3b and c are due to the concentration-dependence of t_+ and D. If t_+ and D were independent of salt concentration and c were proportional to r, all profiles in Figure 4.3 would be linear. Interestingly, the concentration profile at a given current density does not depend on conductivity (see eq. 4.8); the values of the conductivity affect the required cell potential.

Equation 4.7 indicates that the concentration gradient, dr/dx, at a given location, x/L, in the symmetric cell is governed entirely by the local salt concentration, r, regardless of the overall salt concentration, r_{av}, of the electrolyte. Thus, in Figure 4.3 if one moves horizontally from one curve to the next at any chosen value of r, the gradients of the concentration profiles are identical. At steady-state, the overall flux of cations, given by i_{ss}, is independent of position (x/L). The migration and diffusion components of the flux will change with position due to the concentration dependence of t_+ and D. The slope of the concentration profile changes due to this effect.

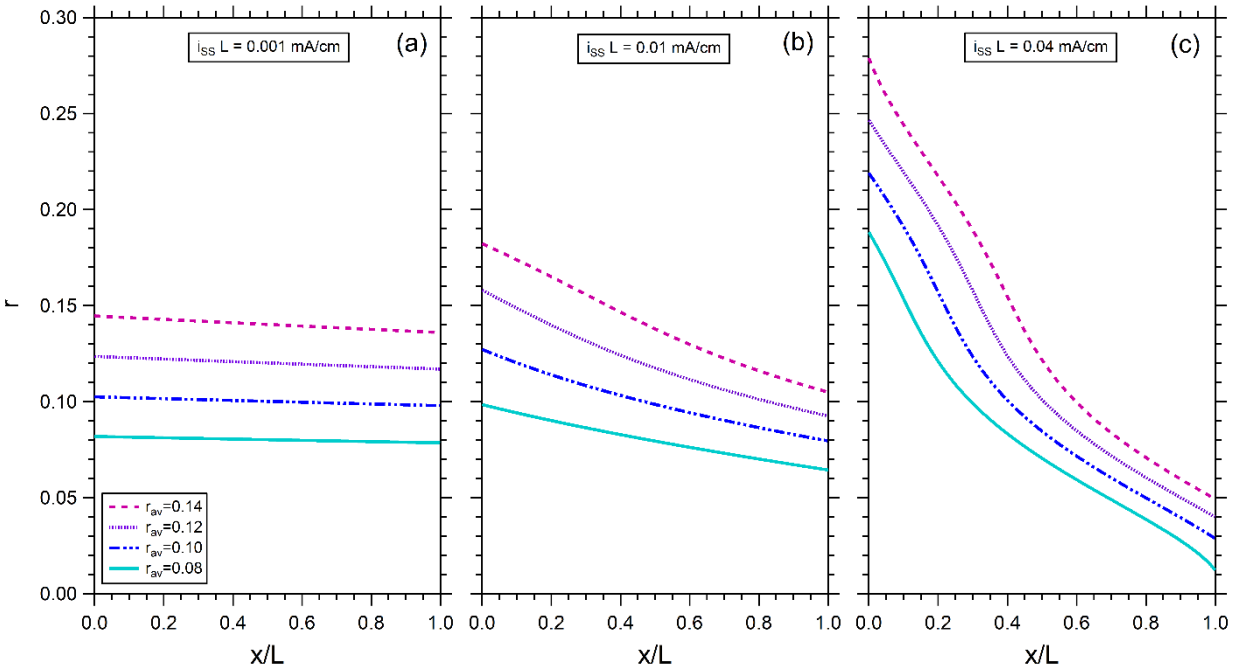

Figure 4.3. Concentration gradients in PEO/LiTFSI electrolytes predicted by the model at steady-state. These are calculated using eq. 4.8 based on the fit of the transport parameter in Figure 4.2.

The limiting current is an important characteristic of an electrolyte, as it defines the maximum current that can be drawn from a cell during operation. Traditionally, equations used to describe this characteristic are based on the assumption of transport properties that are independent of salt concentration.[57] We use our model to calculate the limiting current as a function of salt concentration for PEO/LiTFSI electrolytes. The limiting current, i_{limit}, is defined as the value of i_{ss} when the concentration profile exhibits $r = 0$ at $x/L = 1$. Our expressions for transport properties and the thermodynamic factor were derived from data in the salt concentration range of $0.01 \leq r \leq 0.3$. In other words, $r = 0$ lies outside the parameter window. To overcome this issue, we use our model at a chosen value of r_{av} to obtain values of r at $x/L = 1$ with increasing i_{ss} up to the limit of $r = 0.01$ at $x/L = 1$. Typical data thus obtained at $r_{av} = 0.08$ are shown in Figure 4.4a. Extrapolating these data to $r = 0$ gives the value of the limiting current. Only the product $i_{ss}L$ appears in the governing equation (eq. 4.8); we thus report on this parameter. Figure 4.4b shows the product $i_{limit}L$ as a function of r_{av}. It is evident that $i_{limit}L$ exhibits a nonlinear dependence on salt concentration due to the nonlinear concentration profiles observed in these electrolytes.

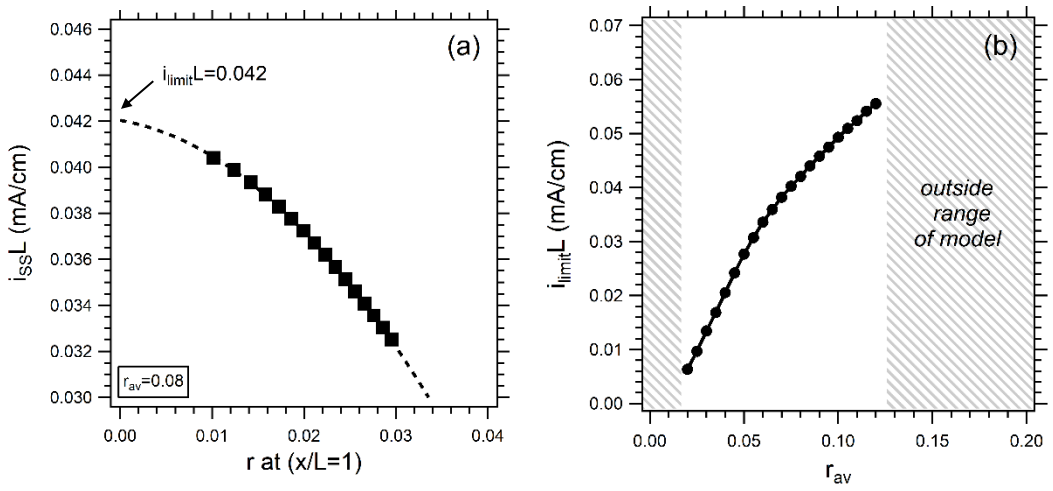

Figure 4.4. (a) The limiting current (here shown as $i_{limit}L$) of r_{av} = 0.08, obtained by extrapolating the data from model to a value of r = 0 at x/L = 1. **(b)** The product $i_{limit}L$ for PEO/LiTFSI predicted by the model as a function of electrolyte salt concentration. Our predictions are limited to 0.02 ≤ r_{av} ≤ 0.12 due to the limited concentration range of the fits used in our model.

To calculate potential gradients in our electrolytes using eq. 4.14, we fit the transport parameter $(D\ c)/(r\ t_-\ \sigma\ t_{+,SS})$ as a continuous function of salt concentration, shown in Figure 4.5. A double exponential gives the most precise fit for this data, and is given by

$$\frac{D\ c}{r\ t_-\ \sigma\ t_{+,ss}} = k_0 + A_1\exp(-\tau_1 r) + A_2\exp(-\tau_2 r), \tag{4.25}$$

with fitting parameters

$$k_0 = 1.202 \times 10^{-5} \qquad A_1 = 1.025 \times 10^{-5} \qquad A_2 = 4.229 \times 10^{-4}$$
$$\tau_1 = 10.186 \qquad \tau_2 = 368.19$$

where D is in cm^2/s, c is in mol/cm^3, and σ is in S/cm.

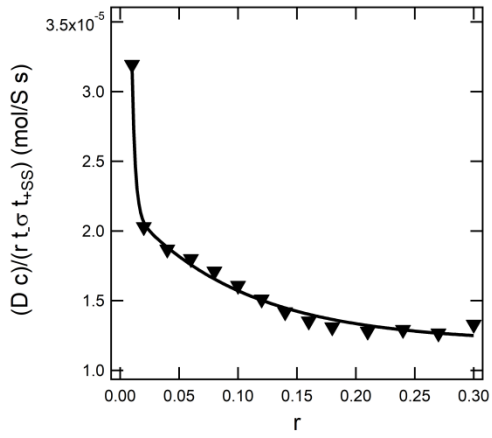

Figure 4.5. Fit of transport coefficient term $(D\ c)/(r\ t_-\ \sigma\ t_{+,SS})$ with LiTFSI salt concentration. The solid curve shows the least-squares fit to the double exponential given in eq. 4.25.

Figure 4.6 shows the dependence of potential, Φ, on position calculated for the electrolytes shown in Figure 4.3 (r_{av} = 0.08, 0.10, 0.12, and 0.14) at the same three values of $i_{ss}L$. We define Φ = 0 at x/L = 1. At the lowest value of $i_{ss}L$, Φ is a linear function of position (Figure 4.6a). Nonlinear dependences of Φ on position are evident at higher values of $i_{ss}L$ (Figure 4.6b and c). There is a close relationship between the nonlinearity in potential seen in Figure 4.6 and the nonlinearity in concentration seen in Figure 4.3. In an experiment, the value of cell potential measured experimentally corresponds to Φ at x/L = 0. It is clear that for a given value of $i_{ss}L$, cells prepared with electrolytes of different salt concentrations will yield different values of Φ at steady-state. Interestingly, the cell potential (Φ at x/L = 0) is a stronger function of salt concentration at $i_{ss}L$ = 0.001 mA/cm when compared to $i_{ss}L$ = 0.04 mA/cm (compare inset in Figure 4.6a with Figure 4.6c). This is because of the large concentration gradients that are obtained at $i_{ss}L$ = 0.04 mA/cm. The transport parameters of our electrolytes are strong functions of salt concentration, but at high currents these properties are integrated over a wide concentration window that is not a sensitive function of r_{av}. Next, we examine the validity of our model by comparing theoretical predictions against experimental measurements of Φ.

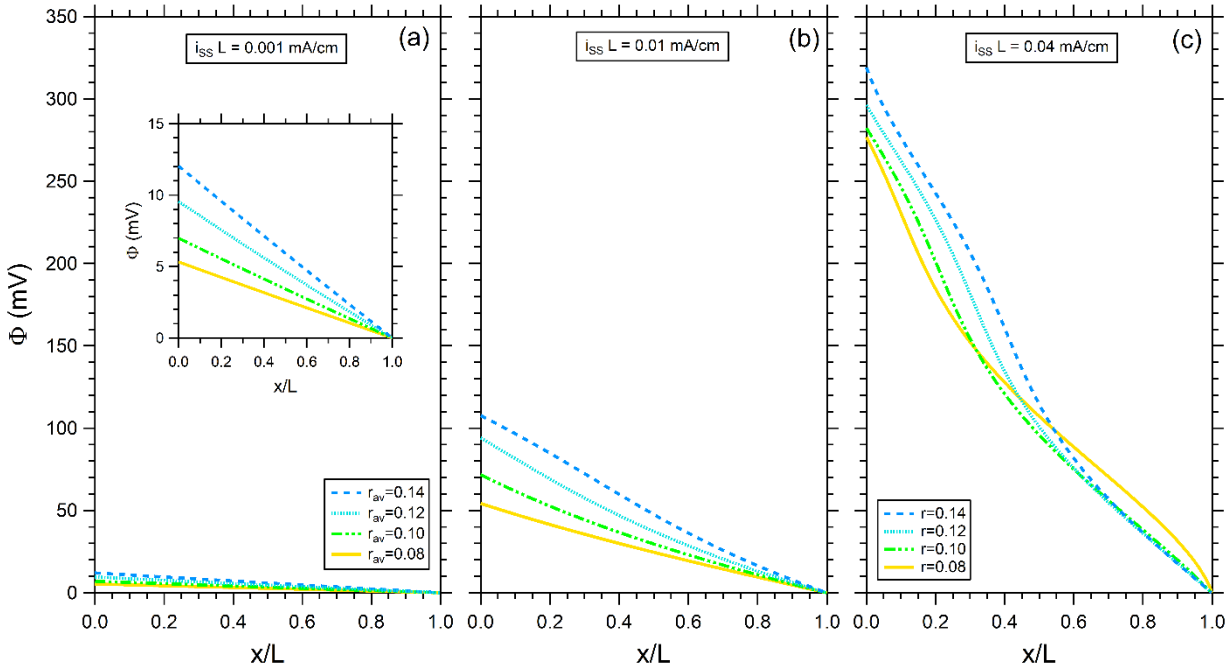

Figure 4.6. Potential profiles in PEO/LiTFSI electrolytes predicted by the model at steady-state. These are calculated using eq. 4.14 based on the fit of the transport parameters in Figure 4.5.

We use the calculations described above to interpret experimental data from lithium symmetric cells with PEO/LiTFSI electrolytes. The cells were cycled at increasing values of i_{ss}, and the measured potential, $\Phi_{measured}$, was recorded as a function of time. Typical time-dependent potential curves thus obtained are shown in Figure 4.7a. These data correspond to an electrolyte with r_{av} = 0.18 cycled at current densities ranging from i_{ss} = 0.02 to i_{ss} = 0.25 mA/cm^2. At each current density, the potential increases with time due to the formation of concentration gradients in the electrolyte, and then plateaus as the cell reaches steady-state. The measured potential, $\Phi_{measured}$, cannot be directly compared to Φ predicted by the model, as it has contributions from the lithium-polymer interfaces that are not included in the model. To correct for this, we subtract the potential drop due to interfacial impedance,

$$\Phi(t) = \Phi_{measured}(t) - R_i i_{ss} A, \tag{26}$$

where R_i is the interfacial resistance obtained from ac impedance and A is the area of the cell. The time-dependent potential curves were obtained after the interfacial impedance had reached a steady value; thus, the product $R_i i_{ss} A$ is taken to be constant at all values of t. For the case of the experimental data, we normalize Φ by the measured thicknesses of the cells, which are in the vicinity of 500 μm. In our comparisons below, all measured potentials are presented after correcting for interfacial impedance and normalizing by thickness (Φ/L). Figure 4.7b shows the data from Figure 4.7a with this correction applied.

The relevant metric for direct comparison between the experimental data in Figure 4.7b and the model based on eq. 4.14 is the potential obtained at steady-state, Φ_{SS}/L. In Figure 4.7c we show this comparison for an electrolyte with r_{av} = 0.18. The model results were obtained for an electrolyte with L = 500 μm at increasing values of i_{ss}. The experimental measurements correspond to the same values of i_{ss} shown in Figure 4.7b; each point represents an average of three samples, and the error bars show the standard deviation. The data in Figure 4.7c are in good agreement with theoretical predictions at low values of i_{ss}, but deviations are evident at higher values of i_{ss}. The explanation for this may be related to the mechanism of cell failure witnessed in the experimental measurements. Upon cycling at increasing i_{ss}, all three cells failed at $i_{ss} \leq 0.25$ mA/cm^2, which is below the limiting current predicted by the model. If the experimental samples had reached the limiting current, one might expect the voltage profile to exhibit a spike indicating depletion of the salt at the electrode. Instead, we observe that cell failure is indicated by an unstable voltage that eventually drops to zero (i_{ss} = 0.25 mA/cm^2 in Figure 4.7a and b), pointing to a short circuit in the cell. Given the low modulus of 5 kg/mol PEO at 90ºC, we believe this can be attributed to the formation of lithium dendrites as the cell reaches high current densities, leading to a deviation of Φ_{SS}/L from the model at high i_{ss} and eventually resulting in cell failure. This experimental constraint prevents us from studying our cells at high current densities. We thus limit the rest of our discussion comparing model and experiment to i_{ss} = 0.02 mA/cm^2, where we expect dendrites are not affecting our results. At this current density, cell potential is a strong function of r_{av} as shown in the inset Figure 4.6a ($i_{ss}L$ = 0.001 mA/cm corresponds to i_{ss} = 0.02 mA/cm^2, as L = 500 μm).

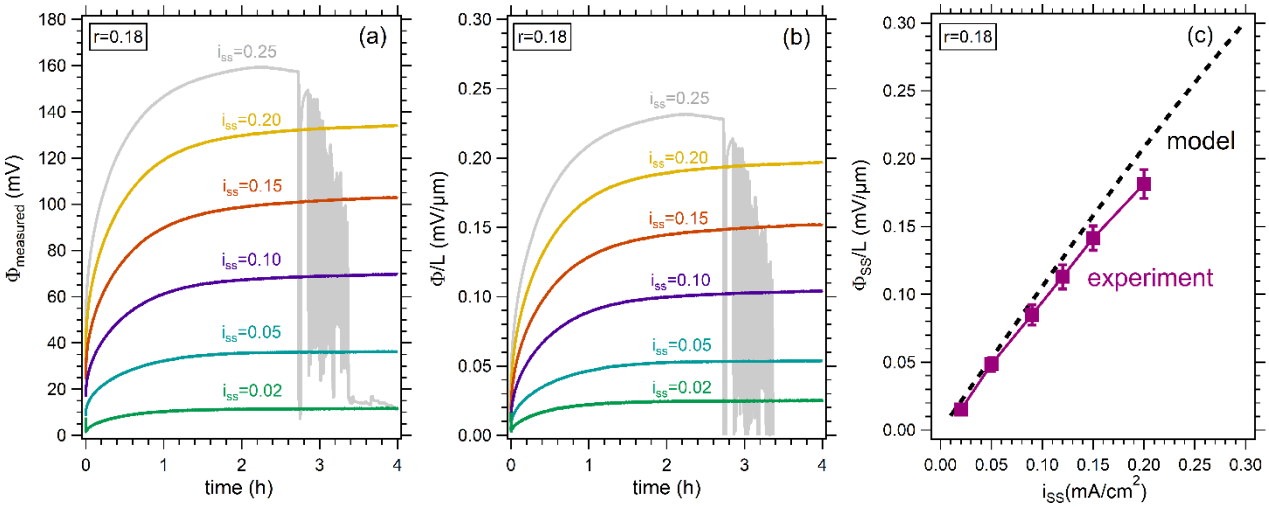

Figure 4.7. (a) Time-dependent voltage profiles measured in r_{av} = 0.18 at different steady-state current densities (i_{ss} = 0.02 mA/cm^2 to i_{ss} = 0.25 mA/cm^2). This cell failed at i_{ss} = 0.25 mA/cm^2. **(b)** Same data as (a) with the interfacial impedance correction (eq. 4.26) and thickness normalization. **(c)** Comparison between predicted potential from model (dashed curve) and experimentally measured potential (markers) for r_{av} =0.18 at different current densities. The experimental measurements are carried out until cell failure, which is below the limiting current predicted by the model.

In Figure 4.8 we compare Φ_{SS}/L over a wide range of salt concentrations, $0.01 \leq r_{av} \leq 0.3$, at a current density of i_{ss} = 0.02 mA/cm^2. The model results correspond to a system where $i_{ss}L$ = 0.001 mA/cm; the concentration and potential profiles shown in Figure 4.3c and Figure 4.6c are thus applicable to the data shown in Figure 4.8. In spite of the fact that the concentration and potential profiles are approximately linear, Φ_{SS}/L is a complex function of salt concentration exhibiting two local minima at r_{av} = 0.05 and r_{av} = 0.23 (model predictions in Figure 4.8). The optimal salt concentration for battery applications would correspond to the case where Φ_{SS}/L is minimized; thus the local minima in Figure 4.8 are of practical significance. Local maxima in Φ_{SS}/L are observed at r_{av} = 0.01, r_{av} = 0.15, and r_{av} = 0.3. These maxima correspond to salt concentrations where D is small and t_+ is close zero or negative (see Table 4.1). At these concentrations, steep concentration gradients result in larger values of Φ_{SS}/L. The agreement between model predictions and experiments in Figure 4.8 is noteworthy.

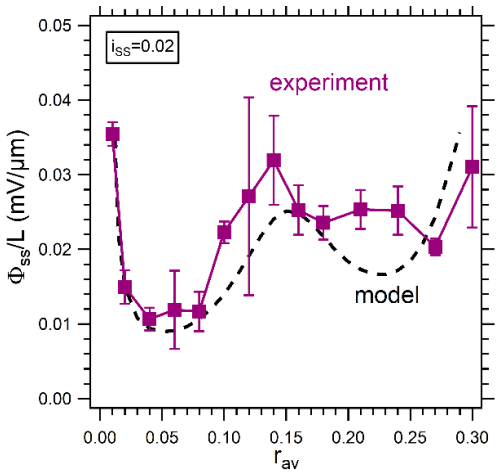

Figure 4.8. Comparison of predicted potential from model (dashed curve) and experimentally measured potential (markers) in PEO/LiTFSI electrolytes at i_{ss} = 0.02 mA/cm^2.

We return to the time-dependent voltage profiles shown in Figure 4.1. The complete data sets for r_{av} = 0.02 and r_{av} = 0.14 are shown in Figure 4.9; the shaded regions signify the range of voltages obtained from three separate cells. The solid yellow and blue curves in Figure 4.9 show averaged potential versus time data from r_{av} = 0.02 and r_{av} = 0.14, respectively. The dashed curves in Figure 4.9 are model predictions obtained by numerically integrating eq. 15 – 20 using Comsol 5.3. It is important to note that the model predictions are based on the same transport coefficients and thermodynamic factors used in the comparisons of steady-state properties. It is evident from Figure 4.9 that the time-dependent potential data are consistent with theoretical predictions with no adjustable parameters. This justifies use of the model to explore current densities that could not be accessed experimentally due to dendrite growth.

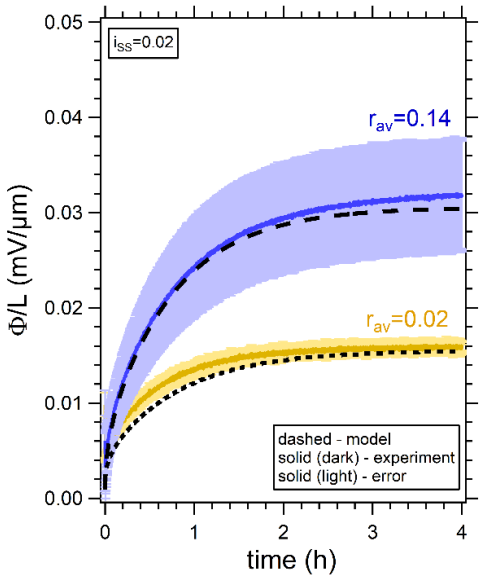

Figure 4.9. Time-dependent voltage curves for cells with r_{av} = 0.02 and r_{av} = 0.14 polarized at i_{ss} = 0.02 mA/cm^2 from experiment (solid lines) and our transient model (dashed lines). The experimental data is an average from multiple lithium symmetric cells (dark solid curves), and the error is given by the standard deviation (light shaded area).

4.5 Conclusions

Using concentrated solution theory, we derive a set of equations that can be used to model salt concentration and potential profiles in symmetric lithium-polymer-lithium cells. Our theory, which accounts for the salt concentration dependence of the electrolyte transport properties and the thermodynamic factor, requires no adjustable parameters. First, we present a steady-state model, used to predict salt concentration and potential profiles in the electrolyte under the application of a steady dc current. Then we present a transient model, used to predict the time-dependence of potential in a symmetric cell during cycling.

Polymer electrolytes are convenient model systems to study ion transport due to the absence of convection. The transport properties of mixtures of polyethylene oxide (PEO) and lithium bis(trifluoromethanesulfonyl) imide (LiTFSI) salt have been previously reported over a wide range of salt concentrations, $0.01 \leq r \leq 0.3$, where $r = [Li^+]/[O]$.[124,126] We use these data as inputs for our model to predict concentration profiles, $r(x)$, and potential profiles, $\Phi(x)$ in PEO/LiTFSI electrolytes with varying current density, i_{ss}, thickness, L, and average electrolyte salt concentration, r_{av}. Both $r(x)$ and $\Phi(x)$ exhibit nonlinearities due to the strong concentration dependence of the transport and thermodynamic properties of the electrolyte; the steepest gradients occur at values of r where both the diffusion coefficient and the transference number exhibit minima. These calculations enable determination of the limiting current. Using our model, we calculate the steady-state potential, Φ_{SS}, across the symmetric cell as a function of r_{av} and i_{ss}. These calculations are compared with experimental data without resorting to any adjustable parameters. At low i_{ss}, we find excellent agreement between the values of Φ_{SS} predicted by the theory and those obtained experimentally in lithium-PEO/LiTFSI-lithium cells. Comparisons at higher i_{ss} are prohibited by the propensity of lithium dendrites to form in the experimental cells. The time-dependence of Φ obtained during cell cycling is consistent with predictions of the transient model, requiring no adjustable parameters or simplifying assumptions.

4.6 Acknowledgements

This work was intellectually led by the Joint Center for Energy Storage Research (JCESR), an Energy Innovation Hub funded by the U.S. Department of Energy (DOE), Office of Science, Basic Energy Sciences (BES), under Contract No. DEAC02-06CH11357.

4.7 Nomenclature

PEO	polyethylene oxide
LiTFSI	lithium bis(trifluoromethanesulfonyl) imide
σ	ionic conductivity (S/cm)
D	salt diffusion coefficient (cm^2/s)
t_+	cation transference number
Th	thermodynamic factor, equal to $1+d\ln\gamma_\pm/d\ln m$
$\gamma_\pm$	mean molal activity coefficient of the salt
m	molality (mol/kg)
r_{av}	moles of Li^+ per mole of ethylene oxide, $[Li^+]/[O]$
i_{SS}	steady-state current density (mA/cm^2)
$\Phi_{measured}$	measured cell potential (mV)

x	position (μm)
z_+, z_-	charge number of cation and anion
ν_+, ν_-	the number of cations and anions into which the salt dissociates
ν	total number of ions into which the salt dissociates
n	number of electrons
L	thickness of the electrolyte (μm)
N_-	anion flux
i	current density
$\mathfrak{D}$	diffusion coefficient of the salt based on a thermodynamic driving force (cm^2/s)
μ_e	chemical potential of the electrolyte (J/mol)
t_-	anion transference number
F	Faraday's constant (96485 C/mol)
R	gas constant (J/mol K)
T	temperature (K)
c	salt concentration (mol/cm^3)
c_0	solvent concentration (mol/cm^3)
c_T	total solution concentration (mol/cm^3)
μ_e^0	chemical potential of the reference state (J/mol)
M_0	molar mass of the solvent (g/mol)
Φ	potential (mV)
Φ_0	initial potential (mV)
Φ_{SS}	steady-state potential (mV)
t	time (h)
i_0	initial current (mA/cm^2)
i_{ss}	steady-state current (mA/cm^2)
Ne	dimensionless number defined by Equation 12
$t_{+,SS}$	transference number obtained using stead-state current method
i_0	exchange current density (mA/cm^2)
α_a, α_c	anodic and cathodic transfer coefficients
Φ_1	potential of the electrode at electrode boundary
Φ_2	potential of the electrolyte at electrode boundary
R_i	interfacial resistance ($\Omega\ cm^2$)
$f_\pm$	mean molar activity of the salt
i_{limit}	limiting current (mA/cm^2)

5 Effect of Monomer Structure on Ionic Conductivity in a Systematic Set of Polyester Electrolytes[*]

ABSTRACT

Polymer electrolytes may enable the next generation of lithium ion batteries with improved energy density and safety. Predicting the performance of new ion-conducting polymers is difficult because ion transport depends on a variety of interconnected factors which are affected by monomer structure: interactions between the polymer chains and the salt, extent of dissociation of the salt, and dynamics in the vicinity of ions. In an attempt to unravel these factors, we have conducted a systematic study of the dependence of monomer structure on ionic conductivity, σ, and glass transition temperature, T_g, using electrolytes composed of aliphatic polyesters and lithium bis(trifluoromethanesulfonyl) imide (LiTFSI) salt. The properties of these electrolytes were compared to those of poly(ethylene oxide) (PEO), a standard polymer electrolyte for lithium batteries. We define a new measure of salt concentration, ρ, the number of lithium ions per unit length of the monomer backbone. This measure enables collapse of the dependence of both the σ and T_g on salt concentration for all polymers (polyesters and PEO). Analysis based on the Vogel-Tammann-Fulcher (VTF) equation reveals the effect of different oxygen atoms on ion transport. The VTF fits were used to factor out the effect of segmental motion in order to clarify the relationship between molecular structure and ionic conductivity. While the conductivities of the newly-developed polyesters were lower than that of PEO, our study provides new insight into the relationship between ion transport and monomer structure in polymer electrolytes.

5.1 Introduction

Replacing conventional organic liquid electrolytes with a nonflammable alternative is a crucial step toward safer rechargeable lithium batteries. Ion-conducting polymers are of particular interest in electrochemical applications due to their non-volatile nature and easily tunable properties.[114,145] Despite 40 years of persistent research, the ionic conductivity of the most promising solvent-free polymer electrolytes remain insufficient for use in commercial batteries. Our ability to design new and improved ion-conducting polymers is compromised by a lack of knowledge of the relationship between monomer structure and ion transport.

The mechanism that enables ion transport in polymers is inherently different from traditional liquids.[9,146,147] Solvent-free polymers solvate low lattice-energy salts through the formation of stable ion-polymer complexes;[26,33,148] hopping from one solvation complex to another is a mechanism that allows ions to travel through polymers.[23,25,149] Therefore, ion-conducting polymers must contain polar groups which interact with at least one of the ions (typically the cation) to

[*] This chapter was reported in *Solid State Ionics* **2016**, *289*, 118–124.

enable salt solvation,[150] but the strength of these interactions will impact hopping dynamics. The solvation of salt and the transport of ions are intrinsically coupled, and the type of polar groups present will directly affect the conductive properties of the material. Furthermore, the location and spacing of these groups influence the stiffness of the chains. More flexible chains exhibit rapid segmental motion which facilitates ion transport, and thus are desirable in polymer electrolytes.[29,151] Due to the complexity of these interrelated factors, determining relationship between molecular structure and ion transport remains an outstanding challenge.

A vast majority of the literature on polymer electrolytes is focused on mixtures of poly(ethylene oxide) (PEO) and lithium salts such as lithium bis(trifluoromethanesulfonyl) imide (LiTFSI) which exhibit reasonable ionic conductivities at temperatures above 60°C, the melting temperature.[23,28–30,58,148] The ionic conductivity of PEO/LiTFSI in the vicinity of 80°C is 1×10^{-3} S/cm,[28,58] significantly lower than the room temperature conductivity of liquid electrolytes used in current electric vehicles. The desire to obtain polymer electrolytes with improved lithium ion transport has motivated studies of conductivity in a variety of polymers such as polyesters,[44–48] polycarbonates,[49,50] polysiloxanes,[51–54] polyphosphazenes,[55] and perflouropolyethers.[56] Changes in the monomer structure affect the glass transition temperature, dielectric constant, ion solvation, salt dissociation, and ion hopping rates in ways that are, at this stage, difficult to predict. It is unclear which of these effects are responsible for the observed differences in conductivity due to the fact that the chemical structure of the monomers listed above are drastically different. Comparison between the results presented in these references is further complicated by differences in salt used to create the electrolytes, salt concentration, and polymer molecular weight; the conductivity of polymer electrolytes is significantly affected by these parameters. To our knowledge, there is no framework that enables quantification of the factors the underlie ion transport in the chemically distinct polymers chains listed above.

In this paper, we have studied ion transport in a series of polyesters wherein the locations of the cation-solvating oxygen atoms in the monomer are systematically changed. The same salt was used in all the electrolytes and our study covers a wide range of overlapping salt concentrations. We ensured that the molecular weight of the polymers exceeded 4 kg/mol. In this regime the conductivity of PEO/LiTFSI mixtures is independent of chain length,[29,58] and the chemical identity of the endgroups.[104] We assume the same holds for the polyester electrolytes. We thus interpret differences in conductivity solely in terms of differences in the chemical structure of the monomers.

The chemical structure of the aliphatic polyesters used in this study are shown in Figure 5.1. We use two different backbones, one with an alkane link between the backbone ester groups, labeled *a*, and another with an ether link between the backbone ester groups, labeled *b*. Polymers labeled 1 have a methyl side chain, polymers labeled 2 have a methoxy-allyl side chain, and polymers labeled 3 have an ethylene-oxide sidechain with three ether oxygens. For completeness we also studied PEO. Careful consideration went into choosing these structures. We explore two polar groups: ethers and carbonyl-containing esters. Ethers are of particular interest in the polymer electrolyte community, while carbonyl groups are used in current lithium battery electrolytes.[9] In contrast to previous reports on polyesters,[44–48] the polymers in Figure 1 all possess sidechains of varying lengths. We chose to avoid linear polyesters to thwart crystallization; the comb polyesters in this study (Figure 5.1) are amorphous over the entire salt concentration and temperature ranges of interest.

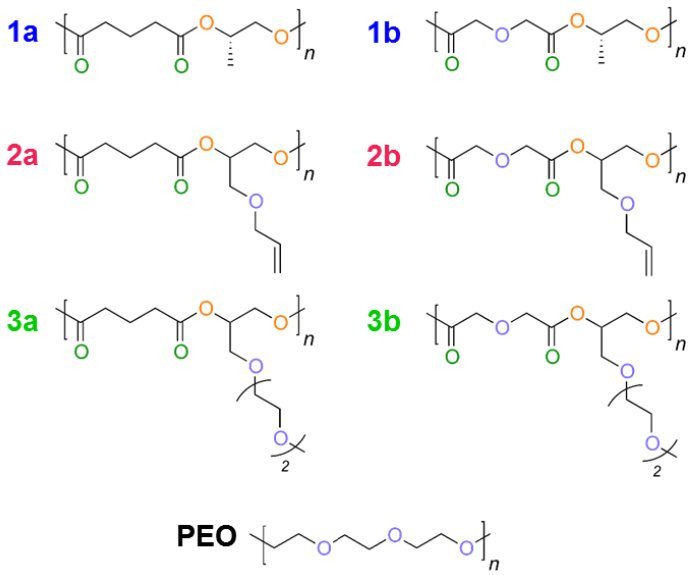

Figure 5.1. Structure and naming convention for polyesters and PEO. The monomer units for all polymers including PEO correspond to 9 atoms along the backbone. Oxygens are distinguished using color: carbonyl oxygens are green, ester oxygens are orange, and ether oxygens are purple.

The properties of the electrolytes listed in Figure 5.1 have been previously studied in the dilute salt concentration limit in reference 127. The focus of that work was to experimentally determine the dilute-ion transport characteristics of polyester electrolytes and utilize simulations for molecular-level insight describing the coordination environment and hopping mechanisms of a lithium ion. It is, perhaps, worth noting at the outset that the ionic conductivities of the newly-developed polyester electrolytes are less than that of PEO (at fixed temperature and salt concentration). The present study is mainly motivated by our desire to begin building a framework for understanding the relationship between monomer structure and ion transport.

5.2 Experimental

5.2.1 Polymer Synthesis and Characterization.

The polyesters used in this study were synthesized and characterized using methods described in reference 127. Table 5.1 provides the number-averaged molecular weight, M_n, and polydispersity, $Đ$, for each polymer.

5.2.2 Electrolyte Preparation

Electrolytes were prepared by mixing each polymer with lithium bis(trifluoromethanesulfonyl) imide (LiTFSI) salt. Due to the hygroscopic nature of LiTFSI, all sample preparation was carried out in an argon glovebox (MBraun) where H_2O and O_2 levels were maintained below 0.1 ppm and 1 ppm respectively. The set of six polyesters were dried, along with 5 kg/mol PEO (Polymer Source), at 90°C under vacuum in the glovebox antechamber for a minimum of 8 h, and then transferred into the glovebox. Dry polymer and LiTFSI salt (Novolyte) were dissolved into anhydrous N-methyl-2-pyrrolidone (NMP) and the solutions were mixed at 90°C for a minimum of 5 h. Once the solutes were fully dissolved, the caps were removed from the vials allowing NMP to evaporate and leave behind a homogeneous polymer/salt mixture. After drying on the hotplate at 90°C for 2 days, the electrolytes were transferred to the glovebox antechamber and dried under

vacuum for 8 h at 90 °C to remove any excess NMP. Most of the dry electrolytes were very viscous liquids at room temperature with the consistency of molasses. Electrolyte 1b was solid-like at room temperature.

It is convenient to define concentration, ρ, as the molar ratio of lithium ions to polymer repeat units, $\rho = [Li^+/monomer]$, wherein the monomer is defined in Figure 5.1. It is perhaps worth noting that a PEO "monomer" is defined as having 3 repeating CH_2-CH_2-O units. The lengths of the backbones of all the monomers are thus comparable. Electrolytes with $\rho = 0$, 0.02, 0.04, 0.08, 0.12, 0.16, 0.2, 0.24, and 0.28 were created for each polyester and PEO. These values were chosen to span the full range of salt concentrations in an attempt identify the maximum conductivity of each polymer.

5.2.3 Differential Scanning Calorimetry

Samples were prepared by depositing 3-7 mg of each electrolyte into hermetically sealed aluminum pans. Differential scanning calorimetry (DSC) experiments were performed on a TA Instruments DSC Q200 instrument with the following temperature scan: heat to 110°C at 20°C/min, cool to -75°C at 5°C/min, heat to 110°C at 20°C/min. The glass transition temperature, T_g, values of the electrolytes were obtained from the second heating scan. T_g measurements were found to be repeatable within 1°C.

5.2.4 Electrochemical Measurements

Stainless steel symmetric cells were prepared for ionic conductivity measurements of electrolytes using ac impedance spectroscopy. Highly viscous liquid electrolytes were pressed into a 3.175 mm diameter hole within a 254 µm thick silicone spacer. Two 200 µm stainless steel electrodes were pressed on either side of the electrolyte-filled spacer. The silicone forms a good seal with stainless steel which prevents the polymers from leaking out of the cell. Due to a high T_g, polymer 1b was heated to 90°C while pressing; all other electrolytes were soft enough to be pressed at room temperature. The thickness of each electrolyte was determined by measuring the thickness of the cell using a micrometer and subtracting the thickness of the electrodes. Aluminum tabs were secured to the electrodes using kapton tape. The entire cell was hermetically sealed within Showa-Denko pouch material leaving only the tab ends exposed. This allows for electrochemical measurements to take place outside of the glovebox while an air-free, water-free environment is maintained for the electrolyte.

Once removed from the glovebox, each cell was placed in a custom-built heating stage to determine conductivity in the range of 25°C to 130°C. Complex impedance measurements were acquired using a Biologic VMP3 potentiostat for a frequency range of 1 Hz to 1 MHz at an amplitude of 50 mV. Figure 5.2 shows a Nyquist plot of the impedance data obtained from polymer 1b with $\rho = 0.08$ at 90°C. As commonly observed with ion-conducting polymer electrolytes, there is a semicircle at high frequencies with a capacitive tail at low frequencies. The data was fit to an equivalent electrical circuit model that is suitable for finding resistance of a polymer electrolyte in a symmetric cell with blocking electrodes, shown in the inset of Figure 5.2. In this circuit, the parallel combination of C_b, the capacitance of the bulk electrolyte, and R_b, the bulk electrolyte resistance, effectively models the semicircle of the data; Q_e, the pseudo-capacitance (constant phase element) of the electrode accounts for the capacitive tail. Apparatus inductance, L_c, and resistance, R_c, were also included.

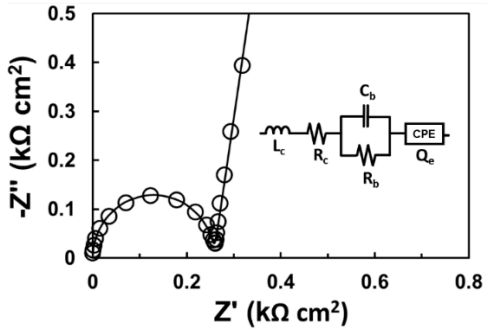

Figure 5.2. Nyquist impedance plot (-Z" vs Z') of polymer 1b with ρ= 0.08 at 90°C for a frequency range of 1 MHz to 25 mHz. Open circles correspond to the experimental data and the solid line shows the least-squares fit obtained using the equivalent circuit shown in the inset.

Conductivity, σ, was then calculated using eq 5.1, where l is the electrolyte thickness, and a is the electrolyte area.

$$\sigma = \frac{l}{aR_b}, \tag{5.1}$$

Subsequent to conductivity measurements, each cell was disassembled in a glovebox and final thicknesses were measured. On average, the electrolyte thickness decreased 7% after annealing. The final sample thicknesses were used for the conductivity calculation. Finally, a visual inspection of the electrolyte was performed to ensure the samples had no bubbles or voids in the polymer. Such defects would alter the electrolyte volume and make conductivity calculations inaccurate, thus, these samples were discarded from the set. Error was calculated based on the standard deviation of three independent conductivity samples prepared for each electrolyte.

5.3 Results and Discussion

Conductivity, σ, was measured at a wide range of salt concentrations and temperatures (25-130°C) for each polymer. Results are shown in Figure 5.3 where conductivity of b-type polyesters and PEO obtained at 90°C is plotted as a function of salt weight fraction, w. The a-type polyesters have been excluded from this figure for clarity but follow similar trends to their b-type counterparts. For the polyesters, the highest conductivity occurs at w values between 0.19 and 0.25, whereas PEO exhibits a broad maximum at w = 0.34. The reason for the non-monotonic dependence of conductivity on salt concentration is well established.[28,151] Conductivity increases with increasing salt concentration in the low concentration regime due to an increase in the number of charge carriers. However, screening effects become important with increasing salt concentration, and this reduces the number of "effective" charge carriers. In addition, interactions between polymer chains and salt molecules slow down segmental motion and this impedes ion transport. On the surface, the qualitative differences between the data obtained from polymers 1b, 2b, 3b, and PEO (Figure 5.3) seem to suggest that the interplay between charge carrier concentration and segmental motion in these systems is fundamentally different.

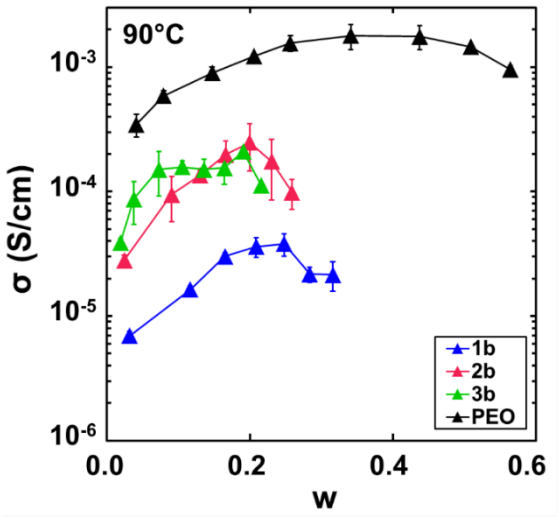

Figure 5.3. Conductivity, σ, as a function of weight fraction, w, of LiTFSI in each polymer. All data shown is at 90°C.

The salt concentration in polymer electrolytes, particularly PEO, is often quantified by the ratio of lithium ions to ether oxygens, r.[18,58] In some cases, $1/r$, the ratio of ether oxygens to lithium ions, is used to quantify salt concentration.[28,30] We prefer to use r as it is directly related to molarity and molality which are standard measures of salt concentration in conventional electrolytes such as aqueous sulfuric acid. It is known, for example, that PEO/LiTFSI mixtures exhibit a maximum conductivity at $r = 0.085$.[18,28] Such a ratio is suitable for describing salt concentration in polymers wherein the interactions between the salt molecules and all of the polar groups on the polymer chains are identical. In contrast to conventional polyethers, the polyesters investigated in this study have three different types of oxygens with varying electron densities (see Figure 5.1). Furthermore, the accessibility of the oxygens will depend on location; oxygens located on sidechains are expected to be more accessible than those located on the main chain. It is likely that the lack of collapse of the conductivity data shown in Figure 5.3 is due to these effects. Defining a measure of salt concentration that enables a collapse of the conductivity data has the potential to provide insight into the interactions between the different polar groups in the polyesters and LiTFSI.

Figure 5.4a shows the same data as Figure 5.3 with a new measure of salt concentration: ρ, the molar ratio of lithium ions to monomers defined in Figure 5.1. The abscissa of Figure 5.3 is restricted to $0.02 \leq \rho \leq 0.28$. It is evident that defining salt concentration in terms of ρ aligns the conductivity trends for each polymer. In particular, the conductivity peaks occur at similar values of ρ and the width of the peaks are also similar. In Figure 5.4b we plot σ/σ_{max} versus ρ, where σ_{max} is the maximum conductivity of each polymer. The values of σ_{max} are given in Table 5.1. We observe that all data sets collapse onto a master curve. Similar collapse is observed for conductivities measured between 40 and 130°C (data not shown for brevity).

The maximum conductivity occurs at $\rho = 0.22 \pm 0.02$ for all polyesters and PEO. This is noteworthy because the monomers as defined in Figure 5.1 contain varying numbers of oxygens, ranging from 3 to 8. If the interactions between salt molecules and all of the oxygens were similar, then the conductivity maximum in polyesters 3a and 3b would occur at ρ values that were significantly higher than that of PEO. As seen in Figure 5.1, all monomers consist of 9 atoms along the backbone. Therefore, our definition of ρ can be thought of as the number of lithium ions per

unit length of the monomer backbone. It appears that there is a spatial limitation in the heavily functionalized polyesters that prevents lithium ions from accessing all available oxygens. In contrast, PEO has only 3 oxygens per monomer, and all are readily accessible to solvate lithium.[127] We examined the possibility of using other definitions of salt concentration such as lithium ions per ether oxygen, lithium ions per carbonyl and ether oxygen, lithium ions per oxygen (including ester, carbonyl, and ether groups) and salt weight fraction. The conductivity data shown in Figure 4 do not collapse when these definitions of salt concentration are used.

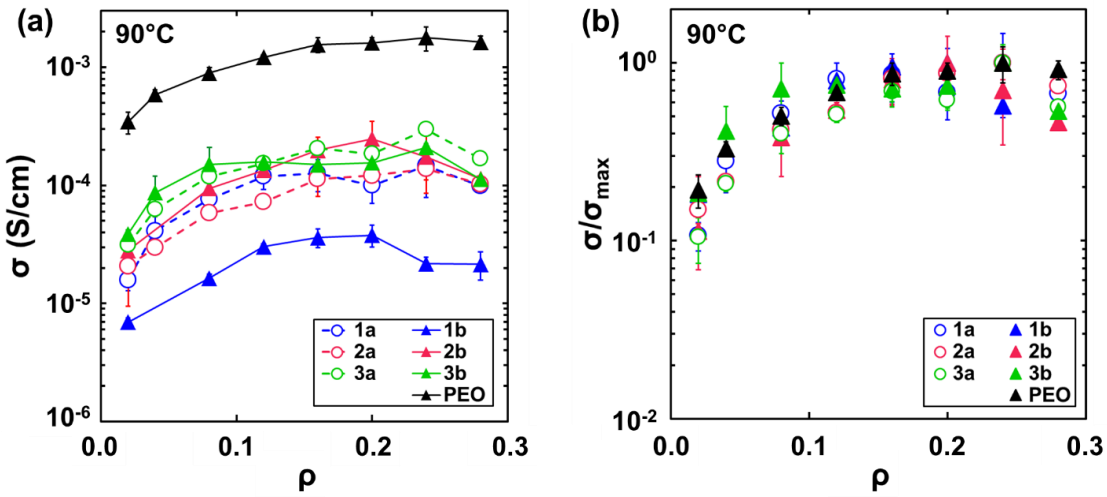

Figure 5.4. (a) Conductivity, σ, and (b) normalized conductivity, σ/σ_{max}, as a function of ρ at 90°C.

We find that σ_{max} for polymers 1a, 2a, 2b, 3a, and 3b all fall in the range of 1.4 x10^{-4} to 3.0x10^{-4} S/cm. The outlier of the polyester set is polymer 1b, which has a σ_{max} approximately one order of magnitude lower than all other polyesters. The glass transition temperature of our polymers at $\rho = 0$, $\rho = 0.02$, and $\rho = 0.2$ are listed in Table 5.1. We find that the T_g of polymer 1b is significantly higher than that of the other polymers in all cases, thus the low value of σ_{max} of polymer 1b is related to slow segmental motion. The most conductive polymer, PEO, has the lowest T_g. There is, however, no correlation between T_g and σ_{max} for polymers with intermediate conductivity. It is evident that factors other than segmental motion are important for ion transport.

Table 5.1. Material properties of polymers and VTF parameters of electrolytes at ρ=0.02 and ρ=0.2.

Polymer	M_n (kg/mol)	$Đ$	$\sigma_{max,\ 90°C}$ (S/cm)	$T_{g,\ neat}$ (°C)	$T_{g,\ \rho=0.02}$ (°C)	$T_{g,\ r=0.2}$ (°C)	$E_{a,\ \rho=0.02}$ (kJ/mol)	$A_{\rho=0.02}$ (SK$^{1/2}$/cm)	$E_{a,\ \rho=0.2}$ (kJ/mol)	$A_{\rho=0.2}$ (SK$^{1/2}$/cm)
1a	8.8	1.9	1.5 x 10^{-4}	-28	-25	-12	8.6 ± 1.1	0.1 ± 0.2	9.2 ± 1.2	2.6 ± 0.2
2a	10.4	2.0	1.4 x 10^{-4}	-41	-40	-26	8.3 ± 1.5	0.1 ± 0.5	8.5 ± 1.0	1.1 ± 0.1
3a	4.2	1.3	3.0 x 10^{-4}	-44	-43	-28	8.6 ± 1.3	0.2 ± 0.3	9.2 ± 1.1	2.5 ± 0.1
1b	6.7	1.6	3.8 x 10^{-5}	12	14	26	10.7 ± 1.2	3.5 ± 0.2	8.9 ± 1.4	7.7 ± 0.2
2b	8.9	1.5	2.5 x 10^{-4}	-14	-13	0	8.7 ± 1.1	0.5 ± 0.1	9.6 ± 2.3	16.6 ± 0.8
3b	6.1	1.8	2.1 x 10^{-4}	-25	-23	-12	9.2 ± 1.1	0.6 ± 0.1	9.8 ± 1.2	6.4 ± 0.2
PEO	5.0	1.1	1.8 x 10^{-3}	-60	-59	-44	7.1 ± 1.6	0.5 ± 0.8	8.4 ± 1.2	7.2 ± 0.2

The glass transition temperature of polymer electrolytes usually increases with salt concentration.[28,30] In many studies, the glass transition of mixtures is correlated with the weight fractions of the components.[152,153] In Figure 5.5a we plot ΔT_g, the increase in T_g at a given salt concentration relative to the neat sample, versus w. Included in this plot are data obtained from all six polyesters in the range $0 \leq \rho \leq 0.28$. The data obtained from PEO samples are limited due to experimental difficulties. Similar difficulties have been noted in previous studies of the glass transition in PEO.[28,154] In particular, we were not able to detect a T_g for the neat sample of PEO due to a high degree of crystallinity. We performed DSC on a 4.6 kg/mol PEO (Sigma Aldrich) with a high polydispersity and obtained T_g = -60°C. We do not expect segmental motion of the polydisperse sample to be significantly different from that of the low polydispersity PEO used in our conductivity experiments. Lacking a better alternative, we assume that T_g of pure PEO is -60 °C. For similar reasons we were unable to determine T_g of PEO/LiTFSI mixtures from ρ =0.02 to ρ = 0.16. At values of ρ > 0.16, PEO/LiTFSI mixtures are amorphous and determining T_g was straightforward. It is evident that ΔT_g at a given value of w depends on the type of polymer, particularly at high concentrations (Figure 5.5a). In Figure 5.5b we plot ΔT_g versus ρ. The data from all samples collapse onto a straight line, $\Delta T_g = 67.7\rho$, which we obtained using a least-squares fit through the data.

Determining a definition of salt concentration that leads to a collapse in both σ and ΔT_g is the first step in relating monomer structure and ion transport. We show below that analysis of data obtained at a fixed value of ρ provides insight regarding the polar groups responsible for salt complexation and steric effects that limit access to certain polar groups.

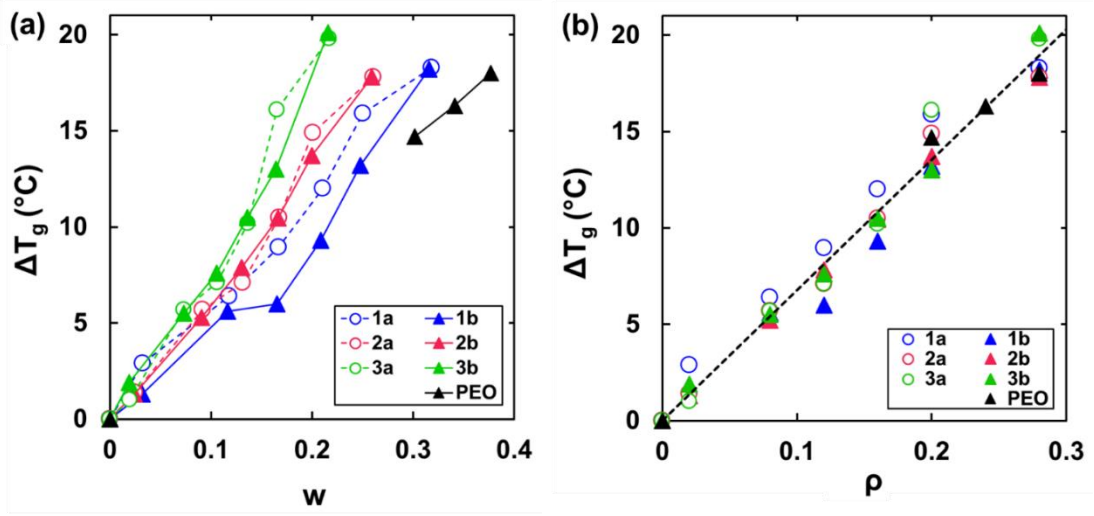

Figure 5.5. Increase in T_g as a function of (a) weight fraction, w, and (b) ρ for the polyester and PEO electrolytes. The T_g at w=0 and ρ=0 is that of the neat polymer.

The ionic conductivity of polymer electrolytes is influenced by a number of interrelated factors: interactions between monomers on the polymer chain and the salt species, extent of dissociation of the salt, and chain conformations and dynamics, i.e. segmental motion, in the vicinity of ions.[28,151] We use the well-known Vogel-Tammann-Fulcher (VTF) equation to factor out the effect of segmental motion on conductivity.[27] The temperature dependence of conductivity of polymer electrolytes is given by the VTF equation,

$$\sigma = A\,T^{-1/2}\exp\left(\frac{-E_a}{R(T-T_o)}\right). \quad (5.2)$$

In this equation T_o is a reference temperature, R is the universal gas constant, and A and E_a are VTF parameters obtained by fitting experimental data. The reference temperature, T_o, is taken to be 50°C below the glass transition temperature of the electrolyte. The parameter A is often related to the concentration of charge carriers in the system, and E_a is the effective activation energy for ion transport.

In Figure 5.6a we plot σ versus 1000/(T-T_g+50) for ρ = 0.02, a dilute salt concentration. The data from all of our samples are approximately linear when plotted in this format indicating agreement with the VTF equation. Note that T_g is the glass transition of the electrolyte with ρ = 0.02 (Table 5.1). The parameters A and E_a, obtained by least-squares fits through the data in Figure 5.6a, are given in Table 5.1. Despite large differences in the chemical formulae of the monomers, E_a values are similar, ranging from 7.1 to 10.7 kJ/mol (Table 5.1). In other words, the VTF plots of all of the polymers are nearly parallel (Figure 5.6a). The vertical offset of the VTF plots of different polymers mainly reflects the magnitude of A. The VTF data of the set of polymers examined here in the dilute limit are segregated into three groups: (1) PEO, (2) b-type polymers, and (3) a-type polymers, in order of decreasing conductivity at fixed T - T_g. The main difference between a-type and b-type polymers is the addition of an ether oxygen on the backbone of b-type polymers (Figure 5.1). We thus conclude that this backbone ether oxygen plays an important role in ion transport through the b-type polymers.

In Figure 5.6b we plot σ versus 1000/(T-T_g+50) for ρ = 0.2, the concentration in the vicinity of the maximum conductivity. The values of T_g, A, and E_a for ρ = 0.2 are provided in Table 5.1. We find that the data of all samples are approximately linear and parallel, and the values of E_a are comparable to those obtained from the data in Figure 5.6a. We thus conclude that the activated process of ion hopping does not significantly change as a function of either polymer type or salt concentration. The VTF data of the set of polymers examined here in the concentrated limit are segregated into two groups: (1) PEO, 1b, and 2b, and (2) 3b and the a-type polymers, in order of decreasing conductivity at fixed T - T_g. Polymer 3b appears to be an outlier of the polyesters, aligning with b-type polymers in the dilute limit and with a-type polymers in the concentrated limit.

Comparison between Figure 5.6a and Figure 5.6b indicate that the trends observed in the VTF plots change as a function of salt concentration. The VTF plot of PEO at ρ = 0.02 lies above that obtained from the polyesters. In contrast, the VTF plot of PEO at ρ = 0.2 was coincident with 1b and 2b. In addition, the VTF plot of 3b at ρ = 0.02 is coincident with that of the other b-type polyesters; in contrast, the VTF plot of 3b at ρ = 0.2 lies below that of 1b and 2b. These differences suggest that the factors that underpin ion transport in the dilute and concentrated regimes may be different in some cases (e.g. PEO and 3b).

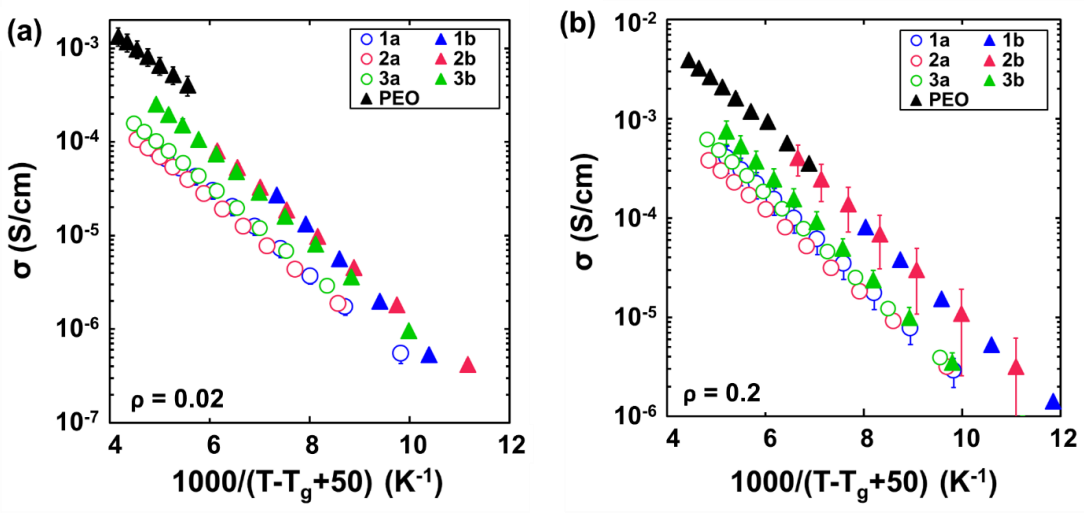

Figure 5.6. Vogel-Tammann-Fulcher plot of conductivity of electrolytes at **(a)** ρ = 0.02 and **(b)** ρ = 0.2. In both figures, the data for PEO is limited to temperatures above the melting point.

To further investigate the effect of salt concentration on ion transport, we use the VTF fit parameters, E_a and A (Tables 5.S2 and 5.S3 in SI), obtained from the temperature dependent data to calculate a reduced conductivity, σ_r, at a set temperature (75 K) away from T_g.

$$\sigma_r = A\,(T_g + 75\ \mathrm{K})^{-1/2} \exp\left(\frac{-E_a}{R(125\ \mathrm{K})}\right), \tag{5.3}$$

Here, T_g is the measured glass transition temperature of the polymer/salt mixture of interest. In the range $0 < \rho < 0.16$, we assume that T_g of PEO is given by the linear fit in Figure 5.5b. Since the VTF lines for the polymers are essentially parallel, the dependence of σ_r on ρ is qualitatively similar at all values of T-T_g. In Figure 5.7 we show the dependence of σ_r on ρ for all the polymers. At first glance, Figure 5.7 appears to be similar to Figure 5.4a. There are, however, important differences that shed light on the underlying factors that affect ion transport. The maxima obtained in σ versus ρ plots of all seven polymers (Figure 5.4a) are not present in the σ_r versus ρ plot (Figure 5.7). The only outlier is polymer 2b wherein a maximum is observed in the σ_r versus ρ plot. It is clear that the maxima in σ versus ρ plots were obtained due to increasing T_g with increasing salt concentration. When this effect is factored out, most σ_r versus ρ plots appear to reach plateaus above ρ = 0.2 (except for 2b). At low ρ, all polymers show an increase in conductivity due to increasing charge carrier concentration. Above ρ = 0.2 the solvation sites become saturated and the reduced conductivity becomes independent of salt concentration. Another significant difference between Figure 5.4a and 5.7 is the vertical offset between different polymers. The distinction between a-type and b-type polymers in σ versus ρ plots is unclear (Figure 5.4a). In contrast, all of the b-type polymers lie above a-type polymers in σ_r versus ρ plots (Figure 5.7). It is evident that factoring out the effect of the glass transition temperature clarifies the relationship between molecular structure and ion transport. At fixed distance from T_g, all b-type polymers have higher conductivity than the a-type polymers at all values of ρ. Figure 5.7 shows that at low ρ, 3b is as conductive as 1b and 2b, but above ρ = 0.08, the conductivity of 3b falls close to the a-type polymers. At low ρ, PEO is more conductive than the b-type polyesters above $\rho < 0.16$; these differences diminish with increasing salt concentration.

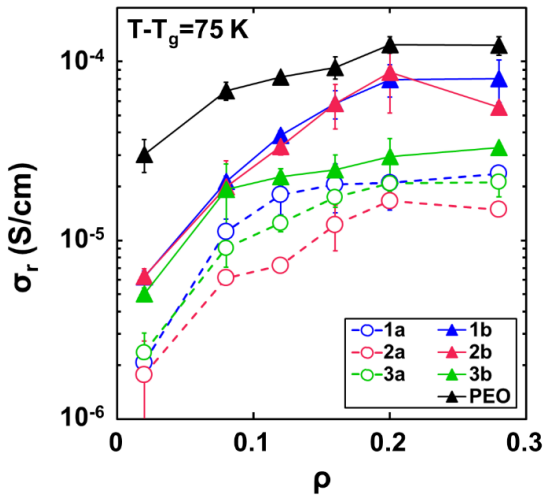

Figure 5.7. Reduced conductivity at T-T_g=75 K, or 1000/(T-T_g+50)=8 K^{-1}, as a function of ρ. Error bars have been adapted from the conductivity error (Figure 5.4a).

5.4 Conclusions

Ion transport in polymer electrolytes depends on a variety of interconnected factors: interactions between the polymer matrix and the salt species (dissociated and undissociated), extent of dissociation of the salt, and chain conformations and dynamics, i.e. segmental motion, in the vicinity of ions. Systematic changes in the monomer structure enable unraveling of these effects. Here, we study ion transport in a set of aliphatic polyester electrolytes and present an approach for analyzing conductivity data that provides insight regarding the relationship between monomer structure and ion transport.

We define a new variable for salt concentration, ρ, which enables collapse of both the σ and T_g measurements for all polymers. This allows us to extract information about the polymer-salt interactions and determine that some oxygens in the heavily functionalized polyesters are inaccessible. A Vogel-Tammann-Fulcher (VTF) analysis reveals the effect of different oxygens on ion transport: backbone ether oxygens enhance conductivity in the absence of sidechain ether oxygens. The VTF fits are used to calculate the reduced conductivity of our electrolytes, σ_r, wherein the effect of segmental motion is factored out. The a-type and b-type polymers are clearly segregated when compared on σ_r versus ρ plots, and PEO lies above the polyesters at all values of ρ. When segmental motion is factored out, the differences in reduced conductivity reflect differences in the dissociation of the salt, solvation environment of the cation, and ion hopping. Distinguishing between these factors will require input from other techniques such as neutron diffraction, NMR, and X-ray absorption spectroscopy. We hope to use these techniques in future studies to further our understanding of the relationship between monomer structure and ion transport in polymer electrolytes.

5.5 Acknowledgements

This research was supported by the National Science Foundation under DMREF Award Number NSF-CHE-1335486. DSC experiments were performed at the Molecular Foundry user facilities at Lawrence Berkeley National Laboratory supported by the Office of Science, Office of

Basic Energy Sciences, of the U.S. Department of Energy under Contract No. DE-AC02-05CH11231.

5.6 Nomenclature

PEO	poly(ethylene oxide)
LiTFSI	lithium bis(trifluoromethanesulfonyl) imide
NMP	N-methyl-2-pyrrolidone
DSC	differential scanning calorimetry
VTF	Vogel-Tammann-Fulcher
C_b	capacitance of the bulk electrolyte (F)
R_b	bulk electrolyte resistance (Ω)
Q_e	pseudo-capacitance of the electrodes (F)
L_c	apparatus inductance (H)
R_c	apparatus resistance (Ω)
l	electrolyte thickness (cm)
a	electrolyte area (cm^2)
σ	conductivity (S/cm)
σ_{max}	maximum conductivity (S/cm)
w	salt weight fraction
r	molar ratio of Li^+ to ether oxygens
ρ	molar ratio of Li^+ to monomer
M_n	number-averaged molecular weight (kg/mol)
$Đ$	polydispersity
T_g	glass transition temperature (°C)
ΔT_g	increase in T_g compared to neat polymer (°C)
T	temperature (°C)
T_o	reference temperature (°C)
R	universal gas constant (kJ/mol K)
A	VTF prefactor ($SK^{1/2}/cm$)
E_a	effective activation energy (kJ/mol)
σ_r	reduced conductivity (S/cm)

5.7 Supporting Information

5.7.1 Chain length considerations

In Table 5.S1, we report the molecular weight, monomer mass, and degree of polymerization of the neat polymers in our study. While the molecular weights fall in a narrow range (4.2-10.4 kg/mol), the degree of polymerization exhibits a much larger range (14-51). Given that the length of each monomer is 9 atoms, it is clear the length of the polymer chains in our study vary greatly. The ionic conductivity of polymer electrolytes are generally thought to be independent of molecular weight above 4 kg/mol based on studies performed in PEO.[58,104] However, a 4 kg/mol molecule of PEO corresponds to N=30, whereas in polymer 3a a molecular weight of 4 kg/mol is only N=14. Thus, due to the large monomer mass of our polyethers, this threshold may be higher in polyesters. The implications of this factor on our results is unknown. More work is needed to establish the molecular weight dependence of conductivity in different polymers.

We also report the concentration of end groups in terms of $\rho_{\text{end groups}}$ in Table 5.S1. In most cases, $\rho_{\text{end groups}} < 0.05$ which is fairly small compared to the range of salt concentrations in our study ($0.02 < \rho < 0.28$). However, in polymer 3a and 3b $\rho_{\text{end groups}}$ is large (0.14 and 0.10). Thus, there is potential for the end groups of the polymer to contribute to the solvation of the salt and the transport of ions in these materials. At this point, we do not know to what extent these end group effects are influencing our conductivity data.

Table 5.S1. Summary of molecular weight, M_n, monomer mass, M_0, and degree of polymerization, N, of each polymer. We use these parameters to calculate the concentration of end groups in each polymer, $\rho_{\text{end groups}}$.

Polymer	M_n (kg/mol)	M_o (g/mol)	N	$\rho_{\text{end groups}}$
PEO	5.0	133	38	0.05
1a	8.8	172	51	0.04
1b	6.7	174	38	0.05
2a	10.4	228	46	0.04
2b	8.9	230	39	0.05
3a	4.2	290	14	0.14
3b	6.1	292	21	0.10

5.7.2 Fitting Parameters E_a *and* A

Table 5.S2. Values of pseudo-activation energy, E_a, obtained from the VTF fits of the temperature dependent conductivity data for each electrolyte. Error corresponds to the standard error of E_a based on a fit of all data collected for a given electrolyte, which typically consists of three independent samples.

	ρ					
	0.02	**0.08**	**0.12**	**0.16**	**0.20**	**0.28**
PEO	7.1 ± 0.8	7.6 ± 0.6	8.1 ± 0.1	8.5 ± 0.3	8.4 ± 0.2	8.8 ± 0.1
1a	8.6 ± 0.2	8.9 ± 0.2	9.3 ± 0.2	9.6 ± 0.2	9.2 ± 0.2	9.4 ± 0.0
1b	10.7 ± 0.2	11.2 ± 0.1	10.1 ± 0.1	9.5 ± 0.2	8.9 ± 0.2	10.1 ± 0.3
2a	8.3 ± 0.5	8.4 ± 0.1	8.8 ± 0.1	8.7 ± 0.2	8.5 ± 0.1	8.9 ± 0.1
2b	8.7 ± 0.1	10.3 ± 0.3	11.0 ± 0.2	10.7 ± 0.3	9.6 ± 0.8	9.4 ± 0.1
3a	8.6 ± 0.3	9.2 ± 0.2	9.2 ± 0.1	9.4 ± 0.1	9.2 ± 0.1	9.4 ± 0.1
3b	9.2 ± 0.1	9.6 ± 0.3	9.6 ± 0.2	9.8 ± 0.1	9.8 ± 0.2	9.5 ± 0.0

Table 5.S3. Values of pre-exponential factor, A, obtained from the VTF fits of the temperature dependent conductivity data for each electrolyte. Error corresponds to the standard error of A based on a fit of all data collected for a given electrolyte, which typically consists of three independent samples.

	ρ					
	0.02	**0.08**	**0.12**	**0.16**	**0.20**	**0.28**
PEO	0.5 ± 1.6	1.8 ± 1.4	3.4 ± 1.1	5.8 ± 1.2	7.2 ± 1.2	10.6 ± 1.1
1a	0.1 ± 1.1	1.1 ± 1.1	2.5 ± 1.2	3.8 ± 1.2	2.6 ± 1.2	3.6 ± 1.0
1b	3.5 ± 1.2	18.8 ± 1.1	12.8 ± 1.2	10.2 ± 1.3	7.7 ± 1.4	25.4 ± 1.3
2a	0.1 ± 1.5	0.3 ± 1.1	0.6 ± 1.1	1.0 ± 1.2	1.1 ± 1.0	1.4 ± 1.0
2b	0.5 ± 1.1	7.7 ± 1.4	24.7 ± 1.3	31.4 ± 1.4	16.6 ± 2.3	8.8 ± 1.1
3a	0.2 ± 1.3	1.1 ± 1.2	1.5 ± 1.1	2.6 ± 1.1	2.5 ± 1.1	3.2 ± 1.1
3b	0.6 ± 1.1	3.6 ± 1.3	4.4 ± 1.2	5.5 ± 1.1	6.4 ± 1.2	5.8 ± 1.0

6 Universal Relationship between Conductivity and Solvation-Site Connectivity in Ether-Based Polymer Electrolytes[§]

ABSTRACT

We perform a joint experimental and computational study of ion transport properties in a systematic set of linear polyethers synthesized via Acyclic Diene Metathesis (ADMET) polymerization. We measure ionic conductivity, σ, and glass transition temperature, T_g, in mixtures of polymer and lithium bis(trifluoromethanesulfonyl) imide (LiTFSI) salt. While T_g is known to be an important factor in the ionic conductivity of polymer electrolytes, recent work indicates that the number and proximity of lithium ion solvation sites in the polymer also plays an important role, but this effect has yet to be systematically investigated. Here, adding aliphatic linkers to a poly(ethylene oxide) (PEO) backbone lowers T_g and dilutes the polar groups; both factors influence ionic conductivity. To isolate these effects, we introduce a two-step normalization scheme. In the first step, Vogel-Tammann-Fulcher (VTF) fits are used to calculate a temperature-dependent reduced conductivity, $\sigma_r(T)$, which is defined as the conductivity of the electrolyte at a fixed value of T-T_g. In the second step, we compute a non-dimensional parameter f_{exp}, defined as the ratio of the reduced molar conductivity of the electrolyte of interest to that of a reference polymer (PEO) at a fixed salt concentration. We find that f_{exp} depends only on oxygen mole fraction, x_o, and is, to a good approximation, independent of temperature and salt concentration. Molecular dynamics simulations are performed on neat polymers to quantify the occurrences of motifs that are similar to those obtained in the vicinity of isolated lithium ions. We show that f_{exp} is a linear function of the simulation-derived metric of connectivity between solvation sites. From the relationship between σ_r and f_{exp} we derive a universal equation that can be used to predict the conductivity of ether-based polymer electrolytes at any salt concentration and temperature.

6.1 Introduction

As the size and energy density of rechargeable lithium batteries continues to be pushed to the limit, the safety of the technology is of growing concern.[145,155] Solvent-free polymer electrolytes (SPEs) are of considerable interest as they offer improved thermal stability and reduced flammability compared to that of conventional organic solvent electrolytes.[114,156] The vast majority of research in the field of SPEs has focused on polyethers such as poly(ethylene oxide) (PEO),[23,28–30] which form stable complexes with alkali metal ions such as Li^+.[26,33,148] Amorphous mixtures of PEO and lithium salts exhibit reasonable ionic conductivities on the order of 10^{-3} S/cm at 90°C.

Substantial effort has been directed towards improving the conductivity of PEO through the incorporation of nanoparticles,[67,68,157,158] plasticizers,[64,159–164] or a second polymer blended into the

[§] This chapter was reported in *Macromolecules* **2016**, *49* (14), 5244–5255.

PEO matrix.[63,64,165] Alternative approaches involve altering the chemical structure of PEO by adding crosslinks,[19,65,66] changing the monomer chemistry,[37–39] incorporating co-monomers into the PEO backbone,[51,166,167] and modifying the architecture of the polymer chain.[40–42,66] However, these materials have not resulted in significant improvement of electrolyte performance or commercial impact, due in part to limited understanding of the molecular mechanisms underpinning ion transport.

We recently identified that the addition of groups that do not interact with the lithium ion can dilute and alter the sites in which a lithium ion can be solvated, leading to overall reductions in ionic conductivity.[127,168] For a set of polyesters, the significantly higher conductivity of PEO relative to that of a set of polyesters was explained using the concept of solvation-site *connectivity*, quantified using molecular simulation by the number and proximity of solvation sites in the polymer matrix.[127] For a series of polyethers, a low density of solvation sites resulted in slow rates of lithium ion hopping.[168] The role of spacing between coordinating centers has also been alluded to recently in the context of poly(ether-thioethers).[75]

In this work, we use experiments and simulations to quantify the relationship between conductivity and solvation-site connectivity in a set of polyethers in which ethylene oxide (EO) segments are regularly interrupted with carbon linkers of varying lengths (Figure 6.1). The polymers, labeled as C_xEO_y, are distinguished by *x*, the number of carbon atoms in the carbon linker, and *y*, the number of consecutive EO monomers in the PEO segment. We show that the conductivity of C_xEO_y electrolytes can be calculated using the known conductivity of PEO electrolytes and a multiplicative correction factor that depends only on oxygen mole fraction. The same correction factor applies to the entire set of electrolytes, irrespective of temperature and salt concentration. Simulations show that introducing carbon linkers of varying lengths and frequencies affects solvation-site connectivity. The experimentally determined correction factor is shown to arise due to this connectivity.

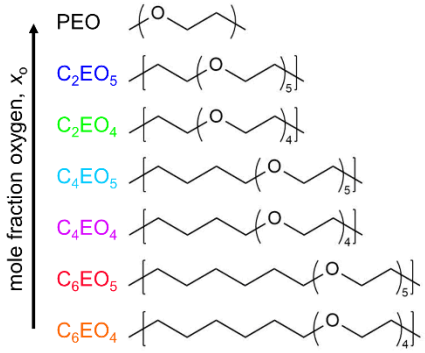

Figure 6.1. Structure of the C_xEO_y polyethers synthesized and characterized in this study. The naming convention specifies x, the length of the carbon linker, and y, the number of consecutive EO monomers on each segment.

6.2 Experimental and Simulation Methods

6.2.1 Polymer Synthesis and Characterization

We synthesized the polyethers shown in Figure 6.1 via Acyclic Diene Metathesis (ADMET) polymerization,[167] followed by hydrogenation with Crabtree's catalyst (Figure 6.2). The diene terminated monomers were synthesized in one step from the facile substitution reaction of the

commercially available poly(ethylene glycol) (PEG) oligomers (tri-, or tetraethylene glycol) with allyl bromide and 5-bromo-1-pentene to yield the C_2EO_y and C_6EO_y monomers respectively. The C_4EO_y monomers were synthesized by mesylating PEG oligomers first and subsequently reacting with 3-butene-1-ol. This alternative procedure was used because the elimination reaction between PEG oligomers and 4-bromo-1-butene significantly lowered the yields of the desired product. The C_xEO_y monomers were then polymerized with Grubbs' first-generation catalyst. The Grubbs' catalyst was used because of its high functional group tolerance and reduced propensity for olefin isomerization reactions.[169] The synthesized unsaturated polyethers were hydrogenated using Crabtree's catalyst to yield the saturated polyethers for this study.

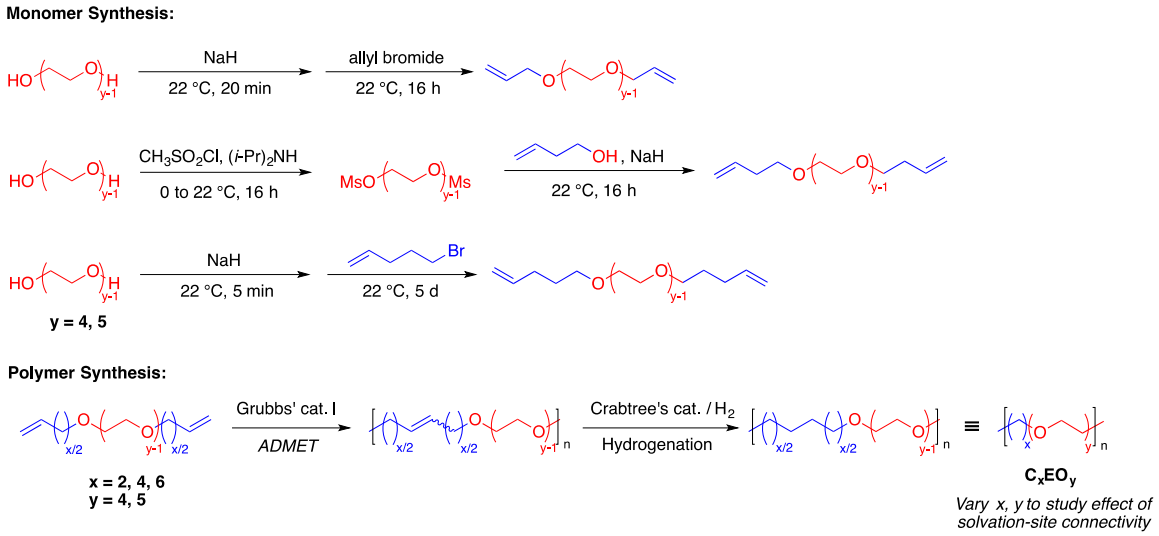

Figure 6.2. Synthesis of C_xEO_y monomers and polymers via Acyclic Diene Metathesis (ADMET) polymerization followed by hydrogenation.

The C_xEO_y polymers synthesized in this study are characterized with gel permeation chromatography (GPC) for the number-averaged molecular weight (M_n) and polydispersity index ($Đ$). Thermal properties of the C_xEO_y polymers are measured with differential scanning calorimetry. The results are summarized in Table 6.1, along with the properties of PEO, which was commercially purchased from Polymer Source. The M_ns of the polymers range between 4.7 and 19.0 kDa (Table 6.1); in this range we expect ionic conductivity to be independent of M_n.[58] The reactivity of the monomers showed some dependence on the number of carbons in the linker with the longest linker (C_6) yielding the polymer with highest M_n. This trend is consistent with the literature on ADMET polymerization of oxygen-containing dienes using Schrock-type catalysts.[170,171] The glass transition temperatures, T_g, of C_2EO_4 (–72.8°C) and C_2EO_5 (–67.0°C) are lower than that of PEO (–60.0°C) likely due to the increased chain flexibility of the carbon linkers. The level of crystallinity in the neat C_4EO_y and C_6EO_y precluded the observation of a T_g, but we expect that those values would decrease as the linker length increases. All of the C_xEO_y polyethers synthesized have a significantly lower T_m relative to PEO.

The mole fraction of oxygen, x_o, in each polymer is calculated according to eq. 6.1,

$$x_{\mathrm{o}} = \frac{\text{oxygen atoms in repeat unit}}{\text{total atoms in repeat unit}}. \quad (6.1)$$

The number of atoms in the repeat unit excludes hydrogen atoms. Values for x_o for each polymer are shown in Table 6.1.

Table 6.1. Properties of C_xEO_y polymers and polyethylene oxide (PEO).

Polymer[a]	M_n (kg/mol)	$Đ$	T_g (°C)	T_m (°C)	ΔH_f (J/g)	x_o
PEO	5.0	1.1	–60.0[c]	60.0[c]	193.0[c]	0.333
C_2EO_4	7.4	1.3	–72.8	–2.8	98.6	0.286
C_2EO_5	6.7	1.5	–67.0	–4.5, 9.0	16.6, 18.4	0.294
C_4EO_4	4.7	1.4	*n.d.*[b]	13.4	118.4	0.250
C_4EO_5	7.1	1.6	*n.d.*[b]	8.0	132.9	0.263
C_6EO_4	12.9	1.8	*n.d.*[b]	24.7, 33.4	144.2, 170.7	0.222
C_6EO_5	19.0	1.8	*n.d.*[b]	23.4	115.3	0.238

[a]See SI of ref 103 for synthesis details. [b]*n.d.* = not detected. [c]The DSC and conductivity measurements are performed on 4.6 kg/mol and 5.0 kg/mol PEO, respectively.

6.2.2 Experimental Characterization

Electrolyte preparation is performed inside of an argon glovebox (MBraun) in order to maintain water and oxygen levels below 1 ppm and 10 ppm respectively. The polyethers synthesized in this study, along with PEO, are dried under vacuum at 90°C for 12 h prior to entering the glovebox. Mixtures of polymer and lithium bis(trifluoromethanesulfonyl) imide (LiTFSI) salt (Novalyte) are dissolved in anhydrous dimethylformamide (DMF) and stirred at 90°C for a minimum of 3 h to form a homogeneous solution. The DMF is then evaporated from the solution, and the polymer/salt mixture is transferred to the glovebox antechamber and dried under vacuum for 8 h at 90°C to remove any excess solvent. Electrolytes are prepared at varying salt concentrations, ranging from $r = 0.06$ to $r = 0.14$, where $r = [Li^+]/[O]$ is the molar ratio of lithium ions to ether oxygens. Electrolytes for C_4EO_5, C_4EO_4 and C_6EO_5 at $r = 0.14$ were not prepared due to limited material.

Stainless steel symmetric cells are prepared for ionic conductivity measurements of electrolytes using ac impedance spectroscopy. Samples are made by pressing the polymer electrolyte into a 254 µm thick silicone spacer and sandwiching between two 200 µm stainless steel electrodes. With the exception of crystalline PEO, all electrolytes are in the form of highly viscous liquids and are soft enough to be pressed at room temperature. The silicone forms a good seal with stainless steel thereby preventing the electrolytes from leaking out of the cell during characterization. A micrometer is used to obtain the thickness of the electrolyte by measuring thickness of the cell and subtracting the thickness of the electrodes. Aluminum tabs are secured to the electrodes to serve as electrical contacts. The assembly is vacuum sealed in a laminated aluminum pouch material (Showa-Denko) before removing from the glovebox for electrochemical characterization.

All reported conductivity results are based on ac impedance spectroscopy performed with a Biologic VMP3 potentiostat which acquires complex impedance measurements for a frequency

range of 1 Hz to 1 MHz at an amplitude of 80 mV. The low-frequency minimum on the Nyquist impedance plot is taken to be the electrolyte resistance, R, which is used along with electrolyte thickness, l, and electrolyte area, a, to calculate the electrolyte conductivity, σ, according to eq. 6.2,

$$\sigma = \frac{l}{a\,R_b}. \tag{6.2}$$

The inner diameter of the spacer, 3.175 mm, is used to calculate a. Thickness, l, is taken to be the final thickness of the electrolyte, measured after conductivity measurements are completed. On average, the electrolyte thickness decreased 3.5% after annealing. The symmetric cells are disassembled to allow for visual inspection of the electrolyte. Any samples that exhibited bubbles or voids in the polymer are discarded from the set, as such defects would alter the electrolyte volume and produce inaccurate conductivity results. Fewer than 5% of samples prepared in this study exhibited such characteristics. The conductivity for each electrolyte is determined by averaging the results from three different samples, and the error bars signify the standard deviation of these measurements. The conductivity of the neat polymer is subtracted from that of the salt-containing electrolytes to account for ionic impurities that may be present. The conductivity at r = 0 at 90°C were below 10^{-5} S/cm for all of the polymers in this study.

DSC experiments are performed on a TA Instruments DSC Q200 instrument to obtain the T_g and T_m of each electrolyte. DSC samples are prepared inside of the glovebox, where aluminum pans are filled with 1-5 mg of electrolyte and hermetically sealed before removing from the glovebox. The following protocol is used for the temperature scan: heat to 110°C at 20°C/min, cool to -90°C at 5°C/min, heat to 110°C at 20°C/min. Values for T_g and T_m are obtained from the second heating scan. DSC measurements are repeatable within 1.0°C.

6.2.3 Molecular Dynamics Simulations

All MD simulations employ a united atom force field, with bonding parameters taken from CHARMM[172] and all other parameters taken from the TraPPE-UA force field;[173] compatible lithium ion parameters are obtained from a previous simulation study.[174] Force field parameters used in this study are provided in SI-2. All simulations are performed using the LAMMPS simulation package[175] with GPU acceleration.[176,177] The equations of motion are evolved using the velocity-Verlet integrator with a 1 fs time step. Particle-particle-particle mesh Ewald summation[176] is used to compute all nonbonded interactions beyond a 14 Å cutoff. The Nosé-Hoover (100 fs relaxation) and Nosé-Hoover barostat (1000 fs relaxation) are used in all simulations to control the temperature and pressure.

Two sets of simulations are performed for the C_xEO_y polymers. For polymers with x = 2, 4, and 6 and y = 3–8, neat-polymer simulations are used to obtain polymer properties and solvation-site connectivity metrics. For polymers with x = 2 and y = 3–8, simulations of a single lithium cation diffusing in a polymer are used to investigate the lithium ion solvation environment.

For the neat-polymer simulations, four independent copies of the simulation cell are generated for each polymer studied. Each copy consists of a single, long polymer chain (M_n ~ 25 kg/mol) with an initial configuration generated via a self-avoiding random walk. For the ion-containing simulations, the same procedure is used, except that a single lithium cation is randomly placed in the simulation cell, and the total charge of the system is neutralized with a uniform background

charge.[178] To generate starting configurations for MD production runs, the systems are equilibrated in five steps. In step 1, the initial configuration is relaxed for 10,000 steps with nonperiodic boundary conditions using steepest descent energy minimization with the maximum atom displacement limited to 0.1 Å for any given step. In step 2, the system is annealed at 726.85°C with periodic boundary conditions using 100,000 steps of Langevin dynamics with a 100 fs damping factor. In step 3, the simulation cell is adjusted at a constant rate over 500 ps at 226.85°C to achieve a cubic simulation cell with a density of 1.0 g/cm^3. In step 4, the system is annealed for 1.5 ns at 226.85°C and 1 atm. In step 5, the system is equilibrated for 10 ns at 90°C and 1 atm. A similar protocol was employed in reference 168.

Following equilibration, production runs of 10 ns for the neat-polymer simulations and of 150 ns for the ion-containing systems are performed at 90°C and 1 atm.

6.3 Results and Discussion

6.3.1 Experimental Characterization

The ionic conductivity, σ, of the C_xEO_y polyethers and PEO was measured as a function of temperature, T, in the range of 27–110°C. Figure 6.3 shows the results at a fixed salt concentration, r = 0.08, which is in the vicinity where PEO conductivity is maximized.[28] Results from Figure 6.3 indicate that the σ of the C_xEO_y polyethers are within one order of magnitude of PEO at all temperatures. The relative ordering of the polymers does not change significantly as T is varied. We observe that at any given T, C_2EO_5 and PEO exhibit the highest σ, which are comparable within error. Of the polyethers synthesized in this study, C_2EO_5 has the shortest carbon linker (two) and the longest consecutive segment of ethylene oxide (EO) monomers (five); thus, C_2EO_5 has the largest mole fraction of oxygen, x_o (Table 6.1), of the C_xEO_y polymers. Similarly, C_6EO_4 has the lowest x_o and exhibits the lowest σ. As one might anticipate, results from Figure 6.3 suggest that there is a relationship between the x_o and σ.

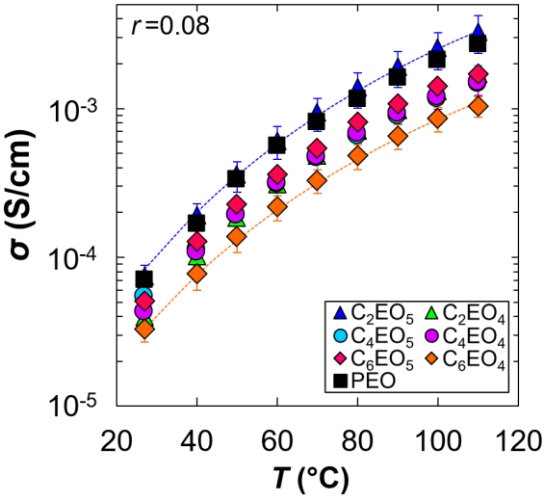

Figure 6.3. Conductivity, σ, with increasing temperature at r = 0.08.

To further explore this relationship, in Figure 6.4a we plot σ of the C_xEO_y polyethers and PEO as a function of x_o at r=0.08 and 90°C. The measured conductivities of the polymers are within a narrow range between 6.5 × 10^{-4} S/cm and 1.7 × 10^{-3} S/cm. In some cases, increasing the linker

length increases σ (C_2EO_4 vs. C_4EO_4), while in other cases it decreases σ (C_2EO_5 vs. C_4EO_5). Similarly, an additional consecutive EO unit in the monomer may either increase σ (C_2EO_4 vs. C_4EO_5) or decrease σ (C_4EO_4 vs. C_4EO_5). The lack of clear trends in this data most likely results from two competing effects upon the addition of carbon linkers. Namely, the presence of the linkers dilutes the density of lithium ion solvation sites (making hopping between sites less probable) but simultaneously changes the thermal properties of the polymer melt. Figure 6.4b shows the glass transition temperature, T_g, of the C_xEO_y and PEO electrolytes at a salt concentration of r = 0.08. It is evident that decreasing x_o decreases T_g due to increased chain flexibility. It is generally accepted that more flexible chains promote ion transport due to rapid segmental motion.[23,179–182]

In an attempt to decouple the effects of solvation-site density and segmental motion, we calculate a reduced conductivity, σ_r. Similar approaches have been used previously in analysis of experimental data from polymer electrolytes.[28,35,104,105] To calculate σ_r we use a modified Vogel-Tammann-Fulcher (VTF) equation where the temperature is defined to be a fixed distance (75 K) above the measured T_g of the electrolyte,

$$\sigma_r = A\,(T_g + 75\text{ K})^{-1/2}\exp\left(\frac{-E_a}{R(125\text{ K})}\right). \tag{6.3}$$

The two dotted curves in Figure 6.3 show VTF fits for C_2EO_5 and C_6EO_4 (other fits are omitted for clarity). These fits enable estimation of a pseudo-activation energy, E_a, and a prefactor, A. Figure 6.4c shows σ_r of the C_xEO_y polyethers and PEO as a function of x_o. Once the contribution from T_g differences is corrected for, it becomes clear that the reduced conductivity is a monotonically increasing function of x_o. In other words, decreasing the linker length or the addition of an EO unit leads to an increase in σ_r. Since the VTF curves for the polymers are essentially parallel, the dependence of σ_r on x_o is qualitatively similar to that seen in Figure 6.4c at all values of T-T_g. All of the electrolytes in Figure 6.4c have a fixed salt concentration of r = 0.08; as r = $[Li^+]/[O]$, electrolytes with a lower x_o value will typically have fewer salt molecules per unit volume. Consequently, it is unclear whether the trend observed in Figure 6.4c is due to changes in molecular structure or simply results from changes in volumetric density of charge carriers in the electrolytes.

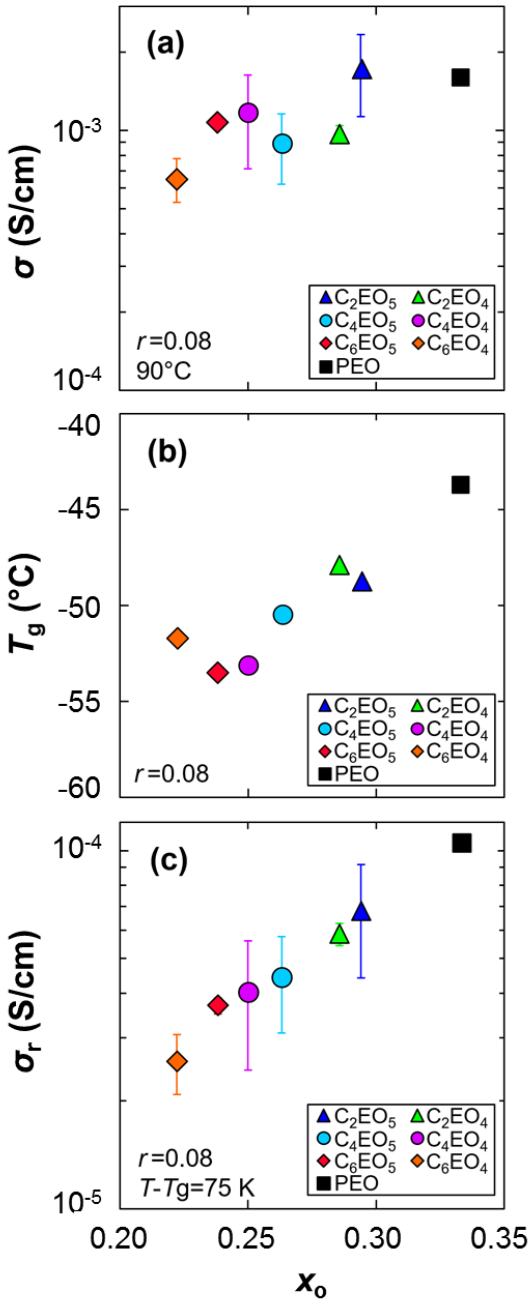

Figure 6.4. (a) Conductivity, σ, at 90°C, (b) glass transition temperature, T_g, and (c) reduced conductivity, σ_r, with increasing mol fraction of oxygen atoms, x_o, on the polymer backbone. All data is collected at a salt concentration of r = 0.08.

To isolate the effect of monomer structure on conductivity, we define a new variable that we call the experimental connectivity, f_{exp}:

$$f_{\mathrm{exp}} = \left(\frac{\sigma_{\mathrm{r}}}{\sigma_{\mathrm{r,PEO}}}\right)_{r,T-T_{\mathrm{g}}} \left(\frac{x_{\mathrm{o,PEO}}}{x_{\mathrm{o}}}\right). \tag{6.4}$$

The ratio of $\sigma_r / \sigma_{r,PEO}$ at a given r and T-T_g quantifies the conductivity of a C_xEO_y electrolyte relative to that of PEO, correcting for the different T_g values of the C_xEO_y electrolyte. The ratio of $x_{o,PEO} / x_o$ represents the ratio of the moles of salt in a C_xEO_y electrolyte relative to that of PEO, given that $r = [Li^+]/[O]$, approximately correcting for differences in the volumetric density of salt (see the SI). The use of mole fractions in eq. 6.4 requires two main assumtions: (1) the salt does not contribute to the overall volume and (2) all atom moeities (i.e., O or CH_2) have the same partial molar volume. Eq. 6.4 is similar to the expression for conductivity in block copolymer systems where a morphology factor is used to describe the constraints on ion transport imposed by the geometry of the conducting phase.[183–185] The strategy is also somewhat similar to work that compared conductivities of liquid electrolytes at the same dielectric constant,[186] but here we compare conductivities in ether-based polymer electrolytes at the same r and T - T_g.

Figure 6.5 is a plot of f_{exp} versus x_o. This plot shows that f_{exp} increases monotonically with increasing x_o. Since other effects have been factored out, the change in f_{exp} with x_o is attributed to changes in the local environment of the lithium ion. As x_o is decreased, there are likely more carbon linker segments and fewer EO segments in the vicinity of each solvated lithium ion. Assuming the carbon linkers are ionically insulating, polymers with a lower x_o are expected to exhibit slower lithium ion diffusion, as it takes longer for the ion to hop to an adjacent solvation site. Thus, f_{exp}, is an experimentally determined quantity that is expected to report on the proximity of lithium ion solvation sites.

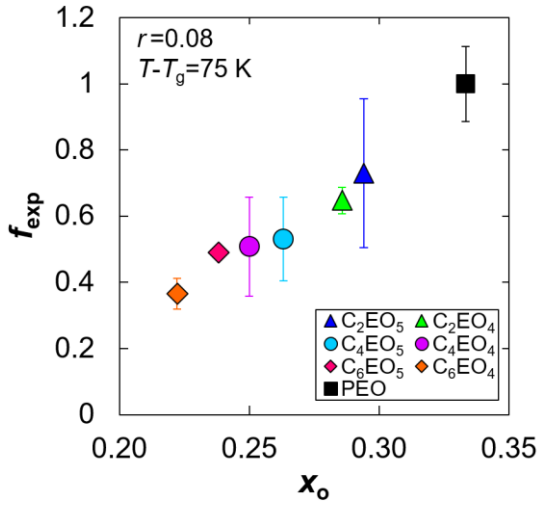

Figure 6.5. Experimental connectivity, f_{exp}, with increasing x_o at r = 0.08 and T-T_g = 75 K.

In Figure 6.6a, we plot f_{exp} versus x_o at r = 0.08 and different reduced temperatures. We find that there is a linear relationship between f_{exp} versus x_o that is, to a good approximation, independent of T - T_g. To investigate the behavior of f_{exp} across different salt concentrations, the analysis was repeated at different values of r, and the results for f_{exp} values are shown in Figure 6.6b. Data for σ, T_g, and σ_r at all salt concentrations used to obtain the f_{exp} values in Figure 6b are provided in SI. In Figure 6.6c we show results for f_{exp} at all values of r at different reduced temperatures. All data in Figure 6.6 is consistent with a line,

$$f_{exp} = 5.39x_o - 0.86, \tag{6.5}$$

obtained by a linear fit of the data in Figure 6.6c.

Figure 6.6 provides justification for the normalization scheme used in this study. It is evident from Figure 6.6 that when polymer electrolytes are compared using σ_r and differences in the volumetric density of salt are factored out using x_o, ion transport is related to a parameter (f_{exp}) that is largely independent of temperature and salt concentration. It appears as though f_{exp} is an intrinsic property of the neat polymer in the absence of salt.

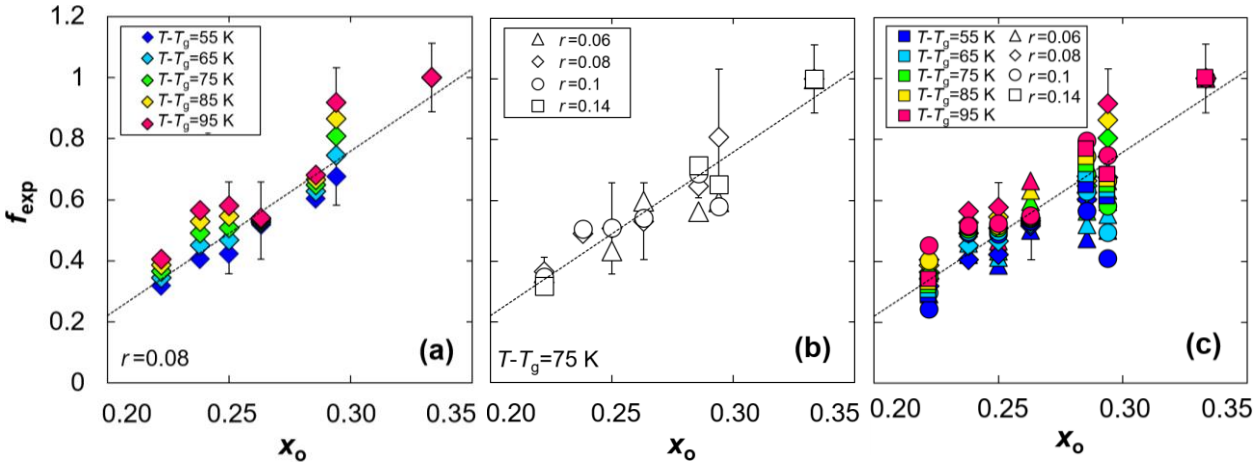

Figure 6.6. Experimental connectivity, f_{exp}, with increasing x_o at varying (a) T - T_g, (b) r, and (c) T - T_g and r. The green diamonds in (a) and (c) and the white diamonds in (b) show the data from Figure 6.5 with r = 0.08 and T-T_g = 75 K; error bars are only shown for this set of data. The dashed line is the same in all three figures and represents the best linear fit of the data in (c), given by eq. 6.5. The correlation coefficients for the linear fits are 0.87, 0.90, and 0.85 for (a-c), respectively.

6.3.2 Molecular Dynamics Simulations

We now use MD simulations to further understand how varying the composition of the C_xEO_y polymers affects lithium ion solvation and polymer properties, including the connectivity between possible lithium ion solvation sites.

Figure 6.7 presents an analysis of the lithium ion solvation environments observed during MD simulations of the C_2EO_y polymers in the presence of an isolated lithium ion. Representative snapshots of the lithium ion solvation shell are shown in Figure 6.7a. In all cases, the lithium ion coordinates with one or two contiguous sequences of oxygen atoms, which is similar to coordination environments previously observed in PEO.[23,127,187] While complexation by a single contiguous sequence of oxygen atoms is expected to be difficult in the presence of carbon linkers, the snapshots for C_2EO_3 and C_2EO_4 depict configurations for which the lithium cation indeed coordinates with oxygen atoms separated by a linker. In general, the snapshots display strikingly similar solvation environments in terms of the number of coordinating oxygen atoms despite the changing frequency of the C_2 linker. This is confirmed in Figure 6.7b, which shows the lithium-oxygen cumulative distribution function (CDF), and in Figure 6.7c, which presents the frequency with which different lithium ion binding motifs are observed in the simulations. Both Figure 6.7b and Figure 6.7c indicate that lithium ions in the C_2EO_y polymers are coordinated by five or six oxygen atoms, irrespective of the number consecutive EO units; similar findings are anticipated for the C_4 and C_6 linkers based on previous simulation studies.[127,168]

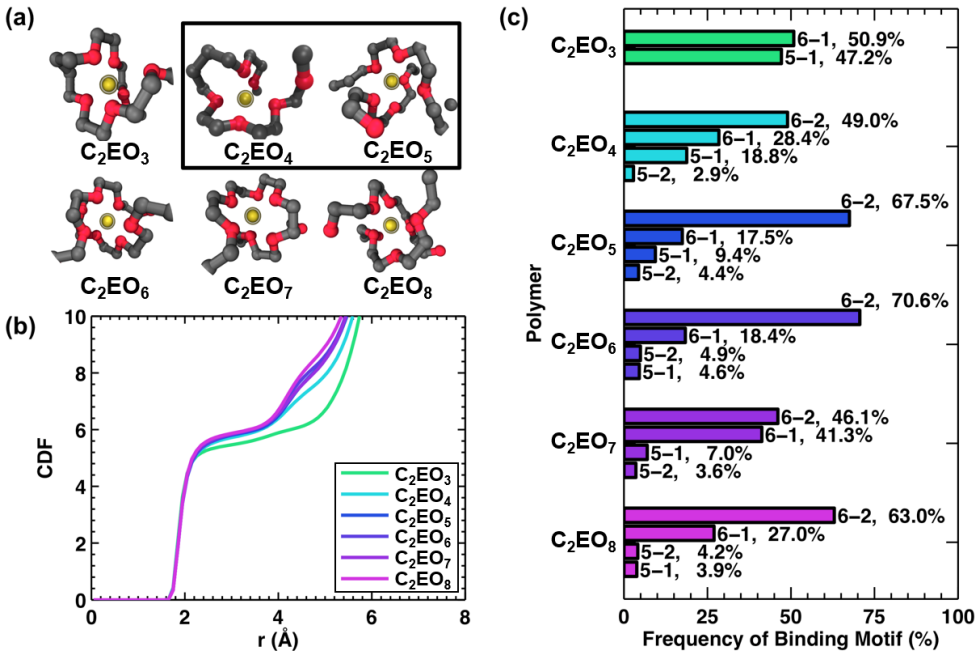

Figure 6.7. Analysis of the lithium ion solvation environment for polymers with C_2 linkers between EO repeat units. **(a)** Simulation snapshots of representative lithium ion solvation structures in polymers with different numbers of repeating EO units. The boxed snapshots correspond to polymers that have experimental data. **(b)** The cumulative number of oxygen atoms as a function of distance from the lithium ion, given by the lithium-oxygen cumulative distribution function (CDF). **(c)** Frequency of occurrence of observed lithium ion binding motifs. The first number indicates the number of oxygen atoms that are within 3.25 Å of the lithium ion; the number after the dash refers to the number of different contiguous polymer chain segments.

We now focus on neat-polymer simulations, i.e. in the absence of the lithium ion, to examine how the addition of carbon linkers affects both the thermal properties of the polymer as well as the distribution of lithium ion solvation sites. Figure 6.8 compares these two properties obtained for the expanded set of polymers (C_xEO_y for x = 2, 4, and 6 and y = 3-8). Figure 6.8a shows that the bulk modulus, B, at 90 °C for the polymers generally increases with increasing x_o. The polymers with C_2 linkers have larger bulk moduli than those with C_4 and C_6 linkers, and PEO (black square) possesses the largest bulk modulus among all the polymers characterized. These results are qualitatively consistent with the experimental observations in Figure 6.4b that the T_g of the electrolytes generally increases with x_o and decreases with increasing linker length.

In contrast to Figure 6.8a, Figure 6.8b shows that the average nearest-neighbor distance, $\langle r_{nn} \rangle$, between lithium ion solvation sites generally decreases with increasing x_o. Here, a solvation site is defined at the centroid of a set of five or more oxygen atoms if each oxygen is also within 3.5 Å of the centroid; two sites are combined if the distance between their centroids is less than r_{min}=1 Å. The figure shows that modifying the number of contiguous EO units and the length of the linker directly influences the number and proximity of solvation sites. Notably, PEO has the shortest average distance between neighboring lithium ion solvation sites. Figure 6.8a and 6.8b combine to highlight a difficulty in designing polymers with enhanced cation diffusivity since increasing the number and proximity of lithium ion solvation sites often increases polymer stiffness, in accordance with the experimental observations in Figure 6.4a.

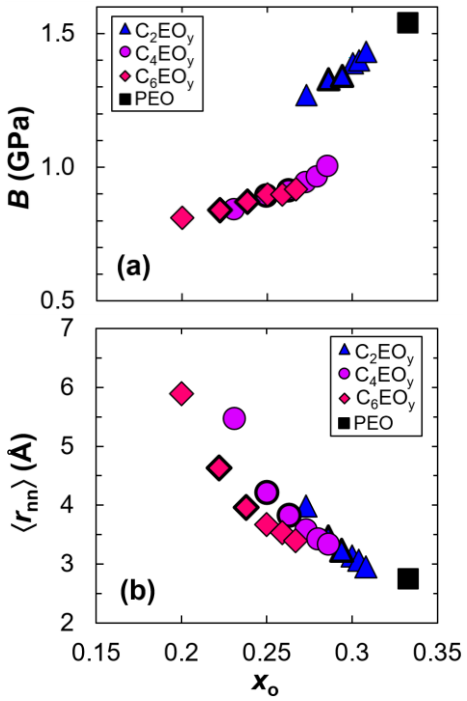

Figure 6.8. Variation of (a) the polymer bulk modulus, *B*, at 90°C and (b) the average nearest-neighbor separation distance between solvation sites, $\langle r_{nn} \rangle$, as a function of x_o for polymers with different linkers. In both (a) and (b), polymers with different linkers are denoted by different symbols. Markers with bold outlines indicate polymers that were also experimentally characterized.

Previous work introduced solvation-site connectivity as an intuitive means of explaining trends in conductivity.[127] To examine this effect for the C_xEO_y polymers, Figure 6.9 compares the distribution and proximity of solvation sites for PEO, which is the most conductive polymer in Figure 6.4c, and C_6EO_4, which is the least conductive. Figures 6.9a and 6.9d depict representative snapshots of the neat PEO and C_6EO_4 melts, respectively. Solvation sites in these snapshots are depicted as blue spheres in Figures 6.9b (PEO) and 6.9e (C_6EO_4). Figures 6.9c and 6.9f depict edges connecting the solvation sites within a cutoff distance, r_{cut}=3 Å. Comparing Figure 6.9b and 6.9e reveals that introduction of the C_6 linker decreases the density of solvation sites in the polymer. Moreover, comparing Figure 6.9c and 6.9f illustrates that C_6EO_4 has far fewer edges than PEO. Because hopping among solvation sites is a primary mode of lithium ion transport and hopping is typically limited to distances less than 3 Å,[23,168] having fewer edges between solvation sites is expected to reduce the overall rate of lithium ion diffusion.

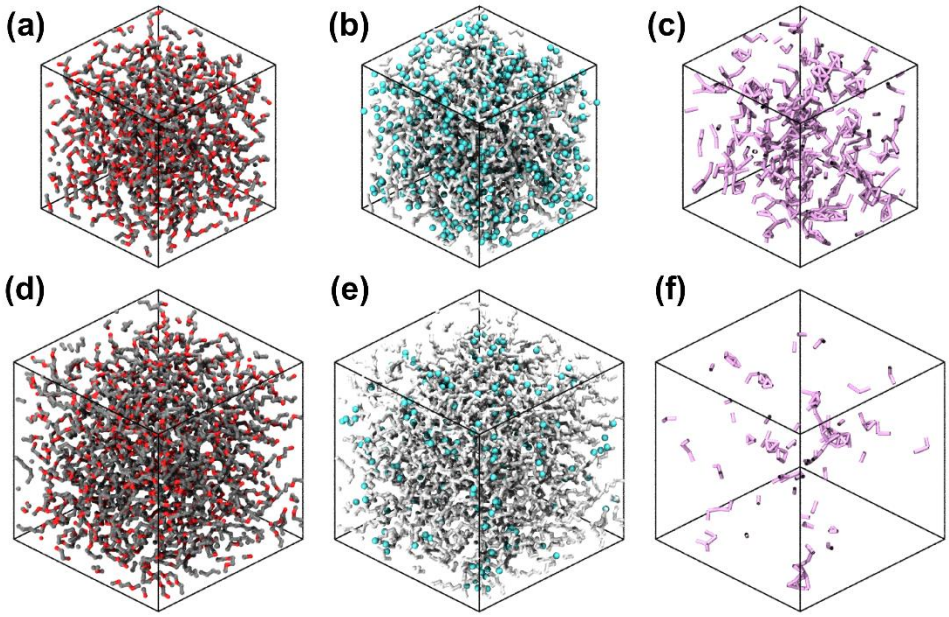

Figure 6.9. A comparison between simulation snapshots for (a-c) PEO and (d-f) C_6EO_4 showing (a, d) a representative configuration of the neat polymer melt; (b, e) possible lithium ion solvation sites within the melt; and (c, f) edges less than 3 Å in length between the solvation sites in (b, e). In (a, d) carbon atoms are gray, and oxygen atoms are red. In (b, e), all polymer atoms are light gray while the solvation sites are depicted as blue spheres. In (c, f), edges between solvation sites are depicted as purple bonds while the polymer is not shown for clarity. The various simulation snapshots have the same size scale; the difference in size between the simulation box for PEO and that of C_6EO_4 is due to the latter having a larger number of atoms and a lower density.

From Figures 6.6, 6.8b, and 6.9, it is clear that x_o plays an important role in both the solvation-site connectivity as well as f_{exp}. To further establish the relationship between solvation-site connectivity and f_{exp}, we examine three possible metrics for characterizing the solvation-site connectivity from the simulations, including κ (the volumetric density of edges between solvation sites), λ (the linear density of edges projected along a given linear direction), and $\exp[-\langle r_{nn}\rangle]$ (a proportionality to a characteristic hopping rate). Figure 6.10 provides a visual representation of these metrics for PEO. The first metric, κ (Figure 6.10a), is computed using

$$\kappa = \frac{1}{V}\sum_{i<j} H\left(r_{\text{cut}} - r_{ij}\right), \tag{6.6}$$

where V is the volume of the simulation cell, the summations run over pairs of solvation sites in the simulation cell, and $H(r)$ is the typical Heaviside step function. Similarly, the second metric, λ (also shown in Figure 6.10a), is computed using

$$\lambda = \frac{1}{L_u}\sum_{i<j} H\left(r_{\text{cut}} - \sqrt{\boldsymbol{r}_{ij}\cdot\boldsymbol{u}}\right), \tag{6.7}$$

where L_u is the length of a given linear dimension in the simulation cell, $\boldsymbol{u}$ is a unit vector in the direction of that linear dimension, and $\sqrt{\boldsymbol{r}_{ij}\cdot\boldsymbol{u}}$ is the magnitude of the distance vector $\boldsymbol{r}_{ij}$ projected onto $\boldsymbol{u}$. The third metric, $\exp[-\langle r_{nn}\rangle]$ (Figure 6.10b), is expected to be proportional to a characteristic hopping rate between solvation sites separate by $\langle r_{nn}\rangle$, which is computed using

$$\langle r_{\mathrm{nn}} \rangle = \frac{1}{N} \sum_{i} \min_{j>i} [r_{ij}] \,, \tag{6.8}$$

where N denotes the number of solvation sites in the simulation cell. All three quantities are likely to increase if the number of sites increases or the distance between solvation sites decreases, and so each reasonably reports on the concept of connectivity.

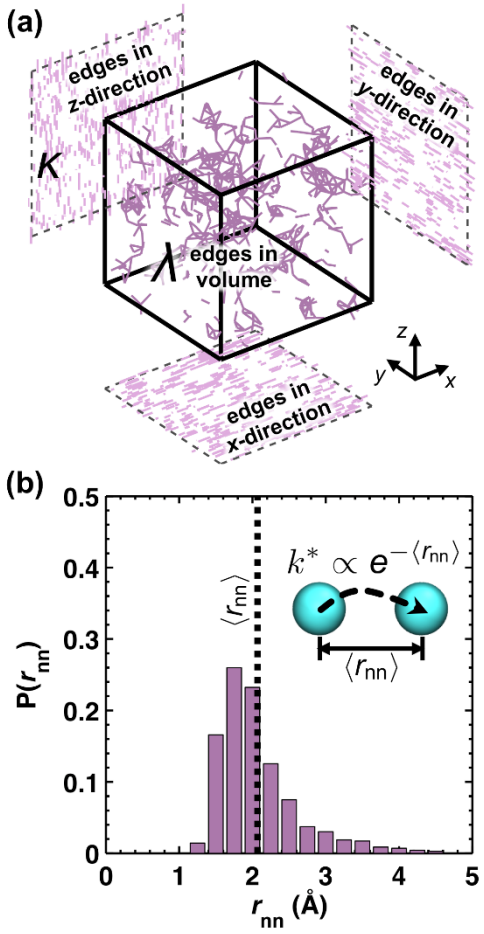

Figure 6.10. The relationship between connectivity metrics in PEO. (a) Edges between solvation sites in the simulation cell, which defines the volumetric edge density κ, and projections of the edges in the x-, y-, and z- directions, which define the linear edge density λ. (b) The distribution of nearest-neighbor separation distances, which defines the average nearest-neighbor separation distance $\langle r_{\mathrm{nn}} \rangle$ used to compute a characteristic hopping rate $\exp[-\langle r_{\mathrm{nn}} \rangle]$.

Figure 6.11 presents the dependence of all three metrics for characterizing the connectivity on x_o. All of the metrics, which are normalized with respect to PEO, increase with increasing x_o for a given linker. This is sensible because the number of consecutive EO units is increasing, making lithium ion solvation sites more prevalent. It is interesting to note that polymers with C_6 linkers are characterized by higher connectivity than polymers with C_4 or C_2 linkers when the oxygen mole fraction is comparable, up to $x_o = 0.27$. This is likely because the C_6EO_y polymers require more contiguous EO units to achieve the same oxygen mole fractions as the polymers with shorter linkers.

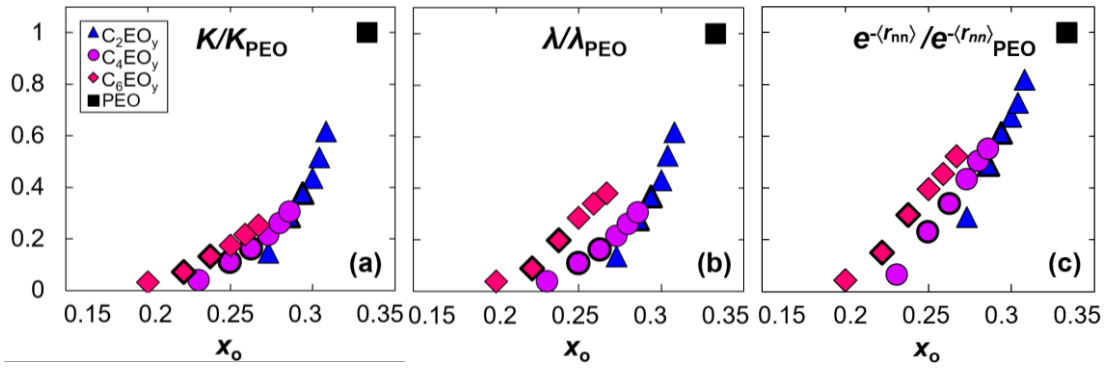

Figure 6.11. Analysis of simulated connectivity metrics as a function of x_o for polymers with different linkers, including (a) κ, the volumetric connectivity (number of edges between solvation sites per unit volume), (b) λ, the linear connectivity (number of edges between solvation sites per unit length), and (c) $\exp[-\langle r_{nn}\rangle]$, a characteristic distance-dependent proportionality for the lithium ion hopping rate. Each metric is normalized by the corresponding value for PEO. In all panels, polymers with different linkers are denoted by different symbols. Markers with bold outlines indicate polymers that were also experimentally characterized.

6.3.3 Comparison of Experiment and Simulations

Figure 6.12 directly examines the correlation between the experimentally calculated f_{exp} and the theoretically derived connectivity metrics. The linear fits shown in Figure 6.12a-c quantify the relationship between f_{exp} and connectivity. The relationships thus obtained are

$$f_{\text{exp}} = a_i + m_i C_i \;\; (i = 1 - 3), \tag{6.9}$$

where C_i represent the three connectivity metrics ($C_1 = \kappa/\kappa_{PEO}$, $C_2 = \lambda/\lambda_{PEO}$, $C_3 = \exp[-\langle r_{nn}\rangle]/\exp[-\langle r_{nn}\rangle_{PEO}]$). The fits give ($a_1 = 0.34$, $m_1 = 0.69$), ($a_2 = 0.31$, $m_2 = 0.72$), and ($a_3 = 0.30$, $m_3 = 0.71$). To a good approximation the relationship between f_{exp} and the connectivity metrics is linear with an intercept of 0.32 and a slope of 0.71 (average values of a_i and m_i, respectively). The behavior of the ether-based electrolytes in the low C_i limit remains an interesting open question. One may expect f_{exp} to approach zero as C_i approaches zero, but the data in Figure 6.12 extrapolates to a finite positive value (0.32) as C_i approaches 0. One possibility is that the linear relationships in Figure 6.12 breaks down at $0 < C_i < 0.15$, perhaps due to a change in ion hopping mechanism in the low connectivity limit ($C_i < 0.15$) or due to the neglect of anion transport or ion-ion interactions in our simulations. Nevertheless, Figure 6.12 makes clear that f_{exp}, which is obtained from analysis of experimentally measured conductivities of a series of ether-based polymer electrolytes, is strongly correlated with the solvation-site connectivity that manifests in simulations of neat polymers. For other classes of polymers, we have found that the calculated solvation-site connectivity does not necessarily correlate directly with x_o,[127] and we likewise do not expect that in general for f_{exp}; in this sense, the results in Figures 6.5 and 6.6 are likely a special feature of the class of polyethers considered here. Nonetheless, generally across polymers, we do expect a strong correlation between the experimental and calculated metrics of connectivity, as shown in Figure 6.12.

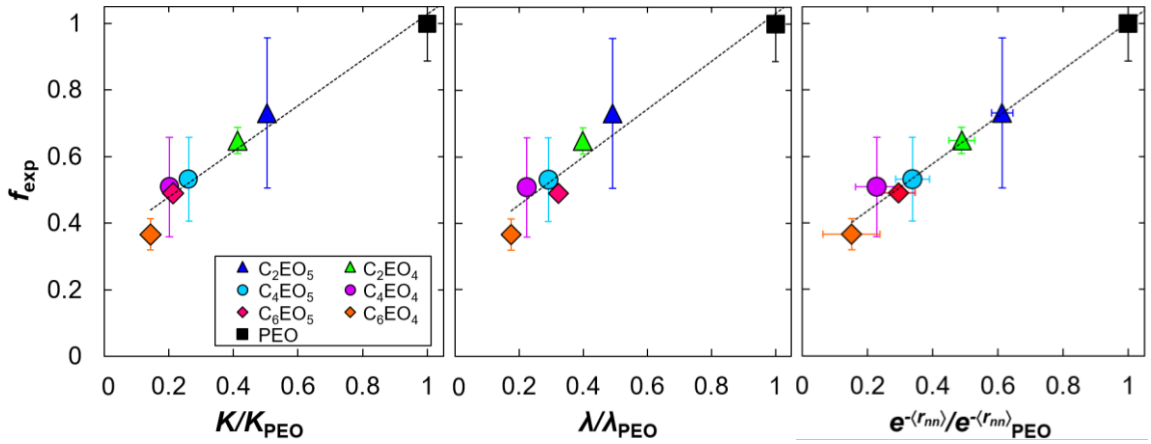

Figure 6.12. Correlation of experimental connectivity, f_{exp}, and the theoretical connectivity metrics in Figure 6.11a-c. The dashed line shows the linear fit to the data. The correlation coefficients for the linear fits are 0.91, 0.89, and 0.98 for a-c, respectively.

6.4 Conclusions

The role of polymer segmental motion and the glass transition temperature on the conductivity of polymer electrolytes has long been appreciated. When comparing polymers with different monomer chemistries, the nature and distribution of ion solvation sites may also play an important role. To investigate these effects, a combined experimental and computational study of ion transport is performed on a systematic set of polymer electrolytes in which aliphatic linkers have been added to a PEO backbone. Experiments are conducted on mixtures of the ether-based polymers and LiTFSI over a wide range of salt concentrations, while the simulations focus on the solvation of lithium ions in the dilute salt limit and the distribution of available lithium solvation sites in neat polymers.

The experimentally measured conductivities are affected by a variety of often competing factors, including T_g and also the density of available ion solvation sites. To isolate the effects of these factors, we employ a two-step normalization scheme. In the first step, VTF fits are used to calculate a temperature-dependent reduced conductivity, $\sigma_r(T\text{-}T_g)$, which is defined as the conductivity of the electrolyte at a fixed value of $T\text{-}T_g$. This step mitigates differences in the conductivity of polymers that arise due to disparities in T_g. In the second step, we compute a dimensionless parameter f_{exp}, defined as the ratio of the reduced molar conductivity of the electrolyte of interest to that of a reference polymer (PEO) at a fixed salt concentration. This parameter is used to assess to what extent changes in conductivity can be attributed to factors other than T_g, such as due to differences in the connectivity of solvation sites. Remarkably, within the set of polyethers studied, f_{exp} is shown to depend only on oxygen mole fraction, x_o, and is largely independent of temperature and salt concentration. This suggests that f_{exp} is an intrinsic property of the neat polymer that distinguishes the conductivity of polymers at a given concentration and $T\text{-}T_g$.

Molecular dynamics simulations conducted on neat polymers and polymers in the presence of an isolated lithium ion are used to develop molecular insight for f_{exp} and its dependence on x_o. The latter simulations are used to identify the nature of lithium ion solvation sites, and the distribution of such sites are examined in simulations of neat polymer systems. We introduce three metrics for quantifying the connectivity among solvation sites using simulation ($C_1 = \kappa/\kappa_{PEO}$, $C_2 = \lambda/\lambda_{PEO}$, C_3

= exp[-⟨r_{nn}⟩] / exp[-⟨r_{nn}⟩$_{PEO}$]). In the range 0.15 < x_o < 0.33, we find that f_{exp} is correlated with the various connectivity metrics according to f_{exp} = 0.32+0.71C_i. The simulations thus provide molecular insight into the underpinnings of f_{exp}. Namely, f_{exp} reports on the proximity of lithium ion solvation sites in the polymer, which is essential in facilitating lithium ion diffusion in polymer electrolytes.

Based on these analyses, we present a universal equation using $\sigma_{PEO}(r,T)$, the well-established dependence of conductivity of PEO electrolytes on salt concentration and temperature,

$$\sigma\left(r, T - T_{g,PEO} + T_g\right) = \sigma_{PEO}(r,T) \times (3x_o) \times (5.39x_o - 0.86), \quad (6.10)$$

where the last term is obtained by linear fit of the f_{exp} data in Figure 6. Note that T_g refers to the glass transition temperature of the polymer/salt mixture, which can either be measured or approximated using the data presented in this paper (see SI for more details). The practical value of eq. 6.10 is that the conductivity of ether-based electrolytes at salt concentrations and temperatures similar to those in this study can be easily predicted on the basis of its molecular composition. This equation highlights two approaches that may be employed for designing polymer electrolytes with improved conductivity: (1) increase f_{exp} while keeping T_g close to that of PEO or (2) decrease T_g while keeping f_{exp} close to unity.

6.5 Acknowledgements

The authors gratefully acknowledge Zhen-Gang Wang for useful discussions. This research was supported by the National Science Foundation under DMREF Award Number NSF-CHE-1335486. DSC experiments were performed at the Molecular Foundry user facilities at Lawrence Berkeley National Laboratory supported by the Office of Science, Office of Basic Energy Sciences, of the U.S. Department of Energy under Contract No. DE-AC02-05CH11231.

6.6 Nomenclature

SPEs	solvent-free polymer electrolytes
PEO	poly(ethylene oxide)
PEG	poly(ethylene glycol)
EO	ethylene oxide
ADMET	Acyclic Diene Metathesis
LiTFSI	lithium bis(trifluoromethanesulfonyl) imide
DMF	dimethylformamide
DSC	differential scanning calorimetry
VTF	Vogel-Tammann-Fulcher
CDF	cumulative distribution function
M_n	number averaged molecular weight (kg/mol)
T_g	glass transition temperature (°C)
T_m	melting temperature (°C)
$Đ$	polydispersity
x_o	mole fraction of oxygen
r	molar ratio of Li^+ to ether oxygens
R_b	bulk electrolyte resistance (Ω)

l	electrolyte thickness (cm)
a	electrolyte area (cm^2)
σ	conductivity (S/cm)
T	temperature (°C)
σ_r	reduced conductivity (S/cm)
A	VTF prefactor ($SK^{1/2}$/cm)
E_a	effective activation energy (kJ/mol)
R	universal gas constant (kJ/mol K)
f_{exp}	experimental connectivity
B	bulk modulus (GPa)
$\langle r_{nn} \rangle$	average nearest-neighbor distance between solvation sites (Å)
r_{min}	minimum distance for edges between solvation sites (Å)
r_{cut}	maximum distance for edges between solvation sites (Å)
κ	weighted volumetric density of edges between viable solvation sites
V	volume of the simulation cell
$w(r)$	function for weighting a particular edge based on distance
$H(r)$	Heaviside step function
λ	linear density of edges projected along a given linear direction
$\boldsymbol{u}$	unit vector in the direction of the linear dimension
L_u	length of a linear dimension (in the direction of $\boldsymbol{u}$) in the simulation cell
$\boldsymbol{r}_{ij}$	distance vector between sites with indices i and j
k^*	lithium ion hopping rate at $\langle r_{nn} \rangle$
C_i	generalized and normalized connectivity metric
a_i	intercept in equation relating C_i and f_{exp}
m_i	slope in equation relating C_i and f_{exp}

6.7 Supporting Information

6.7.1 Derivation of f_{exp} Formula

As indicated in the *Results and Discussion* section of the main text, the experimental solvation-site connectivity, f_{exp}, quantifies differences in conductivity that arise due to differences in monomer structure, as opposed to those due to shifts in the glass transition temperature T_g or the number of charge carriers. To show this, we take f_{exp} to be the ratio of reduced molar conductivities:

$$f_{exp} = \left(\frac{\tilde{\sigma}_r}{\tilde{\sigma}_{r,PEO}} \right)_{r,T-T_g}, \tag{6.S1}$$

where $\tilde{\sigma}_r = \sigma_r / c_{salt}$, σ_r is the reduced conductivity as defined in the main text, c_{salt} is the molar concentration of salt, and $(\ldots)_{r,T\text{-}T_g}$ denotes quantities obtained for a given r = [Li^+]/[O] and T-T_g. In eq. 6.S1, utilizing the reduced conductivities enables comparison between polymers at the same T-T_g, and normalizing the conductivity by the concentration reports the mobility of ions in the system rather than the net conductivity. Eq. 6.S1 can then be rewritten in terms of the reduced conductivity and a ratio of the salt concentration in the two electrolytes:

$$f_{\mathrm{exp}} = \left(\frac{\sigma_{\mathrm{r}}}{\sigma_{\mathrm{r,PEO}}}\right)_{r,T-T_{\mathrm{g}}} \left(\frac{c_{\mathrm{salt,PEO}}}{c_{\mathrm{salt}}}\right) = \left(\frac{\sigma_{\mathrm{r}}}{\sigma_{\mathrm{r,PEO}}}\right)_{r,T-T_{\mathrm{g}}} \left(\frac{n_{\mathrm{salt,PEO}}/V}{n_{\mathrm{salt}}/V}\right), \tag{6.S2}$$

where n_{salt} indicates the moles of salt added to the system with total volume V.

For the C_xEO_y polymers, it is useful to express n_{salt} in terms of r,

$$n_{\mathrm{salt}} = y n_{\mathrm{mon}} r, \tag{6.S3}$$

and V in terms of the partial molar volumes of the system components,

$$V = n_{\mathrm{mon}}\left[(x+2y)\bar{v}_{\mathrm{CH_2}} + y\bar{v}_{\mathrm{O}}\right] + \sum_k n_{\mathrm{salt}}^{(k)} \bar{v}_{\mathrm{salt}}^{(k)}, \tag{6.S4}$$

where $\bar{v}_{\mathrm{CH_2}}$ and $\bar{v}_{\mathrm{O}}$ are the partial molar volumes for a methylene group and an oxygen, respectively, and the summation accounts for the volume of all salt species (free ions, pairs, and aggregates). If the contribution of the salt to the volume is neglected as an approximation, then eq. 6.S2 can be rewritten as

$$f_{\mathrm{exp}} = \left(\frac{\sigma_{\mathrm{r}}}{\sigma_{\mathrm{r,PEO}}}\right)_{r,T-T_{\mathrm{g}}} \left(\frac{\left[(x+2y)\bar{v}_{\mathrm{CH_2}} + y\bar{v}_{\mathrm{O}}\right]}{y\left[2\bar{v}_{\mathrm{CH_2}} + \bar{v}_{\mathrm{O}}\right]_{\mathrm{PEO}}}\right), \tag{6.S5}$$

where the subscript 'PEO' denotes that the partial molar volumes are defined for PEO, in particular. To obtain eq. 6.4 of the main text, we further approximate that the partial molar volumes of all heavy-atom, backbone moeities are the same with respect to each other (i.e., $\bar{v} = \bar{v}_{\mathrm{CH_2}} = \bar{v}_{\mathrm{O}}$) and also that the partial molar volumes are the same for all C_xEO_y polymers and PEO such that eq. 6.S5 becomes

$$f_{\mathrm{exp}} = \left(\frac{\sigma_{\mathrm{r}}}{\sigma_{\mathrm{r,PEO}}}\right)_{r,T-T_{\mathrm{g}}} \left(\frac{x_{\mathrm{o,PEO}}}{x_{\mathrm{o}}}\right), \tag{6.S6}$$

We note that eq. 6.S5 can also be written with a slightly less stringent approximation ($\bar{v}_{\mathrm{O}}$ in the the C_xEO_y polymers is the same as in PEO) as

$$f_{\mathrm{exp}} = \left(\frac{\sigma_{\mathrm{r}}}{\sigma_{\mathrm{r,PEO}}}\right)_{r,T-T_{\mathrm{g}}} \left(\frac{\phi_{\mathrm{o,PEO}}}{\phi_{\mathrm{o}}}\right), \tag{6.S7}$$

where ϕ_{o} is the volume fraction of oxygen in the polymer electrolyte.

6.7.2 Electrolyte Characterization at Different Salt Concentrations

Figure 6.S1 shows conductivity, T_{g} and reduced conductivity for all electrolytes prepared in this experiment. In Figure 6.S1c, we find that factoring out the effect of T_{g} on σ organizes the data at all r, consistent with Figure 4 in the main text.

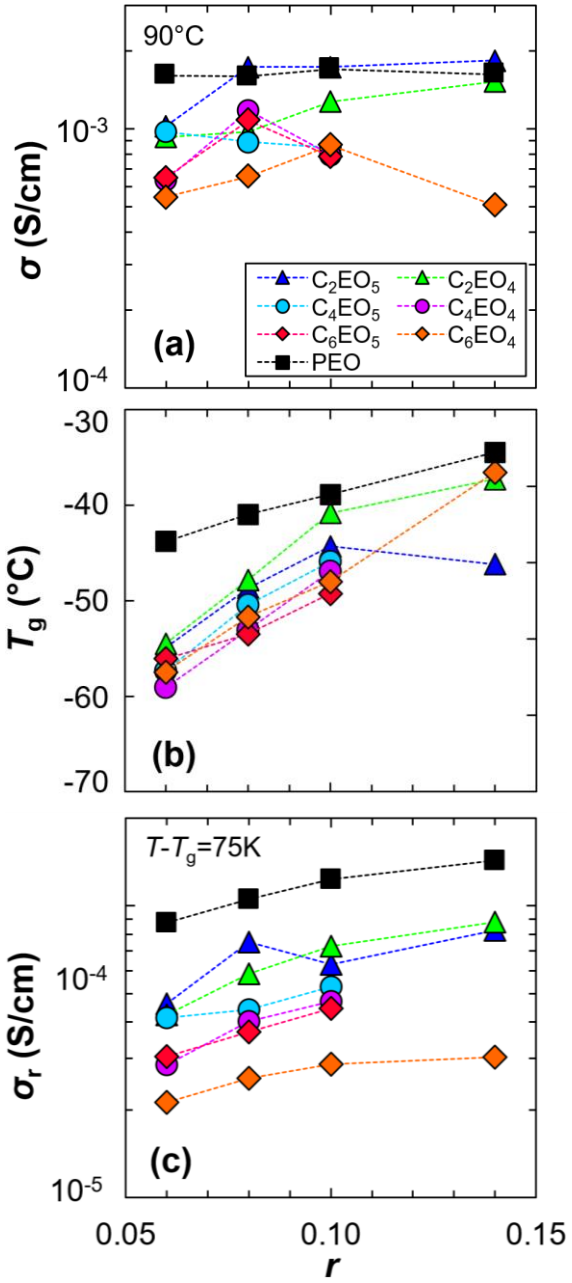

Figure 6.S1. (a) Conductivity, σ, at 90°C and (b) glass transition temperature, T_g, and (c) reduced conductivity, σ_r, with increasing r.

6.7.3 Approximating Conductivity Using the Universal Equation

As described in the *Conclusions* section of the main text, the relationship between f_{exp} and x_o leads us to a universal equation,

$$\sigma\left(r, T - T_{g,PEO} + T_g\right) = \sigma_{PEO}(r, T) \times (3x_o) \times (5.39x_o - 0.86), \quad (6.S8)$$

that can be used to approximate ionic conductivity of any polyether mixed with LiTFSI salt. This approximation relies on four parameters: x_o, the mol fraction of the polymer of interest, $\sigma_{PEO}(r,T)$, the conductivity of PEO at a known temperature and salt concentration, $T_{g,PEO}$, the T_g of PEO at r; and T_g, the T_g of the electrolyte of interest at r. The conductivity approximated using eq. 6.S8 will be at the same r as σ_{PEO} and at a temperature of T-T_g,PEO+T_g, where T is the temperature of σ_{PEO}. Data for σ_{PEO} and $T_{g,PEO}$ as a function of temperature and salt concentration is well reported in the literature. For convenience, we provide our measurements for σ_{PEO} and $T_{g,PEO}$ at varying r and T. We also provide a method for approximating the T_g of any polyether electrolyte based off of x_o and r, in the case that the T_g of the polymer/salt mixture has not been measured.

The relationship between f_{exp} and theoretical connectivity will depend chain architecture of the polymer, especially in cases where all oxygens are not chemically similar and equally accessible. Thus, further work is required to extend our work to cover electrolytes based on comb or branched polymers. Another instance where we can conceive deviation from this relationship is in an ion-paired system, or one where steric hindrance precludes the solvation of the lithium ion. Also, we do not expect the approximation to capture limitations of ion transport due to the presence of a crystalline phase, as our entire analysis was performed on fully amorphous materials. In these cases, eq. 6.S8 would not provide a good estimate of the electrolyte conductivity.

Table 6.S1. Conductivity data for 5 kg/mol PEO at different temperatures and salt concentrations where r = [Li^+/O]. The last row shows the measured T_g of electrolytes at different salt concentrations. All data was obtained using 5 kg/mol PEO mixed with LiTFSI salt.

T (°C)	r=0.02	r=0.04	r=0.08	r=0.10	r=0.12	r=0.14	r=0.16
27	4.12×10^{-7}	8.14×10^{-7}	7.08×10^{-5}	5.08×10^{-5}	5.37×10^{-5}	3.12×10^{-5}	3.15×10^{-5}
40	2.40×10^{-6}	5.19×10^{-6}	1.67×10^{-4}	1.54×10^{-4}	1.53×10^{-4}	1.03×10^{-4}	9.86×10^{-5}
50	9.49×10^{-6}	3.13×10^{-5}	3.34×10^{-4}	3.11×10^{-4}	2.98×10^{-4}	2.19×10^{-4}	2.04×10^{-4}
60	1.57×10^{-4}	5.00×10^{-4}	5.55×10^{-4}	5.54×10^{-4}	5.33×10^{-4}	4.06×10^{-4}	3.77×10^{-4}
70	4.96×10^{-4}	7.05×10^{-4}	8.00×10^{-4}	8.89×10^{-4}	8.84×10^{-4}	6.92×10^{-4}	7.68×10^{-4}
80	6.27×10^{-4}	9.45×10^{-4}	1.17×10^{-3}	1.31×10^{-3}	1.24×10^{-3}	1.09×10^{-3}	9.80×10^{-4}
90	8.16×10^{-4}	1.22×10^{-3}	1.60×10^{-3}	1.84×10^{-3}	1.76×10^{-3}	1.59×10^{-3}	1.45×10^{-3}
100	9.78×10^{-4}	1.53×10^{-3}	2.10×10^{-3}	2.47×10^{-3}	2.40×10^{-3}	2.23×10^{-3}	2.03×10^{-3}
110	1.18×10^{-3}	1.88×10^{-3}	2.69×10^{-3}	3.18×10^{-3}	-	2.95×10^{-3}	-
T_g (°C)	-55.9	-51.9	-43.7	-38.5	-35.6	-30.9	-27.5

Figure 6.S2 shows data for the increase in the glass transition temperature, ΔT_g, relative to the neat polymer at varying r. We find that the data falls on a line,

$$\Delta T_g = 222.6\, r\,, \tag{6.S9}$$

where $\Delta T_g = T_{g,r} - T_{g,neat}$. On average eq. 6.S9 estimates the ΔT_g within 20% for C_xEO_y polymers and will likely provide a good approximation for the T_g at a given value of r for other polyethers, if the T_g of the neat polymer is known.

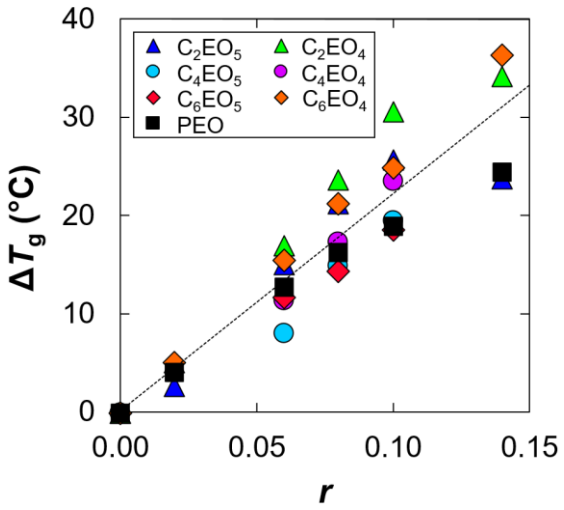

Figure 6.S2. Increase in T_g as a function of salt concentration. The T_g at $r = 0$ is that of the neat polymer.

7 Optimizing Ion Transport in Polyether-based Electrolytes for Lithium Batteries[⁂]

ABSTRACT

We report on the synthesis of poly(diethylene oxide-*alt*-oxymethylene), P(2EO-MO), via cationic ring-opening polymerization of the cyclic ether monomer, 1,3,6-trioxocane. We use a combined experimental and computational approach to study ion transport in electrolytes comprising mixtures of P(2EO-MO) and lithium bis(trifluoromethanesulfonyl) imide (LiTFSI) salt. Mixtures of poly(ethylene oxide) (PEO) and LiTFSI are used as a baseline. The maximum ionic conductivities, σ, of P(2EO-MO) and PEO electrolytes at 90°C are 1.1×10^{-3} S/cm and 1.5×10^{-3} S/cm, respectively. This difference is attributed to the T_g of P(2EO-MO)/LiTFSI (–12°C), which is significantly higher than that of PEO/LiTFSI (–44°C) at the same salt concentration. Self-diffusion coefficients measured using pulsed-field gradient NMR (PFG-NMR) show that both Li^+ and $TFSI^-$ ions diffuse more rapidly in PEO than in P(2EO-MO). However, the NMR-based cation transference number is about a factor of two higher in P(2EO-MO) (0.36) than in PEO (0.19). The transference number measured by the steady-state current technique, $t_{+,SS}$, in P(2EO-MO) (0.20) is higher than in PEO (0.08) by a similar factor. We find that the product $\sigma t_{+,SS}$ is higher in P(2EO-MO); thus, P(2EO-MO) is expected to sustain higher steady-state currents under dc polarization, making it a more efficacious electrolyte for battery applications. Molecular-level insight into the factors that govern ion transport in our electrolytes was obtained using MD simulations. These simulations show that the solvation structures around Li^+ is similar in both polymers. The same is true for $TFSI^-$. However, the density of Li^+ solvation sites in P(2EO-MO) is a factor of two higher than that in PEO. We posit that this is responsible for the observed differences in the experimentally-determined transport properties of P(2EO-MO) and PEO electrolytes.

7.1 Introduction

Rechargeable lithium-ion batteries are an important component of the emerging clean energy landscape, currently being used in both electric vehicles and grid storage. There is considerable interest in finding a replacement for the flammable organic liquids used in conventional lithium-ion batteries. An electrolyte system that has garnered considerable interest is poly(ethylene oxide) (PEO) mixed with lithium salts. The solubility of alkali metal salts in PEO was first reported in the pioneering studies of Fenton, Parker, and Wright.[26] Since then, there have been significant advances in our understanding of the factors that affect the motion of Li^+ ions in polymer electrolytes. Spectroscopic studies and molecular dynamics (MD) simulations reveal that Li^+ is coordinated with ether oxygens on the polymer chain, indicating that ion motion is inherently coupled to polymer segmental motion.[22,32,111,187–191] A consequence of this coupling is that the ionic conductivity of polymer electrolytes is a strong function of the glass transition temperature,

[⁂] This chapter was reported in *Macromolecules* **2018**, *51* (8), 2847–2858.

T_g, which governs segmental motion. Another important factor that affects ion transport is solvation-site connectivity.[103] This parameter is obtained from MD simulations by calculating the density of Li^+ solvation sites that occur naturally in a given polymer due to thermal fluctuations.

There have been numerous attempts to design and synthesize polymer electrolytes that are more efficacious than PEO.[41,44–48,50–53,55,59–72,74,75] In all of these studies, ion transport is characterized by measuring conductivity, σ, using ac impedance spectroscopy. It is, however, known that the performance of an electrolyte in rechargeable batteries depends on many more parameters.[57] In an important study, Bruce and Vincent conducted dc experiments on polymer electrolytes using symmetric lithium-polymer-lithium cells.[88,96] They noted that in the dilute limit, this approach gives the cation transference number. In concentrated electrolytes, however, the relationship between dc current in symmetric cells and the cation transference number is more complex.[101,102,124] Nevertheless, the apparent transference number measured using the approach of Bruce and Vincent, $t_{+,SS}$, is an important attribute of battery electrolytes. It is therefore not surprising that many papers on polymer electrolytes report $t_{+,SS}$.[80–82,87,90,97,98]

The performance of electrolytes in batteries depends on its response to an applied dc potential. Predicting this response requires complete characterization of the electrolyte, i.e. knowledge of three transport parameters, σ, D, and t_+, where t_+ is the true transference number.[57] In the absence of complete characterization, the quantity that reflects the current obtained under an applied dc potential is the product $\sigma t_{+,SS}$. When the dc potential is initially applied, i.e. before concentration gradients have been established, the initial current, i_0, obtained through an electrolyte is given by Ohm's law,

$$i_0 = \frac{\Delta V \sigma}{l}, \tag{7.1}$$

where ΔV is the dc potential and l is the thickness of the electrolyte. The parameter $t_{+,SS}$ is defined as the fraction of the initial current that is sustained at steady-state,

$$t_{+,SS} = \frac{i_{SS}}{i_0}, \tag{7.2}$$

where i_{ss} is the steady-state current. Thus the product $\sigma t_{+,SS}$ is proportional to the steady-state current obtained through an electrolyte under a dc potential,

$$\sigma t_{+,SS} = i_{SS}\left(\frac{l}{\Delta V}\right), \tag{7.3}$$

In this analysis, we restrict our attention to bulk (not interfacial) properties. In addition to the three transport parameters, interfacial impedance and exchange current densities will also affect electrolyte performance in a battery. However, these quantities are inherently dependent on the composition of the solid electrolyte interface (SEI) layer and thus should be considered separately from bulk transport properties.

In this paper we report on the synthesis of a new polymer electrolyte, poly(diethylene oxide-*alt*-oxymethylene), referred to as P(2EO-MO). The monomer comprises two ethylene oxide moieties followed by a methylene oxide moiety, polymerized by ring-opening cationic polymerization. Previous studies of ethylene oxide-*co*-oxymethylene polymer electrolytes have

focused mainly on crosslinked systems.[73,192–194] At least one study has reported on ion transport in a linear version of these copolymers, however the conductivity measurements reported were limited to low temperatures.[195] Here, we characterize ion transport in mixtures of P(2EO-MO) and lithium bis(trifluoromethanesulfonyl) imide (LiTFSI) salt at 90°C. We use transport measurements in PEO/LiTFSI electrolytes as a baseline for comparison. The chemical formulae of the polymers used in this study are shown in Figure 7.1. We demonstrate that $\sigma t_{+,SS}$ is larger in P(2EO-MO) than in PEO. Pulsed-field-gradient NMR (PFG-NMR) experiments are used to characterize the self-diffusion of ionic species in both electrolytes. Calculations of solvation-site connectivity and lithium ion self-diffusion coefficient using MD simulations provide some insight into the molecular underpinnings of our experimental observations.

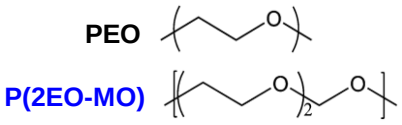

Figure 7.1. Structures for polymers used in this study.

7.2 Experimental

7.2.1 Polymer Synthesis

The synthesis of P(2EO-MO) has been previously reported.[196–198] Step-growth polymerization between diethylene glycol and paraformaldehyde results in the synthesis of an oligomer with a number-averaged molecular weight, M_n, of 1 kg/mol. The oligomer was heated to 150°C under vacuum, depolymerized, and redistilled to yield the cyclic ether monomer, 1,3,6-trioxocane. P(2EO-MO) was synthesized using 2 mol% of $BF_3 \cdot OEt_2$ as the initiator and dichloromethane (DCM) as the solvent at room temperature, as shown in Figure 7.2. The reaction, which was allowed to proceed for 2 hours, resulted in an equilibrium between high molecular weight polymer and oligo-macrocycles. The oligo-macrocycles were removed by precipitation in hexanes. The yielded polymer has an alternating sequence of MO and 2EO units, and no regio-defects are observed based on ^{13}C-NMR; this alternating structure is caused by high reactivity of the acetal group in the monomer. The final M_n of the polymer was 55 kg/mol with a polydispersity index of 2.2, according to gel permeation chromatography (GPC). This chain length was significantly higher than that calculated based on the monomer-to-initiator ratio, suggesting that not all initiators participated in the polymerization. A similar discrepancy between experimental and theoretical M_ns has been reported by Chien and co-workers[196] in polymerizing 1,3,6-trioxocane in toluene with the $BF_3 \cdot OEt_2$ catalyst. The Supporting Information of reference 125 contains a more rigorous description of the synthesis procedure, including NMR spectra and GPC traces of P(2EO-MO).

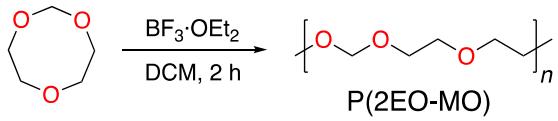

Figure 7.2. Synthesis of P(2EO-MO).

7.2.2 Electrolyte Preparation

The polymers use in this study are 100 kg/mol PEO, purchased from Sigma-Aldrich, and 55 kg/mol 2EO-MO, synthesized according to the procedure outlined in the Polymer Synthesis experimental section. The conductivity[58,104] and Li^+ diffusivity[29] measured in PEO/LiTFSI mixtures has been shown to be independent of chain length above 5 kg/mol. Thus, we expect no significant difference in electrolyte properties to arise from the difference in M_n of our polymers.

Electrolytes were prepared by mixing polymer with lithium bis(trifluoromethanesulfonyl) imide (LiTFSI) salt purchased from Novolyte. All materials (PEO, P(2EO-MO), and LiTFSI) were thoroughly dried prior to use and maintained in an argon environment with H_2O and O_2 levels kept below 2 ppm and 5 ppm respectively. The polymers were dried at 90°C under vacuum in the glovebox antechamber for 24 h. The salt was dried at 120°C under vacuum in the glovebox antechamber for 3 days. Electrolytes were prepared by dissolving dry polymer and LiTFSI salt into tetrahydrofuran (THF) at 55°C until completely dissolved. The THF was evaporated, leaving behind a homogenous polymer/salt mixture. After 12 hours of drying on the hot plate at 55°C, the electrolytes were transferred to the glovebox antechamber to dry under vacuum at 90°C for 24 h to remove any excess THF. The salt concentration in the electrolyte is described as *r*, defined as the molar ratio of lithium ions to oxygen atoms on the polymer: $r = [Li^+]/[O]$. Electrolytes were prepared at r = 0.01, 0.02, 0.04, 0.06, 0.08, 0.10, 0.12, and 0.14 for each polymer.

7.2.3 Differential Scanning Calorimetry

Inside of a glovebox, each sample was prepared by depositing 2-5 mg of electrolyte into a hermetically-sealed aluminum pan. Differential scanning calorimetry (DSC) was performed on each sample in a TA Instruments DSC Q200. The following temperature scan was used, beginning at room temperature: heat to 120°C at 20°C/min, cool to –90°C at 5°C/min, heat to 120°C at 20°C/min. The resulting DSC curves of PEO and P(2EO-MO) electrolytes are shown in the Supporting Information. The glass transition temperature, T_g, and melting temperature, T_m, of each electrolyte was obtained from the second heating scan. Both measurements were reproducible within 1°C.

7.2.4 Electrochemical Measurements

All electrochemical measurements were performed on a VMP3 potentiostat (Bio-Logic). For each measurement, data from three samples were averaged and the error bars signify the standard deviation of these measurements.

Ac impedance spectroscopy was used to determine the ionic conductivity of the electrolytes. Stainless steel symmetric cells were prepared by pressing viscous electrolytes into a 3.175 mm diameter hole in a 508 μm thickness silicone spacer, which was then pressed between two 200 μm thick stainless-steel shims used as electrodes. The electrolyte thickness was determined by measuring the total cell thickness using a micrometer and subtracting the thickness of the electrodes. Aluminum tabs were fastened to the electrodes using Kapton tape. The cell was hermetically sealed in Showa-Denko pouch material, leaving the tab ends exposed. This sample configuration allows for electrochemical measurements to take place outside of the glove box while still maintaining an air- and water-free environment.

Once removed from the glove box, each cell was placed in a custom-built heating stage to determine the ionic conductivity in the temperature range of 25°C to 110°C. Complex impedance

measurements were taken with the frequency range of 1 Hz to 1 MHz at an amplitude of 80 mV. The low-frequency minimum on the Nyquist impedance plot was taken to be the electrolyte bulk resistance, R_b, which was used along with electrolyte thickness, l, and electrolyte area, a, to calculate the electrolyte conductivity, σ, according to eq. 7.4.

$$\sigma = \frac{l}{a\, R_b} \tag{7.4}$$

The inner diameter of the spacer, 3.175 mm, was used to calculate a. Thickness, l, was taken to be the final thickness of the electrolyte, measured after conductivity experiments were completed.

Steady-state current measurements were performed on lithium symmetric cells using a Biologic VMP3 potentiostat. A more detailed description of this experiment is provided in reference 124. Lithium symmetric cells were prepared by pressing electrolyte into a 508 μm thick silicone spacer, then sandwiching between two lithium electrodes (MTI corporation). Nickel tabs were used as electrical contacts. The assembly was vacuum sealed in a laminated aluminum pouch material (Showa-Denko) then transferred to a heating stage at 90°C for electrochemical measurements. Cells were annealed for 4 hours then conditioned for 5 cycles at a low current density of 0.02 mA/cm^2 to introduce a stable interfacial layer. The cell was then polarized at constant potential, ΔV, for 4 h, and the steady-state current, i_{ss}, was recorded. Cell resistances were measured by performing ac impedance spectroscopy before polarization and during steady-state. This experiment was repeated using ΔV = 10 mV, -10 mV, 20 mV, and -20 mV and the results were averaged to ensure that the ion transport characteristics were independent of the sign and magnitude of ΔV.

Ohm's law is used to determine current in the absence of concentration gradients,

$$i_\Omega = \frac{\Delta V}{R_{i,0} + R_{b,0}}, \tag{7.5}$$

where $R_{i,0}$ and $R_{b,0}$ are the interfacial and bulk electrolyte resistances measured prior to polarization. We use this approach to calculate the initial current, i_Ω, resulting from an applied potential, ΔV.

The steady-state current transference number defined by the work of Bruce and Vincent[88,96] is calculated using eq. 7.6.

$$t_{+,SS} = \frac{i_{SS}(\Delta V - i_\Omega R_{i,0})}{i_\Omega(\Delta V - i_{SS} R_{i,SS})} \tag{7.6}$$

7.2.5 PFG-NMR Measurements

PFG-NMR was performed on PEO and P(2EO-MO) electrolytes with salt concentrations of r = 0.08 at temperatures of T = 60°C, 70°C, 80°C, 90°C for PEO and T = 90°C, 100°C, 110°C, and 110°C for P(2EO-MO). NMR measurements were performed on a Bruker Avance 600 MHz instrument fitted with a Z-gradient direct detection broad-band probe and a variable temperature unit. Temperature was calibrated using the chemical shift separation of -OH resonances and -CH_2- resonances of 20% ethylene glycol in dimethyl sulfoxide for the measurements performed between 60-120°C. Diffusion measurements were performed on the isotopes of ^{7}Li and ^{19}F, which produced

peaks around 233 MHz and 565 MHz, respectively, to track the lithium- and fluorine-containing salt species. The 90° pulse lengths were optimized for each sample to achieve maximum signal amplitude. A stimulated echo bipolar gradient pulse sequence was used to measure the self-diffusion coefficients, D_i. The attenuation of the echo E was fit to eq. 7.7,

$$E = e^{-\gamma^2 g^2 \delta^2 D_i \left(\Delta - \frac{\delta}{3}\right)} \tag{7.7}$$

where γ is the gyromagnetic ratio, g is the gradient strength, δ is the duration of the gradient pulse, Δ is the interval between gradient pulses, and D_i is the self-diffusion coefficient. Diffusion time intervals were chosen based on appropriate signal decay and T1 relaxation times. Parameters used for acquisition were diffusion intervals Δ = 0.4–0.5 s (^{7}Li) and 0.5 s (^{19}F), and pulse lengths δ = 10–40 ms (^{7}Li) and 5–10 ms (^{19}F). For each diffusion measurement, 32 experiments of varying gradient strength up to 0.33 T/m were performed and the change in amplitude of the attenuated signal was fit to obtain the parameter D_i. All measured signal attenuations were single exponential decays and the errors in the fits were less than 2%.

7.2.6 Molecular Dynamics (MD) Simulations

All MD simulations were performed within the LAMMPS software suite.[175] All simulations utilized an adapted Trappe-UA force-field that has been reported previously[168] and employed periodic boundary conditions, particle-particle-particle-mesh (pppm) evaluations of long-range interactions beyond a 14 Å cut-off, a Nosé-Hoover barostat with 1000 fs relaxation, and a Nosé-Hoover thermostat with 100 fs relaxation (NPT). Equations of motion were evolved using the velocity-Verlet integrator and a one femtosecond timestep. Intramolecular Lennard-Jones interactions for atom pairs connected by fewer than four bonds were excluded during the MD simulations and electrostatic 1-4 interactions were scaled by 0.5, conforming with Trappe-UA definitions.

Four separate trajectories were run for each polymer at each salt concentration. Each trajectory included a single polymer chain with a mass of approximately 20 kg/mol that was initialized using a protocol to randomize chain orientation and avoid configurations with significant overlap between atoms. Ions were added to random positions in each simulation box at a level consistent with the reported r values. The simulations were initially relaxed at constant NVE with constrained atom displacements of 0.1 Å for 10 ps, followed by five cycles of box compression/expansion between number densities of 0.045 atoms/Å^3 and 0.09 atoms/Å^3 at 2000 K, with each compression/expansion being linearly applied over a 10 ps interval. The simulations were subsequently equilibrated at a temperature of 400 K and a pressure of 1 atm for 10 ns before running long-timescale production runs of 150 ns.

Diffusivities were calculated for each ion according to the Einstein equation,

$$D_i = \lim_{t\to\infty} \frac{d\langle|\boldsymbol{r}_i(t) - \boldsymbol{r}_i(0)|^2\rangle}{6dt} \tag{7.8}$$

where D_i is the diffusion coefficient for ion, i, and the term in brackets is the mean-squared displacement (MSD) evaluated at time t.

7.2.7 Chemically Specific Dynamic Bond Percolation (CS-DBP) Simulations

CS-DBP is a methodology for calculating the long-timescale ion diffusivity using a coarse-grained description of ion-hopping in terms of the ion solvation sites.[168] Here, we use the CS-DBP methodology to calculate and compare the Li^+ ion solvation site distributions in PEO and P(2EO-MO). Sites are generated via trial insertions of the ion into a previously equilibrated polymer simulation, followed by short trajectories to evaluate the stability of the solvation site. Specific details of the protocol can be found in reference 168. The prerequisite MD simulations for CS-DBP were initialized identically to the dilute concentration long-timescale MD simulations for the Li^+ ion, including four separate trajectories for each polymer. Each simulation was equilibrated for 10 ns at 400 K followed by an additional 10 ns trajectory that was used as an input for the CS-DBP site finding simulations. The reported site densities for each polymer reflect the average over four snapshots and reflect the outcome of approximately 5,000 trial insertions of the Li^+ ion into each polymer.

7.3 Results and Discussion

7.3.1 Electrolyte Characterization

DSC was performed on PEO/LiTFSI and P(2EO-MO)/LiTFSI electrolytes to investigate the effect of salt on the thermal properties of the polymer. Figure 7.3a shows the T_g and T_m obtained in PEO electrolytes as a function of salt concentration, r. We find that the T_m of PEO/LiTFSI decreases with increasing salt concentration up to r = 0.08; no T_m is observed from r = 0.1-0.16 indicating that PEO electrolytes in this regime are fully amorphous. DSC measurements of T_g in PEO/LiTFSI exhibit a non-monotonic dependence on r, increasing from r = 0.01 to 0.06, decreasing from r = 0.06 to 0.1, and finally increasing from r = 0.1 to 0.16. For highly crystalline polymers, it has been suggested that segmental motion in the amorphous regions is restricted by the surrounding crystalline regions, and this leads to a measured T_g that is higher than what is representative of the bulk-amorphous phase.[199,200] We attribute the non-monotonic dependence of T_g at $r \leq 0.08$ to this effect. The T_g of the amorphous phase in this regime is thus calculated by extrapolating the least-squares linear fit of the T_g measured in the amorphous electrolytes ($r \geq 0.1$). This fit is shown as the black dotted line in Figure 7.3 and is in the form of $T_g(r) = mr + b$ where m = 198.9°C, b = -59.9°C. Using this equation, we obtain a T_g = -60°C for r=0, which is in agreement with the T_g of neat PEO. Our approach for determining T_g at low salt concentrations is also consistent with observations in non-crystalline polyether-based electrolytes that exhibit a monotonic increase in T_g with increasing salt concentration.[42,59,66,72–74,103]

Figure 7.3b shows the T_g of P(2EO-MO)/LiTFSI electrolytes, along with those obtained for PEO/LiTFSI using the analysis described above. We note that P(2EO-MO) electrolytes are non-crystalline above r = 0.02, thus measured T_gs are presented in Figure 7.3b. Both polymers exhibit a T_g in the vicinity of –60°C in the neat state. As r is increased, the T_gs of both electrolytes increase monotonically. This observation is commonly attributed to the physical crosslinking of the polymer chains mediated by solvated ions in the electrolyte. Interestingly, P(2EO-MO) exhibits a more dramatic increase in T_g with increasing r compared to PEO. This suggests fundamental differences in the mechanism of ion solvation in P(2EO-MO) and PEO electrolytes. In the following section, we use MD simulations to study the solvation of Li^+ and $TFSI^-$; these results provide insight into the concentration dependence of T_g in our electrolytes.

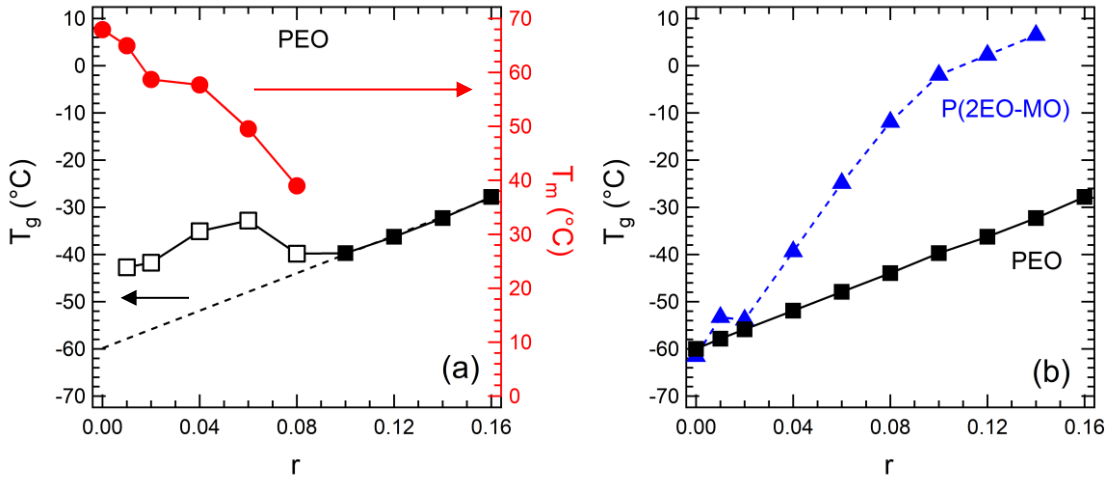

Figure 7.3. (a) Glass transition temperature (left axis) and melting temperature (right axis) of PEO/LiTFSI electrolytes. The black dotted line shows a linear fit of T_g from r=0.1 to r=0.16. (b) Glass transition temperature of PEO and P(2EO-MO) as a function of LiTFSI salt concentration.

Ionic conductivity, σ, of PEO/LiTFSI and P(2EO-MO)/LiTFSI at 90°C is shown as a function of salt concentration, r, in Figure 7.4, where r = [Li^+]/[O]. Both electrolytes exhibit a non-monotonic dependence on r, reaching a maximum conductivity at r=0.08. The maximum conductivity of PEO is 1.5 × 10^{-3} S/cm, while that of P(2EO-MO) is 1.1 × 10^{-3} S/cm. The conductivity of PEO remains above that of P(2EO-MO) for all salt concentrations in this study. This difference is especially significant at the most dilute salt concentration (r = 0.01) and in the highly-concentrated regime (r = 0.10 – 0.14). The differences of PEO and P(2EO-MO) conductivity at high salt concentrations may be attributed to the differences in the glass transition temperatures, T_g, of the electrolytes. In simple electrolytes, one expects conductivity to increase linearly with salt concentration due to the increase in charge carrier concentration. In polymer electrolytes, ion transport is closely coupled to segmental relaxation of polymers,[28,29,151] which slows down with added salt due to associations between ions and the polymer segments. The tradeoff between these two effects results in a conductivity maximum (e.g. Figure 7.4). The glass transition temperature is a simple measure of segmental relaxation. The T_g of P(2EO-MO) increases rapidly with salt concentration relative to PEO resulting in a sharper conductivity peak. Based on the data in Figure 7.4, one might conclude that PEO/LiTFSI is a more efficacious battery electrolyte than P(2EO-MO)/LiTFSI. The discussion below critically examines this statement.

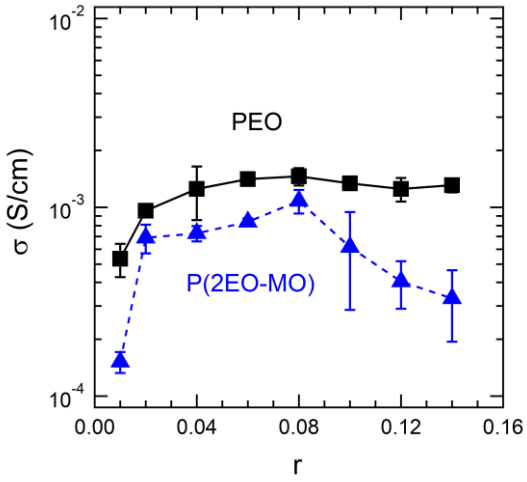

Figure 7.4. Ionic conductivity of PEO and P(2EO-MO) electrolytes as a function of LiTFSI salt concentration. These data are measured at 90°C.

Conductivity is dependent on a number of factors including segmental motion of the polymer chains, the numbers of ions in the electrolyte, and the mobility of the ions. In an attempt to decouple the effect of segmental motion on conductivity, we use the Vogel-Tammann-Fulcher (VTF) equation,[27]

$$\sigma = A\,T^{-1/2}\exp\left(\frac{-E_a}{R(T-T_0)}\right), \tag{7.9}$$

to fit our temperature-dependent conductivity data. In this equation σ is expressed in terms VTF parameters, A and E_a, the universal gas constant, R, and the reference temperature, T_0. We take T_0 to be 50°C below the concentration-dependent T_g of the electrolyte (Figure 7.3b), in accordance with previous literature.[25,201] In Figure 7.5a we plot σ versus $1000/(T\text{-}T_g\text{+}50)$ for PEO and P(2EO-MO) at r = 0.08, the concentration at which both polymers experience a maximum conductivity. Here, we are only interested in observing the temperature-dependence of fully amorphous electrolytes; we have thus excluded the data for PEO when $T \leq$ 40°C, the melting point of PEO/LiTFSI at r = 0.08. All temperatures for P(2EO-MO) are included, as this electrolyte has no detectable melting temperature. Both data sets are approximately linear, indicating good agreement with the VTF equation. Comparing conductivity at a set $T\text{-}T_g$, referred to as reduced temperature, allows us to account for differences in T_g in P(2EO-MO) and PEO electrolytes. We find that the conductivity of P(2EO-MO) is higher than that of PEO at all values of $1000/(T\text{-}T_g\text{+}50)$. Thus, differences in conductivity between these two polymers are not simply explained by differences in segmental motion, i.e., differences in T_g. Instead, our data suggests the mechanism of ion transport in P(2EO-MO) is fundamentally different from that of PEO.

Table 7.1. VTF fit parameters obtained from a least-squares fit to the temperature-dependent conductivity data of each electrolyte according to eq. 7.9.

	PEO		P(2EO-MO)	
r	E_a **(kJ/mol)**	***A*** **(SK$^{1/2}$/cm)**	E_a **(kJ/mol)**	***A*** **(SK$^{1/2}$/cm)**
0.01	7.8	1.1	9.0	0.8
0.02	8.1	2.6	10.7	9.4
0.04	8.4	4.6	9.4	6.9
0.06	8.7	7.1	10.4	29.6
0.08	9.9	18.4	10.2	65.4
0.10	9.2	11.6	9.9	47.1
0.12	9.2	12.2	8.9	17.4
0.14	9.1	13.8	8.7	15.1

To extend this analysis to all salt concentrations in our study, we calculate a reduced conductivity, σ_r, for each electrolyte at a fixed temperature (110 K) above the T_g of the electrolyte,

$$\sigma_r = A\,(T_g + 110\text{ K})^{-1/2} \exp\left(\frac{-E_a}{R(160\text{ K})}\right), \tag{7.10}$$

Eq. 7.10 is obtained by substituting $T = T_g$+110 K in eq. 7.9, where T_g is dependent on the salt concentration of the electrolyte (Figure 7.3b). The parameters A and E_a are obtained by least-squares fits through the temperature-dependent conductivity data; these values are given in Table 7.1 . When compared at the same r, there is good agreement between E_a in PEO and P(2EO-MO) electrolytes, indicating that the VTF lines are nearly parallel (Figure 7.5a). Thus, our choice of 110 K as the reduced temperature is arbitrary; any value of T-T_g would lead to a qualitatively similar dependence of σ_r on r. Figure 7.5b shows σ_r in PEO and P(2EO-MO) electrolytes as a function of r. At low salt concentrations (r < 0.06) PEO has a higher reduced conductivity compared to that of P(2EO-MO), while above r = 0.06 σ_r in P(2EO-MO) electrolytes surpasses that of PEO. Reduced conductivity has been studied for a number of different electrolytes,[28,103–105] and P(2EO-MO)/LiTFSI is the first system to exhibit a σ_r greater than that of PEO/LiTFSI. A greater reduced conductivity could be attributed to improved lithium mobility, improved anion mobility, or a larger degree of dissociation between ions leading to a greater number of effective charge carriers in the system. More information is required to identify which case applies to P(2EO-MO) electrolytes at high salt concentrations.

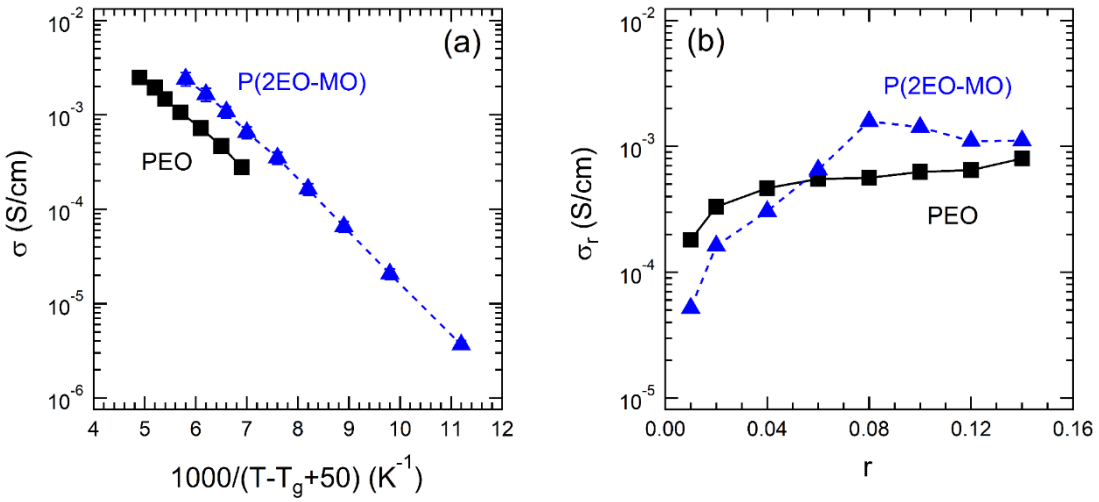

Figure 7.5. (a) Vogel-Tammann-Fulcher plot of conductivity at r = 0.08. (b) Reduced conductivity of PEO and P(2EO-MO) calculated according to eq.10, where $T = T_g$+110 K or 1000/(T-T_g+50) = 6.25.

Self-diffusion coefficients of the lithium- and fluorine-containing species (D_{Li} and D_F) were measured using ^{7}Li and ^{19}F pulsed-field gradient NMR (PFG-NMR). If the salt were fully dissociated, then D_{Li} would reflect the self-diffusion of the cation while D_F would reflect the self-diffusion of the anion. Figure 7.6a shows D_{Li} and D_F for PEO/LiTFSI and P(2EO-MO)/LiTFSI electrolytes at r=0.08. In both polymers, D_F is greater than D_{Li} suggesting the anion is diffusing faster than the cation at a given temperature. This finding is consistent with previous reports of PFG-NMR of PEO electrolytes.[30,36,83,108,109] The slow diffusion of Li^+ is often attributed to the strong interactions with the oxygens on the polymer, whereas the anion moves freely. We find both D_F and D_{Li} are greater in PEO than in P(2EO-MO), likely due to the higher T_g of P(2EO-MO) (–12°C) compared to that of PEO (–44°C) at r = 0.08. The T_g of an electrolyte is related to segmental motion; slow segmental motion often leads to slow ion diffusion, as seen in P(2EO-MO).

Following the same approach used in the conductivity analysis, we decouple the effect of segmental motion on D_{Li} and D_F using the diffusivity form of the VTF equation,

$$D_i = B\,T^{1/2}\exp\left(\frac{-E_a}{R(T-T_0)}\right), \tag{7.11}$$

where all parameters are introduced in eq. 7.9 apart from B, the VTF parameter for diffusivity, analogous to A in eq. 7.9. The values of B and E_a obtained by least-squares fits of the diffusivity data are given in Table 7.2. The E_a values obtained from diffusivity reported in Table 7.2 are in agreement with those determined from conductivity reported in Table 7.1. Figure 7.6b shows D_{Li} and D_F versus reduced temperature for both polymers at r=0.08. When differences in T_g are accounted for, D_F in PEO and P(2EO-MO) are comparable. Thus, the diffusion coefficient of the anion is mainly governed by the T_g of the electrolyte and is not strongly dependent on the chemistry of the monomer. On the other hand, even when differences in segmental motion are accounted for, D_{Li} in P(2EO-MO) remains above that of PEO (Figure 7.6b). Faster Li^+ diffusivity may be attributed to either (1) an increase in solvation-site density which increases the rate of hopping between solvation sites or (2) a difference in the solvation environment of the ion which results in weaker ion-polymer interactions. In discussions below, we use simulations to address this issue.

Table 7.2. VTF fit parameters obtained from a least-squares fit to the temperature-dependent diffusivity data for both electrolytes according to eq. 7.11.

	PEO		P(2EO-MO)	
	E_a (kJ/mol)	B ($cm^2/K^{1/2}s$)	E_a (kJ/mol)	B ($cm^2/K^{1/2}s$)
D_{Li}	11.0	4.0×10^{-6}	9.3	2.9×10^{-6}
D_F	9.7	7.9×10^{-6}	8.8	5.4×10^{-6}

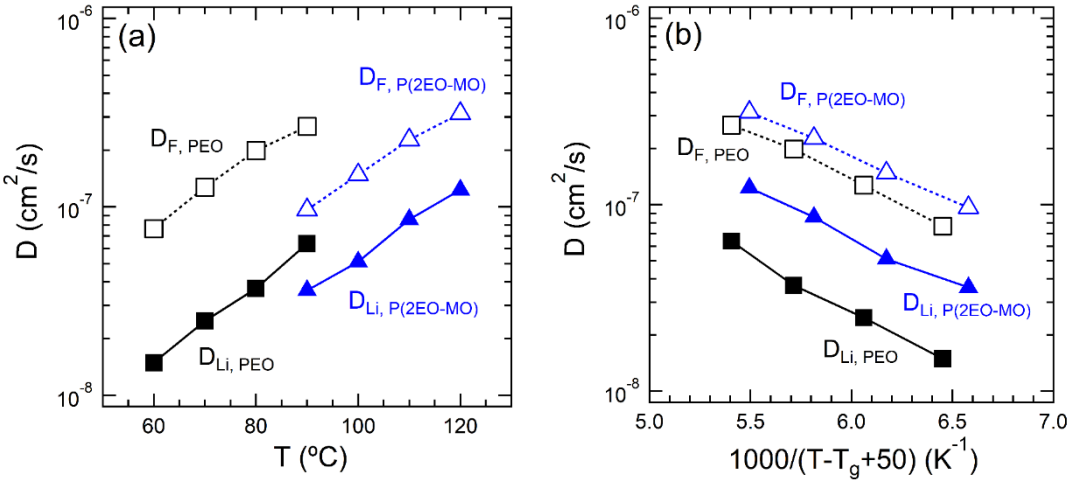

Figure 7.6. (a) Self-diffusion coefficients of lithium- and fluorine- containing species in PEO and P(2EO-MO) at r = 0.08. (b) Same data plotted as a function of reduced temperature.

Using the parameters given in Table 7.2, we calculate a reduced self-diffusion coefficient, $D_{r,i}$, for each electrolyte where the temperature is defined to be 110 K above the T_g of the electrolyte.

$$D_{r,i} = B\,(T_g + 110\ \mathrm{K})^{1/2} \exp\left(\frac{-E_a}{R(160\ \mathrm{K})}\right), \tag{7.12}$$

In PEO $D_{r,Li} = 1.9\times10^{-8}$ cm^2/s and $D_{r,F} = 1.0\times10^{-7}$ cm^2/s while in P(2EO-MO) $D_{r,Li} = 5.1\times10^{-8}$ cm^2/s and $D_{r,F} = 1.4\times10^{-7}$ cm^2/s. The differences in $D_{r,Li}$ provide insight into the observation that reduced conductivity of P(2EO-MO) is higher than that of PEO at r = 0.08 (Figure 7.5b).

Using the self-diffusion coefficients measured at 90ºC (Figure 7.6a), we can calculate the transference number obtained by PFG-NMR using eq. 7.13.

$$t_{+,NMR} = \frac{D_{Li}}{D_{Li} + D_F}, \tag{7.13}$$

We find that $t_{+,NMR}$ in PEO is 0.19 while $t_{+,NMR}$ in P(2EO-MO) is 0.36.

The transference number obtained from the steady-state current technique, $t_{+,SS}$, measured at 90°C is shown as a function of r in Figure 7.7. The $t_{+,SS}$ of both PEO and P(2EO-MO) electrolytes decreases with increasing salt concentration: P(2EO-MO) has a local minima at r = 0.04 while PEO decreases monotonically. The $t_{+,SS}$ of P(2EO-MO) is approximately double that of PEO at all values of r in this study. This finding is consistent with our measurements of $t_{+,NMR}$ in P(2EO-MO), which was also found to be twice that of PEO. The value of $t_{+,SS}$ is lower than that of $t_{+,NMR}$

in both electrolyte systems, consistent previous reports of these quantities in PEO electrolytes.[30,83,99,124] The fact that $t_{+,SS}$ and $t_{+,NMR}$ differ substantially from each other indicates that ion dissociation in our electrolytes is complex. We note that $t_{+,SS}$ nor $t_{+,NMR}$ should be interpreted as approximations of the true transference number; only in the dilute limit wherein ion-pairing and ion-clustering are absent, the transference numbers determined by the steady-state current method and NMR would be identical to the true transference number.[101,102,124]

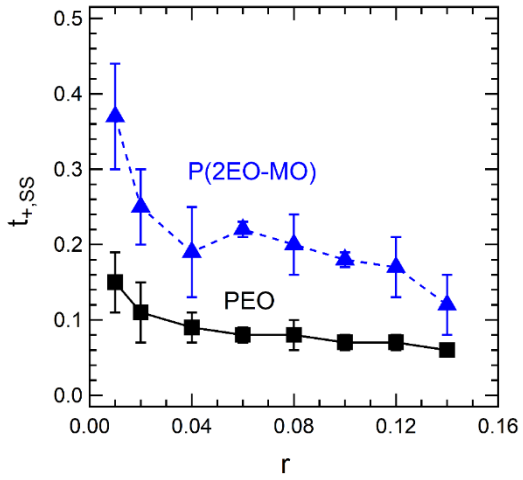

Figure 7.7. Transference number obtained using the steady-state for PEO and P(2EO-MO) as a function of LiTFSI salt concentration. These data are measured at 90°C.

A simple measure of the efficacy of a polymer electrolyte is the product $\sigma t_{+,SS}$. This metric has been reported previously for PEO[99] as well as newly-designed polymer electrolyte systems.[80,202] Figure 7.8 shows $\sigma t_{+,SS}$ as a function of salt concentration in PEO and P(2EO-MO) electrolytes. We find that P(2EO-MO) exhibits a $\sigma t_{+,SS}$ that is higher than PEO from $r = 0.02$ to $r = 0.1$. In this regime of salt concentration, P(2EO-MO) is expected to sustain higher steady-state currents in battery applications.

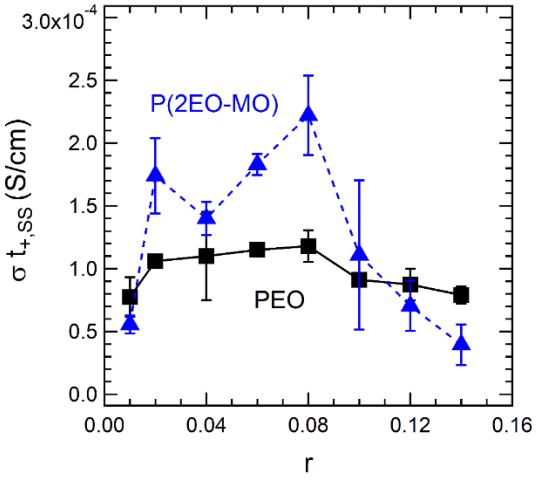

Figure 7.8. Product of conductivity (Figure 7.4) and steady-state current transference number (Figure 7.7) as a function of LiTFSI salt concentration at 90°C.

7.3.2 Molecular Dynamics and Coarse-Grained Simulations

Molecular dynamics (MD) simulations were used to shed light on the molecular origin of the experimental observations described above. Both PEO and P(2EO-MO) electrolytes were studied at r = 0.002, 0.01, 0.02, and 0.06. In addition, the dilute electrolyte was examined by considering a single anion or cation in the simulation box. All simulations were performed at 400 K using a previously reported simulation protocol.[103,168]

These simulations were used to characterize the solvation environment of Li^+ and $TFSI^-$ ions in our electrolytes. The radial distribution functions (rdfs) $g_{\text{Li-O}}(r)$ and $g_{\text{N-Li,C}}(r)$ were parsed from each simulation where "O" includes both the polymer and anion oxygens, "N" is the anion nitrogen atom, "C" corresponds to the CH_2 united atom, and "Li" is the lithium ions. In the dilute systems, the labels "O" and "C" refer exclusively to the polymer ether oxygens and CH_2 united atoms, respectively. The radial distribution functions were calculated according to eq. 7.14,

$$g_{\alpha-\beta}(r) = \frac{V}{4\pi r^2 dr N_\alpha N_\beta} \sum_{i\in\alpha}^{N_\alpha} \sum_{j\in\beta}^{N_\beta} \delta\left(r - \left|\boldsymbol{r}_i - \boldsymbol{r}_j\right|\right), \tag{7.14}$$

where V is the volume of the simulation, N_α and N_β are the number of particles in each set, $4\pi r^2 dr$ is the volume in each shell, r is the position of the atom and the summations run separately over the two sets of atoms. Each rdf in was parsed from 50 ns of trajectory data, using frames spaced by 100 ps.

The Li^+ solvation structures in PEO and P(2EO-MO) electrolytes are characterized using $g_{\text{Li-O}}$ (Figure 7.9a), which gives the radial distribution of oxygens surrounding the lithium ion. The electrolytes exhibit similar Li^+ solvation structures that are independent of salt concentration. In both PEO and P(2EO-MO), Li^+ is surrounded by six oxygen atoms in the first solvation shell, represented by a strong peak at 2 Å. The agreement between the dilute and concentrated electrolytes indicates that Li^+ solvation is dominated by oxygens on the polymer; there is minimal anion presence in the first solvation shell suggesting weak ion pairing in both systems. The main difference between our two polymers is that the 2 Å peak in $g_{\text{Li-O}}$ of P(2EO-MO) is slightly broader, resulting in a smaller peak height. Thus, the oxygens in the P(2EO-MO) solvation shell are slightly more distributed in terms of distance from Li^+. The significance of this observation is unknown. These solvation structures can be visualized in Figure 7.9b, which displays snapshots of typical solvation environments of Li^+ in dilute electrolytes. One notable difference in the two polymers is that two-chain solvation structures predominate in P(2EO-MO), whereas a majority of one-chain solvation structures are observed in PEO.[127] The reason for the two-chain motif in P(2EO-MO) is clearly the structure of the monomer: the presence of two oxygen atoms separated by a single methylene unit is inconsistent with the spacing requirements of typical solvation of Li^+ by ether oxygens. This precludes the possibility of the solvating the ion with oxygens from one chain as is the case with PEO. We posit that the two-chain motif is responsible for the rapid increase seen in the experimentally-measured T_g in P(2EO-MO)/LiTFSI with increasing salt concentration, relative to PEO (Figure 3b).

The $TFSI^-$ environment is examined in Figure 7.9c, which shows $g_{\text{N-Li,C}}$ for PEO and P(2EO-MO). These distribution functions are characterized by one weak shoulder at 6 Å corresponding to 10-12 weakly associated CH_2 groups. The fact that $g_{\text{Li-O}}$ and $g_{\text{N-Li,C}}$ are identical in dilute and concentrated electrolytes indicates that both Li^+ and $TFSI^-$ are surrounded primarily by polymer

chains; the ions are well dissociated in both systems. This is confirmed by Li-TFSI rdf provided in the Supplemental Information. Typical solvation structures for the $TFSI^-$ ion are shown in Figure 7.9d. The arrangements of polymer chains around the central $TFSI^-$ ion are more-or-less random for both electrolytes.

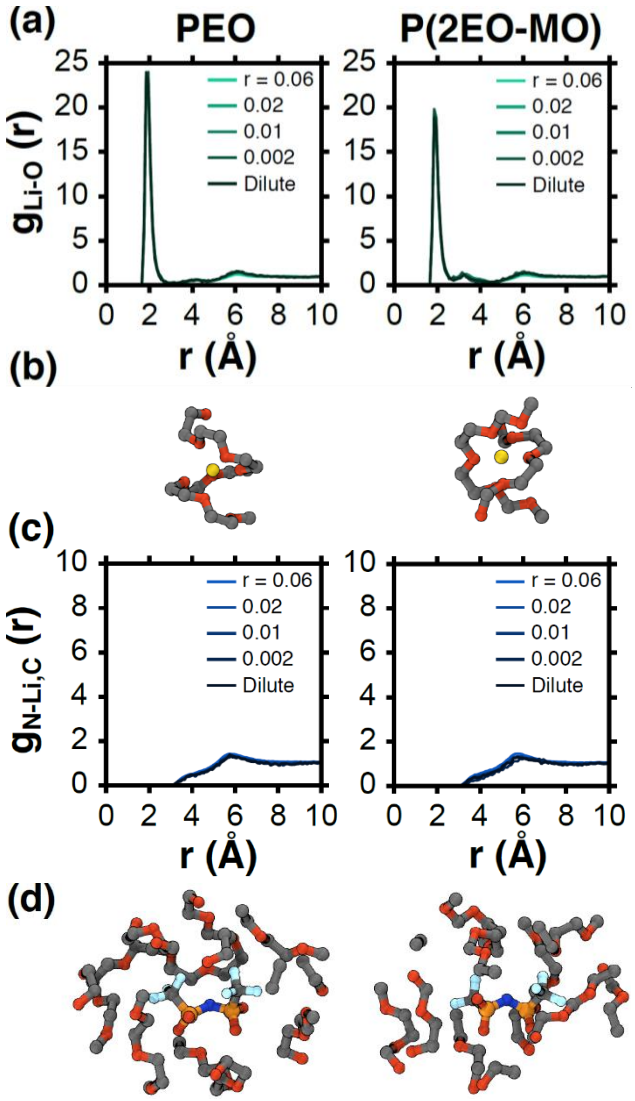

Figure 7.9. Comparison of ion solvation structures in PEO (left) and P(2EO-MO) (right). (a) Li^+ radial distribution functions at different salt concentrations. (b) Representative solvation structures for Li^+ in dilute electrolytes. (c) $TFSI^-$ radial distribution functions at different salt concentrations. (d) Representative solvation structures for $TFSI^-$ in dilute electrolytes. Atoms within 5 Å of Li^+ and 6 Å of nitrogen, sulfur, or fluorine are shown in the solvation structures of Li^+ and $TFSI^-$, respectively. Note, "r" in each legend refers to the salt concentration.

Next, we calculate the Li^+ solvation-site density, ρ_{Li}, in both polymers; ρ_{Li} is the number of solvation sites per unit volume, as defined in reference 103. The solvation-site distributions are generated using the chemically-specific bond percolation (CS-DBP) methodology by analyzing the nascent Li^+ solvation sites that are transiently formed during polymer fluctuations.[168] Figure 7.10 shows the solvation sites in PEO and P(2EO-MO) at a simulation temperature of 400 K (equilibration is challenging at lower temperatures). P(2EO-MO) exhibits approximately a two-

fold increase in ρ_{Li} (20 sites/nm^3) relative to PEO (12 sites/nm^3). Differences in ion transport properties (conductivity, diffusivity, and transference number) in PEO and P(2EO-MO) will be affected by differences in solvation-site density. In particular, the increase in solvation-site density is consistent with the experimentally observed increase in $D_{Li,r}$ and σ_r; holding other factors constant, increased ρ_{Li} has been found to correlate with increased Li^+ transport.[103]

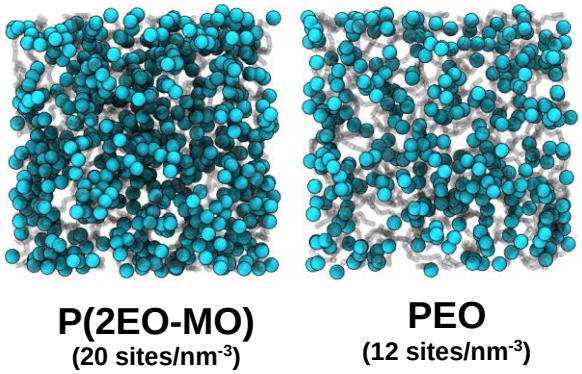

Figure 7.10. Comparison of CS-DBP solvation site densities at 400 K.

The self-diffusion coefficients of both Li^+ and $TFSI^-$ in electrolytes were determined from all-atom MD simulations described in the context of Figure 7.9. The coefficients are obtained from the mean squared displacements of each ion. At the two salt concentrations studied (r = 0.02 and r = 0.06), both Li^+ and $TFSI^-$ diffusivities are suppressed in P(2EO-MO) relative to PEO by approximately a factor of two. For example, at r = 0.06, in P(2EO-MO) Li^+ diffusivity is 8.15×10^{-8} cm^2/s while $TFSI^-$ diffusivity is 4.89×10^{-7} cm^2/s, leading to $t_{+,MD}$ = 0.14. In PEO at r = 0.06, Li^+ diffusivity is 1.26×10^{-7} cm^2/s while $TFSI^-$ diffusivity is 9.23×10^{-7} cm^2/s, leading to $t_{+,MD}$ = 0.12. This is also observed experimentally. The cation transference numbers determined by MD simulations are likewise qualitatively consistent with the NMR measurements.

7.4 Conclusions

In this study, we report on the synthesis and characterization of a new polymer electrolyte, P(2EO-MO). Our characterization work includes both experimental and computational techniques. P(2EO-MO) was synthesized using cationic ring-opening polymerization of the cyclic ether monomer, 1,3,6-trioxocane. Electrolytes were prepared by mixing P(2EO-MO) with lithium bis(trifluoromethanesulfonyl) imide (LiTFSI) salt at a wide range of salt concentrations, r = 0.01-0.14, where r = [Li^+]/[O]. We use the PEO/LiTFSI system as a baseline. The ion transport characteristics of the two electrolytes of interest are compared in Table 7.3.

Table 7.3 contains a summary of the experimental results for PEO and P(2EO-MO) electrolytes at r = 0.08. DSC measurements of both polymers exhibit T_gs in the vicinity of -60°C in the neat state; P(2EO-MO), however, has a much more precipitous increase in T_g with salt concentration. For example, at r = 0.08 the T_g of P(2EO-MO)/LiTFSI (–12°C) is significantly higher than that of PEO/LiTFSI (–44°C) at the same salt concentration (Table 7.3). The conductivity of our electrolytes is affected by T_g. The σ of PEO at 90°C is 1.5×10^{-3} S/cm while that of P(2EO-MO) is 1.1×10^{-3} S/cm. To gain an understanding of transport of individual ions in these systems, we used PFG-NMR to measure the self-diffusion coefficients of Li- and F-containing ions in our electrolytes. Table 7.3 shows that both ions exhibit higher diffusivity in PEO. Based on this set of

information, most studies would conclude that PEO is the superior choice for a battery electrolyte. However, more complete characterization indicates that this is not true. Transference number measurements using the steady-state current technique show that P(2EO-MO) has a $t_{+,SS}$ that is approximately double that of PEO. This is qualitatively consistent with the transference number determined from PFG-NMR (Table 7.3). The steady-state dc current obtained in an electrolyte is governed by the product $\sigma t_{+,SS}$, which is higher in P(2EO-MO) compared to PEO. In other words, batteries made with P(2EO-MO) electrolytes are expected to be more efficacious compared to those made with PEO. We hope to demonstrate this in future studies.

Table 7.3. Summary of parameters obtained in this study for PEO and P(2EO-MO). Experimental measurements are for electrolytes at r=0.08 and T=90°C. MD simulations were performed at r=0.06, and ρ_{Li} was determined in dilute electrolytes. For each column, P(2EO-MO)/PEO (row 3) gives the ratio of the P(2EO-MO) value (row 1) to the PEO value (row 2).

	Experiment							***Simulations***			
	T_g (°C)	σ (S/cm)	D_{Li} (cm^2/s)	D_F (cm^2/s)	$t_{+,NMR}$	$t_{+,SS}$	$\sigma t_{+,SS}$ (S/cm)	ρ_{Li} (nm^{-3})	D_{Li} (cm^2/s)	D_F (cm^2/s)	$t_{+,MD}$
P(2EO-MO)	-12	1.1×10^{-3}	3.8×10^{-8}	9.7×10^{-8}	0.36	0.20	2.2×10^{-4}	20	8.2×10^{-8}	4.9×10^{-7}	0.14
PEO	-44	1.5×10^{-3}	6.4×10^{-8}	2.7×10^{-7}	0.19	0.08	1.2×10^{-4}	12	1.3×10^{-7}	9.2×10^{-7}	0.12
P(2EO-MO) / PEO	-	0.73	0.59	0.36	1.89	2.50	1.83	1.67	0.63	0.53	1.17

Atomistic MD simulations were used to analyze the solvation structure of the Li^+ and $TFSI^-$ ions in PEO and P(2EO-MO) for a range of r; results confirmed that differences in transport properties could not be attributed to differences in solvation structure. The main difference is that P(2EO-MO) preferentially solvates Li^+ using a two-chain solvation motif, whereas PEO has contributions of both one-chain and two-chain solvation. The consequence of this two-chain solvation in P(2EO-MO) may be the rapid increase in T_g with salt concentration. The density of Li^+ solvation sites, ρ_{Li}, calculated from simulations was higher in P(2EO-MO) relative to PEO (Table 7.3). We posit that differences in experimentally-determined ion transport properties in the two electrolytes are primarily due to this effect. The diffusion coefficients of Li^+ and $TFSI^-$ obtained using simulations are qualitatively consistent with experimental data. The simulations do capture the fact that the transference number of P(2EO-MO) electrolytes is higher than that of PEO electrolytes.

The ratio of transport properties of the two polymers of interest are also reported in Table 7.3. We see that conductivity and diffusion coefficients (in both experiments and simulations) are affected by T_g; transport parameters in P(2EO-MO) are lower than those in PEO and all the ratios are less than unity. On the other hand, the transference numbers determined by NMR, electrochemical methods, and MD simulations appear to be governed by factors other than T_g, as they are greater in P(2EO-MO). The same can be said for solvation-site density.

Our work demonstrates that the discovery of new electrolytes is facilitated by the use of complementary experimental and theoretical approaches.

7.5 Acknowledgements

The authors gratefully acknowledge Michael Webb and Zhen-Gang Wang for useful discussions. This research was supported by the National Science Foundation under DMREF Award Number NSF-CHE-1335486. DSC experiments were performed at the Molecular Foundry

user facilities at Lawrence Berkeley National Laboratory supported by the Office of Science, Office of Basic Energy Sciences, of the U.S. Department of Energy under Contract No. DE-AC02-05CH11231.

7.6 Nomenclature

PEO	poly(ethylene oxide)
P(2EO-MO)	poly(diethylene oxide-alt-oxymethylene)
LiTFSI	lithium bis(trifluoromethanesulfonyl) imide
SEI	solid electrolyte interface
NMR	nuclear magnetic resonance spectroscopy
PFG-NMR	pulsed-field-gradient NMR
GPC	gel permeation chromatography
DCM	dichloromethane
THF	tetrahydrofuran
DSC	differential scanning calorimetry
pppm	particle-particle-particle-mesh
MSD	mean-squared displacement
CS-DBP	Chemically Specific Dynamic Bond Percolation
rdf	radial distribution function
T_g	glass transition temperature (°C)
T_m	melting temperature (°C)
M_n	number-averaged molecular weight (kg/mol)
σ	conductivity (S/cm)
σ_r	reduced conductivity (S/cm)
D	salt diffusion coefficient (cm^2/s)
D_i	self-diffusion coefficient (cm^2/s)
D_{Li}	lithium self-diffusion coefficient (cm^2/s)
D_F	fluorine self-diffusion coefficient (cm^2/s)
$D_{r,i}$	reduced self-diffusion coefficient (cm^2/s)
$D_{r,Li}$	reduced lithium self-diffusion coefficient (cm^2/s)
$D_{r,F}$	reduced fluorine self-diffusion coefficient (cm^2/s)
t_+	true cation transference number
$t_{+,SS}$	transference number obtained using stead-state current method
$t_{+,NMR}$	transference number obtained using pulsed-field gradient NMR
$t_{+,MD}$	transference number obtained using MD simulations
i_0	initial current (mA/cm^2)
i_Ω	initial current determined by Ohm's law (mA/cm^2)
i_{SS}	steady-state current (mA/cm^2)
ΔV	dc potential (mV)
R_b	bulk electrolyte resistance ($\Omega\ cm^2$)

$R_{i,0}$	initial interfacial electrolyte resistance (Ω cm^2)
$R_{b,0}$	initial bulk electrolyte resistance (Ω cm^2)
r	moles of Li^+ per mole of ethylene oxide
l	electrolyte thickness (cm)
a	electrolyte area (cm^2)
t	time (s)
T	temperature (°C)
E	attenuation of the echo
γ	gyromagnetic ratio
δ	duration of gradient pulse (s)
Δ	interval between gradient pulses (s)
T_0	reference temperature (°C)
A	VTF prefactor for conductivity (SK$^{1/2}$/cm)
B	VTF prefactor for diffusivity (cm^2/sK$^{1/2}$)
E_a	effective activation energy (kJ/mol)
R	universal gas constant (kJ/mol K)
$g_{Li\text{-}O}$	lithium-oxygen radial distribution function
$g_{N\text{-}Li,C}$	nitrogen-lithium,carbon radial distribution function
r_i	position of the atom (Å)
V	volume of the simulation cell (nm^3)
N_α	number of particles in α
N_β	number of particles in β
ρ_{Li}	Li^+ solvation-site density (nm^{-3})

7.7 Supporting Information

7.7.1 DSC of PEO and P(2EO-MO) Electrolytes

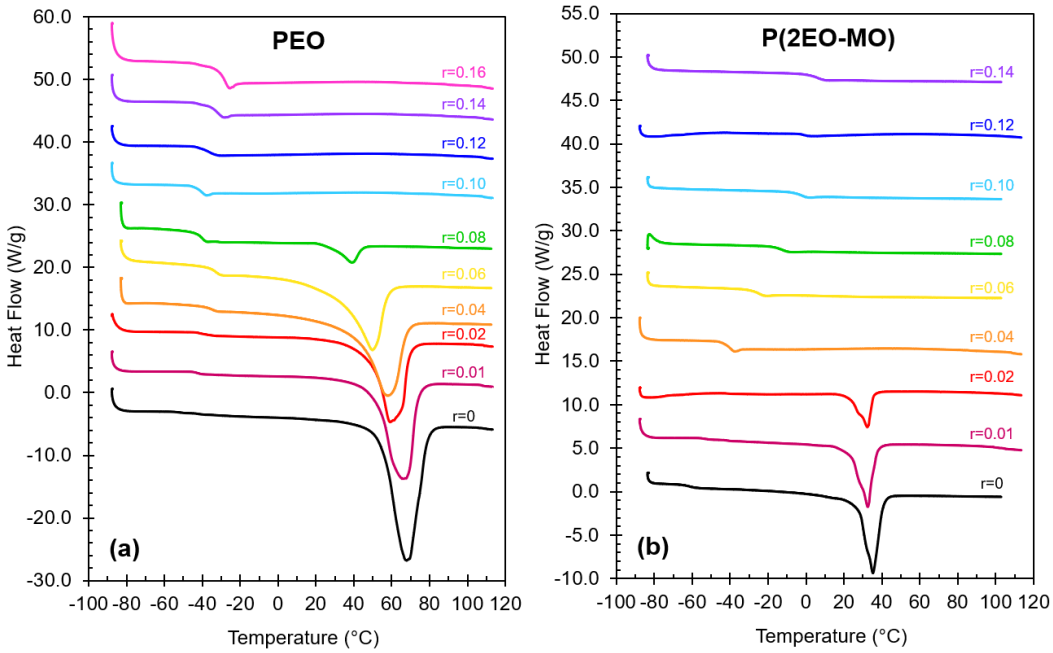

Figure 7.S1. Differential scanning calorimetry (DSC) traces of (a) PEO and (b) P(2EO-MO) electrolytes at different salt concentrations.

7.7.2 Li-TFSI Radial Distribution Functions

Figure 7.S2 shows a comparison of the Li-TFSI radial distribution function (rdf) in PEO and P(2EO-MO) as a function of salt concentration. In each case the rdf is calculated with respect to the Li cations and the oxygen atoms in TFSI. The rdfs show a minimal counter-ion presence in the first solvation shell of the ions. The counter-ion feature in the Li-solvation shell is also much weaker than the corresponding ether oxygen feature in the polymer-Li rdfs. This data is consistent weak ion pairing in both polymers for all studied salt concentrations.

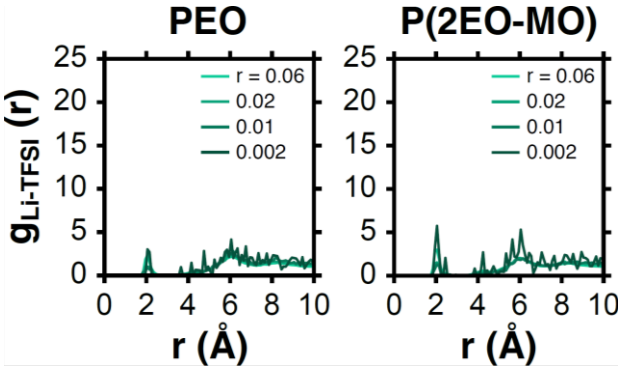

Figure 7.S2. Comparison of Li-TFSI radial distribution functions at different salt concentrations in PEO (left) and P(2EO-MO) (right). Note, "r" in each legend refers to the salt concentration.

Summary

The development of next-generation polymer electrolytes is restricted by a fundamental lack of understanding of ion transport in these systems. In this work, we aim to identify the factors that govern ion transport in polymer electrolytes. We use polyethylene oxide (PEO) mixed with lithium bis(trifluoromethanesulfonyl) imide (LiTFSI) salts as a model system throughout this work. This electrolyte was first used to identify the best techniques for complete characterization of an electrolyte, and then was used as a benchmark to compare against newly-designed polymer electrolytes.

The first two experiments focused on evaluating different approaches for measuring the transference number of concentrated electrolytes. We compared a new approach proposed by Balsara and Newman[102] ($t_{+,\mathrm{Ne}}$) that was derived using concentrated solution theory to more popular approaches that rely on dilute solution theory. All three measurements were performed in 5 kg/mol PEO/LiTFSI electrolytes over a wide range of salt concentrations. The methods that rely on ideal solution assumptions yield positive values throughout the entire concentration window, whereas $t_{+,\mathrm{Ne}}$ exhibits a complex concentration dependence, with negative values at intermediate salt concentrations. These results demonstrate that dilute solution theory is not a valid approximation in polymer electrolytes. More work is needed to understand the nature of the ionic species present in these systems. In the next experiment, $t_{+,\mathrm{Ne}}$ was compared against a more well-established approach proposed by Ma et al.[76] ($t_{+,\mathrm{CI}}$) that is also derived using concentrated solution theory. Both experiments are rigorous, requiring multiple electrochemical measurements to obtain the transference number. In 275 kg/mol PEO/LiTFSI, the values of $t_{+,\mathrm{Ne}}$ and $t_{+,\mathrm{CI}}$ are within experimental error at all concentrations, highlighting the equivalence of these two techniques. In 5 kg/mol PEO, there is a substantial difference between $t_{+,\mathrm{CI}}$ and $t_{+,\mathrm{Ne}}$, particularly at low salt concentrations. We attribute this to the electrochemical measurements used to obtain $t_{+,\mathrm{CI}}$, which are sensitive to the nature of the lithium electrode-electrolyte interfaces, which are complex in 5 kg/mol PEO. The approach of Balsara and Newman is thus believed to be a robust measure of the transference number.

To demonstrate the practical significance of our transport measurements, we presented a theoretical model that was used to predict cycling characteristics of symmetric lithium-polymer-lithium cells. The data previously obtained in 5 kg/mol PEO/LiTFSI electrolytes were used as inputs for the model. First, we showed model predictions of salt concentration profiles, $r(x)$, and potential profiles, $\Phi(x)$, in the electrolyte under steady-state operation of the symmetric cell. Both $r(x)$ and $\Phi(x)$ exhibit nonlinearities due to the strong concentration dependence of the transport and thermodynamic properties of the electrolyte; the steepest gradients occur at salt concentrations where the D is low and t_+ is negative. Our model was then used to predict the limiting current of PEO/LiTFSI electrolytes. Experimentally measured cycling data from a lithium-polymer-lithium cell was compared against theoretical predictions for Φ over a wide range of salt concentrations and current densities. The agreement between experiment and theory is excellent without resorting to adjustable parameters or simplifying assumptions

The next set of experiments focus on identifying the factors that govern ion transport in newly-designed polymers, with the overarching goal of finding a polymer electrolyte superior to PEO/LiTFSI. We first characterized a set of polyester electrolytes wherein systematic changes are made to the sidechains and backbone of the monomer to gain an understanding of the relationship

between monomer structure and ionic conductivity. A new approach for analyzing the conductivity of electrolytes was presented. This analysis centers around the calculation of a reduced conductivity wherein the glass transition temperature is decoupled to gain insight into ion transport in these materials. Next, a similar analysis was used to investigate a systematic set of linear polyethers (C_xEO_y) in which aliphatic linkers have been added to a PEO backbone. A combined experimental and computational approach was used to understand ion transport in these systems. The results highlight the importance of solvation-site connectivity in these materials. In the last experiment, we compared the transport properties in electrolytes based on PEO and a newly-synthesized P(2EO-MO) polymer. The product $\sigma t_{+,SS}$ is identified as the most important transport metric for comparing electrolytes in the absence of complete characterization; $\sigma t_{+,SS}$ is higher in P(2EO-MO) suggesting that it is a more efficacious electrolyte for battery applications. Simulations showed that the improvement in ion transport is likely attributed to increased solvation-site density in P(2EO-MO). More work is needed to fully characterize ion transport in P(2EO-MO) electrolytes.

References

(1) Denholm, P.; Ela, E.; Kirby, B.; Milligan, M. *Role of Energy Storage with Renewable Electricity Generation*; Golden, CO (United States), 2010.

(2) Barton, J. P.; Infield, D. G. Energy Storage and Its Use With Intermittent Renewable Energy. *IEEE Trans. Energy Convers.* **2004**, *19* (2), 441–448.

(3) Dunn, B.; Kamath, H.; Tarascon, J.-M. Electrical Energy Storage for the Grid: A Battery of Choices. *Science* **2011**, *334* (6058), 928–935.

(4) Cairns, E. J.; Albertus, P. Batteries for Electric and Hybrid-Electric Vehicles. *Annu. Rev. Chem. Biomol. Eng.* **2010**, *1* (1), 299–320.

(5) Thackeray, M. M.; Wolverton, C.; Isaacs, E. D. Electrical Energy Storage for Transportation—approaching the Limits of, and Going beyond, Lithium-Ion Batteries. *Energy Environ. Sci.* **2012**, *5* (7), 7854.

(6) Balsara, N. P.; Newman, J. Comparing the Energy Content of Batteries, Fuels, and Materials. *J. Chem. Educ.* **2013**, *90* (4), 446–452.

(7) Bruce, P. G.; Freunberger, S. A.; Hardwick, L. J.; Tarascon, J.-M. Li–O2 and Li–S Batteries with High Energy Storage. *Nat. Mater.* **2012**, *11* (1), 19–29.

(8) Girishkumar, G.; McCloskey, B.; Luntz, A. C.; Swanson, S.; Wilcke, W. Lithium−Air Battery: Promise and Challenges. *J. Phys. Chem. Lett.* **2010**, *1* (14), 2193–2203.

(9) Xu, K. Nonaqueous Liquid Electrolytes for Lithium-Based Rechargeable Batteries. *Chem. Rev.* **2004**, *104*, 4303–4417.

(10) Goodenough, J. B.; Kim, Y. Challenges for Rechargeable Li Batteries †. *Chem. Mater.* **2010**, *22* (3), 587–603.

(11) Marcinek, M.; Syzdek, J.; Marczewski, M.; Piszcz, M.; Niedzicki, L.; Kalita, M.; Plewa-Marczewska, A.; Bitner, A.; Wieczorek, P.; Trzeciak, T.; et al. Electrolytes for Li-Ion Transport – Review. *Solid State Ionics* **2015**, *276*, 107–126.

(12) Brandt, K. Historical Development of Secondary Lithium Batteries. *Solid State Ionics* **1994**, *69* (3–4), 173–183.

(13) Whittingham, M. S. Lithium Batteries and Cathode Materials. *Chem. Rev.* **2004**, *104* (10), 4271–4302.

(14) Li, W.; Dahn, J. R.; Wainwright, D. S. Rechargeable Lithium Batteries with Aqueous Electrolytes. *Science* **1994**, *264* (5162), 1115–1118.

(15) Lin, D.; Liu, Y.; Cui, Y. Reviving the Lithium Metal Anode for High-Energy Batteries. *Nature Nanotechnology*. 2017.

(16) Aurbach, D. *Nonaqueous Electrochemistry*; Marcel Dekker, 1999.

(17) ARMAND, M. Polymer Solid Electrolytes - an Overview. *Solid State Ionics* **1983**, *9–10*, 745–754.

(18) Singh, M.; Odusanya, O.; Wilmes, G. M.; Eitouni, H. B.; Gomez, E. D.; Patel, A. J.; Chen, V. L.; Park, M. J.; Fragouli, P.; Iatrou, H.; et al. Effect of Molecular Weight on the Mechanical and Electrical Properties of Block Copolymer Electrolytes. *Macromolecules* **2007**, *40* (13), 4578–4585.

(19) Khurana, R.; Schaefer, J. L.; Archer, L. A.; Coates, G. W. Suppression of Lithium Dendrite

Growth Using Cross-Linked Polyethylene/Poly(Ethylene Oxide) Electrolytes: A New Approach for Practical Lithium-Metal Polymer Batteries. *J. Am. Chem. Soc.* **2014**, *136* (20), 7395–7402.

(20) Monroe, C.; Newman, J. Dendrite Growth in Lithium/Polymer Systems. *J. Electrochem. Soc.* **2003**, *150* (10), A1377.

(21) Monroe, C.; Newman, J. The Impact of Elastic Deformation on Deposition Kinetics at Lithium/Polymer Interfaces. *J. Electrochem. Soc.* **2005**, *152* (2), A396.

(22) Diddens, D.; Heuer, A.; Borodin, O. Understanding the Lithium Transport within a Rouse-Based Model for a PEO/LiTFSI Polymer Electrolyte. *Macromolecules* **2010**, *43* (4), 2028–2036.

(23) Borodin, O.; Smith, G. D. Mechanism of Ion Transport in Amorphous Poly(Ethylene Oxide)/LiTFSI from Molecular Dynamics Simulations. *Macromolecules* **2006**, *39* (4), 1620–1629.

(24) Borodin, O.; Smith, G. D. Li + Transport Mechanism in Oligo(Ethylene Oxide)s Compared to Carbonates. *J. Solution Chem.* **2007**, *36* (6), 803–813.

(25) Ratner, M. A.; Shriver, D. F. Ion Transport in Solvent-Free Polymers. *Chem. Rev.* **1988**, *88* (1), 109–124.

(26) Fenton, D. E.; Parker, J. M.; Wright, P. V. Complexes of Alkali Metal Ions with Poly(Ethylene Oxide). *Polymer (Guildf).* **1973**, *14* (11), 589.

(27) Armand, M. B.; Chabagno, J. M.; Duclot, M. J. Poly-Ethers as Solid Electrolytes. In *Fast Ion Transport in Solids, eds. Vashishta, P.M., Mundy, J.N., and Shenoy, G.K.*; North-Holland, 1979; pp 131–136.

(28) Lascaud, S.; Perrier, M.; Vallee, A.; Besner, S.; Prud'homme, J.; Armand, M. Phase Diagrams and Conductivity Behavior of Poly(Ethylene Oxide)-Molten Salt Rubbery Electrolytes. *Macromolecules* **1994**, *27* (25), 7469–7477.

(29) Shi, J.; Vincent, C. The Effect of Molecular Weight on Cation Mobility in Polymer Electrolytes. *Solid State Ionics* **1993**, *60* (1–3), 11–17.

(30) Gorecki, W.; Jeannin, M.; Belorizky, E.; Roux, C.; Armand, M.; A, M. J. R. and V. C.; A, B. P. G. and V. C.; M, G. F.; A, S. T.; Takeoka S, O. H. and T. E.; et al. Physical Properties of Solid Polymer Electrolyte PEO(LiTFSI) Complexes. *J. Phys. Condens. Matter* **1995**, *7* (34), 6823–6832.

(31) Gorecki, W.; Belorizky, E.; Berthier, C.; Donoso, P.; Armand, M. NMR Investigation of P(EO)(LiClO4)X. *Electrochim. Acta* **1992**, *37* (9), 1685–1687.

(32) Mao, G.; Saboungi, M.-L.; Price, D. L.; Armand, M. B.; Howells, W. S. Structure of Liquid PEO-LiTFSI Electrolyte. *Phys. Rev. Lett.* **2000**, *84* (24), 5536–5539.

(33) Shriver, D.; Papke, B.; Ratner, M.; Dupon, R.; Wong, T.; Brodwin, M. Structure and Ion Transport in Polymer-Salt Complexes. *Solid State Ionics* **1981**, *5*, 83–88.

(34) Kelly, I. E.; Owen, J. R.; Steele, B. C. H. Poly(Ethylene Oxide) Electrolytes for Operation at near Room Temperature. *J. Power Sources* **1985**, *14* (1–3), 13–21.

(35) Watanabe, M.; Itoh, M.; Sanui, K.; Ogata, N. Carrier Transport and Generation Processes in Polymer Electrolytes Based on Poly(Ethylene Oxide) Networks. *Macromolecules* **1987**, *20* (3), 569–573.

(36) Bhattacharja, S.; Smoot, S.; Whitmore, D. Cation and Anion Diffusion in the Amorphous Phase of the Polymer Electrolyte (PEO) 8LiCF3SO3. *Solid State Ionics* **1986**, *18–19*, 306–314.

(37) Redfern, P. C.; Curtiss, L. A. Quantum Chemical Studies of Li+ Cation Binding to Polyalkyloxides. *J. Power Sources* **2002**, *110* (2), 401–405.

(38) Watanabe, M.; Nagaoka, K.; Kanba, M.; Shinohara, I. Ionic Conductivity of Polymeric Solid Electrolytes Based on Poly(Propylene Oxide) or Poly(Tetramethylene Oxide). *Polym. J.* **1982**, *14* (11), 877–886.

(39) Watanabe, M.; Ikeda, J.; Shinohara, I. Effect of Molecular Weight of Polymeric Solvent on Ion Conductive Behavior in Poly(Propylene Oxide) Solution of LiClO4. *Polym. J.* **1983**, *15* (1), 65–69.

(40) Buriez, O.; Han, Y. B.; Hou, J.; Kerr, J. B.; Qiao, J.; Sloop, S. E.; Tian, M.; Wang, S. Performance Limitations of Polymer Electrolytes Based on Ethylene Oxide Polymers. *J. Power Sources* **2000**, *89* (2), 149–155.

(41) Barteau, K. P.; Wolffs, M.; Lynd, N. A.; Fredrickson, G. H.; Krarner, E. J.; Hawker, C. J. Allyl Glycidyl Ether-Based Polymer Electrolytes for Room Temperature Lithium Batteries. *Macromolecules* **2013**, *46* (22), 8988–8994.

(42) Liu, G.; Reeder, C. L.; Sun, X.; Kerr, J. B. Diffusion Coefficients in Trimethyleneoxide Containing Comb Branch Polymer Electrolytes. *Solid State Ionics* **2004**, *175* (1–4), 781–783.

(43) Watanabe, M.; Hirakimoto, T.; Mutoh, S.; Nishimoto, A. Polymer Electrolytes Derived from Dendritic Polyether Macromonomers. In *Solid State Ionics*; 2002; Vol. 148, pp 399–404.

(44) Armstrong, R. D.; Clarke, M. D. Lithium Ion Conducting Polymeric Electrolytes Based on Poly(Ethylene Adipate). *Electrochim. Acta* **1984**, *29* (10), 1443–1446.

(45) Dupon, R. Ion Transport in the Polymer Electrolytes Formed Between Poly(Ethylene Succinate) and Lithium Tetrafluoroborate. *J. Electrochem. Soc.* **1984**, *131* (3), 586–589.

(46) Watanabe, M.; Rikukawa, M.; Sanui, K.; Ogata, N.; Kato, H.; Kobayashi, T.; Ohtaki, Z. Ionic Conductivity of Polymer Complexes Formed by Poly(Ethylene Succinate) and Lithium Perchlorate. *Macromolecules* **1984**, *17* (12), 2902–2908.

(47) Watanabe, M.; Togo, M.; Sanui, K.; Ogata, N.; Kobayashi, T.; Ohtaki, Z. Ionic Conductivity of Polymer Complexes Formed by Poly(β-Propiolactone) and Lithium Perchlorate. *Macromolecules* **1984**, *17* (12), 2908–2912.

(48) Lee, Y.-C.; Ratner, M. A.; Shriver, D. F. Ionic Conductivity in the Poly(Ethylene Malonate)/Lithium Triflate System. *Solid State Ionics* **2001**, *138* (3–4), 273–276.

(49) Tominaga, Y.; Shimomura, T.; Nakamura, M. Alternating Copolymers of Carbon Dioxide with Glycidyl Ethers for Novel Ion-Conductive Polymer Electrolytes. *Polymer (Guildf).* **2010**, *51* (19), 4295–4298.

(50) Smith, M.; Silva, M.; Cerqueira, S.; MacCallum, J. R. Preparation and Characterization of a Lithium Ion Conducting Electrolyte Based on Poly(Trimethylene Carbonate). *Solid State Ionics* **2001**, *140* (3–4), 345–351.

(51) Nagaoka, K.; Naruse, H.; Shinohara, I.; Watanabe, M. High Ionic Conductivity in Poly(Dimethyl Siloxane-Co-Ethylene Oxide) Dissolving Lithium Perchlorate. *J. Polym. Sci. Polym. Lett. Ed.* **1984**, *22* (12), 659–663.

(52) Hooper, R.; Lyons, L. J.; Moline, D. A.; West, R. A Highly Conductive Solid-State Polymer Electrolyte Based on a Double-Comb Polysiloxane Polymer with Oligo(Ethylene Oxide) Side Chains. *Organometallics* **1999**, *18* (17), 3249–3251.

(53) Hooper, R.; Lyons, L. J.; Mapes, M. K.; Schumacher, D.; Moline, D. A.; West, R. Highly Conductive Siloxane Polymers. *Macromolecules* **2001**, *34* (4), 931–936.

(54) Fonseca, C. P.; Neves, S. Characterization of Polymer Electrolytes Based on Poly(Dimethyl

Siloxane-Co-Ethylene Oxide). *J. Power Sources* **2002**, *104* (1), 85–89.

(55) Blonsky, P.; Shriver, D.; Austin, P.; Allcock, H. Complex Formation and Ionic Conductivity of Polyphosphazene Solid Electrolytes. *Solid State Ionics* **1986**, *18–19*, 258–264.

(56) Wong, D. H. C.; Thelen, J. L.; Fu, Y.; Devaux, D.; Pandya, A. A.; Battaglia, V. S.; Balsara, N. P.; DeSimone, J. M. Nonflammable Perfluoropolyether-Based Electrolytes for Lithium Batteries. *Proc. Natl. Acad. Sci. U. S. A.* **2014**, *111* (9), 3327–3331.

(57) Newman, J.; Thomas-Alyea, K. E. *Electrochemical Systems*, third.; John Wiley & Sons, 2004; Vol. 27.

(58) Teran, A. A.; Tang, M. H.; Mullin, S. A.; Balsara, N. P. Effect of Molecular Weight on Conductivity of Polymer Electrolytes. *Solid State Ionics* **2011**, *203* (1), 18–21.

(59) Nishimoto, A.; Watanabe, M.; Ikeda, Y.; Kohjiya, S. High Ionic Conductivity of New Polymer Electrolytes Based on High Molecular Weight Polyether Comb Polymers. *Electrochim. Acta* **1998**, *43* (10–11), 1177–1184.

(60) Watanabe, M.; Endo, T.; Nishimoto, A.; Miura, K.; Yanagida, M. High Ionic Conductivity and Electrode Interface Properties of Polymer Electrolytes Based on High Molecular Weight Branched Polyether. *J. Power Sources* **1999**, *81–82*, 786–789.

(61) Nishimoto, A.; Agehara, K.; Furuya, N.; Watanabe, T.; Watanabe, M. High Ionic Conductivity of Polyether-Based Network Polymer Electrolytes with Hyperbranched Side Chains. *Macromolecules* **1999**, *32* (5), 1541–1548.

(62) Matoba, Y. Ionic Conductivity and Mechanical Properties of Polymer Networks Prepared from High Molecular Weight Branched Poly(Oxyethylene)S. *Solid State Ionics* **2002**, *147* (3–4), 403–409.

(63) Acosta, J. Structural, Morphological and Electrical Characterization of Polymer Electrolytes Based on PEO/PPO Blends. *Solid State Ionics* **1996**, *85* (1–4), 85–90.

(64) Choi, B. K.; Kim, Y. W.; Shin, H. K. Ionic Conduction in PEO-PAN Blend Polymer Electrolytes. *Electrochim. Acta* **2000**, *45* (8), 1371–1374.

(65) Zhang, Z.; Jin, J.; Bautista, F.; Lyons, L.; Shariatzadeh, N.; Sherlock, D.; Amine, K.; West, R. Ion Conductive Characteristics of Cross-Linked Network Polysiloxane-Based Solid Polymer Electrolytes. *Solid State Ionics* **2004**, *170* (3–4), 233–238.

(66) Watanabe, M. Polymer Electrolytes Derived from Dendritic Polyether Macromonomers. *Solid State Ionics* **2002**, *148* (3–4), 399–404.

(67) Croce, F.; Persi, L.; Scrosati, B.; Serraino-Fiory, F.; Plichta, E.; Hendrickson, M. . Role of the Ceramic Fillers in Enhancing the Transport Properties of Composite Polymer Electrolytes. *Electrochim. Acta* **2001**, *46* (16), 2457–2461.

(68) Johansson, P.; Ratner, M. A.; Shriver, D. F. The Influence of Inert Oxide Fillers on Poly(Ethylene Oxide) and Amorphous Poly(Ethylene Oxide) Based Polymer Electrolytes. *J. Phys. Chem. B* **2001**, *105* (37), 9016–9021.

(69) Baldwin, K. R.; Golder, A. J.; Knight, J. *Polymer Electrolytes: An Investigation of Some Poly (N-Propylaziridine)/Lithium Salt Compositions.*; 1984.

(70) Harris, C. S.; Shriver, D. F.; Ratner, M. A. Complex Formation of Polyethylenimine with Sodium Triflate and Conductivity Behavior of the Complexes. *Macromolecules* **1986**, *19* (4), 987–989.

(71) Morioka, T.; Ota, K.; Tominaga, Y. Effect of Oxyethylene Side Chains on Ion-Conductive Properties of Polycarbonate-Based Electrolytes. *Polymer (Guildf).* **2016**, *84*, 21–26.

(72) Cowie, J. M. G.; Martin, A. C. S. Ionic Conductivity in Poly(Di-Poly(Propylene Glycol) Itaconate)-Salt Mixtures. *Polymer (Guildf).* **1987**, *28* (4), 627–632.

(73) Nekoomanesh H., M.; Nagae, S.; Booth, C.; Owen, J. R. The Effect of Oxyethylene Sequence Length on the Properties of Poly[Oxymethylene-Oligo(Oxyethylene)]/LiClO[Sub 4] Polymer Electrolytes. *J. Electrochem. Soc.* **1992**, *139* (11), 3046.

(74) Watanabe, M.; Nagano, S.; Sanui, K.; Ogata, N. Ion Conduction Mechanism in Network Polymers from Poly(Ethylene Oxide) and Poly(Propylene Oxide) Containing Lithium Perchlorate. *Solid State Ionics* **1986**, *18–19*, 338–342.

(75) Sarapas, J. M.; Tew, G. N. Poly(Ether–thioethers) by Thiol–Ene Click and Their Oxidized Analogues as Lithium Polymer Electrolytes. *Macromolecules* **2016**, *49* (4), 1154–1162.

(76) Ma, Y.; Doyle, M.; Fuller, T. F.; Doeff, M. M.; Jonghe, L. C. De; Newman, J. The Measurement of a Complete Set of Transport Properties for a Concentrated Solid Polymer Electrolyte Solution. *J. Electrochem. Soc.* **1995**, *142* (6), 1859.

(77) Ferry, A.; Doeff, M. M.; Jonghe, L. C. De. Transport Property and Raman Spectroscopic Studies of the Polymer Electrolyte System P(EO)[Sub n]-NaTFSI. *J. Electrochem. Soc.* **1998**, *145* (5), 1586.

(78) Ferry, A.; Doeff, M. M.; DeJonghe, L. C. Transport Property Measurements of Polymer Electrolytes. *Electrochim. Acta* **1998**, *43* (10), 1387–1393.

(79) Doeff, M. M.; Georèn, P.; Qiao, J.; Kerr, J.; Jonghe, L. C. De. Transport Properties of a High Molecular Weight Poly(Propylene Oxide)-LiCF[Sub 3]SO[Sub 3] System. *J. Electrochem. Soc.* **1999**, *146* (6), 2024.

(80) Tominaga, Y.; Yamazaki, K.; Nanthana, V. Effect of Anions on Lithium Ion Conduction in Poly(Ethylene Carbonate)-Based Polymer Electrolytes. *J. Electrochem. Soc.* **2015**, *162* (2), A3133–A3136.

(81) Watanabe, M.; Nagano, S.; Sanui, K.; Ogata, N. Estimation of Li+ Transport Number in Polymer Electrolytes by the Combination of Complex Impedance and Potentiostatic Polarization Measurements. *Solid State Ionics* **1988**, *28*, 911–917.

(82) Kato, Y.; Watanabe, M.; Sanui, K.; Ogata, N. Ionic Transport Number of Network PEO Electrolytes. *Solid State Ionics* **1990**, *40*, 632–636.

(83) Timachova, K.; Watanabe, H.; Balsara, N. P. Effect of Molecular Weight and Salt Concentration on Ion Transport and the Transference Number in Polymer Electrolytes. *Macromolecules* **2015**, *48* (21), 7882–7888.

(84) Sun, B.; Mindemark, J.; V. Morozov, E.; Costa, L. T.; Bergman, M.; Johansson, P.; Fang, Y.; Furó, I.; Brandell, D. Ion Transport in Polycarbonate Based Solid Polymer Electrolytes: Experimental and Computational Investigations. *Phys. Chem. Chem. Phys.* **2016**, *18* (14), 9504–9513.

(85) Edman, L.; Doeff, M. M.; Ferry, A.; Kerr, J.; De Jonghe, L. C. Transport Properties of the Solid Polymer Electrolyte System P(EO) n LiTFSI. *J. Phys. Chem. B* **2000**, *104* (15), 3476–3480.

(86) Rey, I.; Bruneel, J.; Grondin, J.; Servant, L.; Lassègues, J. Raman Spectroelectrochemistry of a Lithium/Polymer Electrolyte Symmetric Cell. *J. Electrochem. Soc.* **1998**, *145* (9), 3034.

(87) Chintapalli, M.; Timachova, K.; Olson, K. R.; Mecham, S. J.; Devaux, D.; DeSimone, J. M.; Balsara, N. P. Relationship between Conductivity, Ion Diffusion, and Transference Number in Perfluoropolyether Electrolytes. *Macromolecules* **2016**, *49* (9), 3508–3515.

(88) Evans, J.; Vincent, C. A.; Bruce, P. G. Electrochemical Measurement of Transference Numbers in Polymer Electrolytes. *Polymer (Guildf).* **1987**, *28* (13), 2324–2328.

(89) Bruce, P. G.; Evans, J.; Vincent, C. A. Conductivity and Transference Number Measurements on Polymer Electrolytes. *Solid State Ionics* **1988**, *28*, 918–922.

(90) Tominaga, Y.; Yamazaki, K. Fast Li-Ion Conduction in Poly(Ethylene Carbonate)-Based Electrolytes and Composites Filled with TiO2 Nanoparticles. *Chem. Commun.* **2014**, *50* (34), 4448.

(91) Capiglia, C.; Saito, Y.; Kageyama, H.; Mustarelli, P.; Iwamoto, T.; Tabuchi, T.; Tukamoto, H. 7Li and 19F Diffusion Coefficients and Thermal Properties of Non-Aqueous Electrolyte Solutions for Rechargeable Lithium Batteries. *J. Power Sources* **1999**, *81*, 859–862.

(92) Valoen, L. O.; Reimers, J. N. Transport Properties of LiPF[Sub 6]-Based Li-Ion Battery Electrolytes. *J. Electrochem. Soc.* **2005**, *152* (5), A882.

(93) Zhao, J.; Wang, L.; He, X.; Wan, C.; Jiang, C. Determination of Lithium-Ion Transference Numbers in LiPF[Sub 6]–PC Solutions Based on Electrochemical Polarization and NMR Measurements. *J. Electrochem. Soc.* **2008**, *155* (4), A292.

(94) Zugmann, S.; Fleischmann, M.; Amereller, M.; Gschwind, R. M.; Wiemhöfer, H. D.; Gores, H. J. Measurement of Transference Numbers for Lithium Ion Electrolytes via Four Different Methods, a Comparative Study. *Electrochim. Acta* **2011**, *56* (11), 3926–3933.

(95) Aihara, Y.; Bando, T.; Nakagawa, H.; Yoshida, H.; Hayamizu, K.; Akiba, E.; Price, W. S. Ion Transport Properties of Six Lithium Salts Dissolved in γ-Butyrolactone Studied by Self-Diffusion and Ionic Conductivity Measurements. *J. Electrochem. Soc.* **2004**, *151* (1), A119.

(96) Bruce, P. G.; Vincent, C. A. Steady State Current Flow in Solid Binary Electrolyte Cells. *J. Electroanal. Chem. Interfacial Electrochem.* **1987**, *225* (1–2), 1–17.

(97) Jo, G.; Jeon, H.; Park, M. J. Synthesis of Polymer Electrolytes Based on Poly(Ethylene Oxide) and an Anion-Stabilizing Hard Polymer for Enhancing Conductivity and Cation Transport. *ACS Macro Lett.* **2015**, *4* (2), 225–230.

(98) Geiculescu, O. E.; Rajagopal, R.; Creager, S. E.; DesMarteau, D. D.; Zhang, X.; Fedkiw, P. Transport Properties of Solid Polymer Electrolytes Prepared from Oligomeric Fluorosulfonimide Lithium Salts Dissolved in High Molecular Weight Poly(Ethylene Oxide). *J. Phys. Chem. B* **2006**, *110* (46), 23130–23135.

(99) Pożyczka, K.; Marzantowicz, M.; Dygas, J. R.; Krok, F. IONIC CONDUCTIVITY AND LITHIUM TRANSFERENCE NUMBER OF POLY(ETHYLENE OXIDE):LiTFSI SYSTEM. *Electrochim. Acta* **2017**, *227*, 127–135.

(100) Lu, Y.; Tikekar, M.; Mohanty, R.; Hendrickson, K.; Ma, L.; Archer, L. A. Stable Cycling of Lithium Metal Batteries Using High Transference Number Electrolytes. *Adv. Energy Mater.* **2015**, *5* (9), 1402073.

(101) Doyle, M.; Newman, J. Analysis of Transference Number Measurements Based on the Potentiostatic Polarization of Solid Polymer Electrolytes. *J. Electrochem. Soc.* **1995**, *142* (10), 3465.

(102) Balsara, N. P.; Newman, J. Relationship between Steady-State Current in Symmetric Cells and Transference Number of Electrolytes Comprising Univalent and Multivalent Ions. *J. Electrochem. Soc.* **2015**, *162* (14), A2720–A2722.

(103) Pesko, D. M.; Webb, M. A.; Jung, Y.; Zheng, Q.; Miller III, T. F.; Coates, G. W.; Balsara, N. P. Universal Relationship between Conductivity and Solvation-Site Connectivity in Ether-Based

Polymer Electrolytes. *Macromolecules* **2016**, *49* (14), 5244–5255.

(104) Devaux, D.; Bouchet, R.; Glé, D.; Denoyel, R. Mechanism of Ion Transport in PEO/LiTFSI Complexes: Effect of Temperature, Molecular Weight and End Groups. *Solid State Ionics* **2012**, *227*, 119–127.

(105) Pesko, D. M.; Jung, Y.; Hasan, A. L.; Webb, M. A.; Coates, G. W.; Miller III, T. F.; Balsara, N. P. Effect of Monomer Structure on Ionic Conductivity in a Systematic Set of Polyester Electrolytes. *Solid State Ionics* **2016**, *289*, 118–124.

(106) Mullin, S. A.; Stone, G. M.; Panday, A.; Balsara, N. P. Salt Diffusion Coefficients in Block Copolymer Electrolytes. *J. Electrochem. Soc.* **2011**, *158* (6), A619.

(107) Stewart, S.; Newman, J. Measuring the Salt Activity Coefficient in Lithium-Battery Electrolytes. *J. Electrochem. Soc.* **2008**, *155* (6), A458.

(108) Hafezi, H.; Newman, J. Verification and Analysis of Transference Number Measurements by the Galvanostatic Polarization Method. *J. Electrochem. Soc.* **2000**, *147* (8), 3036.

(109) Orädd, G.; Edman, L.; Ferry, A. Diffusion: A Comparison between Liquid and Solid Polymer LiTFSI Electrolytes. *Solid State Ionics* **2002**, *152*, 131–136.

(110) Georén, P.; Lindbergh, G. Characterisation and Modelling of the Transport Properties in Lithium Battery Polymer Electrolytes. *Electrochim. Acta* **2001**, *47* (4), 577–587.

(111) Rey, I.; Lassègues, J. C.; Grondin, J.; Servant, L. Infrared and Raman Study of the PEO-LiTFSI Polymer Electrolyte. *Electrochim. Acta* **1998**, *43* (10–11), 1505–1510.

(112) Edman, L. Ion Association and Ion Solvation Effects at the Crystalline−Amorphous Phase Transition in PEO−LiTFSI. *J. Phys. Chem. B* **2000**, *104*, 7254–7258.

(113) Meyer, W. H. Polymer Electrolytes for Lithium-Ion Batteries. *Adv. Mater.* **1998**, *10* (6), 439–448.

(114) Scrosati, B.; Vincent, C. A. Polymer Electrolytes: The Key to Lithium Polymer Batteries. *MRS Bull.* **2011**, *25* (03), 28–30.

(115) Hittorf, J. W. Ueber Die Allotropie Des Selens. *Ann. der Phys. und Chemie* **1851**, *160* (10), 214–220.

(116) Spiro, M. Historical Highlights in Transference Number Research; 1989; pp 92–114.

(117) Tubandt, C.; Reinhold, H. Über Gemischte Elektrische Leitung in Einheitlichen Festen Verbindungen. *Zeitschrift für Anorg. und Allg. Chemie* **1927**, *160* (1), 222–236.

(118) Longsworth, L. G. A Differential Moving Boundary Method for Transference Numbers. *J. Am. Chem. Soc.* **1943**, *65* (9), 1755–1765.

(119) Taylor, P. B. Electromotive Force of the Cell with Transference and Theory of Interdiffusion of Electrolytes. *J. Phys. Chem.* **1926**, *31* (10), 1478–1500.

(120) Holz, M. Electrophoretic NMR. *Chem. Soc. Rev.* **1994**, *23* (3), 165.

(121) Ravn Sørensen, P.; Jacobsen, T. Conductivity, Charge Transfer and Transport Number—an Ac-Investigation of the Polymer Electrolyte LiSCN-Poly(Ethyleneoxide). *Electrochim. Acta* **1982**, *27* (12), 1671–1675.

(122) Pollard, R. Determination of Transport Properties for Solid Electrolytes from the Impedance of Thin Layer Cells. *J. Electrochem. Soc.* **1989**, *136* (12), 3734–3748.

(123) Price, W. S. Pulsed-Field Gradient Nuclear Magnetic Resonance as a Tool for Studying Translational Diffusion: Part 1. Basic Theory. *Concepts Magn. Reson.* **1997**, *9* (5), 299–336.

(124) Pesko, D. M.; Timachova, K.; Bhattacharya, R.; Smith, M. C.; Villaluenga, I.; Newman, J.; Balsara, N. P. Negative Transference Numbers in Poly(Ethylene Oxide)-Based Electrolytes. *J. Electrochem. Soc.* **2017**, *164* (11), E3569–E3575.

(125) Zheng, Q.; Pesko, D. M.; Savoie, B. M.; Timachova, K.; Hasan, A. L.; Smith, M. C.; Miller, T. F.; Coates, G. W.; Balsara, N. P. Optimizing Ion Transport in Polyether-Based Electrolytes for Lithium Batteries. *Macromolecules* **2018**, *51* (8), 2847–2858.

(126) Villaluenga, I.; Pesko, D.; Timachova, K.; Feng, Z.; Newman, J.; Srinivasan, V.; Balsara, N. Negative Stefan-Maxwell Diffusion Coefficients and Complete Electrochemical Transport Characterization of Homopolymer and Block Copolymer Electrolytes. *J. Electrochem. Soc.* **2018**.

(127) Webb, M. A.; Jung, Y.; Pesko, D. M.; Savoie, B. M.; Yamamoto, U.; Coates, G. W.; Balsara, N. P.; Wang, Z.-G.; Miller, T. F. Systematic Computational and Experimental Investigation of Lithium-Ion Transport Mechanisms in Polyester-Based Polymer Electrolytes. *ACS Cent. Sci.* **2015**, *1* (4), 198–205.

(128) Stone, G. M.; Mullin, S. A.; Teran, A. A.; Hallinan, D. T.; Minor, A. M.; Hexemer, A.; Balsara, N. P. Resolution of the Modulus versus Adhesion Dilemma in Solid Polymer Electrolytes for Rechargeable Lithium Metal Batteries. *J. Electrochem. Soc.* **2012**, *159* (3), A222–A227.

(129) Lu, Y.; Tu, Z.; Archer, L. A. Stable Lithium Electrodeposition in Liquid and Nanoporous Solid Electrolytes. *Nat. Mater.* **2014**, *13* (10), 961–969.

(130) Qian, J.; Henderson, W. A.; Xu, W.; Bhattacharya, P.; Engelhard, M.; Borodin, O.; Zhang, J. G. High Rate and Stable Cycling of Lithium Metal Anode. *Nat. Commun.* **2015**.

(131) Appetecchi, G. B.; Scaccia, S.; Passerini, S. Investigation on the Stability of the Lithium-Polymer Electrolyte Interface. *J. Electrochem. Soc.* **2000**, *147* (12), 4448.

(132) Han, X.; Gong, Y.; Fu, K. (Kevin); He, X.; Hitz, G. T.; Dai, J.; Pearse, A.; Liu, B.; Wang, H.; Rubloff, G.; et al. Negating Interfacial Impedance in Garnet-Based Solid-State Li Metal Batteries. *Nat. Mater.* **2016**, *16* (5), 572–579.

(133) Thomas, K.; Newman, J.; Darling, R. Mathematical Modeling of Lithium Batteries. In *Advances in Lithium-Ion Batteries*; 2002; pp 345–392.

(134) Doyle, M.; Newman, J.; Gozdz, A. S.; Schmutz, C. N.; Tarascon, J. Comparison of Modeling Predictions with Experimental Data from Plastic Lithium Ion Cells. *J. Electrochem. Soc.* **1996**, *143* (6), 1890.

(135) Doyle, M.; Fuller, T. F.; Newman, J. Modeling of Galvanostatic Charge and Discharge of the Lithium/Polymer/Insertion Cell. *J. Electrochem. Soc.* **1993**, *140* (6), 1526.

(136) Kim, U. S.; Shin, C. B.; Kim, C.-S. Modeling for the Scale-up of a Lithium-Ion Polymer Battery. *J. Power Sources* **2009**, *189* (1), 841–846.

(137) Arora, P.; Doyle, M.; Gozdz, A. S.; White, R. E.; Newman, J. Comparison between Computer Simulations and Experimental Data for High-Rate Discharges of Plastic Lithium-Ion Batteries. *J. Power Sources* **2000**, *88* (2), 219–231.

(138) Srinivasan, V.; Newman, J. Discharge Model for the Lithium Iron-Phosphate Electrode. *J. Electrochem. Soc.* **2004**, *151* (10), A1517.

(139) Liu, J.; Monroe, C. W. Solute-Volume Effects in Electrolyte Transport. *Electrochim. Acta* **2014**, *135*, 447–460.

(140) Ehrl, A.; Landesfeind, J.; Wall, W. A.; Gasteiger, H. A. Determination of Transport Parameters in Liquid Binary Lithium Ion Battery Electrolytes. *J. Electrochem. Soc.* **2017**, *164* (4), A826–A836.

(141) Ehrl, A.; Landesfeind, J.; Wall, W. A.; Gasteiger, H. A. Determination of Transport Parameters in Liquid Binary Electrolytes: Part II. Transference Number. *J. Electrochem. Soc.* **2017**, *164* (12), A2716–A2731.

(142) Wu, S.-L.; Javier, A. E.; Devaux, D.; Balsara, N. P.; Srinivasan, V. Discharge Characteristics of Lithium Battery Electrodes with a Semiconducting Polymer Studied by Continuum Modeling and Experiment. *J. Electrochem. Soc.* **2014**, *161* (12), A1836–A1843.

(143) Newman, J.; Tiedemann, W. Porous-Electrode Theory with Battery Applications. *AIChE J.* **1975**, *21* (1), 25–41.

(144) Fuller, T. F.; Doyle, M.; Newman, J. Simulation and Optimization of the Dual Lithium Ion Insertion Cell. *J. Electrochem. Soc.* **1994**, *141* (1), 1.

(145) Scrosati, B.; Garche, J. Lithium Batteries: Status, Prospects and Future. *J. Power Sources* **2010**, *195* (9), 2419–2430.

(146) Baril, D.; Michot, C.; Armand, M. Electrochemistry of Liquids vs. Solids: Polymer Electrolytes. *Solid State Ionics* **1997**, *94* (1–4), 35–47.

(147) Fergus, J. W. Ceramic and Polymeric Solid Electrolytes for Lithium-Ion Batteries. *J. Power Sources* **2010**, *195* (15), 4554–4569.

(148) Borodin, O.; Smith, G. D. Molecular Dynamics Simulations of Poly(Ethylene Oxide)/LiI Melts. 1. Structural and Conformational Properties. *Macromolecules* **1998**, *31* (23), 8396–8406.

(149) Druger, S. D.; Nitzan, A.; Ratner, M. A. Dynamic Bond Percolation Theory: A Microscopic Model for Diffusion in Dynamically Disordered Systems. I. Definition and One-Dimensional Case. *J. Chem. Phys.* **1983**, *79* (6), 3133–3142.

(150) Vincent, C. A. Polymer Electrolytes. *Prog. Solid State Chem.* **1987**, *17* (3), 145–261.

(151) Killis, A.; LeNest, J.; Cheradame, H.; Gandini, A. Ionic Conductivity of Polyether-polyurethane Networks Containing NaBPh4: A Free Volume Analysis. *Die Makromol. Chemie* **1982**, *183* (11), 2835–2845.

(152) Fox, T. G. Influence of Diluent and of Copolymer Composition on the Glass Temperature of a Polymer System. *Bull. Am. Phys. Soc.* **1956**, *1* (123), 22060–26218.

(153) Couchman, P. R. Compositional Variation of Glass-Transition Temperatures. 2. Application of the Thermodynamic Theory to Compatible Polymer Blends. *Macromolecules* **1978**, *11* (6), 1156–1161.

(154) Faucher, J. A. Glass Transitions of Ethylene Oxide Polymers. *J. Appl. Phys.* **1966**, *37* (11), 3962–3964.

(155) Tarascon, J. M.; Armand, M. Issues and Challenges Facing Rechargeable Lithium Batteries. *Nature* **2001**, *414* (6861), 359–367.

(156) Meyer, W. H. Polymer Electrolytes for Lithium-Ion Batteries. *Adv. Mater.* **1998**, *10* (6), 439–448.

(157) Bruce, P. G.; Scrosati, B.; Tarascon, J.-M. Nanomaterials for Rechargeable Lithium Batteries. *Angew. Chem. Int. Ed. Engl.* **2008**, *47* (16), 2930–2946.

(158) Croce, F.; Appetecchi, G. B.; Persi, L.; Scrosati, B. Nanocomposite Polymer Electrolytes for Lithium Batteries. **1998**, *394* (6692), 456–458.

(159) Bandara, L. R. a. K.; Dissanayake, M. a. K. L.; Mellander, B.-E. Ionic Conductivity of Plasticized(PEO)-LiCF3SO3 Electrolytes. *Electrochim. Acta* **1998**, *43* (10–11), 1447–1451.

(160) Kim, Y. T.; Smotkin, E. S. The Effect of Plasticizers on Transport and Electrochemical Properties

of PEO-Based Electrolytes for Lithium Rechargeable Batteries. *Solid State Ionics* **2002**, *149* (1–2), 29–37.

(161) Shin, J. H.; Henderson, W. A.; Passerini, S. Ionic Liquids to the Rescue? Overcoming the Ionic Conductivity Limitations of Polymer Electrolytes. *Electrochem. commun.* **2003**, *5* (12), 1016–1020.

(162) Rhoo, H.-J.; Kim, H.-T.; Park, J.-K.; Hwang, T.-S. Ionic Conduction in Plasticized Blend Polymer Electrolytes. *Electrochim. Acta* **1997**, *42* (10), 1571–1579.

(163) Ito, Y.; Kanehori, K.; Miyauchi, K.; Kudo, T. Ionic Conductivity of Electrolytes Formed from PEO-LiCF3SO3 Complex Low Molecular Weight Poly(Ethylene Glycol). *J. Mater. Sci.* **1987**, *22* (5), 1845–1849.

(164) Michael, M. .; Jacob, M. M. .; Prabaharan, S. R. .; Radhakrishna, S. Enhanced Lithium Ion Transport in PEO-Based Solid Polymer Electrolytes Employing a Novel Class of Plasticizers. *Solid State Ionics* **1997**, *98* (3–4), 167–174.

(165) Tanaka, R.; Sakurai, M.; Sekiguchi, H.; Mori, H.; Murayama, T.; Ooyama, T. Lithium Ion Conductivity in Polyoxyethylene/Polyethylenimine Blends. *Electrochim. Acta* **2001**, *46* (10–11), 1709–1715.

(166) Kerr, J. B.; Liu, G.; Curtiss, L. A.; Redfern, P. C. Towards Room-Temperature Performance for Lithium–polymer Batteries. *Electrochim. Acta* **2003**, *48* (14–16), 2305–2309.

(167) Qiao, J.; Chen, Y.; Baker, G. L. Polymer Electrolytes Based on Unsaturated Ethylene Oxide-Segmented Polymers. *Chem. Mater.* **1999**, *11* (9), 2542–2547.

(168) Webb, M. A.; Savoie, B. M.; Wang, Z.-G.; Miller III, T. F. Chemically Specific Dynamic Bond Percolation Model for Ion Transport in Polymer Electrolytes. *Macromolecules* **2015**, *48* (19), 7346–7358.

(169) Schmidt, B. Catalysis at the Interface of Ruthenium Carbene and Ruthenium Hydride Chemistry: Organometallic Aspects and Applications to Organic Synthesis. *European J. Org. Chem.* **2004**, *2004* (9), 1865–1880.

(170) Wagener, K. B.; Brzezinska, K. Acyclic Diene Metathesis (ADMET) Polymerization: Synthesis of Unsaturated Polyethers. *Macromolecules* **1991**, *24* (19), 5273–5277.

(171) Wagener, K. B.; Brzezinska, K.; Bauch, C. G. Acyclic Diene Metathesis (ADMET) Polymerization. The Preparation of Sym-unsaturated Polyethers by the Use of Mo(CH-t-Bu)(N-2,6-C6H3-i-Pr2)[OCCH3(CF3)2]2 Catalyst. *Die Makromol. Chemie, Rapid Commun.* **1992**, *13* (2), 75–81.

(172) Vanommeslaeghe, K.; Hatcher, E.; Acharya, C.; Kundu, S.; Zhong, S.; Shim, J.; Darian, E.; Guvench, O.; Lopes, P.; Vorobyov, I.; et al. CHARMM General Force Field: A Force Field for Drug-Like Molecules Compatible with the CHARMM All-Atom Additive Biological Force Fields. *J. Comput. Chem.* **2010**, *31* (4), 671–690.

(173) Stubbs, J. M.; Potoff, J. J.; Siepmann, J. I. Transferable Potentials for Phase Equilibria. 6. United-Atom Description for Ethers, Glycols, Ketones, and Aldehydes. *J. Phys. Chem. B* **2004**, *108* (45), 17596–17605.

(174) Wu, H.; Wick, C. D. Computational Investigation on the Role of Plasticizers on Ion Conductivity in Poly(Ethylene Oxide) LiTFSI Electrolytes. *Macromolecules* **2010**, *43* (7), 3502–3510.

(175) Plimpton, S. Fast Parallel Algorithms for Short-Range Molecular-Dynamics. *J. Comput. Phys.* **1995**, *117* (1), 1–19.

(176) Brown, W. M.; Kohlmeyer, A.; Plimpton, S. J.; Tharrington, A. N. Implementing Molecular Dynamics on Hybrid High Performance Computers - Particle-Particle Particle-Mesh. *Comput. Phys. Commun.* **2012**, *183* (3), 449–459.

(177) Brown, W. M.; Wang, P.; Plimpton, S. J.; Tharrington, A. N. Implementing Molecular Dynamics on Hybrid High Performance Computers - Short Range Forces. *Comput. Phys. Commun.* **2011**, *182* (4), 898–911.

(178) Figueirido, F.; Del Buono, G. S.; Levy, R. M. On Finite-Size Effects in Computer Simulations Using the Ewald Potential. *J. Chem. Phys.* **1995**, *103* (14), 6133.

(179) Maitra, A.; Heuer, A. Cation Transport in Polymer Electrolytes: A Microscopic Approach. *Phys. Rev. Lett.* **2007**, *98* (22), 1–4.

(180) Diddens, D.; Heuer, A.; Borodin, O. Understanding the Lithium Transport within a Rouse-Based Model for a PEO/LiTFSI Polymer Electrolyte. *Macromolecules* **2010**, *43* (4), 2028–2036.

(181) Nitzan, A.; Ratner, M. a. Conduction in Polymers : Dynamic Disorder Transport. *J. Phys. Chem.* **1994**, *98*, 1765–1775.

(182) Mogurampelly, S.; Borodin, O.; Ganesan, V. Computer Simulations of Ion Transport in Polymer Electrolyte Membranes. *Annu. Rev. Chem. Biomol. Eng.* **2016**, *7* (1), 349–371.

(183) Panday, A.; Mullin, S.; Gomez, E. D.; Wanakule, N.; Chen, V. L.; Hexemer, A.; Pople, J.; Balsara, N. P. Effect of Molecular Weight and Salt Concentration on Conductivity of Block Copolymer Electrolytes. *Macromolecules* **2009**, *42* (13), 4632–4637.

(184) Yuan, R.; Teran, A. A.; Gurevitch, I.; Mullin, S. A.; Wanakule, N. S.; Balsara, N. P. Ionic Conductivity of Low Molecular Weight Block Copolymer Electrolytes. *Macromolecules* **2013**, *46* (3), 914–921.

(185) Chintapalli, M.; Chen, X. C.; Thelen, J. L.; Teran, A. A.; Wang, X.; Garetz, B. A.; Balsara, N. P. Effect of Grain Size on the Ionic Conductivity of a Block Copolymer Electrolyte. *Macromolecules* **2014**, *47* (15), 5424–5431.

(186) Petrowsky, M.; Frech, R. Temperature Dependence of Ion Transport: The Compensated Arrhenius Equation. *J. Phys. Chem. B* **2009**, *113* (17), 5996–6000.

(187) Mullerplathe, F.; Vangunsteren, W. F. Computer-Simulation of a Polymer Electrolyte - Lithium Iodide in Amorphous Poly(Ethylene Oxide). *J. Chem. Phys.* **1995**, *103* (11), 4745–4756.

(188) Papke, B. L.; Ratner, M. A.; Shriver, D. F. Vibrational Spectroscopic Determination of Structure and Ion Pairing in Complexes of Poly(Ethylene Oxide) with Lithium Salts. *J. Electrochem. Soc.* **1982**, *129* (7), 1434.

(189) Mao, G.; Saboungi, M.-L.; Price, D. L.; Badyal, Y. S.; Fischer, H. E. Lithium Environment in PEO-$LiClO_4$ Polymer Electrolyte. *Europhys. Lett.* **2001**, *54* (3), 347–353.

(190) Wen, S. J.; Richardson, T. J.; Ghantous, D. I.; Striebel, K. A.; Ross, P. N.; Cairns, E. J. FTIR Characterization of PEO + LiN(CF3SO2)2 Electrolytes. *J. Electroanal. Chem.* **1996**, *408* (1–2), 113–118.

(191) Borodin, O.; Smith, G. D. Mechanism of Ion Transport in Amorphous Poly(Ethylene Oxide)/LiTFSI from Molecular Dynamics Simulations. *Macromolecules* **2006**, *39* (4), 1620–1629.

(192) Nagae, S.; Nekoomanesh, H. M.; Booth, C.; Owen, J. R. The Effect of Salt Concentration on the Properties of Poly[Oxymethylene-Oligo (Oxyethylene)]/LiClO4 Polymer Electrolytes. *Solid State Ionics* **1992**, *53–56*, 1118–1124.

(193) Sloop, S. E.; Lerner, M. M. Study of the Poly[Oxymethylene Oligo-(Oxyethylene)]/Lithium Metal

Interface. *J. Electrochem. Soc.* **1996**, *143* (4), 1292.

(194) Nicholas, C. V.; Wilson, D. J.; Booth, C.; Giles, J. R. M. Improved Synthesis of Oxymethylene-Linked Poly(Oxyethylene). *Br. Polym. J.* **1988**, *20* (3), 289–292.

(195) Linden, E.; Owen, J. R. Conductivity Measurements on Amorphous PEO Copolymers. *Solid State Ionics* **1988**, *28–30*, 994–1000.

(196) Xu, B.; Lillya, C. P.; Chien, J. C. W. Cationic Polymerizations of 1,3,6-Trioxocane and 2-Butyl-1,3,6-Trioxocane. *Macromolecules* **1987**, *20* (7), 1445–1450.

(197) Okada, M.; Kozawa, S.; Yamashita, Y. Kinetic Studies on the Polymerization of 1.3.6-trioxocane Catalyzed by Triethyl Oxonium Tetrafluoroborate. *Macromol. Chem. Phys.* **1969**, *127* (1), 66–77.

(198) Kawakami, Y.; Yamashita, Y. Macrocyclic Formals. 3. Two-Stage Polymerization of 1,3-Dioxacycloalkanes. *Macromolecules* **1977**, *10* (4), 837–839.

(199) Alves, N. M.; Mano, J. F.; Balaguer, E.; Meseguer Dueñas, J. M.; Gómez Ribelles, J. L. Glass Transition and Structural Relaxation in Semi-Crystalline Poly(Ethylene Terephthalate): A DSC Study. *Polymer (Guildf).* **2002**, *43* (15), 4111–4122.

(200) Mano, J. F.; Gómez Ribelles, J. L.; Alves, N. M.; Salmerón Sanchez, M. Glass Transition Dynamics and Structural Relaxation of PLLA Studied by DSC: Influence of Crystallinity. *Polymer (Guildf).* **2005**.

(201) J.R. MacCallum, C. A. V. *Polymer Electrolyte Reviews, Volume 1*; Springer Science & Business Media, 1987.

(202) Shah, D. B.; Olson, K. R.; Karny, A.; Mecham, S. J.; DeSimone, J. M.; Balsara, N. P. Effect of Anion Size on Conductivity and Transference Number of Perfluoroether Electrolytes with Lithium Salts. *J. Electrochem. Soc.* **2017**, *164* (14), A3511–A3517.

(203) Harry, K. J.; Hallinan, D. T.; Parkinson, D. Y.; MacDowell, A. A.; Balsara, N. P. Detection of Subsurface Structures underneath Dendrites Formed on Cycled Lithium Metal Electrodes. *Nat. Mater.* **2014**, *13* (1), 69–73.

(204) Thompson, S. D.; Newman, J. Differential Diffusion Coefficients of Sodium Polysulfide Melts. *J. Electrochem. Soc.* **1989**, *136* (11), 3362–3369.

Appendix A1 – Lithium Symmetric Cell Experimental Design

A variety of the electrochemical characterization measurements employed in this dissertation rely on the polarization of lithium-polymer-lithium symmetric cells. While the experimental sections in each chapter provide a detailed description of the techniques performed, the purpose of this section is to provide insight into some of the considerations that should be taken into account when designing these experiments.

A1.1 Cell Configuration and Thickness Effects

While the optimal configuration of a lithium-polymer-lithium cell is highly dependent on the physical properties of the polymer, there are some considerations for cell assembly that are useful to consider. The polymer electrolyte must be in good contact with the lithium electrodes throughout the entire interface. If a spacer is used, the polymer must perfectly fill the volume of the spacer as closely to the spacer surface as possible; underfilling or overfilling the spacer may force the lithium to adopt a convex or concave curvature. Curvature of the electrode surface is known to lead to complex electric potentials[20] which are likely to reduce the accuracy of the steady-state current and restricted diffusion measurements. To avoid deformation of the electrode surface during cell assembly, it is helpful to press the lithium against a solid surface to provide support. Stainless-steel shims were used as backing for the lithium electrodes in this work.

Perhaps the most important factor of the cell design for these experiments is the thickness of the electrolyte. The electrolyte must be thin enough such reasonable current densities can be achieved during polarization; this upper thickness limit is dependent on the transport properties of the electrolyte, primarily conductivity, which determines the overall cell resistance. However, thick electrolytes help to prevent surface effects like SEI layers from contaminating the measurements of transport properties in the bulk. The restricted diffusion measurement is particularly sensitive to the electrolyte thickness, as thickness determines the timescale over which the voltage relaxation occurs. A longer voltage decay likely enables increased accuracy in the fit of the data. Furthermore, small applied potentials create sufficient concentration polarization in thick electrolytes whereas larger potentials are necessary to create such polarization in thinner electrolytes; these potentials could lead to complex effects. The effect of applied potential is discussed in Section A1.3.2.

Most importantly, the error in the thickness measurement will contribute to error in D and consequently $t_{+,Ne}$ for a given electrolyte. A 5 μm error in cell thickness is not unreasonable for measurements obtained using a micrometer. Figure A1.1a demonstrates the range in D that can be expected for a cell with a thickness of 20 ± 5 μm compared to a thickness of 500 ± 5 μm. The experimental measurements, which were obtained using 500 μm thick cells, are shown for comparison. It is clear that using a 20 μm for these measurements may lead to large error bars and a dependence of D on r that is more difficult to establish compared to the 500 μm thick sample. Using the upper and lower bounds of D to calculate the bounds of $t_{+,Ne}$ clarifies the importance of accurate thickness measurements and large electrolyte thicknesses.

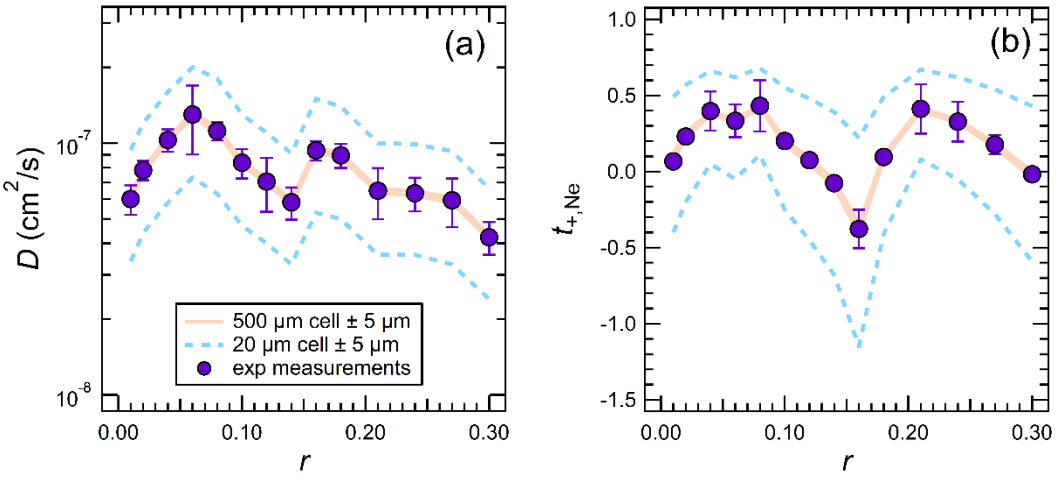

Figure A1.1. Upper and lower bounds of (a) D and (b) $t_{+,Ne}$ based on a thickness measurement error of ± 5 µm in electrolytes that are 20 µm and 500 µm thick.

A1.2 Conditioning Cycles

Conditioning cycles should always be performed prior to any electrochemical measurement on a lithium symmetric cell. The purpose of this cycling is to introduce stable SEI layers at the lithium surface to allow the cell to reach steady-state before any data is acquired. In other words, the goal of the conditioning cycles is to obtain bulk and interfacial resistances, R_b and R_i, that are stable with time.

This work followed the conditioning cycling procedure previously established by Harry et al.[203] for lithium symmetric cells with approximately 20 µm thick PS-PEO electrolytes. Each cycle consisted of a 4-hour charge at a constant current density of i = 0.02 mA/cm^2, a 45-minute rest, a 4-hour discharge at i = -0.02 mA/cm^2, and a 45-minute rest as shown in Figure A1.2a. A total of 5 cycles were performed in all cases. Figure A1.2b and c shows the resistances measured during the conditioning of a 5 kg/mol PEO electrolyte at r = 0.08. In this cell, we find that R_b is independent with time whereas R_i is increasing with each additional conditioning cycle; reasons for this observation in 5 kg/mol PEO electrolyte were discussed in Chapter 3. In an ideal experiment, the cycling would continue until R_i has reached a plateau with the number of conditioning cycles. It is clear that this is not always the case in our experiments (Figure A1.2c) due to the length of time required for each additional cycle.

The optimal current density for the conditioning cycles is an interesting open question. The potential reached at the electrode interface during cycling will be dependent on the overall cell configuration and will change based on the conductivity and thickness of the electrolyte. One might imagine the makeup of the final SEI layers, and consequently the interfacial resistance, to be dependent on the potential reached during the conditioning cycles. In our experiments, the steady-state potential reached during conditioning was less than 20 mV. However, using the same current density on an electrolyte lower conductivity would lead to significantly higher potentials. At this point it is not clear what effect this would have on the electrochemical characterization performed subsequent to conditioning. In the absence of a thorough understanding of the influence of different conditioning cycle parameters, one might consider using the following relationship to approximate an appropriate current density for a given cell configuration:

$$i = \left(0.02\,\frac{mA}{cm^2}\right)\left(\frac{0.05\ cm}{L}\right)\left(\frac{\sigma}{\sigma_{PEO}}\right) \tag{A1.1}$$

Here, the conductivity, σ, and thickness, L, of the electrolyte are used to scale i. The units for σ are S/cm, for L are cm, and for i are mA/cm^2.

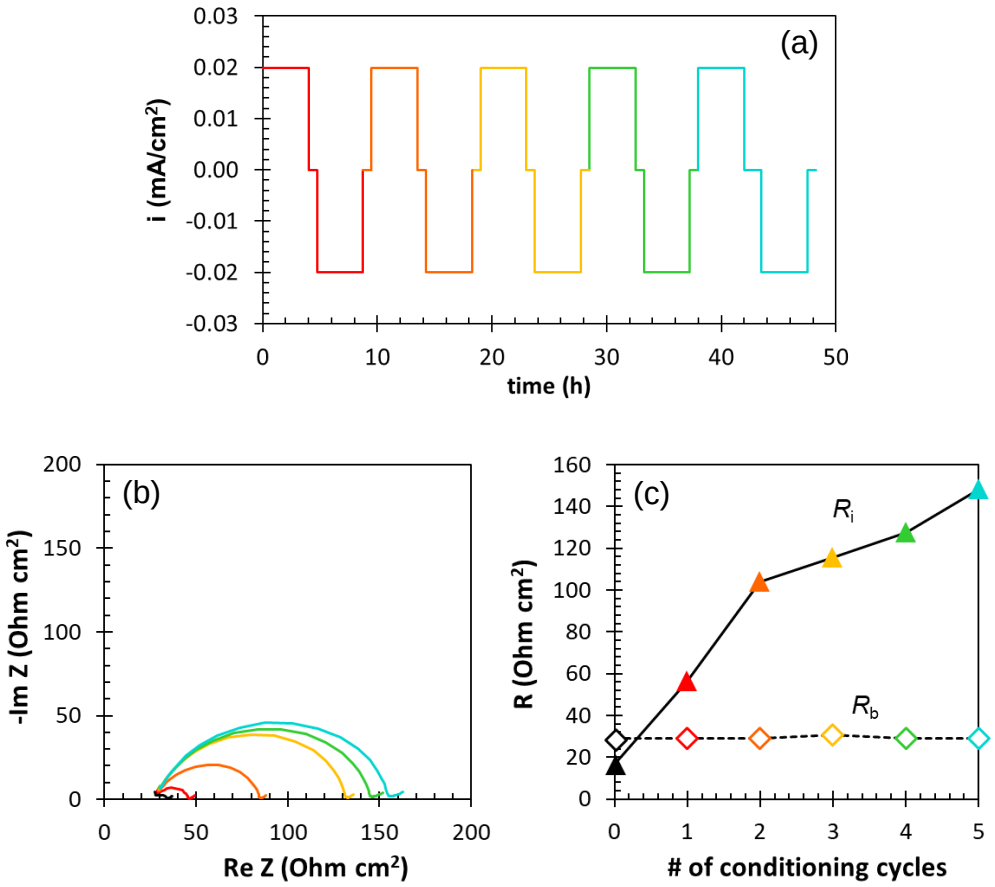

Figure A1.2. (a) Conditioning cycling protocol performed on all lithium symmetric cells in this work. (b) Nyquist plots and (c) bulk and interfacial resistance data from a cell with a 5 kg/mol PEO electrolyte with LiTFSI at r = 0.08.

A1.3 Electrochemical Experiments to Obtain $t_{+,SS}$ and D

A1.3.1 Steady-State Current

To obtain $t_{+,SS}$ using the steady-state current approach, a lithium-polymer-lithium symmetric cell is polarized at constant potential, ΔV, for a long period of time and the response of the current density, i, is recorded. During operation of the cell, concentration gradients propagate through the electrolyte leading to a decrease in i with time. As the cell reaches steady-state, the current density will plateau to a constant value, i_{ss}. Figure A1.3a shows the current density response in a typical cell for four different values of ΔV. It is important to err on the side of caution when choosing the polarization time, as the time required for the cell to reach steady-state depends on a variety of factors (transport properties of the electrolyte, overall salt concentration, applied potential, and cell thickness) and is often hard to predict. In this work, the polarization was applied for 4.75 hours

although in most cases steady-state was achieved in under 2 hours. From the data in Figure A1.3a, it is evident that the value of i_{ss} is dependent on ΔV.

The measured value of i_{ss} is used to calculate $t_{+,SS}$ according to the relationship defined by Bruce and Vincent[88,96]

$$t_{+,SS} = \frac{i_{SS}(\Delta V - i_{\Omega} R_{i,0})}{i_{\Omega}(\Delta V - i_{SS} R_{i,SS})}, \tag{A1.2}$$

where i_{Ω} is given by

$$i_{\Omega} = \frac{\Delta V}{R_{i,0} + R_{b,0}}. \tag{A1.3}$$

Impedance spectroscopy is used to obtain the resistances of the cell prior to polarization ($R_{i,0}$ and $R_{b,0}$) and at steady-state ($R_{i,SS}$ and $R_{b,SS}$). For accuracy, it is important to use the measured values of ΔV from the output file as opposed to the ΔV defined in the parameter settings. At times these values are different. Equations A1.2 and A1.3 assume that the OCV of the cell is zero. Section A1.4 addresses the corrections required for cells with non-negligible OCVs.

The value of $t_{+,SS}$ should be independent of the magnitude and sign of the applied potential. Thus, it is useful to perform multiple experiments with different values of ΔV. In this work, ΔV = 10, -10, 20, and -20 mV was performed on each sample (Figure A1.3a). Chintapalli et al.[87] have reported a normalization of the current response using the parameter i/i_{Ω}. We use a similar approach to normalize the data in Figure A1.3a, however an interfacial resistance correction analogous that used in eq. A1.2 is also taken into account. Figure A1.3b shows the normalized current density response for different values of ΔV. It is clear that the results are independent of ΔV. The steady-state values of the data in Figure A1.bb are $t_{+,SS}$ = 0.10 in all cases.

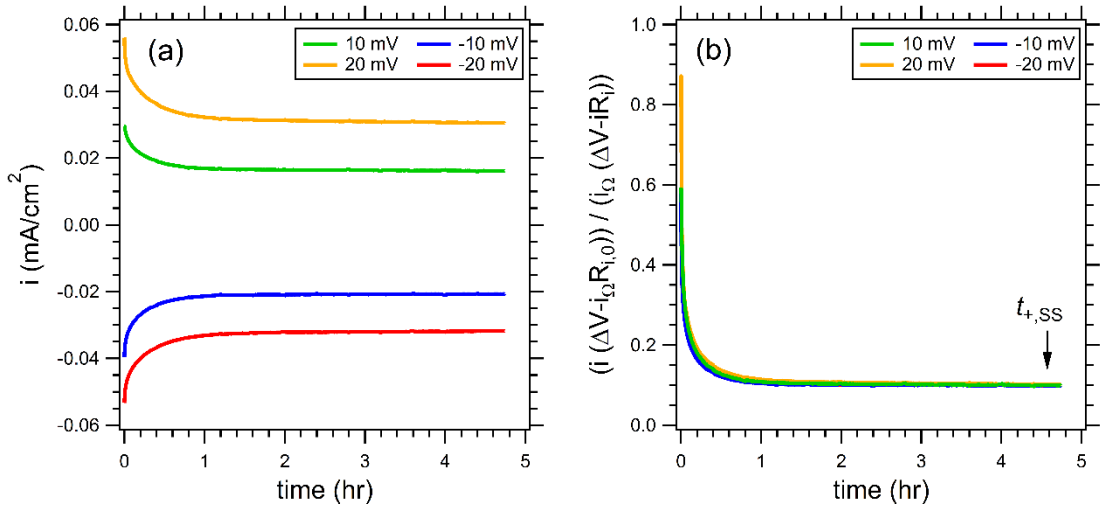

Figure A1.3. (a) Current density measured during steady-state current experiment for four different applied potentials: 10, -10, 20, -20 mV. This cell was comprised of a 5 kg/mol PEO/LiTFSI electrolyte at r = 0.08 at 90°C. (b) Normalized current density for the same data in (a).

A1.3.2 Restricted Diffusion

The restricted diffusion experiment is performed in a lithium-polymer-lithium symmetric cell where concentration gradients are present in the electrolyte, where the cell is no longer actively being polarized. The concentration difference at the electrodes creates a non-zero cell potential, U; the relaxation of U with time is governed by the salt diffusion coefficient. In theory, any form of polarization can be used to set up the concentration gradients for this experiment, i.e. constant current or constant potential. In this work, it is convenient to use the concentration gradients induced by the steady-state current experiment to obtain D. Figure A1.4a shows the relaxation of U for four different polarizations (ΔV = 10, -10, 20, and -20 mV).

The change in voltage with time is related to D through the relationship

$$-\frac{d\,ln[U]}{dt} = \frac{\pi^2 D}{L^2}, \tag{A1.4}$$

where L is the measured thickness of the electrolyte.

The change in ln(U) is expected to be constant with time regardless of the initial state of polarization. In Figure A1.4b, we plot the data in the linearized form of -ln(U) × (L^2/π^2) versus t. In all cases, the data is linear in the intermediate regime (5 to 80 min). The nonlinearly of the data at short timescales is attributed to the discharge of the double layer and other such relaxation processes; these processes are predicted to have a negligible effect on the relaxation of U when $Dt/L^2 > 0.05$[204] which corresponds to t > 15 min in the data in Figure A1.4. Calculating this parameter for each set of data is the most rigorous approach for determining timescales over which eq. A1.4 is relevant, however the accuracy of this prediction has yet to be evaluated. After 80 min, U is approaching zero such that the values of ln(U) are dominated by noise. Thus, it is only within the linear section ($5 \leq t \leq 80$ min) of the data that the relaxation processes are representative of the diffusion of the salt; a least-squares linear fit is used to obtain the slope of the data in this range, which is D. While, in theory, a nonlinear fit of the data in Figure A1.4a can be used to obtain D, it is difficult to identify the correct range over which the data should be fit. For this reason, analyzing the data in the form of -ln(U) × (L^2/π^2) versus t is the preferred approach. The slope of the data in Figure A1.4b are independent of ΔV, and $D = 1.2 \times 10^{-7}$ cm^2/s is obtained in all cases.

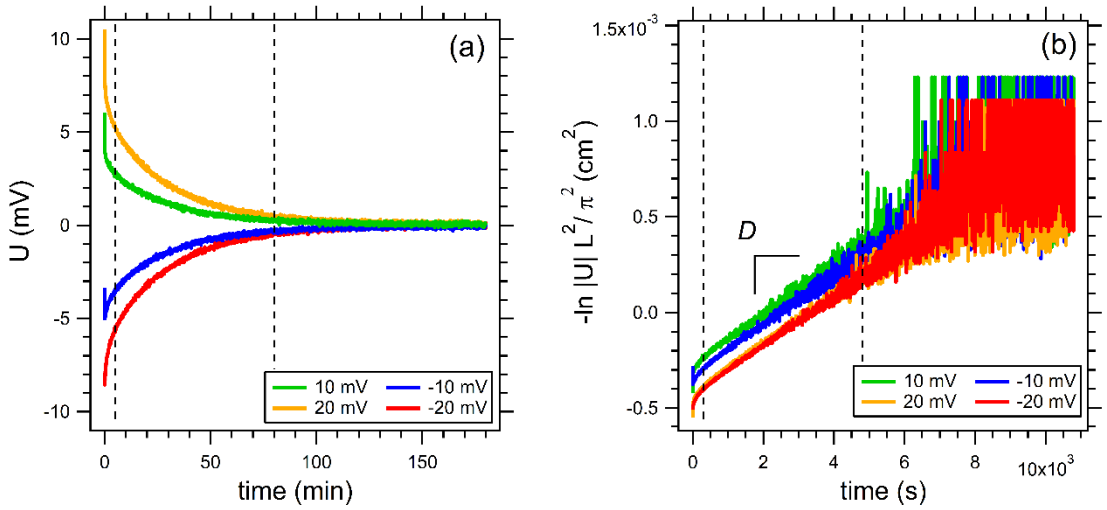

Figure A1.4. (a) Voltage relaxation measured during restricted diffusion experiment for four different applied potentials: 10, -10, 20, -20 mV. This cell was comprised of a 5 kg/mol PEO/LiTFSI electrolyte at r = 0.08 at 90°C. (b) Linearized version of voltage relaxation in (a). The vertical dotted lines represent the range in which the fit of the data was obtained.

A1.3.2 Effect of Applied Potential on $t_{+,SS}$ and D

Despite the fact that $t_{+,SS}$ and D are found to be independent of ΔV in Figure A1.3 and A1.4, choosing the potential to use in these experiments is not trivial. The steady-state current approach defined by Bruce and Vincent is only valid in the limit of small potentials, such that the concentration gradients in the electrolyte are small and approximately linear.[96] An applied potential of 10 mV was used for the steady-state current in the work of Evans et al.[88] Similarly, the restricted diffusion experiments also have polarization limitations.[204] The applied polarization must be large enough to induce a sufficient concentration polarization such that the relaxation process is long enough for the data to be fit. However, large applied potentials can induce strong concentration gradients and complex ionic speciation leading to a variety of competing relaxation processes.

In both experiments, a small, linear concentration gradient should lead to improved accuracy of the measurement. Predicting concentration gradients in PEO/LiTFSI electrolytes under steady-state operation is straightforward given the model described in Chapter 4. Figures 4.3a shows the concentration profiles in the limit of small potentials (< 10 mV); the gradients are small and the profiles are linear across the electrolyte. Using small applied potentials is particularly important in thick electrolytes, as the concentration profiles for a given potential are highly dependent on thickness (Chapter 4). On the other hand, thinner electrolytes may require higher potentials to establish a sufficient gradient across the cell.

The best way to determine the ideal value of ΔV is to perform these experiments as a function of applied potential. Figures A1.5a and A1.5b the measurements of $t_{+,SS}$ and D in PEO/LiTFSI electrolytes as a function of applied potential from 20 mV to 100 mV. For both parameters, an increase in ΔV results in an increased value of $t_{+,SS}$ or D in addition to larger error bars. The value of D is independent of ΔV for $\Delta V \leq 60$ mv whereas $t_{+,SS}$ is strongly dependent on ΔV in this range. The results Figure A1.5 suggests that polarizations of 20 mV or less should be used in 500 µm

thick PEO/LiTFSI electrolytes. A different electrolyte or cell configuration may have a different optimal value of ΔV.

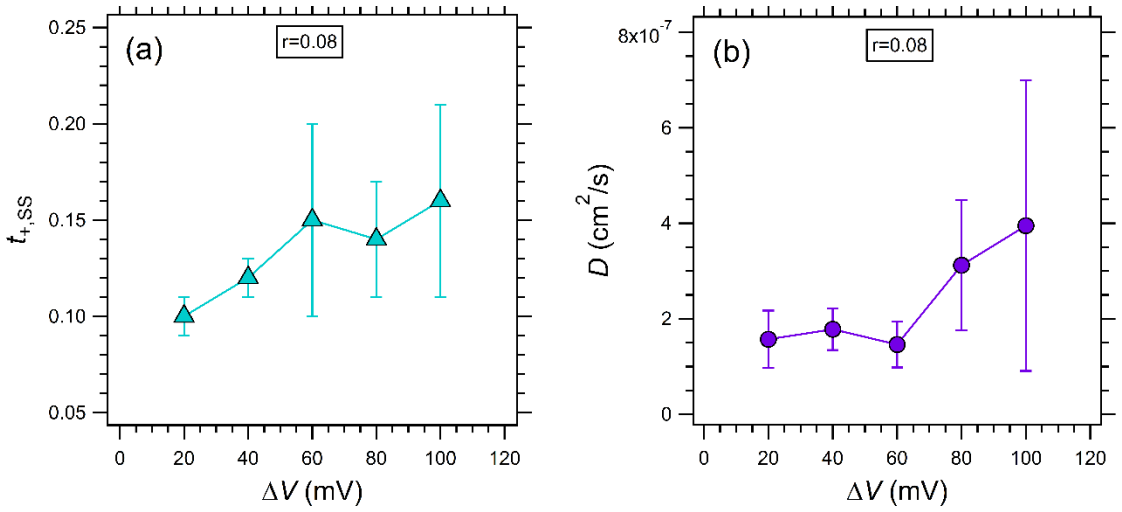

Figure A1.5. Values of (a) $t_{+,SS}$ and (b) D obtained using different values of applied potential. This cell was comprised of a 5 kg/mol PEO/LiTFSI electrolyte at r = 0.08 at 90°C.

A1.4 Correcting for the Seebeck Effect

It is a well-known principle in the field of thermoelectrics that a temperature gradient within a conductive material provides a driving force for charge carriers to move from hot to cold, creating a potential within the cell. The magnitude of the potential depends on the temperature difference as well as the electrode and electrolyte materials. This phenomenon, demonstrated in Figure A1.6, is formally known as the Seebeck effect.

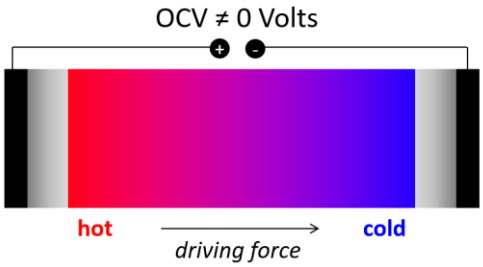

Figure A1.6. Temperature gradients within an electrochemical cell cause a potential for ions to move from hot to cold according to the Seebeck Effect.

Electrochemical cells tested in a heating stage may exhibit a temperature distribution across the cell due to the non-uniform heating in this setup. The open circuit potential (OCV) measured in lithium-polymer-lithium symmetric cells in a (see Figure A1.7). The OCV values range from 0.15 to 1.18 mV for PEO-275K and 0.59 to 1.09 mV for PEO-5K. The sign of the potential depends on the direction in which the leads are hooked up: connecting the working electrode to the electrode with a higher temperature results in a positive potential. Thinner cells are likely to have a smaller temperature gradient between the electrodes and therefore smaller OCV values. Electrochemical cells heated using an oven with a uniform temperature are expected to have negligible OCVs and may not require a correction.

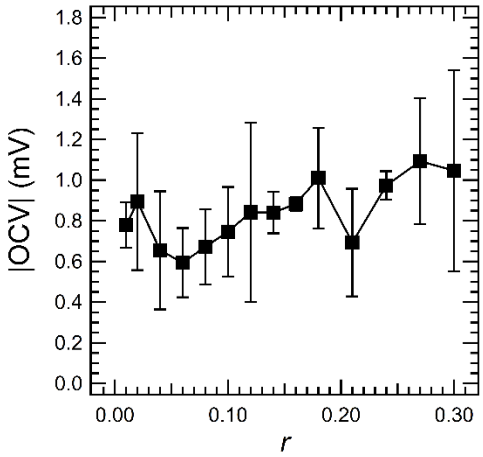

Figure A1.7. Absolute value of open circuit voltage measured in lithium-polymer-lithium cells with electrolytes of 5 kg/mol PEO with LiTFSI at 90°C. The non-zero OCV is attributed to the temperature gradient introduced by the heating stage. Thicknesses were around 500 μm.

The magnitude of the OCVs in Figure A1.7 are significant relative to the applied potential used in the experiments (10, -10, 20, and -20 mV). Figure A1.8 shows the voltage of a cell during the $t_{+,SS}$ and D experiments at 10 and -10 mV. The OCV must be subtracted as a baseline in both measurements: the applied potential used to calculate $t_{+,SS}$ is (ΔV – OCV) and the potential of the cell used to calculate D is (U – OCV). It is important to note that the OCV should be remeasured each time before a new potential is applied.

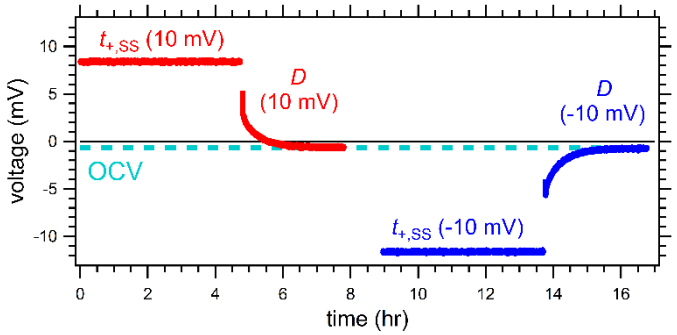

Figure A1.8. Measured voltage versus time in a 10 mV and -10 mV polarization experiment. This cell had a 5 kg/mol PEO / LiTFSI electrolyte at r = 0.08. The OCV of the cell is -0.67 mV.

It is instructive to explicitly write the equations used to calculate $t_{+,SS}$ and D. The general forms of these equations that are given in Chapter 2 assume uniform heating in the cell. The steady-state current transference number in a cell with a non-negligible OCV is calculated according to

$$t_{+,SS} = \frac{i_{SS}((\Delta V - OCV) - i_{\Omega} R_{i,0})}{i_{\Omega}((\Delta V - OCV) - i_{SS} R_{i,SS})}, \tag{A1.5}$$

where ΔV - OCV is the true potential applied in the cell, and i_{Ω}, the initial current, is calculated according to

$$i_{\Omega} = \frac{(\Delta V - OCV)}{R_{i,0} + R_{b,0}}. \tag{A1.6}$$

For accuracy, it is important to use the measured values of ΔV from the output file. Sometimes these values do not exactly match the 10, -10, 20, and -20 mV input in the settings file, as is evident in Figure A1.8. This may be easily fixed with an adjustment of the settings.

The salt diffusion coefficient in a cell with a non-negligible OCV is calculated by

$$-\frac{d\ ln\ [U - OCV]}{dt} = \frac{\pi^2 D}{L^2}, \tag{A1.7}$$

where the OCV is subtracted from the potential, *U*, before the derivative is evaluated. In the absence of a measured OCV, it is acceptable to use the plateau voltage of the restricted diffusion measurement as a baseline as long as the cell is allowed enough time to relax to a stable resting state. It is clear from Figure A1.8 that this would yield similar results.

Appendix A2 – Programs for Data Analysis

A2.1 AC Impedance Spectroscopy

This program is used for high throughput analysis of multiple text files of impedance data from cells with blocking electrodes. The text files to be analyzed must be in the following form:

```
freq/Hz      Re(Z)/Ohm    -Im(Z)/Ohm
1.0000193E+006      1.7294982E+003      2.2462722E+003
6.3095681E+005      1.8944200E+003      2.0078296E+003
3.9810538E+005      2.5964595E+003      2.0095253E+003
2.5119136E+005      3.3371379E+003      1.7315834E+003
1.5848628E+005      3.8537810E+003      1.3048267E+003
…
```

The items highlighted in red should be changed based on the naming convention of the file and the location on your computer. An example of a possible file name that is consistent with this format would be `‘011018_01_1heating_20C_02_PEIS_C10’` where the object `openfile` is `[‘011018’, ’01’, ‘1heating’, ‘20C’, ‘02’, ‘PEIS’, ‘C10’]`. Thus, `openfile[0]` is the date, `openfile[2]` is the heating/cooling, `openfile[3]` is the temperature, and `openfile[-1]` is the channel.

Once the program is running, a window pops up asking the user to select the text files to be analyzed. Multiple text files can be selected at one time. Then each set of data is plotted individually on a Nyquist plot and the minimum obtained from the program is circled in red. This program works by locating the low frequency minimum on the Nyquist plot, which is taken to be the bulk resistance of the electrolyte. The program asks “Correct minimum?”. If ‘yes’ is selected, the data will be saved in the output file. If ‘no’ is selected, the resistance of that cell will read 0 in the output file. The data is output as a file called ‘Results_ conductivity.csv’, which appears in the working directory once the program is finished running. This file can be opened in Excel.

```
import numpy as np
import csv
import Tkinter, tkFileDialog, tkSimpleDialog, tkMessageBox
import scipy.optimize
import matplotlib.pyplot as plt

i=0
j=1j

# Select files-----------------------------------------------------------------
root = Tkinter.Tk()
root.withdraw()
files = tkFileDialog.askopenfilenames()
files = files.strip('{}')
files = str(files).split('} {')

dtype=[('Date',np.str_,512),('Heating/Cooling',np.str_,512),('Temperature',np.str_,51
2),('Channel',np.str_,512),('Resistance',float)]
```

```
results = np.zeros((len(files)),dtype=dtype)

# Open individual files and load data-----------------------------------------------
for i in range(len(files)):
openfile = files[i]
freq = np.trim_zeros(np.loadtxt(openfile, skiprows=1, usecols = (0,)))
rez = np.trim_zeros(np.loadtxt(openfile, skiprows=1,usecols = (1,)))
imz = np.trim_zeros(np.loadtxt(openfile, skiprows=1,usecols = (2,)))
Z = rez+j*imz
# Input parameters from file name into 'results' ----------------------------------
openfile = str(openfile).replace('C:\Users\danie\Documents\Conductivity data', '')
openfile = str(openfile).replace('.txt', '')
openfile = str(openfile).split('_')

results[i]['Date'] = openfile[0]
results[i]['Heating/Cooling'] = openfile[2]
results[i]['Temperature'] = openfile[3]
results[i]['Channel'] = openfile[6]

# Find minimum ---------------------------------------------------------------------
Xmin = Z.real[np.diff(np.sign(np.diff(Z.imag)/np.diff(Z.real)))!=0][-1]
Ymin = -Z.imag[np.diff(np.sign(np.diff(Z.imag)/np.diff(Z.real)))!=0][-1]

# Create figure --------------------------------------------------------------------
plt.figure(i)
plt.plot(Z.real,-Z.imag,'-o', color='lime')
plt.plot(Xmin, Ymin,'o', color='b', markersize=80, mfc='none')
plt.show(i)
plt.xlabel('ReZ')
plt.ylabel('-ImZ')
plt.xlim([0, Xmin*(5)])
plt.ylim([0, Ymin*(50)])

# Ask question ---------------------------------------------------------------------
question = tkMessageBox.askquestion('?','Correct minimum?')
if question == 'yes':
results[i]['Resistance'] = Xmin
plt.close(i)
else:
plt.close(i)

#Export data to csv file ----------------------------------------------------------
with open('Results_conductivity.csv', 'wb') as fp:
a = csv.writer(fp, delimiter=',')
a.writerows(results)
```

A2.2 Steady-State Current

This program is used for high throughput analysis of multiple text files from steady-state current measurements. The text files to be analyzed must be in the following form:

```
time/s Ewe/V  I/mA
5.416386038304336E+002    8.2065770E-003      1.5858422E-003
```

```
5.426386038051714E+002    8.1874868E-003     1.5743197E-003
5.436386037799093E+002    8.0920365E-003     1.5594864E-003
5.446386037546472E+002    8.2638469E-003     1.5479000E-003
5.456386037293851E+002    8.2829371E-003     1.5379689E-003
…
```

For each file, this program extracts three parameters: the voltage in V, the initial current in mA, and the steady-state current in mA. The output file is 'Results_t+SS.csv', which appears in the working directory once the program is finished running. This file can be opened in Excel.

```
import numpy as np
import csv
import Tkinter, tkFileDialog, tkSimpleDialog, tkMessageBox
import matplotlib.pyplot as plt

# Select files-------------------------------------------------------------------------
root = Tkinter.Tk()
root.withdraw()
files = tkFileDialog.askopenfilenames()
files = files.strip('{}')
files = str(files).split('} {')

dtype=[('A',np.str_,512),('V',float),('Io',float),('Iss',float)]
results = np.zeros((len(files)),dtype=dtype)

# Open individual files and load data-------------------------------------------------
for i in range(len(files)):
    openfile = files[i]

    time = np.loadtxt(openfile, skiprows=1, usecols = (0,))
    voltage = np.loadtxt(openfile, skiprows=1, usecols = (1,))
    current = abs(np.loadtxt(openfile, skiprows=1, usecols = (2,)))
    data=np.zeros((len(time),3),dtype=float)

    openfile = str(openfile).replace('C:\Users\danie\Documents\t+ss and D
measurements', '')
    openfile = str(openfile).replace('.txt', '')
    openfile = str(openfile).split('_')
    results[i]['A'] = openfile[-1]

# Finding Io and Iss ------------------------------------------------------------------
    V=np.mean(voltage)
    Io=max(current)
    results[i]['V'] = V
    results[i]['Io'] = Io

    for j in range(len(current)):
        if current[j]==0:
            if j==0:
                current[0]=current[1]
            else:
                current[j]=current[j-1]
```

```
    Iss=np.mean(current[-100])
    results[i]['Iss'] = Iss

    current=current/Io
    time=(time-time[0])/60/60

# Plotting data ------------------------------------------------------------------
    plt.figure(0)
    plt.plot(time,current,label=(results[i]['A'],"%.2f" % results[i]['V'] ))
    plt.legend()
    plt.show(0)
    plt.xlabel('time (h)')
    plt.ylabel('I (mA)')
    plt.ylim([0, 1])

with open('Results_t+SS.csv', 'wb') as fp:
    a = csv.writer(fp, delimiter=',')
    a.writerows(results)
```

A2.3 Restricted Diffusion

This program is used for high throughput analysis of multiple text files of restricted diffusion data. The text files to be analyzed must be in the following form:

```
time/s Ewe/V
1.783265852643803E+004    7.2272238E-003
1.783765852637749E+004    5.2005001E-003
1.784265852631695E+004    5.2196099E-003
1.784765852625642E+004    5.0667296E-003
1.785265852619588E+004    5.0858399E-003
1.785765852613535E+004    5.0285095E-003
…
```

Also located in the working directory must be a text file entitled ‘Results_OCV.txt’, which contains the OCV of each cell. These values are used by the program to account for the OCV offset in the restricted diffusion data, as is discussed in section A1.4. Thus, the order and overall number of lines in ‘Results_OCV.txt’ should correspond exactly to the order and overall number of the text files selected for analysis. For example, if restricted diffusion data from channels 9-16 are being analyzed, ‘Results_OCV.txt’ should be in the following form:

```
C09    0.001069362
C10    0.000750788
C11    0.000284206
C12    0.000272218
C13    0.001007124
C14    0.000254972
C15    0.000791762
C16    0.00050473
…
```

Constructing this file carefully is important, as the diffusion coefficients obtained are strongly dependent on the OCV that is used.

The output of the program is the slope of -ln(*V*) vs. *t*. The parameters `t_low` and `t_high` set the upper and lower limits of the data that is fit, which was consistently 5 to 80 min in this work. The output file is called Results_diffusion.csv, which will appear in the working directory once the program is finished running. This file can be opened in Excel.

```
import numpy as np
import csv
import Tkinter, tkFileDialog
import matplotlib.pyplot as plt

t_low = 5 #low cutoff time in min
t_high = 80 #high cutoff time in min

# Select files-----------------------------------------------------------------
root = Tkinter.Tk()
root.withdraw()
files = tkFileDialog.askopenfilenames()
files = files.strip('{}')
files = str(files).split('} {')
dtype=[('Date',np.str_,512),('Channel',np.str_,512),('V',np.str_,512),('OCV',float),(
'Slope',float)]
results = np.zeros((len(files)),dtype=dtype)

# Open OCV.txt-----------------------------------------------------------
OCV=np.loadtxt('C:/Users/danie/Documents/t+ss and D measurements/Results_OCV.txt',
usecols = (1,))

# Open individual files and load data------------------------------------------------
for i in range(len(files)):
    openfile = files[i]

    time = np.loadtxt(openfile, skiprows=1, usecols = (0,))
    time = time-time[0]
    time_inc = time[1] - time[0] #seconds between each point
    t1 = t_low*60/time_inc #low cutoff point
    t2 = t_high*60/time_inc #high cutoff point

    voltage = np.loadtxt(openfile, skiprows=1, usecols = (1,))
    ln_V = -np.log(abs(voltage-OCV[i]))

# Input parameters from file name into 'results' ----------------------------------
    openfile = str(openfile).replace('C:/Users/danie/Documents/t+ss and D
measurements/', '')
    openfile = str(openfile).replace('.txt', '')
    openfile = str(openfile).split('_')

    results[i]['Date'] = openfile[0]
    results[i]['Channel'] = openfile[-1]
    results[i]['V'] = openfile[3]
    results[i]['OCV'] = OCV[i]

# Find slope of data ----------------------------------------------------------
    par = np.polyfit(time, ln_V, 1, full=False)
```

```
    par = np.polyfit(time[t1:t2], ln_V[t1:t2], 1, full=False)
    results[i]['Slope'] = par[0]

# Plot data ----------------------------------------------------------------
    plt.figure(0)
    plt.plot(time[t1:t2]/60,ln_V[t1:t2]-
min(ln_V[t1:t2]),label=(results[i]['Channel'], results[i]['V']))
    plt.legend()
    plt.show(0)
    plt.xlabel('time', fontsize=16)
    plt.ylabel('-ln V',fontsize=16)

#Export data to csv file ---------------------------------------------------
with open('Results_diffusion.csv', 'wb') as fp:
    a = csv.writer(fp, delimiter=',')
    a.writerows(results)
```

A2.4 Modeling Concentration and Potential Profiles

This program is used to predict the concentration and potential profiles that form within electrolytes under steady-state operation of the cell. Use of this program requires knowledge of the transport properties of the electrolyte over a wide range of salt concentrations. The constants `a1, b1, c1, d1, e1, f1` correspond to the fitting parameters for $(D\,c)/(r\,t_-)$ and the constants `y0, A_1, A_2, tau_1, tau_2` correspond to the fitting parameters of $(D\,c)/(r\,t_-\,\sigma\,t_{+,SS})$, as discussed in Chapter 4. The current parameters correspond to 5 kg/mol PEO with LiTFSI salt. The object `r_av` should be changed depending on the average salt concentration of the electrolytes which are being modeled. The values of steady-state current `iss` and electrolyte thickness `L` can be adjusted to model a variety of cell conditions.

For each concentration in `r_av`, one output file is created with the name 'Results_r_av csv' containing the concentration and potential profiles calculated by the program. The three columns in this file correspond to the position, x/L, local concentration, r, and potential, Φ. The program also plots these profiles on two separate figures. In addition, a summary file named 'Results_summary.csv' is created, which contains the cell potential for each electrolyte in `r_av` divided by thickness, Φ_{SS}/L, in units of mV/μm. This data is shown in a third figure.

```
import numpy as np
import matplotlib.pyplot as plt
import csv

#Choose electrolyte concentration-----------------------------------------------
r_av=[0.012, 0.02, 0.04, 0.06, 0.08, 0.1, 0.12, 0.14, 0.16, 0.18, 0.20, 0.22, 0.24,
0.26, 0.28, 0.3]

#Choose cell parameters---------------------------------------------------------
iss=0.02 #mA/cm^2
L=500 #microns

#Constants----------------------------------------------------------------------
F=96485 #C/mol
```

```
a1=1.088e-4
b1=-9.889e-5
c1=3.280e-5
d1=-4.750e-6
e1=2.670e-7
f1=-9.425e-10

y0=1.2017e-5
A_1=1.0246e-5
A_2=4.2287e-4
tau_1=10.186
tau_2=368.19

#Functions-------------------------------------------------------------------------
def evaluate_r(r):
    #Function that computes int. parameter for a given r
    return a1/6*r**6+b1/5*r**5+c1/4*r**4+d1/3*r**3+e1/2*r**2+f1*r #mol/s*cm

def evaluate_phi(r):
    #Function that computes int. parameter for a given r
    return y0*r-A_1/tau_1*np.exp(-tau_1*r)-A_2/tau_2*np.exp(-tau_2*r)

def calcx(r0,r1):
    #Function that computes position x for a given r1
    return -(evaluate_r(r1)-evaluate_r(r0))*F/iss*1000*10000

def calcphi(r1,rL):
    #Function that computes position x for a given r1
    return (evaluate_phi(r1)-evaluate_phi(rL))*F

def findr(r0):
    #Function that calculates r as a function of x for a given value of r0, then
computes ravg
    r1=np.linspace(r0, 0, 10000)
    ravg=0
    arr = []
    for i in range (len(r1)):
        x = calcx(r0,r1[i])
        if x/L<1:
            arr.append([x/L, r1[i]])
    for j in range (len(arr)-1):
        ravg=ravg+(arr[j][1]+arr[j+1][1])/2*(arr[j+1][0]-arr[j][0])
    return ravg

def give_array(r0):
    #Function that outputs the final profiles of r_av
    r1=np.linspace(r0, 0, 10000)
    arr = []
    for i in range (len(r1)):
        x = calcx(r0,r1[i])
        if x/L<1:
            arr.append([x/L, r1[i], 0])
    for j in range (len(arr)-1):
        arr[j][2]=calcphi(arr[j][1], arr[-1][1])*1000
```

```
    return arr

def iterate_r (r, upper, lower):
    #Function that takes in r with an upper and lower bound, computes new bounds
    bounds=np.linspace(upper, lower, 10)
    print bounds
    i=0
    if findr(bounds[0]) > r:
        while findr(bounds[i]) > r:
            print (findr(bounds[i]), r)
            i=i+1
        upper = bounds[i-1]
        lower = bounds[i]
        return (upper, lower)
    else:
        print 'r=%s is too high'%(r)
        return (0,0)

#Find concentration and potential profile-----------------------------------------
summary = []

for k in range (len(r_av)):
    r0=0.3
    rlow=0.005
    while round(findr(r0),3) != round(r_av[k],3) and r0 != 0:
        r0, rlow = iterate_r(r_av[k], r0, rlow)
    if r0 != 0:
        ravg=round(findr(r0),3)

        arr=give_array(r0)
        position= [row[0] for row in arr]
        conc = [row[1] for row in arr]
        potential = [row[2] for row in arr]

        if max(position) < 0.99:
            print 'r=%s is too low'%(ravg)
        else:
            summary.append([r_av[k],potential[0]/L])

#Plot and export data-------------------------------------------------------------
            plt.figure(0,figsize=(6,10))
            plt.plot(position,conc, label='r_av=%.2f'%(ravg))
            plt.figure(1,figsize=(6,10))
            plt.plot(position,potential, label='r_av=%.2f'%(ravg))

            with open('Results_%.2f.csv'%r_av[k], 'wb') as fp:
                  a = csv.writer(fp, delimiter=',')
                  a.writerows(arr)

    with open('Results_summary.csv', 'wb') as fp:
          a = csv.writer(fp, delimiter=',')
          a.writerows(summary)

plt.figure(0,figsize=(6,10))
plt.ylim(0, 0.31)
```

```
plt.xlim(0, 1)
plt.legend()
plt.xlabel('x/L', fontsize=14)
plt.ylabel('r', fontsize=14)
plt.show(0)

plt.figure(1,figsize=(6,10))
plt.xlim(0, 1)
plt.legend()
plt.xlabel('x/L', fontsize=14)
plt.ylabel('phi (mV)', fontsize=14)
plt.show(1)

plt.figure(2, figsize=(6,5))
plt.plot([row[0] for row in summary], [row[1] for row in summary],'-o', color =
'lime')
plt.xlabel('r_av', fontsize=14)
plt.ylabel('delta phi/L (mV/micron)', fontsize=14)
plt.xlim(0, 0.31)
plt.show(2)
```

A2.5 Predicting the Limiting Current

This program is used to predict the limiting current of electrolytes. Use of this program requires knowledge of the transport properties of the electrolyte over a wide range of salt concentrations. The constants `a1, b1, c1, d1, e1, f1` correspond to the fitting parameters for $(D\,c)/(r\,t_-)$ and the constants `y0, A_1, A_2, tau_1, tau_2` correspond to the fitting parameters of $(D\,c)/(r\,t_-\,\sigma\,t_{+,SS})$, as discussed in Chapter 4. The current parameters correspond to 5 kg/mol PEO with LiTFSI salt. The object `r_av` should be changed depending on the average salt concentration of the electrolytes which are being modeled. The values of steady-state current `iss` and electrolyte thickness `L` can be adjusted to model a variety of cell conditions.

The input values are `r_av` the average salt concentration of the electrolytes and the electrolyte thickness `L`. The range of `iss` should be adjusted, beginning with large bounds at first then narrowing in. The constants `a1, b1, c1, d1, e1, f1` correspond to the fitting parameters for $(D\,c)/(r\,t_-)$ and the constants `y0, A_1, A_2, tau_1, tau_2` correspond to the fitting parameters of $(D\,c)/(r\,t_-\,\sigma\,t_{+,SS})$, as discussed in Chapter 4.

The approach for obtaining limiting current is described in Chapter 4. This program functions by calculating the concentration profile in the electrolyte as a function of `iss`. The values of r at the position $x = L$ are plotted versus `iss`. This data is fit to a polynomial expression which is extrapolated to obtain `iss` when $r = 0$ at $x = L$, i.e. the limiting current. The output in the display text reads ‘limiting current for `r_av` = `iss`’.

```
import numpy as np
import matplotlib.pyplot as plt
import csv
```

```
#Choose electrolyte concentration-----------------------------------------------------
r_av=0.08

#Choose cell parameters---------------------------------------------------------------
iss=np.linspace(0.65, 0.85, 20) #mA/cm^2
L=500 #microns

#Constants----------------------------------------------------------------------------
F=96485 #C/mol

a1=1.088e-4
b1=-9.889e-5
c1=3.280e-5
d1=-4.750e-6
e1=2.670e-7
f1=-9.425e-10

#Functions----------------------------------------------------------------------------
def evaluate_r(r):
    #Function that computes int. parameter for a given r
    return a1/6*r**6+b1/5*r**5+c1/4*r**4+d1/3*r**3+e1/2*r**2+f1*r #mol/s*cm

def calcx(r0,r1):
    #Function that computes position x for a given r1
    return -(evaluate_r(r1)-evaluate_r(r0))*F/iss[k]*1000*10000

def findr(r0):
    #Function that calculates r as a function of x for a given value of r0, then
computes ravg
    r1=np.linspace(r0, 0, 10000)
    ravg=0
    arr = []
    for i in range (len(r1)):
        x = calcx(r0,r1[i])
        if x/L<1:
            arr.append([x/L, r1[i]])
    for j in range (len(arr)-1):
        ravg=ravg+(arr[j][1]+arr[j+1][1])/2*(arr[j+1][0]-arr[j][0])
    return ravg

def give_array(r0):
    #Function that outputs the final profiles of r_av
    r1=np.linspace(r0, 0, 10000)
    arr = []
    for i in range (len(r1)):
        x = calcx(r0,r1[i])
        if x/L<1:
            arr.append([x/L, r1[i]])
    return arr

def iterate_r (r, upper, lower):
    #Function that takes in r with an upper and lower bound, computes new bounds
    bounds=np.linspace(upper, lower, 10)
    print iss[k]
    i=0
```

```
    if findr(bounds[0]) > r:
        while findr(bounds[i]) > r:
            i=i+1
        upper = bounds[i-1]
        lower = bounds[i]
        return (upper, lower)
    else:
        print 'iss=%s is out of range'%(iss[k])
        return (0,0)

#Find concentration and potential profile-----------------------------------------
summary = []
in_range = 'yes'

for k in range (len(iss)):
    if in_range == 'yes':
        r0=0.30
        rlow=0.01

        while round(findr(r0),4) != round(r_av,4) and r0 != 0:
            r0, rlow = iterate_r(r_av, r0, rlow)
        if r0 != 0:
            ravg=round(findr(r0),4)

            arr=give_array(r0)
            position = [row[0] for row in arr]
            conc = [row[1] for row in arr]

            if min(conc) < 0.01:
                print 'iss=%s is above limit'%(iss[k])
                in_range = 'no'
            else:
                if conc[-1] <= 0.03:
                    summary.append([iss[k], conc[-1]])
                    plt.figure(0,figsize=(6,10))
                    plt.plot(position,conc, label='iss=%.2f'%(iss[k]))

#Determine limiting current-------------------------------------------------------
par = np.polyfit([row[1] for row in summary], [row[0] for row in summary], 2,
full=False)
x=np.linspace(0, max([row[1] for row in summary]), 100)
y=par[0]*x**2+par[1]*x+par[2]
print 'limiting current for %s = %s'%(r_av, par[2])

#Plot and export data-------------------------------------------------------------
plt.figure(0,figsize=(6,10))
plt.ylim(0, 0.31)
plt.xlim(0, 1)
plt.legend()
plt.xlabel('x/L', fontsize=14)
plt.ylabel('r', fontsize=14)
plt.show(0)

plt.figure(2, figsize=(6,5))
```

```
plt.plot([row[1] for row in summary], [row[0] for row in summary],'-o', color =
'lime')
plt.plot(x,y,'-', color = 'blue')
plt.ylabel('iss', fontsize=14)
plt.xlabel('r at x=L', fontsize=14)
plt.xlim(xmin=0)
plt.show(2)
```
